Lehrstuhl für Raumfahrttechnik
Prof. Prof. h.c. Dr. Dr. h.c. Ulrich Walter

Technische Universität München

Master Thesis

Development of a Dynamic Simulation Model for Performance Prediction of Photobioreactors in Biological Life Support Systems for Human Spaceflight

RT-MA 2018/16

Author:

Thomas Ruck, B.Sc.

Betreuer: Daniel Pütz, M. Sc.
Lehrstuhl für Raumfahrttechnik / Institute of Astronautics
Technische Universität München

LRT-Nummer: RT-MA 2018/16

Titel der Arbeit: Development of a Dynamic Simulation Model for Performance Prediction of Photobioreactors in Biological Life Support Systems for Human Spaceflight

Autor: Thomas Ruck, B.Sc.

Erklärung

Mir als vertraulich genannte Informationen, Unterlagen und Erkenntnisse werde ich nach meiner Tätigkeit am Lehrstuhl nicht an Dritte weitergeben.

Ich erkläre mich außerdem damit einverstanden, dass meine Bachelor-, Semester-, Master-/Diplomarbeit vom Lehrstuhl auf Anfrage fachlich interessierten Personen, auch über eine Bibliothek, zugänglich gemacht wird, und dass darin enthaltene Ergebnisse sowie dabei entstandene Entwicklungen und Programme vom Lehrstuhl für Raumfahrttechnik uneingeschränkt genutzt werden dürfen. (Rechte an evtl. entstehenden Programmen und Erfindungen müssen im Vorfeld geklärt werden.)

Ich erkläre außerdem, dass ich diese Arbeit ohne fremde Hilfe angefertigt und nur die in dem Literaturverzeichnis angeführten Quellen und Hilfsmittel benutzt habe.

Garching, den 12.12.2018

_____

Unterschrift

Acknowledgments

This thesis was mainly written during my time as a visiting researcher at the University of Colorado Boulder, USA. This special placement was only possible with the help of a variety of people, who I would like to acknowledge here.

I would like to say thank you to my advisor Daniel Pütz, M.Sc. from the Institute of Astronautics at the Technical University of Munich who not only helped me on all the programming questions I had, but also helped me organise this placement in probably record-braking time after a very sudden change of plans on my end. Daniel, I am incredibly grateful you made this experience possible for me.

And I would like to thank my second advisor and algae expert Dr. Tobias Niederwieser from the University of Colorado Boulder, who was not just source of great ideas and always available for help, but also became a friend over many barbecues in his backyard.

Thanks are also owed to Dr. Claas Olthoff, who was always supportive of my ambitions at the Institute of Astronautics over the years and helped me in finding a placement for my Master's Thesis.

Furthermore, I would like to thank Dr. Alexander Höhn and M.Eng Carla Höhn, who put so much work into the invitation paperwork, and then set me up with everything I could have asked for to start my new life in Boulder.

I would like to express my gratitude to Professor Dr. David Klaus from the University of Colorado Boulder and Professor Dr. Ulrich Walter from the Technical University of Munich for keeping this exchange between our two institutes alive and strong. The experiences you are offering your students with this opportunity are amazing.

I would also like to extend my thanks to the Heinrich und Lotte Mühlfenzl Stiftung, who generously supported my stay in Boulder and Dr. Martin Rott from the Institute of Astronautics at the Technical University of Munich for advocating for me and organizing this scholarship. Further support that I am grateful for came from the German Academic Exchange Service as PROMOS scholarship, which was awarded through the Technical University of Munich.

Zusammenfassung

Die Verwendung physikalisch-chemischer Lebenserhaltungssysteme wird, wegen der begrenzten Möglichkeit von Nachschublieferungen, ein begrenzender Faktor auf zukünftigen bemannten Langzeit-Raumflugmissionen sein. Der Anbau von Algen in Photobioreaktoren ist eine vielversprechende bio-regenerative Alternative für die kombinierten Aufgaben der Atemluftaufbereitung, Urinaufbereitung und Produktion von Nahrungsergänzungsmitteln.

Diese Arbeit präsentiert die Entwicklung eines dynamischen Wachstumsmodells der grünen Mikroalge Chlorella vulgaris. Das Modell kann dynamisch auf variierende Einflüsse reagieren. Diese sind die Kohlenstoffdioxid- und Nährstoffverfügbarkeit für Photosynthese, pH Wert des Wachstumsmediums, Temperatur, Kohlenstoffdioxid- und Sauerstoffkonzentrationen im Wachstumsmedium und die Verfügbarkeit von photosynthetisch aktiver Strahlung. Bestandteil des Modells sind zudem komplexe Submodelle zur Berechnung des pH Werts des Wachstumsmediums sowie der Verbreitung von photosynthetisch aktiver Strahlung durch die Photobioreaktorgeometrie bei variierenden Biomassenkonzentrationen.

Experimente werden im Rahmen dieser Arbeit durchgeführt und deren Ergebnise präsentiert um Daten in Bereichen zu generieren, in denen die Literaturwerte große Varianz zeigen oder nur spärlich verfügbar sind. In das entwickelte Modell integriert sind Ergebnisse der Experimente in den Bereichen der Bestimmung von Wachstumsraten, Abschwächung von photosynthetisch aktiver Strahlung mit variierender Biomassenkonzentration und benötigte Oberflächenstrahlungsdichte für optimales Wachstum.

Das Chlorella vulgaris Wachstumsmodell ist in V-HAB implementiert, einem MATLAB basierten Simlationsprogramm für Lebenserhaltungssyste, welches seit 2006 am Lehrstuhl für Raumfahrttechnik der Technischen Universität München entwickelt wird. In der V-HAB Simulationsumgebung ist das Modell in einem hocheffizienten Photobioreaktor integriert, welcher derzeit an der University of Colorado Boulder entwicklet wird. Dieser Photobioreaktor ist wiederum in eine simulierte Kabine eines Raumfahrzeuges mit einem Menschmodell integriert. Die Kombination aus Algenmodell in einem Photobioreaktor und den breiten Funktionalitäten von V-HAB erlauben die Simulation eines Lebenserhaltungssystems für zukünftige bemannte Raumfahrtmissionen. Das simulierte system kann 100 % Luft- und Urinaufbereitung leisten und zusätzlich eine Ergänzung zur täglichen Nahrung produzieren. Mit einer optimistischen Wachstumsrate ist, abhänging von der erreichbaren Flußkanaldicke des Reaktors, ein Wachstumsvolume der Algen von nur 21.5 Litern oder 32 Litern nötig, mit einer pessimistischeren werden 500 Liter benötigt, um Luft- und Urinaufbereitung für einen Menschen zu gewährleisten.

Zusätzlich zeigt das Modell die Möglichkeit der Optimierung des Photobioreaktordesigns und operationeller Entscheidungen, wie dem Wachstumsvolumen, der Kulturtiefe, der optimale Biomassenkonzentration im kontinuierlichen Betrieb, dem Profil der photosynthetisch aktiven Strahlung und Parametern der Luftversorgung des Reaktors.

Abstract

The use of physico-chemical life support systems will be a limiting factor on future long-duration human spaceflight missions due to the lack of frequent resupply capability. Cultivation of algae in a photobioreactor is a promising bioregenerative alternative for combined air revitalization, waste water treatment, and food supplement production.

This thesis presents the development of a dynamic growth model for the green microalgae Chlorella vulgaris. The model can dynamically react to the varying influences of carbon dioxide and nutrient availability for photosynthesis, growth medium pH, temperature, carbon dioxide and oxygen concentration in the medium and the availability of photosynthetic active radiation. Complex sub-models for the representation of pH changes in the growth medium and the propagation of photosynthetically active radiation through a photobioreactor geometry at varying biomass concentrations are also part of the overall model.

Experiments are conducted and presented in this thesis, which generate data in areas where literature sources show a large variance or only scarce data is available. The experimental results in the areas of growth rate determination, varying radiation attenuation in a growing microalgal culture and required surface irradiances for optimum growth are integrated into the model to increase its confidence level.

The Chlorella vulgaris growth model is implemented in V-HAB, a MATLAB based life support system simulation tool, which has been under development at the Institute of Astronautics at the Technical University of Munich since 2006. In the V-HAB environment, the growth model is implemented in a newly designed high-efficiency photobioreactor developed at the University of Colorado Boulder and integrated in a simulated cabin environment with a sophisticated human model in the loop. The combination of the algae model in a photobioreactor and the borad functionalities of the V-HAB simulation environment allows the simulation of a biological life support system for future human spaceflight missions. The simulated system is able to reach 100 % air revitalization and urine processing capability, as well as some food supplement production. With an optimistic growth model an algal culture volume of 21.5 liters or 32 liters is required depending on the attainable flow channel thickness, with a more pessimistic one, 500 liters are necessary to support one human in terms of air revitalization and urine processing.

Furthermore, the developed model is shown to have the capability of optimizing photobioreactor-designs and operational decisions such as the overall growth volume, culture depth, optimum continuous biomass concentration, the profile of provided photosynthetically active radiation and air supply parameters.

Table of Contents

List of Figures

List of Tables

Symbols

A	$\frac{1}{m}$	Attenuation coefficient
A_{max}	$\frac{1}{m}$	Maximum attenuation coefficient
A_M	m^2	Membrane area
b	-	Empirical constant for attenuation model
c_{light}	$\frac{m}{s}$	Speed of light
c^0	$\frac{mol}{m^3}$	Standard molar concentration
c_a	$\frac{mol}{m^3}$	Molar concentration in Water
C_{cells}	$\frac{1}{ml}$	Cell concentration
C_T	$\frac{mol}{m^3}$	Total inorganic carbon concentration
c_p	$\frac{J}{K}$	Heat capacity
d_M	m	membrane thickness
Δ	-	difference
E_{ph}	J	Energy of a photon
E_{PAR}	J	Photosynthetically active radiation energy
η_{solar}	-	Solar energy conversion efficiency
f_{dil}	-	Dilution factor
h	$J * s$	Planck's Constant
H	$\frac{mol}{m^3 * Pa}$	Henry's constant
H^{ref}	$\frac{mol}{m^3 * Pa}$	Reference Henry's Constant
I	$\frac{W}{m^2}$	Irradiance
J	$\frac{mol * m}{m^2 * Pa * s}$	Membrane permeability
K_{a_X}		Acid constant of X
L	m	Length parameter
L_{min}	m	Position below surface of minimum photon flux density
L_{sat}	m	Position below surface of saturation photon flux density
λ	m	Wavelength
m	kg	Mass
m_{cell}	kg	Mass of one cell
$\dot{M}$	$\frac{mol}{s}$	Molar flow rate
M_{rel}	$\frac{kg}{mol}$	Relative molar mass
μ	$\frac{kg}{m^3 * s}$	specific biomass concentration increase rate
μ_{ach}	$\frac{kg}{m^3 * s}$	Achievable specific biomass concentration increase rate
μ_{max}	$\frac{kg}{m^3 * s}$	Maximum specific biomass concentration increase rate
μ_{opt}	$\frac{kg}{m^3 * s}$	Optimum specific biomass concentration increase rate
$\mu_{rel_{CO_2}}$	-	Carbon dioxide concentration influence relative growth rate
$\mu_{rel_{O_2}}$	-	Oxygen concentration influenced relative growth rate
μ_{rel_P}	-	Photosynthetically active radiation influenced relative growth rate
$\mu_{rel_{pH}}$	-	pH influenced relative growth rate

μ_{rel_T}	-	Temperature influenced relative growth rate
N_A	-	Avogadro constant
OD	-	Optical density
OD_{corr}	-	Corrected optical density
OD_{dil}	-	Diluted optical density
P	$\frac{\mu mol}{m^2 * s}$	Photosynthetic photon flux density
P_0	$\frac{\mu mol}{m^2 * s}$	Surface photon flux density
P_{att}	$\frac{\mu mol}{m^2 * s}$	Attenuated photon flux density
$P_{avg_{lin}}$	$\frac{\mu mol}{m^2 * s}$	Average photon flux density in linear radiation growth domain
P_{exit}	$\frac{\mu mol}{m^2 * s}$	Photon flux exiting the photobioreactor on bottom
P_{heat}	$\frac{\mu mol}{m^2 * s}$	Photon flux density turned to heat
P_{min}	$\frac{\mu mol}{m^2 * s}$	Minimum photon flux density
P_{sat}	$\frac{\mu mol}{m^2 * s}$	Saturation photon flux density
$P_{inhibit}$	$\frac{\mu mol}{m^2 * s}$	Inhibition photon flux density
$P_{av_{lin}}$	$\frac{\mu mol}{m^2 * s}$	Average photon flux density in linear radiation growth domain
$pH_{extr_{low}}$		Lower extreme pH Boundary
$pH_{opt_{low}}$		Lower pH boundary for optimum growth
$pH_{opt_{up}}$		Upper pH boundary optimum growth
$pH_{extr_{up}}$		Upper extreme pH Boundary
p_g	Pa	Partial pressure of a substance in gas phase
p_{eq}	Pa	Equivalent partial Pressure
$\dot{Q}_{PAR}$	W	Heating power from photosynthetically active radiation
ρ_b	$\frac{kg}{m^3}$	Biomass concentration
$\rho_{b_{max}}$	$\frac{kg}{m^3}$	Maximum biomass Concentration
$\rho_{b_{opt}}$	$\frac{kg}{m^3}$	Optimum biomass concentration for highest growth rate
t	s	Time
t_{lag}	s	Lag time
T	K	Temperature
T^{ref}	K	Reference temperature
$T_{max_{life}}$	K	Maximum survivable temperature
$T_{max_{opt}}$	K	Maximum temperature for optimum growth
$T_{min_{opt}}$	K	Minimum temperature for optimum growth temperature
V_{lin}	m^3	Volume of linear radiation growth domain
V_{sat}	m^3	Volume of saturated radiation growth domain
V_{tot}	m^3	Total growth volume

V_{solute}	m^3	Volume of solute
$V_{solution}$	m^3	Volume of solution
$\frac{-\Delta_{sol}H}{R}$	K	Temerpature influence Factor (Henry's Law)

Abbreviations

Ac.	Acid
BBM	Bold's Basal Medium
Bs.	Base
EDTA	Ethylenediaminetetraaeceitic acid
LED	Light-emitting diode
M.	Mineral
Nut.	Nutrient
PAR	Photosynthetically active radiation
PBR	Photobioreactor
PPFD	Photosynthetic Photon Flux Density

1 Introduction

The use of physico-chemical life support systems will be a limiting factor on future long-duration human spaceflight missions due to the lack or high expense of frequent resupply capability. Biological life support systems are a sustainable alternative to maintain breathable air, water and food supply for the astronauts on these missions.

The working mechanism behind a plant-based biological life support system is what initially turned Earth's anoxic (oxygen-free) atmosphere into a liveable place at least 2.5 bilion years ago: photosynthesis [1]. It has the potential to consume carbon dioxide and water by utilizing photosynthetically active radiation energy and produce carbohydrates and oxygen. Since humans do exactly the opposite, consume oxygen and produce carbon dioxide, photosynthetic assimilation is a good counter-mechanism to human respiration when a constant atmospheric composition is required.

Organisms capable of performing photosynthesis are called phototrophs, among which are plants, algae and cyanobacteria. While plants need to grow structures (e.g. woody stalks in trees) and reproductive organs, in algae none of the tissue is unused in terms of photosynthetic growth [2]. Furthermore, algae are ready to perform photosynthesis within only 3 to 5 days, which can be an advantage after a catastrophic failure [3]. Therefore, the cultivation of algae in a photobioreactor is a promising bioregenerative alternative to traditional physico-chemical systems for combined air revitalization, waste water treatment, and food supplement production.

The prediction of algal growth behavior in a photobioreactor is of vital importance to the design of a biological life support system, since it determines rate of carbon dioxide fixation and oxygen assimilation. While the performance could be assessed with hardware tests and compared for different photobioreactor designs and integration architectures, this approach would be rather time consuming and costly. It is therefore desirable to have high confidence data on a design before it is built for hardware testing in order to minimize hardware development and testing iterations.

An option to generate this data is the use of averages. When talking about averages, usually time-averages are meant, which by definition cannot display behavior at a time-resolution smaller than the time-interval over which they were averaged. However, for spaceflight, where every additional kg launch mass is connected to high cost, a system with as little mass-overhead as possible yet high operational confidence is necessary. These requirements call for high resolution analysis and optimization which can only be done with dynamic calculations, which re-evaluate all system parameters at short time intervals. Since this requires a large number of calculation steps, these calculations are done with a computer and then called dynamic simulations.

In order to dynamically simulate the behavior of algal growth, an algal growth model is required that can adapt to dynamically changing environmental influences. Such a dynamic algal growth model is developed in this thesis, integrated in a photobioreactor and then used to simulate the photobioreactor's behavior as a biological life support system component with a human in the loop. This is done with the dynamic life support system tool V-HAB, which has been under development at the Institute of Astronautics at the Technical University of Munich since 2006 [4].

1.1 Scope

This thesis documents the development of an algal growth model, its integration into a photobioreactor and the simulation of the photobioreactor's performance in a spacecraft cabin with a human in the loop. More specifically, a proposed high-efficiency photobioreactor design by Tobias Niederwieser [5] is used, which was initially sized with averages and is simulated with a dynamic approach in this thesis.

The developed model is implemented with values for the green algae Chlorella vulgaris on which a lot of data exists since it is widely used in scientific experiments. All the mechanisms that govern the behavior of Chlorella vulgaris growth are outlined in this thesis in two separate chapters. One of them describes the scientific background of algal growth in detail and the other is more focused on the implementation of these mechanisms in the V-HAB simulation system. Therefore, this thesis should also be regarded as a description of algal growth from an engineer's point of view and not just a presentation of simulation results.

The Chlorella vulgaris growth model can dynamically react to the following varying influences:

- Growth medium temperature
- Growth medium pH
- Availability of nutrients for photosynthetic growth
- Availability of carbon dioxide for photosynthetic growth
- Oxygen concentration in the medium
- Carbon dioxide concentration in the medium (not for photosynthetic assimilation but as limiting effect at high concentrations)
- Availability of photosynthetically active radiation

Since literature provides strongly varying or only scarce information on some of the influences mentioned above, some experiments with regard to growth and radiation parameters are done within the scope of this thesis. The results of the experiments are presented in this thesis and implemented in the model.

The model can be used to simulate the use of a Chlorella vulgaris photobioreactor as a biological life support system. The most important simulation results consider:

- Air revitalization (carbon dioxide consumption, oxygen evolution)
- Water processing (urine processing, potable water harvesting)
- Food supplement production (biomass harvesting)

Furthermore, the model was developed with the clear intent of providing information on potential design optimizations by indicating what factors are limiting the growth at any given time during the simulation.

1.1.1 Limitations

Biological processes are not always calculable as engineers are commonly used to and have a certain degree of unpredictable probability. However, for a computer simulation, the description of scientific, biological and natural behaviors and effects in a mathematical way is essential. In order to do so, the inherent uncertainty of biological systems has to be reduced to a degree by using assumptions and averages.

The used abstractions are usually only valid on a certain range, for example a certain temperature or pH range. The range for which the assumptions are made usually coincides with that range that can be expected in a controlled photobioreactor environment. The model should therefore not be regarded as a universal algal growth model, but specifically as a model for growth in a controlled photobioreactor. For example, it is not intended to simulate the algal growth in salty water in an ocean at 280 K but can simulate the algal growth in a specific culture medium at 300 K in a photobioreactor in a spacecraft cabin.

The model is implemented with the behavior of Chlorella vulgaris. However, not for all factors affecting the growth of this microalgae, specific values on the Chlorella vulgaris species could be found more general value for the Chlorella genus or simply values stated for *microalgae* were used. It is clearly stated in this thesis in which areas of the model this is done.

Since the abstraction of scientific problems is necessary in most engineering disciplines, cell internal processes (for example the assimilation pathway of carbon atoms during the photosynthetic process) are not regarded in this model. The Chlorella vulgaris cells are treated as a black box. The model should demonstrate how a Chlorella vulgaris culture can be incorporated into an engineering system by accepting biological findings from experts on biological matters. Nevertheless, all important scientific mechanisms are explained in this thesis to that degree that is represented in the model.

One aim of this thesis, besides developing an algae simulation model, was to simulate a photobioreactor design proposal by Niederwieser [5]. Since this is a flat panel photobioreactor, the areas of the simulation where geometry plays a role are designed for such a reactor. Especially the propagation of photosynthetically active radiation through the growth medium would have to be extended if cylindrical photobioreactors should be modeled in the future.

1.2 Methods

This thesis is written in collaboration between the Institute of Astronautics at the Technical University of Munich and the Bioastronautics Department at the University of Colorado Boulder. Since two parties are involved, two different aims can be expected from them and are both reflected in this thesis.

The Institute of Astronautics at the Technical University of Munich started developing the life support system simulation tool V-HAB in 2006 [4] and is continuing this effort with the work of PhD, master and bachelor students. This thesis shall therefore provide a further contribution to the V-HAB simulation system by developing an algae model that is functioning in a photobioreactor and can be used for future simulations.

Tobias Niederwieser from the Bioastronautics Department at the University of Colorado Boulder, presented a highly efficient photobioreactor design for spaceflight life support [5]. Since this design was done with averages the other overall goal of this thesis is to verify the design in a dynamic simulation environment. The design is therefore to be implemented in the dynamic simulation tool V-HAB, combined with the developed algae model and its behavior simulated in a spacecraft cabin with a human in the loop.

1.2.1 Mission Statement and Requirements

In an early phase, when the project goals were defined, a mission statement and main tasks were formulated and communicated with both involved university advisors.

The originally formulated mission statement reads as follows:

> *This thesis aims at updating the existing algal model and creating the flow-through photobioreactor (under development at the University of Colorado, Boulder) in the VHAB Simulation environment. The simulation should be able to predict the reactor's carbon dioxide consumption, oxygen generation and the algal growth under varying influences of pressure, carbon dioxide content, light and temperature. The simulation should be validated and improved with test data and eventually used to size a reactor capable of providing sufficient oxygen to a human in a day/night cycle.*

After some initial research, the existing V-HAB algal models were deemed unusable for the task at hand. Two of them were too inflexible with regard to changing environmental parameters and and the other one aimed at producing hydrogen in a discontinuous process instead of oxygen (more information see 2.4).

From the initially defined main tasks for the work conducted within the scope of this thesis, the following top-level requirements were derived and used as a baseline for the work in this thesis.

1. A Chlorella vulgaris growth model shall be created capable of dynamically reacting to varying influences of
   1.1. atmospheric pressure
   1.2. carbon dioxide concentration
   1.3. oxygen concentration
   1.4. nitrogen concentration
   1.5. light intensity
   1.6. temperature
2. The use of urine as a nutrient should be investigated and implemented
3. The algal growth model shall be implemented in V-HAB
4. The algal growth model shall be incorporated in a photobioreactor design in order to simulate
   4.1. carbon dioxide consumption
   4.2. oxygen generation
   4.3. biomass production
5. Two gas transfer technologies between the photobioreactor and the atmosphere shall be implemented
   5.1. sparging
   5.2. hollow fiber membranes
6. Areas where biological and hardware tests are sensible shall be identified.
7. Simulations shall be run that to size a photobioreactor capable of providing sufficient air revitalization capability to a human in a day/night cycle with special consideration of the
   7.1. interplay between assimilation coefficient (algae) and respiration coefficient (human)
   7.2. predicting the waste water input (urine as nutrition) and purified water output
   7.3. predicting the produced biomass

After the arrival in Boulder and more communications about the goals of the thesis, it became clear that a newly proposed photobioreactor design and integration architecture by Tobias Niederwieser shall act as baseline for the simulation cases in order to verify the validity of that design. Therefore, two more requirements are added to the list:

8. The newly proposed photobioreactor design and integration architecture shall be simulated
   8.1. with values exactly as proposed in the paper
   8.2. with the values as implemented in the model (found in other literature sources)
9. Means of optimization shall be identified through the simulation results

1.2.2 Model Development Process

The development process of the model was governed by the analysis of literature. Where possible, journal articles were used, which mainly came from scientific, biological or biotechnological journals rather than purely engineering journals. When journal articles were unavailable, further resources like conference papers, university courses or technical product sheets were used.

In the initial development phase, a top-level V-HAB system with a growth chamber and air supply was implemented with a simplistic growth model. Since the backbone of simulated algal growth is a model that calculates the growth rate itself, this was implemented as first subsystem.

Over time, features were added that simulate a certain influence on the algal growth (for example temperature, pH, nutrients). And since the calculation of the magnitude of these influences require the simulation of the cause of the influence, further mechanisms had to be implemented. For example, the influence of pH on the growth rate requires the simulation of the pH in the medium, which can then act as a cause of the influence.

Each implemented influence was tested for its individual performance. For example, titration experiments with the pH calculation module were made to reproduce known behaviors. In a next step they were combined with the existing growth model and other factors implemented thus far. This approach ensures the validity of the individual calculation mechanisms and gives confidence that they are also capable of functioning in a larger context.

A further step in the model development was the generation of experimental data in areas where data was only available scarcely (such as the attenuation of photosynthetically active radiation in an algal culture) or showed a wide variance (such as the growth rate and maximum achievable cell concentrations). The materials and methods used for these experiments are presented in chapter 5, where also their results are presented.

Scaling up to at a larger system context, the developed Chlorella vulgaris model was integrated in a photobioreactor V-HAB system. During this integration, certain boundary conditions previously set in the algae model were moved up one level to be defined by the photobioreactor. This concerned mainly parameters of the photosynthetically active radiation, the gas exchange with the atmosphere and the integration of a dedicated biomass harvester.

Each time a feature was added to the model, it was connected with subsystems that were already part of the model. Furthermore, each time a higher order system (e.g. photobioreactor or spacecraft cabin) was integrated, more interdependencies were added. A map of top-level interdependencies can be drawn that gives an idea of how connected the eventually developed model is. This furthermore shows how important a dynamic simulation is for an accurate prediction of algal growth, since it depends on a variety of factors that can influence its growth. The map is shown in Figure 1-1.

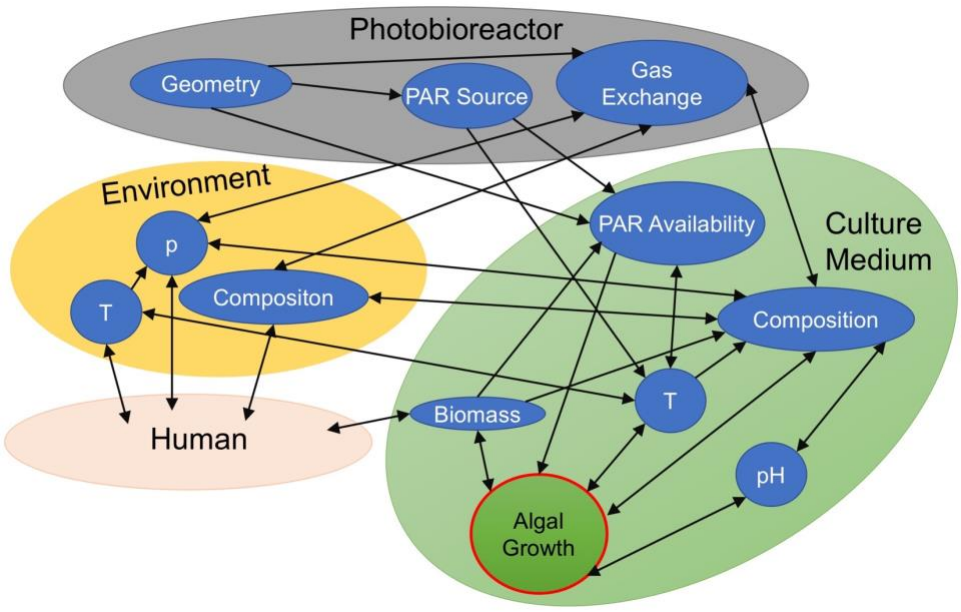

Figure 1-1: Map of dependencies between components of the developed algal growth model and its integration in a photobioreactor as a life support system component.

1.3 Nomenclature

This thesis uses no abbreviations in the running text. Only units and chemical symbols are abbreviated. In figures and tables, the use of abbreviations is also avoided where possible but used sometimes for the sake of space. For the few abbreviations that had to be used in figures and tables, the full word is mentioned in the text and in the list of abbreviations.

This thesis describes the development of a Chlorella vulgaris model. Nevertheless, sometimes also terms such as *algal culture* (instead of *Chlorella vulgaris culture*) or *algal growth* (instead of *Chlorella vulgaris growth*) are used in the thesis. These terms refer to the same model in which the algal species Chlorella vulgaris is modeled. For a non-native English speaker some confusion about the words *alga*, *algae* or *algal* can arise which should be explained here. *Alga* is singular (i.e. one cell), *algae* the plural and *algal* an adjective.

Throughout the published literature there is a lot of ambiguity around the words describing how many cells are in a volume of growth medium and to how much biomass these cells in the volume equate. For this thesis a consistent nomenclature shall be used, which is explained here

- *Cell density* is the density of the cell itself, measured in kg cell mass per m^3 volume of a single cell.
- *Cell concentration* is the number of cells per m^3 volume of growth medium.
- *Biomass concentration* is the combined mass of all cells in kg per m^3 volume of growth medium.

The source from which the photosynthetic process draws its energy is often referred to as *light*. However, the term *light* or more precisely *visible light* is defined as the radiation between 400 and 700 nm wavelength, which the human eye can detect [6] and since plants do not receive energy or information through eyes, the term *light* should not be used when referring to plant research [7]. Hence, this thesis uses the correct term, which is *photosynthetically active radiation*, where many other publications use *light*. In tables and figures it may be used in its abbreviated form *PAR*.

2 Chlorella Vulgaris Biology, Cultivation and Technology

The microalgal species Chlorella vulgaris, which will be defined in more detail in 2.1, can be utilized in a broad spectrum of useful applications. These applications can be both terrestrial and extraterrestrial and are presented in 2.2. When cultivated in an industrial manner, Chlorella vulgaris is usually grown in photobioreactors, to which an introduction and technology overview is given in 2.3. Lastly this chapter discusses previous V-HAB simulation models of algal biotechnology applications in 2.4, which also serves as a direct introduction to the main work conducted within the scope of this thesis.

2.1 Algae

For most people the word *algae* will call forth images of *seaweed* or a green film on bodies of water. And as different as the appearances of seaweed and a seemingly homogenous green film on a pond is, they can still both be referred to as algae. In fact, algae is a very broad term for aquatic organisms capable of performing photosynthesis, which can range from microscopic unicellular species, such as Chlorella vulgaris used in this thesis, to 60 meter long Kelps, spanning seven orders of magnitude in size [8]. Alone among the microalgae, 40 000 different types have been discovered so far [9].

Algae are eukaryotic organisms, which means that their cells have an organism with an enclosed nucleus [10]. They do not have multicellular reproductive structures such as plants [8]. The so called blue-green algae or cyanobacterium (also sometimes considered for spaceflight applications [10]), has many similarities with eukaryotic algae but technically is not considered one [11], [12]. A further means of classifying algae is often done by their visual appearance due to the different pigments they contain such as green, brown or blue-green algae [8].

Since this thesis mainly deals with the green freshwater microalgal species Chlorella vulgaris, it shall be introduced in more detail hereafter.

2.1.1 Chlorella Vulgaris

First discovered in 1890 by Dutch researcher Martinus Willem Beyerinck [13], Chlorella vulgaris is a green eukaryotic fresh water microalgae with a diameter between 2 and 10 µm [14].

The Chlorella vulgaris cell, which is pictured in Figure 2-1, is characterized by a rigid outer cell wall, which shields the active components of the cell from harsh environments. The single chloroplast inside the Chlorella vulgaris cell holds the chlorophyll and carotenoid pigments that capture the photosynthetically active radiation energy for the photosynthetic processes that happens in the chloroplast and its lower level components [14].

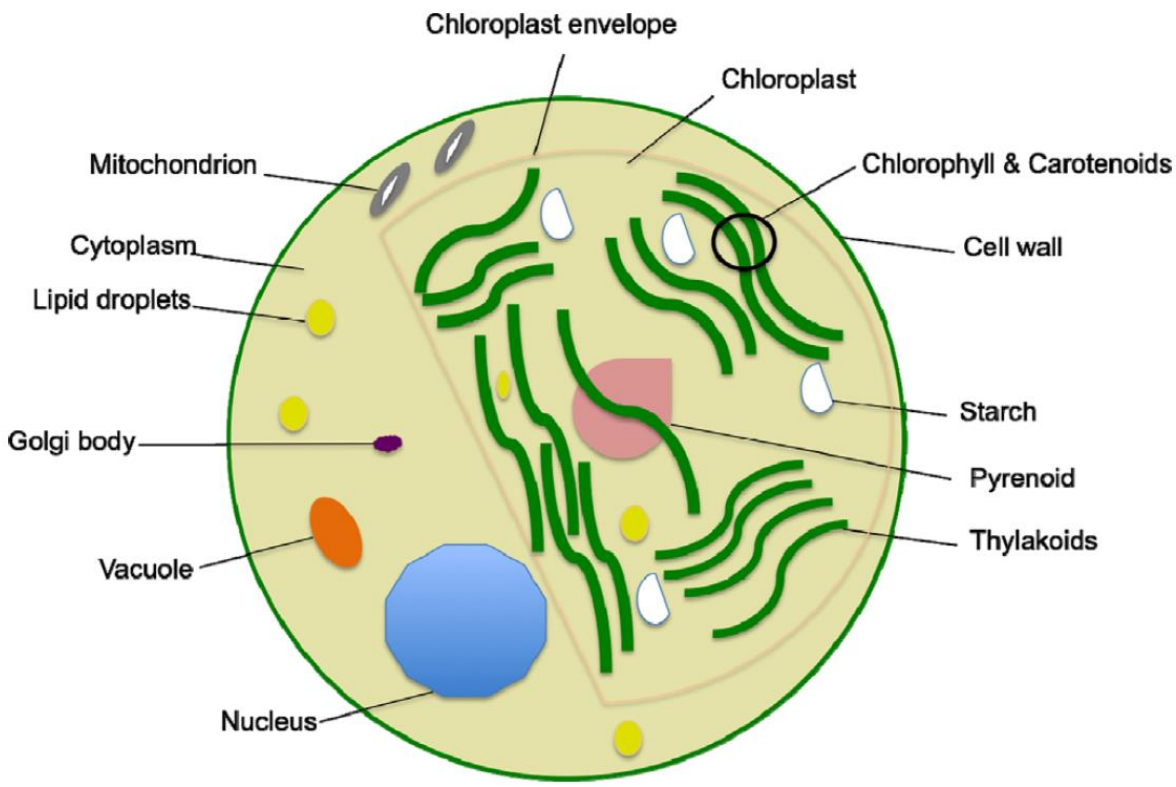

Figure 2-1: Schematic overview of Chlorella vulgaris cell with cell organelles. Copied from [14].

The reproductive process of Chlorella vulgaris is asexual and happens in a process called autosporulation. During this process, four daughter-cells are formed within the mother-cell and burst out of the (at that point no longer existing) mother-cell, when they become too large. These daughter-cells each have their own nucleus and chloroplast and consume the remainder of the mother cell [14].

When looking at Chlorella vulgaris' macromolecular composition, there is a variance that can be influenced by the cultivation method and growth medium composition [15]. It is composed of 42-58 % proteins, 5-40 % lipids (depending on growth conditions), 12-55 % carbohydrates (depending on growth medium) and 1-2 % pigments [14]. Another source states the following values: 51-58 % proteins, 12-17 % carbohydrates and 14-22 % lipids [16].

This sub-chapter only serves as a short introduction to cell internal characteristics of Chlorella vulgaris. Chapter 3 covers the photosynthetic growth, nutrient metabolism and reaction to varying environmental influences of Chlorella vulgaris in detail.

2.2 Applications of Chlorella Vulgaris

Applications of Chlorella vulgaris are found in various different fields. Their rigid cell walls, make the cells resistant to harsh conditions and invaders and, combined with their rapid growth rate, this circumstance makes them well suited for commercial industrial production. The terrestrial applications in which these commercially produced Chlorella vulgaris cells can be put to use are abundant and outlined in 2.2.1. For space applications, which are outlined in 2.2.2, the production will not be of a commercial nature and most likely also would not be considered large-scale.

2.2.1 Terrestrial

With an increasing carbon dioxide content in Earth's atmosphere due to the burning of fossil fuels, sustainable biofuels become ever more important. Chlorella vulgaris can be used as a feedstock for so called *third-generation* biofuels, which have the advantage of not competing with food sources for humans, not requiring deforestation when cultured sensibly [14] and even have the potential to be grown in otherwise unusable brackish water [15]. For this application, a high lipid content in the algal cells is desired and research regarding the maximization of lipid content is ongoing [14], [15]. However, currently the processes of culturing the algal cells and the chemical processes to eventually turn them into fuel cannot compete with fossil fuel sources from economic and production-energy perspectives [14].

Chlorella vulgaris is used as a food supplement in the form of tablets, powders and extracts due to its "richness in proteins, lipids, polysaccharides, pigments and vitamins" [14]. However, breaking the rigid cell walls is a challenge since it is a costly process but required to make the cells digestible and the internal components extractable [14].

Chlorella vulgaris cells can be used as food for animals, which made up about 30 % of total Chlorella vulgaris production in 2007 [16]. The carotenoid pigments in Chlorella vulgaris can have a positive pigmentation effect on fish flesh and egg yolk and increase health and life expectancy of animals. Furthermore, Chlorella vulgaris as animal food can protect the animals against the effects of heavy metals [14].

The treatment of municipal, agricultural or industrial wastewaters can be done with Chlorella vulgaris cells [14] in a cheaper and more efficient manner than with traditional methods [17]. A lot of research, historic and present, is connected to the metabolism of water contaminants (especially urine, ammonia and phosphorus) that can serve as nutrients to a growing algal culture [15], [18], [19], [20].

Other areas of application, which are not further discussed here are the use of Chlorella vulgaris as fertilizer for higher plants, in cosmetics and for the production of pharmaceutical products [14].

2.2.2 Extraterrestrial

Some of the previously described terrestrial applications of Chlorella vulgaris can be transferred to an extraterrestrial application, where algae can also be used in a beneficial way. Among these already discussed ones are the potential for food production and waste water cleaning. One additional major functionality a growing algal culture can have in a spacecraft is air revitalization. An algal culture can turn carbon dioxide into oxygen through the process of photosynthesis while producing edible biomass and processing urine to potable water.

The concepts for algae based life support systems vary from a full air revitalization and water processing capability [5], over hybrid systems[21] to backup systems for carbon dioxide regulation during times of emergency or strong fluctuations in the cabin atmosphere [3].

While some full scale biological life support system experiments have been done on Earth in Russia and the United States as early as the 1960s (involving humans, apes dogs and rats) [10], no data on full scale system tests in space could be found.

Nevertheless, smaller-scale algal experiments have been done in space. A review study [22] found that algal experiment have been done in space since as early as 1960 and have totaled to 50 individual experiments until the end of 2017 with one additional one to be launched in 2018. Not all of these experiments used green algae or Chlorella vulgaris specifically, but the main genus used was Chlorella. While most of these experiments were done inside the pressurized cabin, one experiment proved the survivability of algae and cyanobacteria in the vacuum of space, which indicates that they could survive a catastrophic failure and help to recover the atmosphere after such an event. [22]

2.3 Cultivation in Photobioreactors

When algae are cultured in a controlled manner, this is done in photobioreactors. This sub-chapter gives an overview of different photobioreactor designs in open and closed types of system architectures.

At this point two opposing cultivation methods for photobioreactors can also be explained. A photobioreactor is usually either run in batch or continuous operation.

Batch growth refers to starting the culture once and leaving it untouched until it no longer grows due to reaching its maximum biomass concentration. The biomass can then be harvested as a batch.

Continuous growth refers to keeping an algal culture growing continuously by harvesting biomass and adding nutrients. Biomass is usually harvested to that degree that the culture always stays at its highest productivity.

2.3.1 Open Photobioreactors

Open systems are typically used for economic large-scale production. They are not sealed from the environment, which puts them at a higher risk of pollution, contamination with other algal species or invasion of bacteria and evaporative water loss [14]. Since the growth in open systems is usually almost uncontrolled, the achievable productivity and biomass concentration is low [2].

2.3.1.1 Open Pond

This is the most common, simple and cheap system of a photobioreactor for large scale biomass production [14]. As the name already suggests, it is simply an artificial pond in which algae can grow without any control or stirring device [2].

2.3.1.2 Raceway Pond

Raceway ponds are an open pond enhanced with a stirring device – usually a paddle wheel – to prevent sedimentation and improve the aeration. They are considerably more productive and stable than open ponds at the cost of higher infrastructure, power and maintenance investments [2]. A picture of an experimental raceway pond is seen in Figure 2-2.

Figure 2-2: Open raceway pond at Texas A&M University [23]

2.3.2 Closed Photobioreactors

Closed photobioreactors provide a controlled environment to the growing algal culture. The main controlled parameters usually are the radiation intensity, temperature, carbon dioxide content and temperature, which are kept at optimum for the growing algal culture or can be altered to generate experimental data. They come at the cost of construction and maintenance investments and smaller irradiated area and culture volume than an open pond system.

2.3.2.1 Tubular

Tubular photobioreactors consist of a loop in which the culture is exposed to photosynthetically active radiation and moved through an impulsion device to prevent sedimentation, and a degasser in which the air exchange happens. Both of these devices can be optimized individually to fulfill the needs of the growing algal culture [2].

Since it does not rely on rising air to be moved, a tubular photobioreactor could be conceptualized for an orbiting spacecraft if the degasser can function in microgravity.

Figure 2-3: Tubular photobioreactor, degasser not shown [24].

2.3.2.2 Vertical

Vertical (or air column) photobioreactors are those most commonly used, when studying literature or algal experiments. They are single bodied tubes or flat panels in which every aspect of the cultivation (gas exchange, illumination, mixing) takes place [2]. Air column photobioreactors are stirred through air rising from the bottom to the top through density differences. They can either be implemented as bubble column photobioreactors, in which an air stream is induced at the bottom (also called sparging) and rises as bubbles or air lift photobioreactors, in which the air is induced into a stream of moving culture medium [25]. An image of a vertical bubble column photobioreactor is shown in Figure 2-4.

Issues with these reactors can arise at a large scale, when the pressure at the bottom becomes damagingly high to the algae [2].

Since they rely on a rising air column, and this cannot happen in microgravity, vertical photobioreactors could not be implemented in an orbiting spacecraft.

Figure 2-4: Vertical bubble column photobioreactors [26].

2.3.2.3 Membrane

Membrane based photobioreactors are characterized through a membrane that is permeable to at least carbon dioxide and oxygen but not to the algal culture and growth medium. The air exchange can either be realized through a membrane wall on a flat panel reactor or through hollow fiber membranes submerged in the algal culture. An impulsion or stirring device in these reactors is needed since there is no other means of mixing.

These photobioreactors are well suited for microgravity environments since they do not rely on aeration through rising gas bubbles. The simulations run within the scope of this thesis discuss a flat panel photobioreactor with membrane air exchange for a biological life support system in high detail in 6.1.

2.4 Current V-HAB Algae Simulation Models

Since this thesis presents the development of an algal growth model, which is then integrated into a photobioreactor, previously developed models shall be introduced and discussed in this section. In fact, three previous models of algae have been implemented in V-HAB alone, which is the simulation tool that is also used for this thesis.

One model by Steigenberger [27] implemented the unicellular green microalgae Chlamydomonas reinhardtii in a photobioreactor in V-HAB. This model aims at representing the discontinuous process of producing hydrogen. During this process the algae die and a new batch culture with a very specific procedure must be started again, when new hydrogen shall be produced. Since this model describes a very different process from what this thesis is aimed at, (discontinuous, hydrogen vs continuous, oxygen) it was not further investigated.

Another model, developed by Beck, which was implemented in the first version of V-HAB also modeled the behavior of Chlorella (without specifying a species) [28]. Its implementation approach was to use a given amount of power that is provided to the photobioreactor, which is primarily used to keep the optimum temperature and only with second priority provides photosynthetically active radiation to the algal culture. The growth modeled in this thesis is based on a stoichiometric composition, consumes carbon dioxide and nutrients and produces oxygen and biomass according to the biomass growth rate. However, the only actual influence on the growth rate that varies with time is the available photosynthetically active radiation and that is also only implemented in a way of requiring a certain amount of power in Watts to maintain growth. This might be true for a given photobioreactor depth at one certain biomass concentration but seems too general an approach for the level of detail desired for this thesis. The appearance of the results presented in the thesis allow the assumption that the behavior described as *dynamic* was in fact only time-dependent and not a reaction to changing parameters modeled in the simulation environment. This model was therefore deemed not to be useful (only available power in Watts dictates the simulation behavior in the end) and no benefit was seen in adapting it to new ideas and a newer version of V-HAB, since the creation of a new model would probably be faster.

A third model, developed by Schneider, which was also implemented in the first version of V-HAB modeled the growth behavior for the cyanobacterium Spirulina platensis in a flat panel photobioreactor [25]. Like the Chlorella model mentioned before, mainly the availability of photosynthetic active radiation is what is modeled as influencing factor. While the previous model by Beck [28] used only a given amount of power in watts, this one at least uses the commonly used photosynthetic photon flux density, but only by tying it to result from a certain power level. The modeled influence is not continuous but divided into four discrete levels depending on the available overall power. Interesting aspects of this thesis are the consumption of power of different components such as pumps and heaters, and the ability of algae to respire at low power availability. Nevertheless, it was also deemed to inflexible (four discrete photon flux density levels tied directly to power, no geometry influence, no other influences modeled) for what wanted to be done and therefore the decision was made to not use the old models and create an entirely new one.

3 Scientific Background of Chlorella Vulgaris Model

This chapter provides an overview of the scientific background of the processes and effects that are part of the dynamic Chlorella vulgaris model and the photobioreactor that the algae are growing in. These modeled processes can either be the algal growth itself, affect the growth or be a result of the growing algal culture.

The Chlorella vulgaris model is separated into four modules, which each represent a distinct part of algal growth in a growth medium. The growth rate calculation module determines how much the algae can currently grow. The photosynthesis module uses the calculated growth rate to synthesize Chlorella vulgaris cells from carbon dioxide, water and nutrients based on stoichiometric relations. The growth medium module represents all aspects that happen in the growth medium, while the algae are growing such as air exchange or pH changes. The photosynthetically active radiation module determines how radiation propagates through the culture medium and photobioreactor geometry based on the current biomass concentration. These four modules shall act as a logical division for the explanation of the modeled features in this chapter.

While this chapter exclusively deals with the scientific and mechanistic background by describing technical, physical, chemical or biological characteristics of processes happening in the growth model and photobioreactor, it does not cover the programmatic implementation of the model. However, all aspects, mechanisms and phenomena described in this chapter are implemented in the model and a description of the implementation can be found in Chapter 4.

3.1 Growth Rate Calculation Module

The *growth rate calculation module* determines how much the algal culture in the photobioreactor can increase in the current time step. Initially, an ideal growth rate is calculated, which is based on an exponential growth curve and then factors for various environmental influences are calculated, which determine how strongly the actually achievable growth rate differs from the calculated optimum.

The growth behavior of microalgae and a mathematical model for the optimum growth is presented in 3.1.1, the influence of various environmental parameters on the growth rate is described in 3.1.2 and the calculation of the actually achievable growth rate is shown in 3.1.3.

3.1.1 Optimum Growth

In a batch culture (i.e. one without harvesting or refilling of nutrient during the cultivation time), microalgal biomass increase typically follows a distinct growth curve over time as shown in Figure 3-1.

This curve starts with an initial lag phase, in which the algal culture adapts to the conditions in the medium (e.g. pH, Temperature) and photobioreactor (e.g. lighting conditions). The lag phase is followed by an exponential phase in which the growth rate is neither limited by nutrients nor by available radiation energy (i.e. all available in abundance). In the linear phase, biomass is produced at a constant rate until nutrients become limited and the growth rate starts to decline in the declining growth phase. The stationary phase is characterized through a steady biomass concentration in which no

net growth occurs, but the macromolecular composition of the cells can change. It is followed by the death phase in which the microalgal cells die [29].

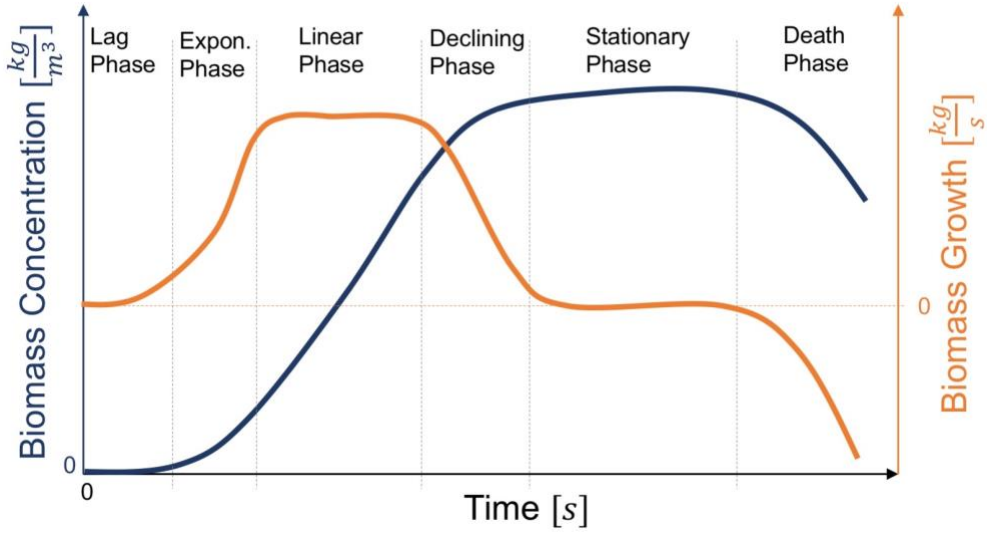

Figure 3-1: Phases of microalgal growth over time. The blue line represents the qualitative evolution of biomass concentration over time and is, along with the phase names, adapted from [29]. The orange line represents a qualitative sketch of the growth rate over time.

In order to mathematically approximate the microalgal growth curve shown in Figure 3-1, the Gompertz Model can be used [30], [31]. It is a three parameter model and commonly used in various fields of biology such as plant, animal, bacteria and cell growth [32].

The Gompertz Model does not show a linear phase but therefore expands the exponential and declining growth phases with the maximum specific growth rate at the inflection point between these two phases. It should be noted, that the time dependent growth rate described with this model is not symmetric to the inflection point [33], which lies at approximately 36.8% of the maximum biomass concentration [32]. The lag time of this model is described as the point where 6.6% of the maximum biomass concentration (the upper asymptote) are reached [32] and the model furthermore does not show a death phase.

One of the numerous parametrizations of the Gompertz Model is the Zwietering modification [34],[32]. It is represented by a relatively simple equation, that uses “parameters with a biologically meaning” [34] shown in Eq. (3-1), which was adapted from [34]. In order to calculate the time dependent biomass concentration, it requires the input of a lag time, maximum specific growth rate at the inflection point between the exponential and declining growth phase and the maximum biomass concentration in the stationary phase.

$$\rho_b(t) = \rho_{b_{max}} * \exp(-\exp\left(\frac{\mu_{max} * \exp(1)}{\rho_{b_{max}}} * (t_{lag} - t) + 1\right)) \qquad \textbf{Eq. (3-1)}$$

In the above equation, $\rho_b(t)$ is the biomass concentration in $[\mathrm{kg/m^3}]$ as a function of time, $\rho_{b_{max}}$ the upper asymptote or, in other words, the maximum achievable biomass concentration $[kg/m^3]$, μ_{max} is the maximum specific biomass concentration increase

in $[kg/(m^3 * s)]$ in the inflection point, t_{lag} the lag time in $[s]$, and t the evaluated time in $[s]$.

3.1.1.1 Time Dependent Cell Density Increase Rate

The biomass concentration increases as a function of time as shown in Eq. (3-2) can be achieved by deriving Eq. (3-1) with respect to time.

$$\mu(t) = \frac{d\rho_b(t)}{dt} = \mu_{max} * \exp(-\exp\left(\frac{\mu_{max} * \exp(1)}{\rho_{b_{max}}} * (t_{lag} - t) + 1\right) + \frac{\mu_{max} * \exp(1)}{\rho_{b_{max}}} * (t_{lag} - t) + 2) \qquad \textbf{Eq. (3-2)}$$

In the above equation, $\mu(t)$ is the time dependent biomass concentration increase rate in $[kg/(m^3 * s)]$.

Experiments were conducted in order to determine the values that define the growth model. The results are shown in 5.2.4.

An exemplary graph of the evolution of biomass concentration and biomass concentration increase rate over time as described by the Gompertz Model is shown in Figure 3-2.

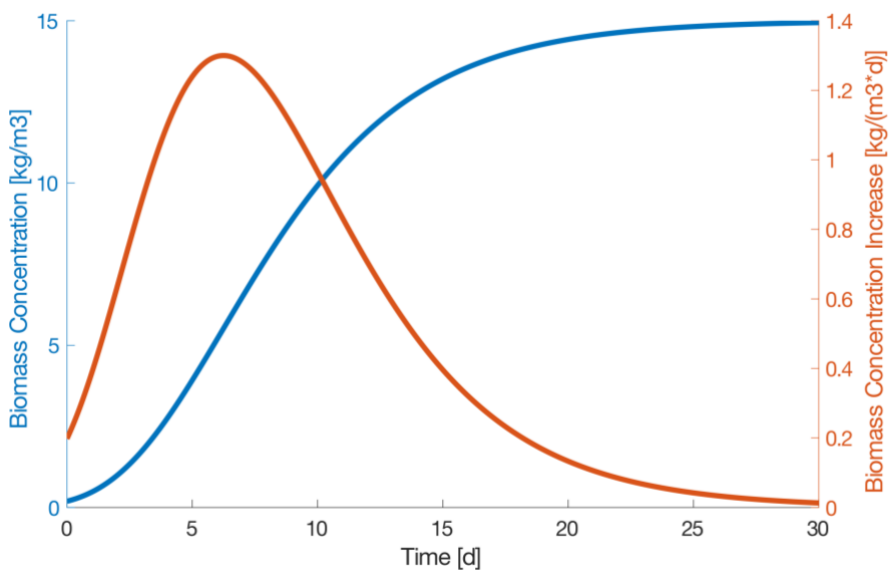

Figure 3-2: Evolution of biomass concentration and biomass concentration increase rate over time as described by the Gompertz Model. Graphs calculated with Eq. (3-1) and Eq. (3-2) for a time span of $t = 30\ d$ with $t_{lag} = 2\ d$, $\rho_{b_{max}} = 15\ \frac{kg}{m^3}$ and $\mu_{max} = 1.3\ \frac{kg}{m^3 * d}$.

3.1.1.2 Biomass Concentration Dependent Calculation

A photobioreactor in a life support system will not be operated in batch mode. It will rather be operated continuously to enable a constant stream of carbon dioxide into and oxygen out of the photobioreactor. In order to enable the continuous operation, biomass must be continuously harvested, and nutrients resupplied into the medium at the same time. As soon as the process of harvesting begins, the time is still increasing,

but the biomass concentration remains constant or even decreases. As long as sufficient nutrients are available and the biomass concentration neither increases nor decreases during the harvesting process, the growth rate stays at a constant level. Therefore, the time dependent calculation of biomass concentration and growth rate cannot be used for a continuously operating photobioreactor.

Furthermore, non-ideal but survivable growth conditions can lead to a momentarily decreased (possibly to zero) growth rate. Since time progresses independently, a wrong growth rate would be observed, when ideal conditions are reestablished (i.e. the one that would be present at the current time). The effect is similar to a photobioreactor with an operating harvester: the actual biomass concentration differs from what it would be in a time-controlled ideal growth behavior. The time-dependent growth rate can therefore no longer represent the growth rate that would actually be achievable after a disturbance is induced. The challenges harvesting, and non-ideal conditions pose to the use of a time-dependent growth rate are graphically explained in Figure 3-3.

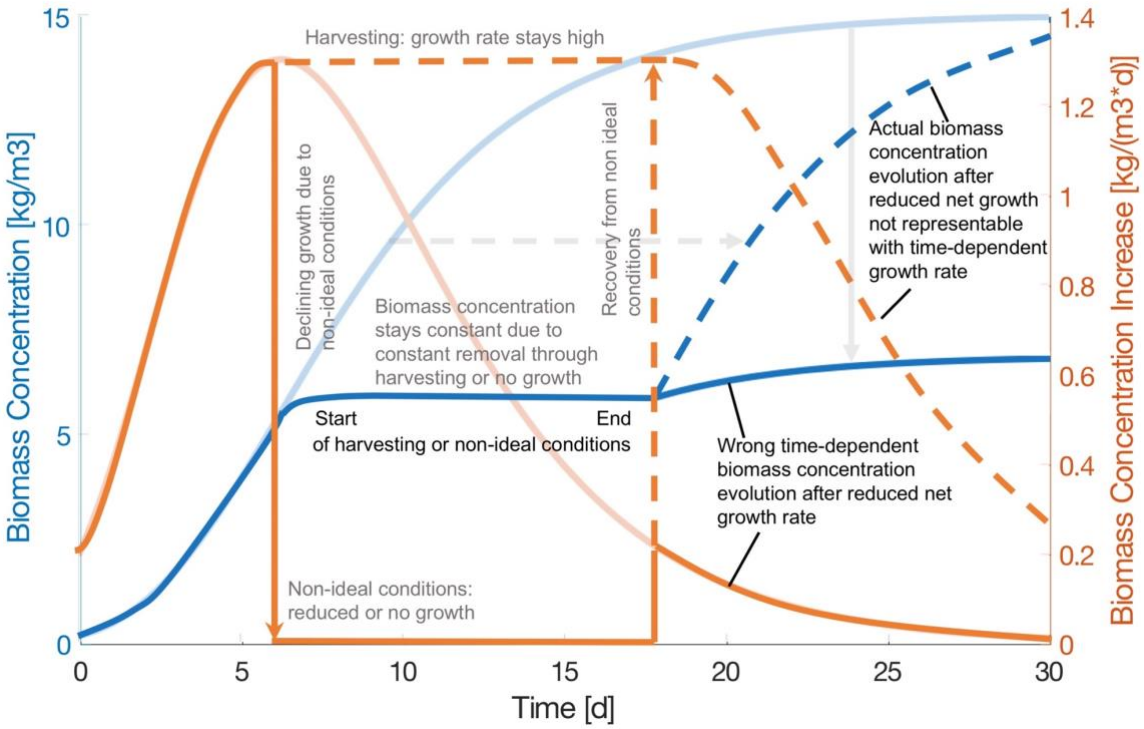

Figure 3-3: Challenges to a purely time-dependent growth calculation model after disturbances such as harvesting or non-ideal conditions are induced between the 6th and 17th day. The transparent blue and orange lines in the background show the ideal time-dependent behavior. The bold blue and orange lines show the time-dependent behavior with an induced disturbance. The dashed blue and orange lines show the behavior of biomass concentration and growth rate that would be observed in reality but are not representable with a time-dependent growth model. The transparent grey arrows indicate the similarities between the ideal behavior and the actual (dashed) and wrongly represented behavior (bold).

In order to predict the current optimum growth rate in a continuously operating photobioreactor, which can also be affected by non-ideal growth conditions, the cell density increase rate must be determined as a function of the current biomass concentration instead of being time dependent.

The required equation can be obtained by rearranging the previously presented equations Eq. (3-1) and Eq. (3-2). First, the biomass concentration equation Eq. (3-1) must be rearranged in a way, so it shows the time at which a certain biomass concentration is reached. This rearranged form of Eq. (3-1) is Eq. (3-3).

$$t(\rho_b) = t_{lag} - \frac{\rho_{b_{max}} * (\ln(-\ln\left(\frac{\rho_b}{\rho_{b_{max}}}\right)) - 1)}{\mu_{max} * \exp(1)} \qquad \textbf{Eq. (3-3)}$$

Since the required equation to calculate the biomass concentration increase should be independent of time, the time variable t in in Eq. (3-2) must be substituted for the expression in Eq. (3-3). The time independent equation for the biomass concentration increase can then be simplified to Eq. (3-4).

$$\mu(\rho_b) = \mu_{max} * \exp(-\exp\left(\left(\ln\left(-\ln\left(\frac{\rho_b}{\rho_{b_{max}}}\right)\right) - 1\right) + 1\right) + (\ln(-\ln\left(\frac{\rho_b}{\rho_{b_{max}}}\right)) - 1) + 2) \qquad \textbf{Eq. (3-4)}$$

The behavior of the time independent biomass concentration increase rate $\mu(\rho_b)$ as a function of biomass concentration is shown in Figure 3-4 and can be compared to the graph shown in Figure 3-2, since the same values were used where necessary.

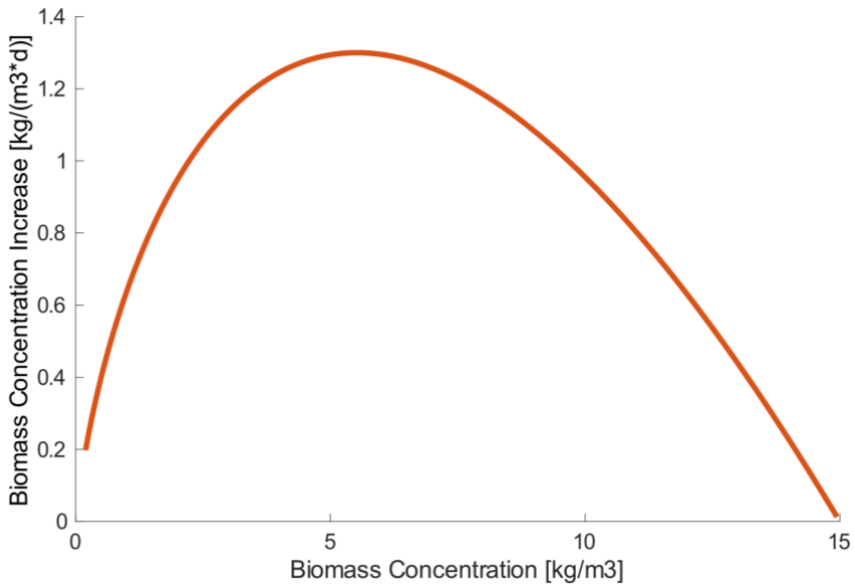

Figure 3-4: Biomass concentration increase as a function of current biomass concentration. The graph was created using Eq. (3-4) with $\rho_{b_{max}} = 15\ \frac{kg}{m^3}$ and $\mu_{max} = 1.3\ \frac{kg}{m^3 * d}$.

The challenges previously depicted in Figure 3-3 can be overcome with this method of growth rate calculation. When biomass is harvested, the growth rate adapts accordingly to the changed biomass concentration. At the end of the harvesting or non-ideal conditions, the growth rate can be determined based on the current biomass concentration and not on the time which would then lead to the evolution shown as a dashed line instead of the wrong and time-dependent solid line in Figure 3-3.

By integrating Eq. (3-4) with respect to time (or from a programmatic standpoint: adding resulting growth rates over time), considering that ρ_b can be time dependent

when biomass is being harvested, and using a starting biomass concentration $\rho_{b_{start}}$, the biomass concentration at any time can be calculated. When the starting biomass concentration is used that is calculated when the time dependent Gompertz Model Eq. (3-1) is evaluated at $t = 0$, and no biomass is harvested, the evolution of biomass concentration shows the same behavior as in Figure 3-2, in which the time dependent growth rate equation Eq. (3-1) is used.

3.1.2 Limiting Factors on Optimum Growth

The parameters that affect the Gompertz Model should be selected in a way that represent ideal conditions. If the conditions of the photobioreactor or medium deviate from these ideal conditions, the cell density increase rate is decreased.

This sub-chapter presents different limiting factors, establishes their optimum range and discusses how they affect the optimum cell density increase rate, which for simplicity, is also referred to as growth rate.

3.1.2.1 Temperature Limitation

The temperature of the growth medium can strongly affect the growth of microalgae, when it deviates from its optimum. Typically, there are lower and upper temperature extremes beyond which the culture is lethally damaged. In between these extreme boundaries, the algal culture can grow at varying levels depending on how strongly the temperature differs from the narrow optimum temperature band, in which the maximum growth can be achieved as shown in Figure 3-5.

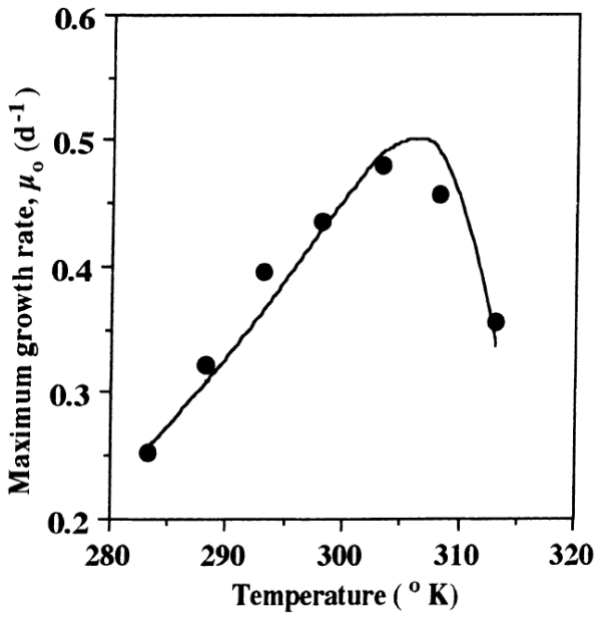

Figure 3-5: Growth Rate as a function of medium temperature. Steady climb from the lowest temperature to the optimum (around 303 K) and then a steep decline to the maximum survivable temperature. Copied from [35].

Since this temperature values differ between microalgal species and therefore no universal statement for all microalgae can be made [35], the values stated here are specifically for Chlorella vulgaris. A compilation of literature values is shown in Table 3-1.

Table 3-1: Compilation of literature values for lower and upper extreme temperature boundaries $T_{min/max_{life}}$ and the boundaries of the optimum temperature band $T_{min/max_{opt}}$ for Chlorella vulgaris. Comments about the source are added for further information in some cases.

Source	$T_{min_{life}}$ $[K]$	$T_{min_{opt}}$ $[K]$	$T_{max_{opt}}$ $[K]$	$T_{max_{life}}$ $[K]$	Comment
[15]	-	301	305	311	Review paper, values from different sources.
[36]	-	293	303	> 303	States that conditions above 303 K are critical
[37]	-	297	299	-	Not stated that best, but used for experiment
[38]	-	303	303	-	States multiple sources
[9]		297	303		
[35]	< 283	303	308	> 313	State that 305.4 K is optimum. No statement about minimum, but lowest reported growth rate is ta 283 K
[39]	<278	-	-	-	Fig. 1 shows growth (albeit low) still possible at 5°C. “Cut-off temperature very close to 0°C” [39]. Storage at 4°C possible for longer durations (22 weeks tested in this article)

The data in Table 3-1 shows, that the optimum temperature for Chlorella vulgaris is around 300 K and the maximum survivable temperature around 310 K. Since the optimum operating temperature is rather close to the maximum tolerable temperature, a reliable temperature control is vital, especially when considering that the required radiation energy can present a significant heat flux into the medium.

On the other hand, temperatures close to 273 K seem tolerable without long-term damage and even a long term storage at 253 K for 22 weeks still yielded a photosynthetic activity of 50 % compared to pre-exposure activity in Chlorella vulgaris in one article [39].

In order to account for temperatures as low as 278 K [39], where Chlorella vulgaris can still grow (albeit at a low rate) and a minimum survivable temperature of (at least) 274 K [39], the behavior shown in Figure 3-5 [35], is amended. The assumption is made, that the relative population growth rate in the graph in [1/day] can be translated to a

relative cell density increase rate [μ/μ_{opt}] which is 1 at the temperature optimum, and 0 at the lower and upper survivable temperatures. Furthermore, while a steady increase of relative growth is assumed between the lower survivable temperature and the optimum, a steep drop-off to 0 is assumed when the highest survivable temperature documented in the graph in Figure 3-5 is passed. The resulting behavior of the relative growth rate with regard to varying medium temperature is shown in Figure 3-6.

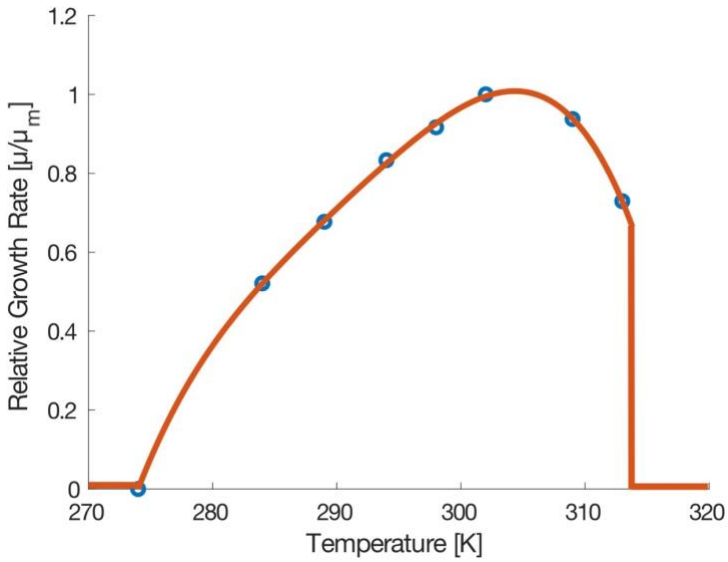

Figure 3-6: Relative growth rate of Chlorella vulgaris with respect to medium temperature. Data points are blue circles and the orange line represents the growth/rate temperature behavior which is a 4th order polynomial on the interval between the lower and upper survivable temperatures [274 K, 314 K], and 0 outside of the survivable temperature range. Derived from values in [35] and [39].

The function representing this graph on the interval between the lower and upper survivable temperatures [274 K, 314 K] is a 4th order polynomial and can be obtained by entering the data points and applying a curve fitting algorithm. Outside the minimum and maximum survivable temperatures, the relative growth rate is zero, since this model does not regard negative growth (however, theoretically it is possible due to respiration). The equation is shown in Eq. (3-5).

$$\mu_{rel_T}(T) = \begin{cases} 0 & \mid T < 274 \\ 2.1 * 10^{-6} * T^4 + 0.0024 * T^3 - 1.07 * T^2 \ldots \\ \quad \ldots + 206.8 * T - 1.5 * 10^{-4} & \mid T \in [274, 314] \\ 0 & \mid T > 314 \end{cases} \qquad \textbf{Eq. (3-5)}$$

In the above equation $\mu_{rel_T}(T)$ is the unitless relative growth rate as a result of temperature limitation and T is the current medium temperature in $[K]$.

3.1.2.2 pH Limitation

Besides the temperature, the pH of the medium is one of the important parameters that affect algal growth [35]. The pH is defined as the negative decadic logarithm of hydrogen ion activity in the solution [40]. However, throughout this thesis, the assumption of an ideal solution is used, which allows to disregard activities and replace

them with concentrations [41]. The pH can then be defined as the negative logarithm of hydrogen ion concentration (instead of activity) as shown in Eq. (3-6). For more information on activities and the assumption that allows to use concentrations instead, see 3.3.5.1.

$$pH = -\log_{10}\left(\frac{[H^+]}{c^0}\right) \qquad \textbf{Eq. (3-6)}$$

In the above equation, pH is the unitless pH value, which typically ranges between 0 and 14 and $[H^+]$ is the concentration of hydrogen ions in $[mol/L]$ and c^0 the standard concentration of $1\,mol/L$ to normalise the units inside the logarithm.

The medium pH can be altered through components manually added to the medium (e.g. acidic and basic salt compounds), components taken up through atmospheric exchange (eg. carbon dioxide) and by the algal metabolism (e.g. release of hydroxide ions in the nitrate metabolism). More information on how different components affect the pH and how it is calculated, see 3.3.5.3.

Similar to how the growth of Chlorella vulgaris is affected by temperature, there are extreme lower and upper pH boundaries, beyond which no growth is possible Furthermore, there are lower and upper boundaries of optimum growth between which the growth is not affected [35]. Inbetween the extreme boundaries and the bounadries of optimum growth, the growth linearly climbs or falls. Inbetween the pH boundaries for optimum growth, the growth rate is not affected by the pH. However, these boundaries are not static but depend on the current medium temperature as shown in Figure 3-7.

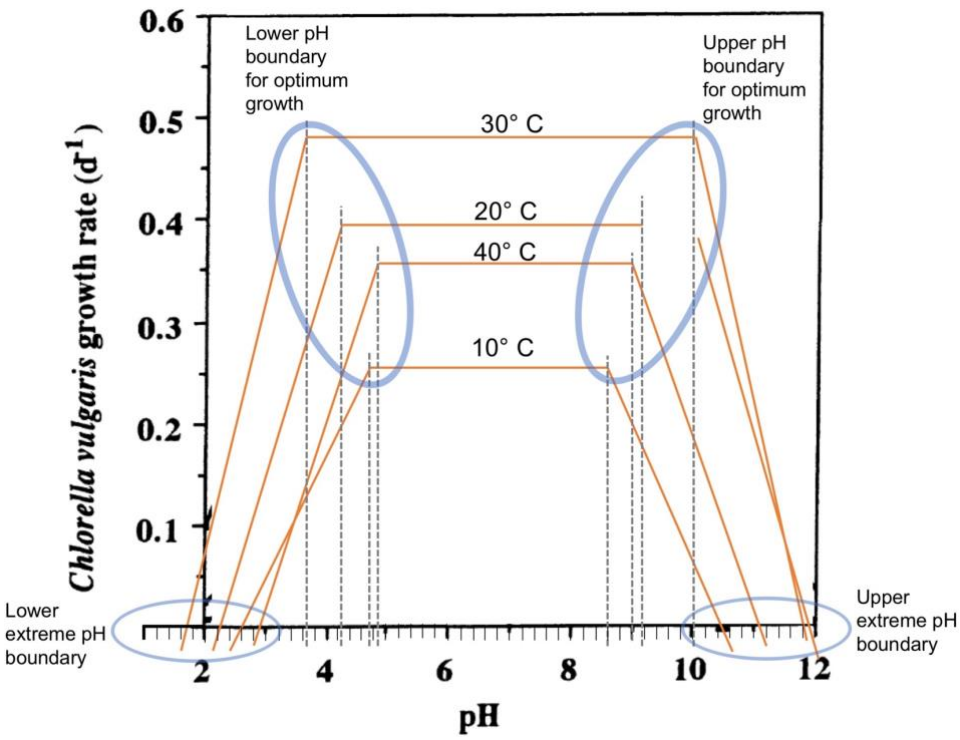

Figure 3-7: Effect of pH on growth affected by the current temperature level. The orange lines represent the growth rate as a function of varying pH on four different temperature levels. The graph is taken from [35], exchanged lines for better visibility, added grey visual guides for better readability and onward data point extraction, added description and visual markers for the four boundary categories.

Since the effect of the temperature on the growth rate is already covered in the previous sub-chapter 3.1.2.1, Figure 3-7 is used to derive a relationship between the four pH boundaries and temperature. The absolute level of growth rate is reflected in the temperature effect previously outlined and therefore not regarded here.

When the pH values for the four different boundaries are extracted from the above guide are extracted and plotted over the temperature they correspond to, they can interpolated with a curve fitting algorithm to yield four separate third order polynomials representing the upper and lower extreme and optimum growth pH boundaries as a function of medium temperature. The graphs of these functions are shown in Figure 3-8 - Figure 3-11.

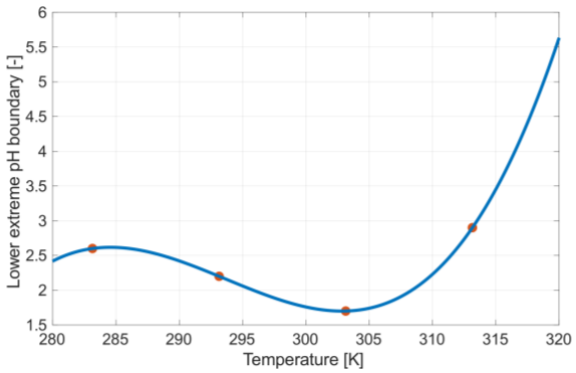

Figure 3-8: Lower extreme pH boundary as a function of medium temperature. Derived from data (orange dots) in [35].

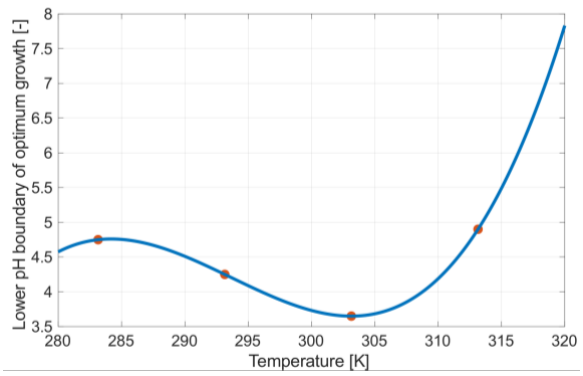

Figure 3-9: Lower pH boundary of optimum growth as a function of medium temperature. Derived from data (orange dots) in [35].

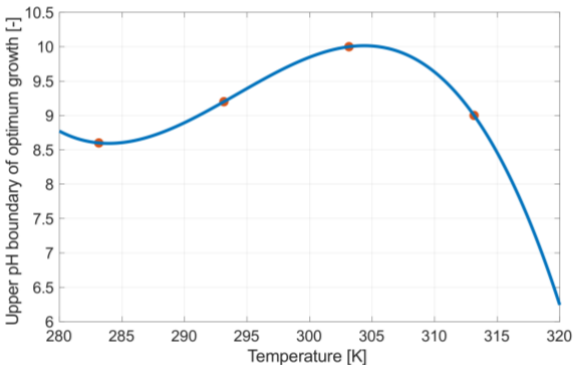

Figure 3-10: Upper pH boundary of optimum growth as a function of medium temperature. Derived from data (orange dots) in [35].

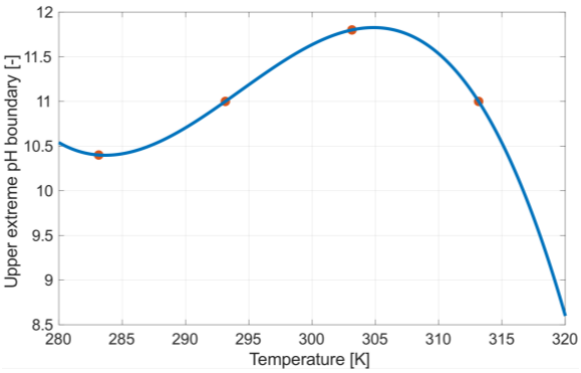

Figure 3-11: Upper extreme pH boundary as a function of medium temperature. Derived from data (orange dots) in [35].

The corresponding third order polynomials, which relate the pH boundaries to the medium temperature, are shown in Eq. (3-7) - Eq. (3-10).

$$pH_{extr_{low}}(T) = 0.00030 * T^3 - 0.264 * T^2 + 77.56 * T - 7577 \qquad \textbf{Eq. (3-7)}$$

$$pH_{opt_{low}}(T) = 0.00033 * T^3 - 0.286 * T^2 + 83.99 * T - 8201 \qquad \textbf{Eq. (3-8)}$$

$$pH_{opt_{up}}(T) = -0.00033 * T^3 + 0.294 * T^2 - 86.42 * T + 8462 \qquad \textbf{Eq. (3-9)}$$

$$pH_{extr_{up}}(T) = -0.00030 * T^3 + 0.265 * T^2 - 77.83 * T + 7625 \qquad \textbf{Eq. (3-10)}$$

In the above equations, $pH_{extr_{low}}(T)$ corresponds to the temperature-dependent lower extreme pH boundary below which no growth is possible. $pH_{opt_{low}}(T)$ corresponds to the temperature-dependent lower pH boundary of optimum growth above which the growth rate is not affected by pH. $pH_{opt_{up}}(T)$ corresponds to the temperature-dependent upper pH boundary of optimum growth below which the growth rate is not affected by pH. $pH_{extr_{up}}(T)$ corresponds to the temperature-dependent upper extreme pH boundary above which no growth is possible and T to the temperature in $[K]$.

Once the temperature dependent pH boundaries are established, the relative growth rate $\mu_{rel_{pH}}$ can be determined as shown in Figure 3-12.

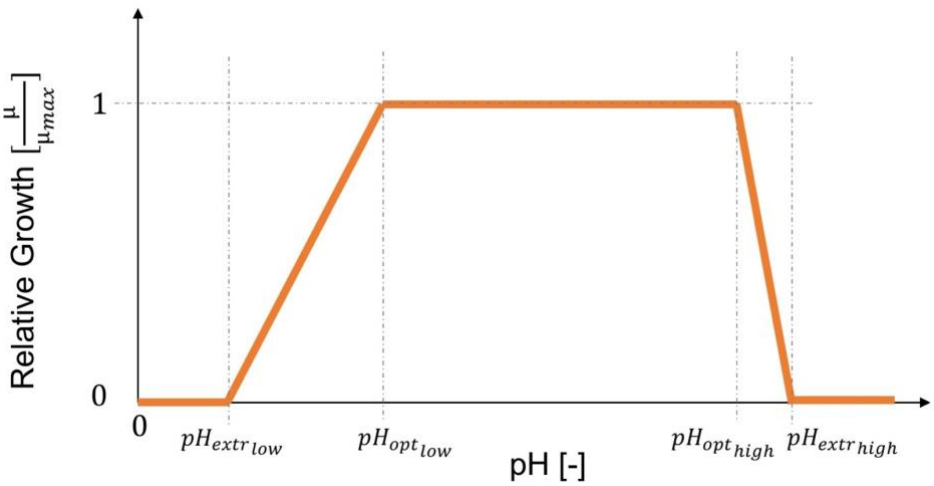

Figure 3-12: Relative growth as a function of temperature-dependent pH boundaries.

Figure 3-12 shows that the relative growth rate is 0, when the pH lies below the extreme lower pH value as calculated with the previously stated formulas. Between the lower extreme boundary and the lower boundary for optimum growth, the relative growth rises linearly with increasing pH. For any pH value between the lower and upper pH boundary for optimum growth, the growth rate is not affected by changes in pH. For a medium pH above the upper boundary for optimum growth, the relative growth rate decreases linearly with rising pH until it reaches 0 for pH values larger than the upper extreme pH boundary.

Since the current pH of the medium is an important aspect when calculating the growth of microalgae, a dedicated part of the *Medium Module* in the simulation calculates the current pH based on the medium constitution. More information on this module and the pH calculation, which then feeds back to determining the relative growth with respect to pH, can be found in 3.3.5.

3.1.2.3 Photosynthetically Active Radiation Limitation

When regarding radiation energy for photosynthesis and how it can potentially limit algal growth, two aspects must be considered: the correct waveband and the right amount of photon flux density. The photosynthetically active radiation, the radiation

that plants can use as energy source for photosynthesis, lies within the same wave spectrum of 400-700 nm as the radiation that the human eye can sense as light [7].

The right dose of photosynthetically active radiation is required to enable growth at the algal culture's full potential. In dense algal cultures, radiation energy can quickly become the limiting resource due to attenuation. The availability of radiation energy is not homogenous throughout the culture and the limiting effect on growth can therefore be a local one (as opposed to temperature or pH limitation, which are assumed to be homogenous throughout the medium). This makes the determination of growth limitation through photosynthetically active radiation more complex and a dedicated module in the simulation accounts for the underlying physical effects. It is described in detail in 3.4, where the growth limitation the available radiation energy can have on the algal culture is discussed in more detail.

In general, a relationship between the available photosynthetically active radiation, measured in photosynthetic photon flux density $[\mu mol/(m^2 * s)]$, and the relative growth can be formulated which is divided into four domains as shown in Figure 3-13.

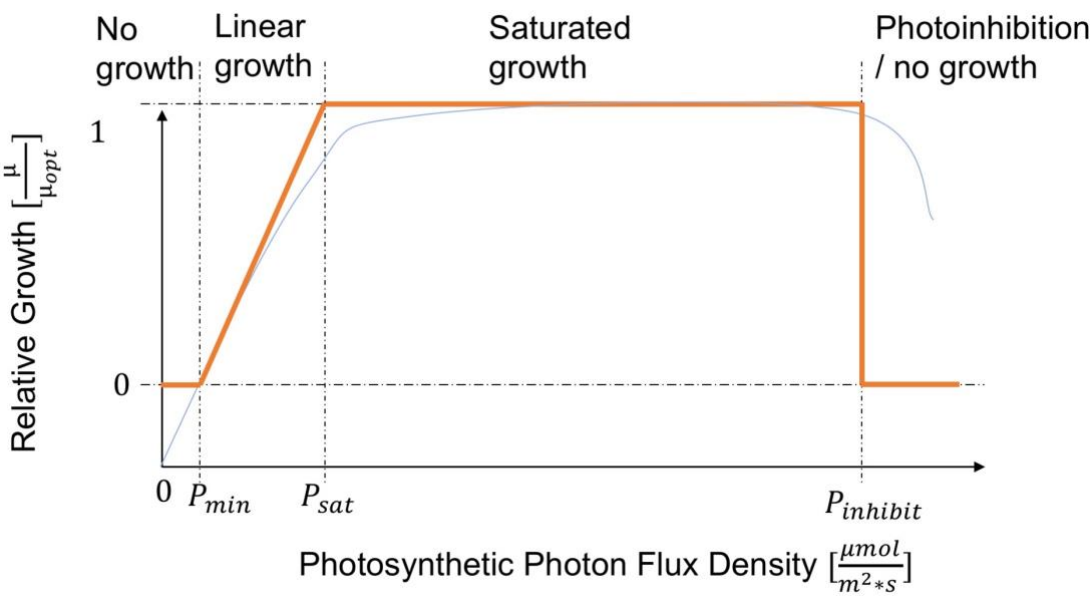

Figure 3-13: Radiation saturation curve of photosynthesis with four growth domains: respiration, linear growth, photo-saturated growth and photoinhibition / no growth. The blue line represents the realistic evolution of relative growth (approximated from [42]) and the orange line a simplified one, which is used for the model.

More details on the background on why the four different domains exist can be found in 3.4.2 and only an overview shall be provided here.

Below the minimum photon flux density not enough radiation energy is available for photosynthesis. The algal culture only respires, and oxygen and biomass are being consumed, which leads to a negative growth but is regarded to be zero for the purposes of this thesis. Once a minimum photon flux density is reached, the relative growth rate increases linearly until the saturation photon flux density is reached. Beyond this point, a further increase in photon flux density does not increase the growth rate because all cells are provided with sufficient radiation power but the speed of cell-internal processes is limiting photosynthetic reproduction [42]. However, the radiation can penetrate deeper into the algal culture and provide deeper lying cells with

sufficient energy for photosynthesis. At a certain point, when the photon flux density is further increased, the growth becomes photoinhibited due to cell-internal mechanisms which are sensitive to high photon flux [43], [2]. During photoinhibition the growth quickly decreases but is assumed to instantly drop to zero in the model, and a further increase of photon flux can be lethal to the algal culture.

The domains of the radiation-saturation curve are defined by their photon flux boundary points:

- P_{min} below which negative growth occurs due to photorespiration
- P_{sat} which defines the end of the linear light/radiation-limited growth behavior and above which saturated growth behavior exists
- $P_{inhibit}$ which defines the end of the saturated growth behavior domain and above which rapidly declining growth occurs due to photoinhibition.

The literature offers very different values on the radiation properties which, along with some comments, are compiled in Table 3-2.

Table 3-2: Irradiation values from different literature sources

Source	P_{min} $[\frac{\mu mol}{m^2 * s}]$	P_{sat} $[\frac{\mu mol}{m^2 * s}]$	$P_{inhibit}$ $[\frac{\mu mol}{m^2 * s}]$	Comments
[43]	1 - 3	200 - 300	300 - 500	For green algae, different species listed but not Chlorella vulgaris
[44]	n/a	≤ 197	≥ 848	Compared different irradiances but didn't determine boundaries. Growth at 848 $\frac{\mu mol}{m^2 * s}$ the same as 197 $\frac{\mu mol}{m^2 * s}$ which is an indicator for saturation.
[42]	~ 50	~ 400	~ 2000	Values extracted from a graph.
[45]	> 400	> 1600	<2400	Values seem extremely high. Experimentally determined but possibly stated light intensity, not surface irradiance.
[9]	n/a	150	369	State that Chlorella vulgaris performs well between 150-350 $\frac{\mu mol}{m^2 * s}$
[46]	5 – 10	250	n/a	

While one source states an inhibition value as low as 150 $\mu mol/m^2 * s$, another one indicates that it is higher than 1600 $\mu mol/(m^2 * s)$ which is a difference by a factor of more than 10. The situation is similar for the inhibition photon flux density which varies from 300 $\mu mol/(m^2 * s)$ to 2400 $\mu mol/(m^2 * s)$.

When looking at the irradiances that were actually used in experiments documented in papers and journal articles, they are a lot closer together. It is advisable to select a surface irradiance that is above the saturation and close to the inhibition photon flux density. This ensures that deeper lying layers of algal cells also receive a sufficient number of photon flux to be growing in the saturated growth domain and, at the same

time, prevents the higher layers from being photoinhibited. The values are compiled in Table 3-3 along with some comments.

Table 3-3: Surface irradiances used in documented experiments

Source	$P_0\ [\frac{\mu mol}{m^2 * s}]$	Comments
[47]	200 ± 50	
[48]	150	
[3]	300	Was supposed to be maintained at around 300 $\mu mol/(m^2 * s)$ but was actually 350 $\mu mol/(m^2 * s)$.
[49]	~ 90	Was ramped up with increasing biomass but not higher than 90 $\mu mol/(m^2 * s)$.
[50]	300	White light used. Value selected with reference to [9]
[51]	600	Chlorella sp., not specifically vulgaris. Fluorescent lamps used with 320 $\mu mol/(m^2 * s)$ each.

From the data in Table 3-2 and Table 3-3 the conclusion can be drawn, that there is no one correct set of values that can be universally agreed on. Since there is such a large variation in reported values, experiments were conducted in order to evaluate the radiation values that define the radiation-saturation curve. The results are shown in 5.3.4. The experimentally determined values are $P_{sat} = 100\ \mu mol/(m^2 * s)$and $P_{inhibit} = 400\ \mu mol/(m^2 * s)$. While the minimum photon flux density could not be determined in the experiments conducted for this thesis, it can be assumed to be $P_{min} = 10\ \mu mol/(m^2 * s)$ from the data stated in the tables above.

Once the photon flux density values that define the radiation saturation curve are selected, the relative growth can be determined as shown in Figure 3-13. A mathematical equation with the assumption of zero growth for lower than the minimum photon flux density and higher than the inhibition flux density, is given in Eq. (3-11).

$$\mu_{rel_P}(P) = \begin{cases} 0 & | \ P < P_{min} \\ \dfrac{P_{sat} - P}{P_{sat} - P_{min}} & | \ P_{min} < P < P_{sat} \\ 1 & | \ P_{sat} < P < P_{inhibit} \\ 0 & | \ P > P_{inhibit} \end{cases} \qquad \textbf{Eq. (3-11)}$$

In the above equation, $\mu_{rel_P}(P)$ refers to the unitless relative growth rate with regard to the current (two-dimensional consideration) or the current local (three-dimensional consideration) photon flux density P in $[\mu mol/(m^2 * s)]$. P_{min} is the minimum photosynthetic photon flux density in $[\mu mol/(m^2 * s)]$ required for photosynthesis, P_{sat} the saturation photosynthetic photon flux density in $[\mu mol/(m^2 * s)]$ and $P_{inhibit}$ the photosynthetic photon flux density in $[\mu mol/(m^2 * s)]$ beyond which no growth occurs due to photoinhibition.

Since the calculation of growth domains and therefore the relative growth factor with respect to photosynthetically active radiation is a complex three-dimensional task, a dedicated module in the simulation is responsible for this. The purpose of the *Photosynthetically Active Radiation Module* in the simulation is to determine the photon

flux in every part of the three-dimensional photobioreactor and then derive the volumes of each growth domain. Based on these volumes, an overall relative growth factor can be determined.

For each of these four volumes, the relative growth rate is calculated. For the no-growth volume (irradiated below minimum photon flux density and above inhibition photon flux density), the relative growth rate is 0. For the saturated growth domain volume, the relative growth rate is 1. In the linear growth domain, the growth rate is linearly dependent on the available radiation power, not on the spatial position within that domain, which shows an exponential decrease of growth rate due to exponential attenuation. The relative growth rate is determined by relating a dynamically calculated average photon flux density in that zone and relating that to the saturation photon flux density at which the relative growth rate would be 1.

The overall relative growth rate due to photosynthetically active radiation limitation is comprised of the three relative growth rates from the growth domains (no, linear and saturated growth). Each of the volume's growth factors is weighted with the relation of how much the volume takes up of the total culture volume. The overall growth factor is calculated by with Eq. (3-12).

$$\mu_{rel_P} = 1 * \frac{V_{sat}}{V_{tot}} + \frac{P_{av_{lin}}}{P_{sat}} * \frac{V_{lin}}{V_{tot}} \qquad \textbf{Eq. (3-12)}$$

The overall relative growth rate with regard to photosynthetically active radiation in the photobioreactor's entire volume V_{tot} in $[m^3]$ is the unitless μ_{rel_P}. V_{sat} in $[m^3]$ is the volume of the photobioreactor irradiated in the saturated growth domain, $P_{av_{lin}}$ is the current average photon flux density in the linear growth domain volume V_{lin} in $[m^3]$, and P_{sat} in $[\mu mol/(m^2 * s)]$ the saturation photon flux density in $[\mu mol/(m^2 * s)]$

More information on the calculation module can be found in 3.4 and details on the model implementation in 4.6.

3.1.2.4 Nutrient Limitation

The availability of nutrients, especially carbon dioxide, nitrogen (in form of nitrate or urea) and phosphorus, can be a limiting factor on algal growth. However, the limitation is not represented through a limiting factor or relative growth as is the case for pH, radiation energy or temperature. Instead the *Photosynthesis Module*, which is described in 3.2, reacts to a lack in nutrient availability by preventing growth, since it is not able to synthesize Chlorella vulgaris macromolecules. In contrast to the relative growth factors that are determined for pH, radiation energy or temperature and then affect the growth rate, the nutrient limitation is not dictated by a calculated relative growth factor. If nutrients are not sufficiently available, the optimum growth rate is decreased and then a resulting relative growth factor can be calculated by comparing how much the algal culture was able to grow compared to what would have been possible with abundant nutrients. In other words, if the growth rate is decreased due to nutrient limitation, this is not the consequence of a calculated relative growth factor but rather a relative growth factor is calculated as a consequence of a reduced growth rate.

Carbon dioxide enters the growth medium through atmospheric exchange based on Henry's Law and membrane transport mechanisms as outlined in 3.3.2. Furthermore, it can speciate to bicarbonate and carbonate with increasing pH and therefore not

always be abundantly available – especially when the atmospheric exchange can only happen at a slow rate. Therefore, carbon dioxide limitation can most likely occur when the growth rate of the algal culture is high, and the membrane transport cannot support the rapid carbon dioxide uptake into the algal culture. A high growth medium pH will increase the lack of carbon dioxide even further since a fraction of the carbon entering the medium speciates to bicarbonate and carbonate and therefore is not available as a nutrient to the algal culture. This is problematic, since the Rubisco enzyme in the photosynthetic process of carbon dioxide fixation can only use carbon dioxide as a substrate [52]. For more information on the speciation of carbon dioxide, see 3.3.3.

Another nutrient that is required for the algal metabolism is nitrogen. It can be supplied as nitrate or from urine in the shape of urea, which is a viable form of nitrogen supply for Chlorella vulgaris [53]. In order to not become limiting on growth, its content in the medium has to be monitored and frequently added to the medium. More information on the nitrogen metabolism in Chlorella vulgaris is given in 3.2.2.

Furthermore, phosphorus is required as a nutrient to Chlorella vulgaris growth but disregarded here, since it only occurs in small quantities and is also not modeled in the V-HAB human model's urine composition. In theory, the lack of phosphorus can therefore also limit the growth of Chlorella vulgaris, but for the purposes of this thesis, this is not the case.

3.1.2.5 Oxygen Concentration Limitation

Oxygen is the main product of photosynthesis besides biomass. However, if it is not transported out of the medium, its concentration rises and a high oxygen concentration can become limiting on algal growth [54], [55]. The limiting effect arises from the competition with carbon dioxide for the RuBisCO enzyme, which is required for the process of photosynthetic biomass synthesis through carbon dioxide fixation [56].

Although the concept of partial pressures does not apply to liquids, the tolerable and inhibitory limits of dissolved oxygen on algal growth are often stated as partial pressures or in fractions of atmospheres. What is meant in this context is the equivalent concentration the substance would have in equilibrium with the atmosphere according to Henry's law at the stated partial pressure. The stated partial pressure can therefore also be regarded as an equivalent partial pressure. For more information on Henry's law see 3.3.2.1. The concept of equivalent (or imaginary) partial pressure is explained in more detail in 3.3.2.2.

Since the effects of oxygen limitation on algal growth vary with literature sources, two concepts are presented here.

Experimental data from [54] is plotted in Figure 3-14 and shows, that the relative growth rate due to oxygen concentration in water can be 0.7 at oxygen concentrations equivalent to 65 kPa oxygen partial pressure in the medium. It should be noted though, that the data showed a varying result for 65 kPa oxygen, where the relative growth was 0.83 in one run and 0.7 in another. Even stronger reductions in relative growth could be observed under conditions where the carbon dioxide concentration was lowered to 0.4 kPa.

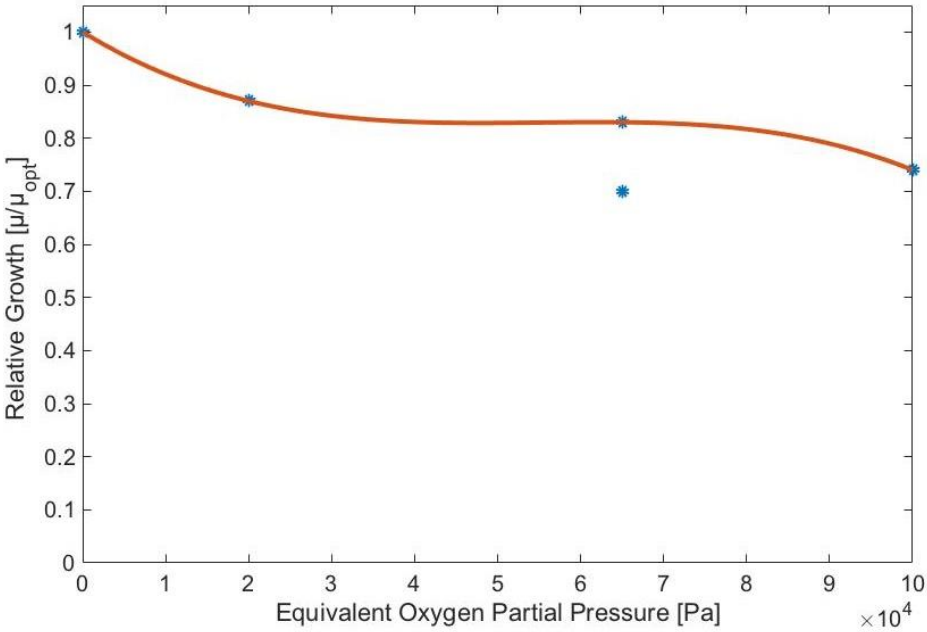

Figure 3-14: Oxygen equivalent partial pressure influence (i.e. concentration) on relative growth rate. Blue dots represent experimental data from [54] and the orange line a function that was generated with a curve fitting tool. Second data point at 65000 Pa was disregarded for the curve fitting. The carbon dioxide partial pressure for these data points was 1 kPa.

The experimental results from [54], which are shown in Figure 3-14, suggest that the growth is already reduced by 13 % at the typical oxygen partial pressure of 20 kPa. However, most experiments that determine the growth rate of Chlorella vulgaris happen under oxygen partial pressures of 20 kPa, since that is roughly the oxygen partial pressure at sea level. One could argue that the reported reduction in relative growth at 20 kPa should be normalized to be the norm and oxygen partial pressures closer to 0 could represent a means of improvement yielding a higher growth than was determined as optimum in other experiments.

Mathematically, the model can be described by Eq. (3-13).

$$\mu_{rel_{O_2}}\left(p_{eq}(O_2)\right) = -1.074 * 10^{-15} * p_{eq}(O_2)^3 + 1.776 * 10^{-10} * p_{eq}(O_2)^2 - 9.622 * 10^{-06} * p_{eq}(O_2) + 1 \quad \textbf{Eq. (3-13)}$$

In the above equation, $\mu_{rel_{O_2}}\left(p_{eq}(O_2)\right)$ refers to the unitless relative growth rate as a function of equivalent partial pressure of oxygen $p_{eq}(O_2)$ in $[Pa]$, which results from the concentration of oxygen being in equilibrium with the surrounding atmosphere through Henry's law.

In a different article, it was reported that algae can grow under conditions of elevated oxygen concentration in the medium, as long as the concentration is increased in small steps. These steps shall not be larger than 0.2 atm. and sufficient time for the culture to stabilize should be given before a new step is made. Until an oxygen equivalent partial pressure of 80 kPa, the growth is not affected and drops to around 0.65 (graphically extracted) at a partial pressure of 95 kPa (equivalent partial pressure values are stated as percentages of atmospheres in the source) [57]. The evolution of

relative growth with respect to an increasing atmospheric partial pressure of oxygen is shown in Figure 3-15.

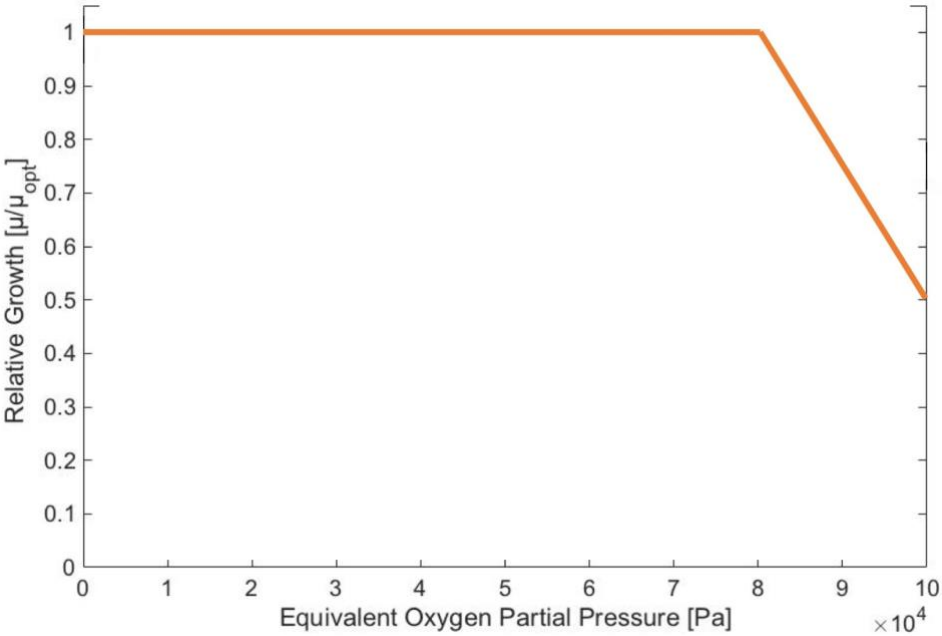

Figure 3-15: Oxygen equivalent partial pressure influence (i.e. concentration) on relative growth rate. Adapted from [57] by graphically extracting values and changing absolute growth rate to relative growth by assuming the stated maximum growth rate is the optimum growth. Carbon Dioxide partial pressure was maintained at 0.5 kPa.

The effect of oxygen concentration on Chlorella vulgaris in this publication [57] is far less severe than the one from [54], which was previously shown. Again, it should be noted that this is only possible, when the increase is not done in large steps and the culture can adapt to the changed conditions. This model will be used henceforth since it does not see a reduced relative growth rate at 20 kPa oxygen partial pressure and with the assumption that the changes in a photobioreactor interacting with a spacecraft cabin will not be rapid.

Mathematically, the model can be described by Eq. (3-14).

$$\mu_{rel_{O_2}}\left(p_{eq}(O_2)\right) = \begin{cases} 1 & \mid p_{eq}(O_2) < 80\ kPa \\ -2.33 * 10^{-5} * p_{eq}(O_2) + 2.867 & \mid p_{eq}(O_2) \geq 80\ kPa \\ 0 & \mid p_{eq}(O_2) \geq 122\ kPa \end{cases} \quad \textbf{Eq. (3-14)}$$

In the above equation, $\mu_{rel_{O_2}}\left(p_{eq}(O_2)\right)$ refers to the unitless relative growth rate as a function of equivalent partial pressure of oxygen $p_{eq}(O_2)$ in $[Pa]$, which results from the concetration of oxygen being in equilibrium with the surrounding atmosphere through Henry's law.

3.1.2.6 Carbon Dioxide Concentration Limitation

Carbon dioxide is an important nutrient for photosynthetic processes. However, at high concentrations in the growth medium it can become a limiting factor on growth. This

sub-chapter does not deal with the lack of carbon dioxide for photosynthetic growth, as discussed in 3.1.2.4, but rather with the opposite: the excessive abundance of carbon dioxide.

As is the case for the oxygen limitation, which was discussed in the previous sub-chapter 3.1.2.5, the tolerable and inhibitory limits of dissolved carbon dioxide on algal growth are often stated as partial pressures or in fractions of atmospheres. What is meant in this context is the equivalent concentration the substance would have in equilibrium with the atmosphere according to Henry's law at the stated partial pressure. The stated partial pressure can therefore also be regarded as an equivalent partial pressure. For more information on Henry's law see 3.3.2.1. The concept of equivalent (or imaginary) partial pressure is explained in more detail in 3.3.2.2.

A conflict arises because carbon dioxide in the atmosphere above the medium needs to be at a sufficiently high pressure to support a transfer through the membrane (or even just the medium surface) that matches the rate of uptake into algal cells through photosynthesis. At the same time, Henry's law dictates, that an increased partial pressure will also lead to an increased concentration in the medium, which then can limit the algal growth. A photobioreactor therefore requires close carbon dioxide monitoring and control to provide sufficient carbon dioxide to the algal metabolism but also not exceed a critical threshold, where it can become limiting on the growth rate.

A compilation of literature values of carbon dioxide equivalent partial pressures that limit algal growth is given in Table 3-4.

Table 3-4: Compilation of literature values for carbon dioxide concentration growth limitation.

Source	$p_{eq}(CO_2)\ [Pa]$	$\mu_{rel}\ [-]$	Comment
[15]	15 000	-	Review of other papers. 15% for Chlorella vulgaris. Higher values (30-50 % of atm.) stated for Chlorella sp.
[52]	60 000	0	Even in a high-CO2-tolerant microalga, growth is suppressed at > 60% CO2 in air (Satoh et al., 2004) [52]
[57]	65 000 100 000	- 0.15	Start of inhibition when c(CO2) is only increased slowly.
[9]	15 000	0.33	4 % stated as optimum "at 15 % CO2 concentration there is a 3-fold decline in biomass yield when compared to the yield produced at a 4% CO2 concentration." [9]

Due to its simplicity and continuous availability of data over a wide range of carbon dioxide equivalent partial pressure, the data from [57] is used. It states that Chlorella vulgaris growth is not affected until a partial pressure of 65 kPa and then declines to a relative growth of 0.15 at 100 kPa (equivalent partial pressure values are stated as percentages of atmospheres in the source) [57].

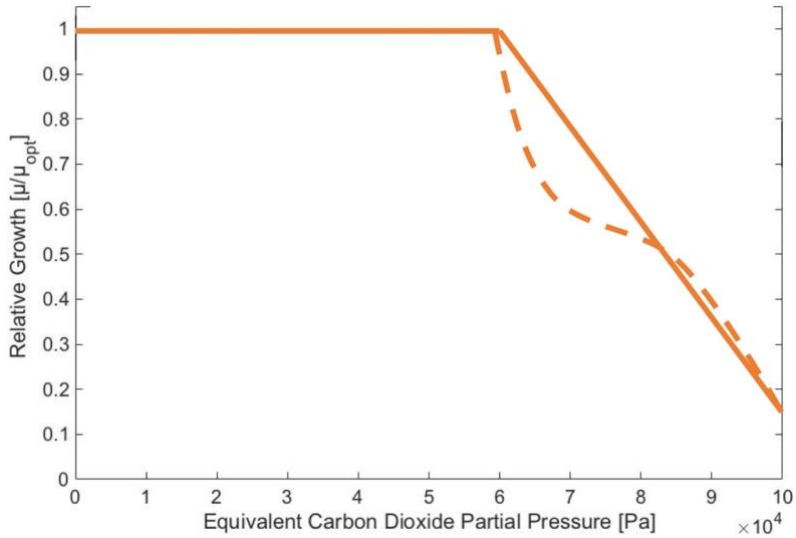

Figure 3-16: Carbon dioxide equivalent partial pressure (i.e. concentration) influence on relative growth rate. Adapted from [57] by changing absolute growth rate to relative growth by assuming the stated maximum growth rate is the optimum growth and simplifying the reported evolution (dashed line, approximated) to a linear one.

The model for the limitation of algal growth through carbon dioxide that is graphically represented in Figure 3-16 can be formulated as given in Eq. (3-30). This equation assumes a linear drop in relative growth between 65 kPa and 100 kPa, which actually has a more complex course in the source (see dashed line in Figure 3-16).

$$\mu_{rel_{CO_2}}\left(p_{eq}(CO_2)\right) = \begin{cases} 1 & \mid p_{eq}(CO_2) < 80\ kPa \\ -2.125 * 10^{-5} * p_{eq}(CO_2) + 2.275 & \mid p_{eq}(CO_2) \geq 80\ kPa \\ 0 & \mid p_{eq}(CO_2) \geq 107\ kPa \end{cases} \quad \textbf{Eq. (3-15)}$$

In the above equation, $\mu_{rel_{CO_2}}\left(p_{eq}(CO_2)\right)$ refers to the unitless relative growth rate as a function of equivalent partial pressure of carbon dioxide $p_{eq}(CO_2)$ in $[Pa]$, which results from the concetration of carbon dioxide being in equilibrium with the surrounding atmosphere through Henry's law.

It is important to note, that the above graph does not regard the fact that an extremely low carbon dioxide equivalent partial pressure will most likely lead to the lack of carbon dioxide as nutrient. In fact, it has been stated, that the growth of Chlorella sp. increases with increasing carbon dioxide percentage between 0.5 % and 5 % in the atmosphere, while for Chlorella vulgaris an optimum of 2 % was reported and no beneficial effects with further increase to 4 % and 8 % [15]. However, the limitation that arises through insufficient availability of carbon dioxide is a nutrient limitation and is regarded in the *Photosynthesis Module* as described in 3.1.2.4. The effects previously described in this chapter solely deal with a too high carbon dioxide concentration and its limitation on growth.

3.1.3 Achievable Biomass Concentration Increase Rate

The achievable biomass concentration increase rate can be calculated after the current optimum biomass concentration increase rate and the relative growth rates due to

limiting factors are determined. Since multiple factors can be limiting algal growth at the same time, a decision must be made with regard to how strongly each of these factors can affect the biomass concentration increase rate.

Two main types of models can be applied to the determination of achievable biomass concentration increase rate for problems like this one: threshold and multiplicative models [29].

Threshold models, also called minimum law models, assume that the optimum biomass concentration increase rate is only affected by the most limiting factor and even if the other relative growth rates also deviate from optimum (but to a lesser degree), they are disregarded. Therefore, the achievable biomass concentration increase rate is calculated as if there were only one factor limiting the optimum growth. The achievable biomass concentration increase rate as a result of a threshold model can be calculated with Eq. (3-16) [29].

$$\mu_{ach} = \mu_{opt} * \min(\mu_{rel_T}, \mu_{rel_{pH}}, \mu_{rel_P}, \mu_{rel_{O_2}}, \mu_{rel_{CO_2}}) \qquad \textbf{Eq. (3-16)}$$

Multiplicative models regard all limiting factors in the calculation of the achievable biomass concentration increase rate by multiplying the relative growth rates of the limiting factors. The achievable biomass concentration increase rate as a result of a multiplicative model can be calculated with Eq. (3-17) [29].

$$\mu_{ach} = \mu_{opt} * \mu_{rel_T} * \mu_{rel_{pH}} * \mu_{rel_P} * \mu_{rel_{O_2}} * \mu_{rel_{CO_2}} \qquad \textbf{Eq. (3-17)}$$

In the two equations stated above, μ_{ach} is the achievable biomass concentration increase rate in $[kg/(m^3 s)]$. It is calculated from the optimum biomass concentration increase rate μ_{opt} (as calculated by the Gompertz model) $[kg/(m^3 s)]$ by factoring in the unitless relative growth rates μ_{rel_T} for the temperature dependence, $\mu_{rel_{pH}}$ for the pH dependence, μ_{rel_P} for the photosynthetically active radiation dependence, $\mu_{rel_{O_2}}$ for the oxygen concentration dependence and $\mu_{rel_{CO_2}}$ for the carbon dioxide concentration dependence.

A terminological differentiation must be made between the optimum, achievable and actual biomass concentration increase rates. The optimum biomass concentration increase rate is the rate calculated by the Gompertz model based on the current biomass concentration as outlined in 3.1.1 and the achievable and actual biomass concentration increase rates are derived from it.

The achievable biomass concentration increase is not necessarily the actually observable growth since it does not regard nutrient limitation (carbon dioxide, nitrogen and phosphorus) in the simulation model. While the effect of limiting factors such as temperature and pH affect the ability of the biochemical photosynthetic processes to be performed at their optimum rate in a calculable manner, the transformation of nutrients is part of the biochemical processes themselves and their limitation is therefore regarded in the *Photosynthesis Module*. When all required nutrients are available in the growth medium, the achievable (derived from optimum growth rate with limiting factors) and actual biomass concentration increase rate (including possible nutrient limitation) are equal. Both models are available to select from, the multiplicative model is used for simulations in this thesis, since small deviations are expected and these should all be respected.

3.2 Photosynthesis Module

Algal growth is the product of photosynthesis which uses radiation energy (photosynthetically active radiation, see 3.4) to transform carbon dioxide and water to carbohydrates (e.g. sugar) and oxygen as shown in Eq. (3-18). The chemical energy stored in carbohydrates can then be used by other biochemical processes in the algal cell to metabolize nutrients such as nitrogen (in the form of nitrate, urea or ammonia) or phosphorus.

$$6CO_2 + 12H_2O\ (+E_{PAR}) \Longrightarrow C_6H_{12}O_6 + 6O_2 \qquad \textbf{Eq. (3-18)}$$

For the purpose of this thesis, the photosynthetic transformation of carbon dioxide and water to carbohydrates and oxygen, along with the nitrogen and phosphorus metabolism are regarded as one overall process, while the algal cell itself is regarded as a black box. Therefore, the processes happening inside the cell are disregarded.

The *Photosynthesis Module* is responsible for the photosynthetic and biochemical transformation of carbon dioxide, water and nutrients to chlorella cells, oxygen and further waste products based on the growth rate calculated by the previously discussed growth rate calculation module. This chapter presents different stoichiometric Chlorella vulgaris composition models in 3.2.1, outlines the chemical reactions responsible for the photosynthetic growth and metabolism of Chlorella vulgaris and discusses the metabolism of different nitrogen sources and how these affect the overall reactant consumption and reaction product evolution.

3.2.1 Chlorella Vulgaris Composition Model

In order to describe the overall photosynthetic growth and biochemical nutrient metabolism of algal cells, a stoichiometric model is required. A stoichiometric model of the algal cell allows to relate the increase in biomass of the algal culture to the amount of carbon dioxide and other nutrients required for the growth and also how much oxygen is produced in the process.

Since algal cells are living organisms that can adapt their composition to changing nutrient availability [58], finding a universal stoichiometric composition always requires averaging and simplifications. Furthermore, data on the stoichiometric composition of Chlorella vulgaris specifically is scarce and the sources typically rather refer to the broader genus Chlorella or, even more generalizing, simply microalgae.

A list of relative stoichiometric compositions from different sources is given in Table 3-5. Relative in this sense means that the number of atoms stated is relative to the absolute number of atoms of that element in an algal cell and therefore also relative to the number of atoms in the biomass of the entire algal culture. Stating an absolute value for a single cell is nonsensical since the algal cells grow before they separate (see 2.1.1) and also because the simulation logic only considers an absolute biomass and does not regard the number of discrete algal cells for the growth rate calculation.

Table 3-5: Relative stoichiometric composition of microalgae (mostly Chlorella / Chlorella vulgaris) compiled from different literature sources. Only carbon, hydrogen, oxygen, nitrogen and phosphorus are regarded. Entries list the relative number of atoms in a molecule normalized to carbon and below the mass percentages of each atom in the molecule. The resulting relative molar mass is also listed.

Source	C	H	O	N	P	M_{rel} $[kg/mol]$	Comment
[59]	1 66.9 %	1.6243 9.1 %	0.2394 21.4 %	0.0128 1.0 %	0.0092 1.6 %	0.0179	Compiled from averaged mass fractions for Chlorella from [60]. Disregarded materials with less percentage than P. Data used by [61].
[10]	1 55.0 %	1.6775 7.7 %	0.3648 26.8 %	0.1629 10.8 %	0 0 %	0.0218	Equations provided on p. 272, normalized to carbon. No further references. Used by [30].
[62]	1 49.9 %	1.6296 6.8 %	0.4025 26.8 %	0.1852 10.8 %	0.0446 5.8 %	0.0241	No specific type of microalgae stated. Microalgae grown in a medium (clarified domestic waste water) containing microorganisms. Normalized to carbon
[63]	1 53.3 %	1.7 7.6 %	0.4 28.4 %	0.15 9.3 %	0.0094 1.3 %	0.0225	Corresponding chemical photosynthesis equation in [64]
[18]	1 52.4 %	2.4811 7.4 %	1.0377 29.6 %	0.1509 9.2 %	0.0094 1.3 %	0.0335	No specific algal type stated. Normalized to carbon
[58]	1 54.8 %	1.68 7.7 %	0.365 26.7%	0.168 10.7 %	0.0 0 %	0.0219	Chlorella with Nitrate as N source. Normalized to carbon. Equations provided in [65], used by [37].
[61]	1 52.8 %	1.8 7.9 %	0.432 30.4%	0.143 8.8 %	0.0 0 %	0.0227	Chlorella with Ammonia as N source. Normalized to carbon. Equations provided in [65], used by [37].
[66]	1 52.6 %	1.75 7.7 %	0.42 29.4%	0.15 9.2 %	0.008 1.1%	0.0228	Chlorella sorokiniana. Normalized to carbon

In order to make them comparable, all values in Table 3-4 are normalized to contain one carbon atom. When comparing the stoichiometry and mass percentages listed in, a similarity between the values can be recognized.

When disregarding the first Chlorella composition, which was stated in [59], the carbon content ranges between 50 % and 55 %, hydrogen around 8 %, oxygen between 25 % and 30 %, nitrogen around 10 % and phosphorus (if considered at all), around 1 % (with one exception). The differentiation between different Chlorella species (vulgaris, sorokiniana, etc.) therefore seems unnecessary when regarding the stoichiometric composition and the statement of values simply for Chlorella, without further specifications, seem sufficient.

One of the benefits of the implementation of an algal photobioreactor in a spacecraft cabin is the ability to process urine to clean or even potable water. Therefore the Chlorella composition $C_1H_{1.75}O_{0.42}N_{0.15}P_{0.008}$ is chosen for this simulation since the source which provided this composition uses urine as growth medium and also provides experimentally derived chemical reaction equations for the photosynthetic growth and nutrient consumption [65]. Although the stated composition is used for a different Chlorella species in the original source, the similarity of stoichiometric compositions shown in Table 3-4 allows to assume it can also be used for Chlorella vulgaris.

One set of data even lists a different composition with regard to what nitrogen source is used [61]. Since microalgae can adapt their composition to different nutrients and media, this can provide an approach to modeling a varying composition of the biomass in a simulation environment in the future.

3.2.2 Algal Growth Reactions

Since the selected algal composition $C_1H_{1.75}O_{0.42}N_{0.15}P_{0.008}$ differs from the previously stated "pure" photosynthesis biomass $C_6H_{12}O_6$, Eq. (3-18) cannot be used. A chemical reaction has to be found that also considers the nitrogen and phosphorus uptake. An overall equation for the Chlorella growth, which is stated in the same source as the used stoichiometric composition is shown in Eq. (3-19) [65].

$$CO_2 + 0.15\,NH_3 + 0.008\,H_2PO_4^- + 0.646\,H_2O \Longrightarrow C_1H_{1.75}O_{0.42}N_{0.15}P_{0.008} + 1.125\,O_2 + 0.008\,OH^- \qquad \textbf{Eq. (3-19)}$$

Since the human model of the V-HAB simulation environment does not contain phosphorus in its urine, an abstraction is made that excludes phosphorus from the algal composition, which is then $C_1H_{1.75}O_{0.42}N_{0.15}$. The resulting equation is slightly different and makes up for the lost hydrogen and oxygen from $0.008\,H_2PO_4^-$ on the reactant side by using more water and producing less oxygen on the product side. The reaction equation is shown in Eq. (3-20).

$$CO_2 + 0.15\,NH_3 + 0.65\,H_2O \Longrightarrow C_1H_{1.75}O_{0.42}N_{0.15} + 1.115\,O_2 \qquad \textbf{Eq. (3-20)}$$

The provided equations us ammonia (NH_3) as nitrogen source, which is in an equilibrium with ammonium (NH_4^+) in an aqueous solution. The mechanism of nitrogen uptake into algae is often reported with ammonium [67] [68] [69], which releases a hydrogen ion into the medium when consumed by the algae [65] [67]. The assimilation of ammonia has the same overall mass and proton balance as consuming ammonium and releasing a hydrogen ion. Since cell-internal processes are not of concern for this thesis, only the assimilation of ammonia will be regarded for simplicity. Ammonia shall henceforth act as the baseline for nitrogen assimilation and any other nitrogen source (such as nitrate or urea), is first transformed to ammonia before it is assimilated by the algal cell.

Since the growth medium pH is a factor in growth rate determination, not only the mass balance of the growth reactions must be considered, but also the proton uptake or hydroxide ion production. Special care has to be given to ensuring a correct charge and proton balance, since the proton balance is often disregarded in literature sources when dealing with photosynthetic growth [69]. This is especially the case when dealing with nitrate as nitrogen source.

This sub chapter presents equations used in the simulation based on the previously selected Chlorella composition. The chemical equations are divided into two sections depending on the nitrogen source, which can either be nitrate (see 3.2.2.1) or urine (see 0). Since the human model of the V-HAB simulation environment does not contain phosphorus in its urine, simplified equations without phosphorus are also presented.

3.2.2.1 Reactions with Nitrate as Nitrogen Source

Algae such as Chlorella vulgaris can grow on nitrate ions (NO_3^-) as nitrogen source. In the assimilation process, nitrate is first reduced to nitrite (NO_2^-,) then further reduced to ammonium [69] [70] and incorporated into amino acids through further cell internal processes [68]. Since ammonium is an intermediate step in this process and releases a hydrogen ion into the medium when incorporated into biomass, the assumption of using ammonia (NH_3) as nitrogen source is valid, as long as the process of reducing nitrate to ammonia is respected in the overall equation.

When nitrate is consumed, the medium pH rises steadily [69]. Since nitrate itself is not acidic or basic (at a considerable level), the pH increase must be a result of hydrogen ion consumption or hydroxide ion production.

No uniform quantification of proton uptake per nitrate molecule is found in literature. The redox state of the nitrogen atom in nitrate is +5 and that in ammonium is -3 [71]. One (non-peer-reviewed) source states that 8 hydrogen ions (i.e. protons) are required in the process of nitrate reduction [2], which can be assumed to be derived from the redox state difference. Other sources state, and experimentally verify, that two hydrogen ions are consumed in the reduction of nitrate to ammonium and one hydrogen ion released when ammonium is assimilated [67] [72]. When regarding the overall reduction of nitrate to ammonium and subsequent uptake of ammonia then one proton is consumed, and one hydroxide ion released to the medium. A further article, which deals with the pH changes in the soil surrounding roots of higher plants, compares different sources and acknowledges that the quantification of proton uptake in nitrate reduction is “under discussion” but is larger than 1 per nitrate ion reduced [73].

It therefore seems fair to assume 1 hydrogen ion per mole nitrate ion reduced to ammonia. When assuming water to be the source for the hydrogen atoms in ammonia and the oxygen of the nitrate ion to be released as molecular oxygen the overall reaction equation is Eq. (3-21).

$$NO_3^- + 2\,H_2O \Longrightarrow NH_3 + 2\,O_2 + OH^- \qquad \textbf{Eq. (3-21)}$$

This equation can then be integrated in the previously stated equations of algal growth with phosphorus (Eq. (3-22)) and without phosphorus (Eq. (3-23), both (adapted from [65])), which represent the algal growth reaction with nitrate as nitrogen source.

$$CO_2 + 0.15\,NO_3^- + 0.008\,H_2PO_4^- + 0.946\,H_2O \Longrightarrow C_1H_{1.75}O_{0.42}N_{0.15}P_{0.008} + 1.425\,O_2 + 0.158\,OH^- \qquad \textbf{Eq. (3-22)}$$

$$CO_2 + 0.15\,NO_3^- + 0.95\,H_2O \Longrightarrow C_1H_{1.75}O_{0.42}N_{0.15} + 1.415\,O_2 + 0.15\,OH^- \qquad \textbf{Eq. (3-23)}$$

Generally speaking, nitrate is not the most suitable nitrogen source since it is expensive [74] and its metabolism is rather energy intensive [68]. Other viable sources are based on ammonium, ammonia or urea, which are preferred by algae over nitrate [71].

3.2.2.2 Reactions with Urine as Nitrogen Source

Urine can be the source of nitrogen for Chlorella [51] [53] and other algal species [75] [76]. The nitrogen is assimilated by metabolizing urea $CO(NH_2)_2$, which is the main nitrogen containing component in fresh urine [65].

In an enzymatic reaction, urea is broken up into ammonia and carbon dioxide as shown in Eq. (3-39) [53]. Ammonia then enters an equilibrium with ammonium in an aqueous solution but is disregarded here since it yields the same overall equation as regarding ammonia.

$$CO(NH_2)_2 + H_2O \Longrightarrow 2\,NH_3 + CO_2 \qquad \textbf{Eq. (3-24)}$$

This equation can then be integrated in the previously stated equations of algal growth with phosphorus Eq. (3-25) [65] and without phosphorus Eq. (3-26) (adapted from [65]), which represent the algal growth reaction with urea from urine as nitrogen source.

$$0.925CO_2 + 0.075\,CO(NH_2)_2 + 0.008\,H_2PO_4^- + 0.721\,H_2O \Longrightarrow C_1H_{1.75}O_{0.42}N_{0.15}P_{0.008} + 1.125\,O_2 + 0.008\,OH^- \qquad \textbf{Eq. (3-25)}$$

$$0.925\,CO_2 + 0.075\,CO(NH_2)_2 + 0.725\,H_2O \Longrightarrow C_1H_{1.75}O_{0.42}N_{0.15} + 1.115\,O_2 \qquad \textbf{Eq. (3-26)}$$

The pathway of urea assimilation is less complex than that of nitrate, which also poses some major advantages that the algal growth on urea instead of nitrate as nitrogen source has.

The metabolism of urea uptake does not consume any hydrogen ions or produce hydroxide ions like nitrate does [69] [77]. It therefore does not affect the medium pH when used as a nitrogen source.

Furthermore, the uptake of urea is less energy demanding. It only requires an enzymatic hydrolysis to ammonia and not a redox reaction, like nitrate does, which competes for energy with other photosynthetic mechanisms [68]. When both nitrate and ammonium are available in the growth medium, algal cells prefer the uptake of ammonium since it requires less energy [71].

Being a waste product which is produced by the human metabolism, urine is a cheaper nitrogen source than nitrate [74]. In a spacecraft the use of urine does not only have a monetary advantage but also requires less stored supplies, which would contribute toward an increased launch mass and storage space.

3.3 Growth Medium Module

The growth medium is the liquid in which the algal cells grow. Ideally, it is composed in a way that supports high algal growth and provides sufficient nutrients and also

allows the transportation of radiation energy to the algal cells in order to perform photosynthesis.

In a natural environment the growth medium can be an outdoor pond or an ocean. In a laboratory environment, a defined medium is used – meaning it is made up of defined quantities of ingredients [78]. It is typically water based and consists of a selection of chemicals that are added to the photobioreactor. For batch cultures these chemicals are added once in the beginning of batch growth and for continuous cultures the chemicals have to be provided continuously as they are taken up by the continuously growing algae population.

Besides the manually added chemicals, there are also components in the medium that enter the medium through an exchange with the surrounding atmosphere such as carbon dioxide and oxygen. Furthermore, products of the algal metabolism enter the medium (and may exit to the atmosphere in a next step) and therefore also alter its composition.

The components of the medium, either manually added or taken up from the atmosphere, may also react with the water molecules of the medium and create an acidic or basic solution. The pH of the solution can then affect the solubility of some medium components and therefore determine how much of a certain component can be dissolved in the medium under the existing conditions. A schematic overview of processes and components of an algal growth medium is shown in Figure 3-17.

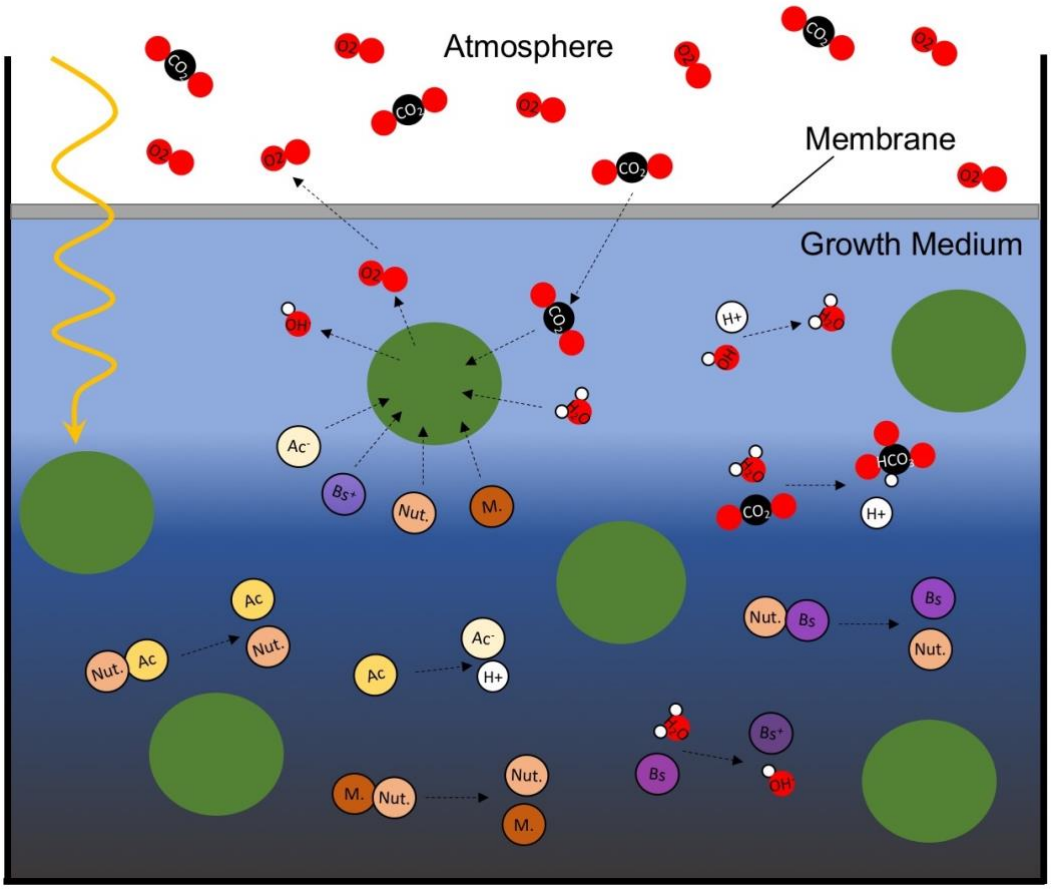

Figure 3-17: Growth medium components and reactions. Compounds are dissolved in the water and split up into their ionic constituent parts and may further react with water if either of their compounds is acidic (Ac.) or basic (Bs.) to form hydrogen ions (H^+) or hydronium ions (OH^-). Molecular nutrients (Nut.) and mineral ions (M.) are dissolved in the solution and used for photosynthetic processes. Carbon dioxide (CO_2) is absorbed from and oxygen (O_2) released to the atmosphere through the membrane. Carbon dioxide that is not used for photosynthesis may react with water to other carbon species. Furthermore, photosynthetically active radiation (yellow arrow) penetrates the membrane and medium and provides energy for photosynthetic processes in the algal cells (green circles).

3.3.1 Bold's Basal Medium

Depending on what type of algae are grown and what the culture should be used for, a variety of growth media recipes exist [78]. Typically, these recipes can be bought as a premade concentrate and have to be mixed with a defined amount of water to form the desired growth medium.

Chlorella vulgaris is the algal species of interest within the scope of this thesis and one of the most suitable mediums for this species is Bold's Basal Medium [79]. It is an artificial freshwater algae medium made up of inorganic components such as minerals and trace metals [80]. A detailed list of Bold's Basal Medium components and their concentrations is shown in Table 3-6.

Table 3-6: Bold's Basal Medium composition. Adapted from [80].

Component	Chemical Formula	Concentration [kg/m^3]
Sodium Nitrate	$NaNO_3$	0.25
Magnesium Sulfate, anhydrous	$MgSO_4*7H_2O$	0.03663
Sodium Chloride	NaCl	0.025
Potassium Phosphate, dibasic	K_2HPO_4	0.075
Potassium Phosphate, monobasic	KH_2PO_4	0.175
Calcium Chloride. anhydrous	$CaCl_2*2H_2O$	0.0187
Zink Sulfate * 7 H2O	$ZnSO_4*7H_2O$	0.00882
Manganese Chloride *4 H2O	$MnCl_2*4H_2O$	0.00144
Cupric Sulfate	$CuSo_4*5H_2O$	0.00157
Cobalt Nitrate	$Co(NO_3)_2*6H_2O$	0.00049
Boric Acid	H_3BO_3	0.01142
Disodium Ethylenediaminetetraacetic acid (EDTA) Salt	$Na_2C_{10}H_{14}N_2O_8$	0.06361
Potassium Hydroxide	KOH	0.031
Ferrous Sulfate, anhydrous	$FeSO_4*7H_2O$	0.00498
Na2MoO4	Na_2MoO_4	0.0019
Sulfuric Acid	H_2SO_4	0.00184

When prepared correctly with deionized water, it initially has a pH of 4.4 and should be adjusted with Potassium Hydroxide to a pH of 6.6 [80]. It should be noted, that the word "basal" in this context refers to a medium that supports the growth of a broad variety of microorganisms that do not require special nutrient supplements [81] and should not be confused with having a pH in the basic range (7-14).

3.3.2 Atmospheric Exchange of Components

The surrounding atmosphere composition, to which the medium in a photobioreactor is exposed, can also influence the medium composition through matter exchange based on Henry's Law. Among the most notable components in the growth medium that are affected by atmospheric exchange are carbon dioxide that enters from the atmosphere, and oxygen that is produced in the photosynthetic metabolism and exits the medium to the atmosphere.

It should be noted, that oxygen (like any other atmospheric component) also enters the medium through atmospheric exchange, but more importantly, also leaves the medium when produced by the algal culture and the oxygen content surpasses what is currently dissolvable in the medium.

3.3.2.1 Henry's Law

In 1803, William Henry introduced a law [82] that postulated the solubility of a species in water to be proportional to the partial pressure of the gaseous species above the water. The proportionality factor in this relationship is temperature dependent and commonly referred to as Henry's constant [83].

Although varying definitions of the involved terminology and units exist, the law can be defined as given in Eq. (3-27) [83].

$$H = \frac{c_a}{p_g} \qquad \textbf{Eq. (3-27)}$$

Where H is the Henry's constant in $[mol/(m^3 * Pa)]$, c_a is the molar concentration of a substance in the aqueous phase in $[mol/m^3]$ and p_g is the partial pressure of the substance in the gaseous phase above the water in $[Pa]$ in equilibrium conditions [83]. For a given temperature, each substance will reach its own equilibrium concentration and the Henry constant is therefore individually defined for each substance. A compilation of values for 4632 substances can be found in [83].

Furthermore, the Henry's constant not only differs between substances but is also temperature dependent. Based on a reference temperature, at which the Henry's constant is known, and a factor that represent the temperature dependence, the Henry's constant as a function of temperature can be written as seen in Eq. (3-28) [83].

$$H(T) = H^{ref} * \exp\left(\frac{-\Delta_{sol}H}{R}\left(\frac{1}{T} - \frac{1}{T^{ref}}\right)\right) \qquad \textbf{Eq. (3-28)}$$

$H(T)$ is the temperature dependent Henry constant in $[mol/(m^3 * Pa)]$ at the evaluated Temperature T in $[K]$, H^{ref} is the Henry constant in $[mol/(m^3 * Pa)]$ at a reference temperature T^{ref} in $[K]$ and $-\Delta_{sol}H/R$ is a tabulated temperature dependency factor in $[K]$ (H in this temperature dependency factor refers to enthalpy, not the henry's law constant H). It should be noted, that with the above equation the temperature dependent henry factor can only be accurately calculated for temperatures close to the selected reference temperature [83]. Since the reference temperature $T^{ref} = 298.15\ K$ for the used values is close to the ideal operating point of the photobioreactor at $T \approx 303\ K$, the observed temperature range will be sufficiently small to maintain a high accuracy.

For carbon dioxide the values of interest are: $H^{ref} = 3.3 * 10^{-4}\ mol/(m^3 * Pa)$ at $T^{ref} = 298.15\ K$ and $-\Delta_{sol}H/R = 2400\ K$ [83]. A plot of Eq. (3-28) shown in Figure 3-18 over a temperature range from $T_{min} = 283\ K$ to $T_{min} = 313\ K$ shows, that the soluble concentration of carbon dioxide in water (assumed partial pressure $p_g = 5000\ Pa$) decreases with increasing temperature.

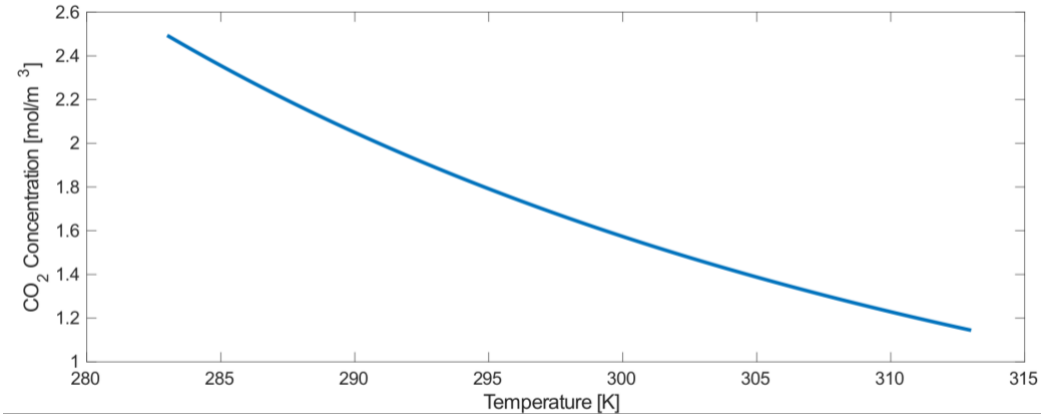

Figure 3-18: Concentration variation in aqueous phase (with constant partial pressure in gas phase) as a result of Henry constant temperature dependence.

3.3.2.2 Membrane Transport

In order to separate the growth medium from the atmosphere, to prevent excessive water evaporation and contamination but still allow the exchange of carbon dioxide and oxygen, a membrane can be utilized. In a weightlessness environment a membrane is also required to prevent the liquid from leaving the photobioreactor.

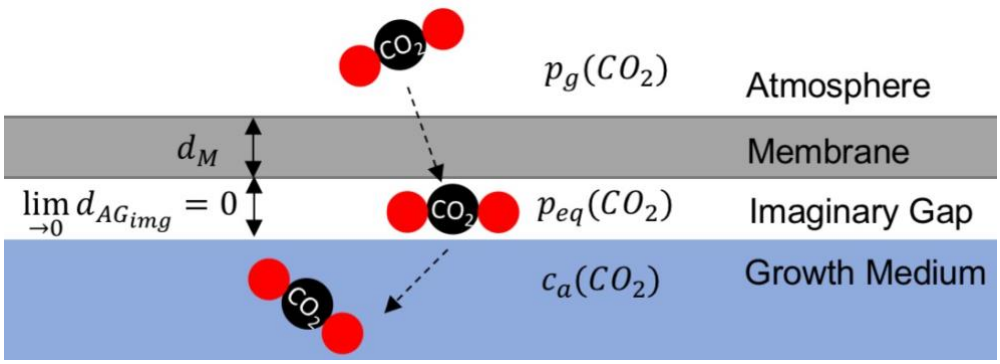

Figure 3-19: Membrane transport from the atmosphere to the growth medium where the difference of partial pressures is the driving force. Carbon dioxide is shown as an example.

Membrane flow depends on a multitude of variables, that can be adjusted to allow the desired flow rate of a certain substance. At all times, a partial pressure gradient between both sides must be present as a driving force for the membrane transport. In the medium the ideal gas law does not apply, and the definition of a partial pressure is therefore not sensible. From the concentration of the substance in the medium, an equivalent partial pressure in an infinitesimally small volume between the medium and the membrane must be used as shown in Figure 3-19. This equivalent partial pressure represents the pressure the gas would have if it were in equilibrium with the medium and can be calculated with Eq. (3-29) using the Henry constant at the current temperature.

$$p_{eq} = \frac{c_a}{H(T)} \qquad \textbf{Eq. (3-29)}$$

Where p_{eq} is the equivalent partial pressure of the substance in the imaginary air gap in $[Pa]$ and c_a is the current molar concentration of the substance in the aqueuous phase in $[mol/m^3]$.

This equivalent partial pressure, along with characteristics of the utilized membrane, can then be used in Eq. (3-30) to calculate the transport rate through the membrane.

$$\dot{\mathrm{M}} = \frac{J * A_M * (p_g - p_{eq})}{d_M} \qquad \textbf{Eq. (3-30)}$$

Where $\dot{\mathrm{M}}$ is the molar flowrate through the membrane in $[mol/s]$, J the membrane's permeability in $[mol * m/(m^2 * Pa * s)]$, A_M the membrane surface in $[m^2]$ and d_M the membrane's thickness in $[m]$.

The flow of carbon dioxide through the membrane must be sufficiently high to provide ample supply to the growing algal culture at all times. Furthermore, it must transport the produced oxygen away from the culture sufficiently fast to not be limiting on algal growth. The membrane must therefore be able to support the carbon dioxide uptake rate and oxygen production rate during the peak of the algal growth rate. Most easily this can be achieved by adjusting the membrane surface or the partial pressure difference between algal medium and the outside.

3.3.3 Total Inorganic Carbon Balance

Carbon dioxide is an essential nutrient to photosynthetic growth and enters the growth medium through gas exchange with the atmosphere based on Henry's Law. However, it can speciate to bicarbonate and carbonate ions which means that it is no longer available to the photosynthetic processes. Furthermore, the process of aqueous carbon speciation releases hydrogen ions to the medium and make it more acidic. The involved reactions are shown in Eq. (3-31), Eq. (3-32) and Eq. (3-33) [84].

$$CO_2 + H_2O \overset{K_{a_{CO2}}}{\Longleftrightarrow} H_2CO_3 \qquad \textbf{Eq. (3-31)}$$

$$H_2CO_3 \overset{K_{a_{H_2CO3}}}{\Longleftrightarrow} HCO_3^- + H^+ \qquad \textbf{Eq. (3-32)}$$

$$HCO_3^- \overset{K_{a_{HCO3^-}}}{\Longleftrightarrow} CO_3^{2-} + H^+ \qquad \textbf{Eq. (3-33)}$$

The sum of these three carbon species concentrations is referred to as total inorganic carbon concentrations as shown in Eq. (3-30) [2].

$$\mathrm{C_T} = [CO_2^*] + [HCO_3^-] + [CO_3^{2-}] \qquad \textbf{Eq. (3-34)}$$

$\mathrm{C_T}$ refers to the total inorganic carbon concentration in $[mol/m^3]$ and the brackets around the three different species indicate concentrations of these in $[mol/m^3]$. The combined concentrations of carbon dioxide and carbonic acid are often represented by $[CO_2^*]$ as defined in Eq. (3-35).

$$[CO_2^*] = [CO_2] + [H_2CO_3] \qquad \textbf{Eq. (3-35)}$$

Furthermore, a combined acid constant $K_{a_{CO_2^*}}$ is used that describes the reaction of CO_2^* to HCO_3^- and H^+.

Not only does the introduction of carbon dioxide into the medium change the medium pH through speciation, but the variation of pH due to other acids or bases will also influence the distribution of carbon species. Reason for this is, that the equilibrium

reactions are not just influenced by the initial CO2 concentration on the left side, but also by the hydrogen ion concentration, which is on the right. If that concentration is changed (taken away through bases or increased through other acids, the equilibrium of the whole equation is shifted accordingly. Reactions must be strictly regarded as a process that can go in both directions, not just left to right, but also right to left.

The concentration of the individual species of the total inorganic carbon balance can be regarded as a function of pH as shown in Figure 3-20. The species concentration equivalency points (i.e. where the lines cross) are defined by the temperature dependent pK_a-values (the negative logarithm of the respective acid constants).

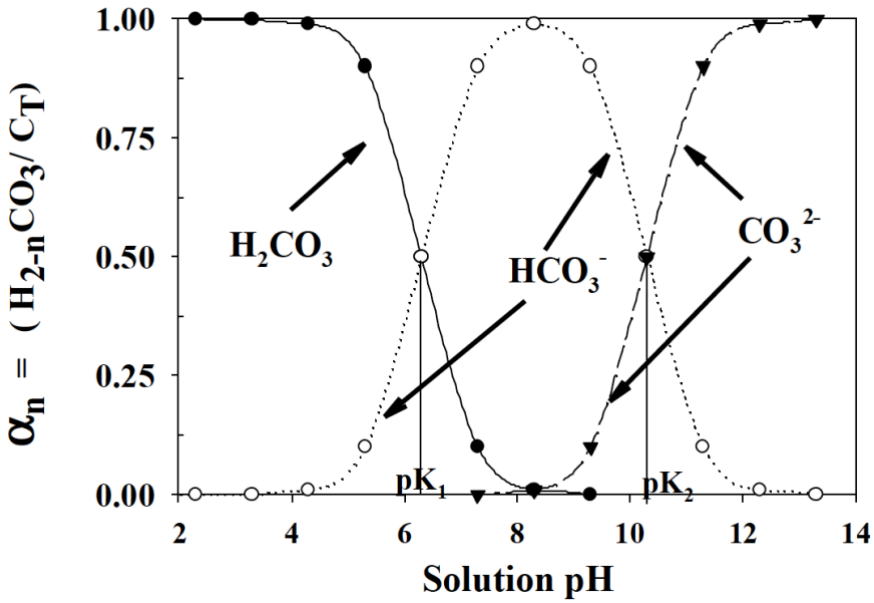

Figure 3-20: Relation of inorganic carbon species concentration to the total inorganic carbon concentration as a function of pH. pK1 in the figure represents $-\log_{10}(K_{a_{CO_2^*}})$ and pK2 represents $-\log_{10}(K_{K_{a_{HCO3^-}}})$ Copied from [85].

Since some of the carbon dioxide, that is dissolved in the water, is directly speciated to bicarbonate and carbonate ions, the effective Henry's constant for carbon dioxide is in fact higher than the previously stated $H_{CO_2}^{ref} = 3.3 * 10^{-4}\, mol/(m^3 * Pa)$. The actual value depends on the pH of the medium and current, temperature dependent, equilibrium constants of the carbon species reactions $K_{a_{CO_2^*}}$ and $K_{a_{HCO3^-}}$.

In a closed system (with no contact to a surrounding atmosphere) or one that is partially closed due to a transience-inducing behavior of membrane transport (which is limiting the flow of carbon dioxide into the medium), the concentration of carbon dioxide varies with pH (e.g. induced by other acids/bases) while the total inorganic carbon concentration stays equal (or changes only slowly due to limited membrane transport capabilities). In a completely open system, where instantaneous exchange with the atmosphere is possible, the variation of pH leads to a varying concentration of total inorganic carbon, while the concentration of carbon dioxide remains constant [86] (the relative distribution still follows that shown in Figure 3-20, the absolute concentrations just become higher or lower).

As a result, at high pH and transport limitation through the medium surface, even if the total inorganic carbon concentration is high, potentially not enough carbon dioxide is

available for photosynthesis because the total inorganic carbon equilibrium lies far on the side of carbonate ions. Carbon dioxide ions entering the medium are speciated to bicarbonate and carbonate before they can be used otherwise. Another consequence of the pH dependent concentration of carbon dioxide in a (partially) closed system is that other acidic or basic components in the medium can influence how much carbon dioxide can be dissolved in medium if the Henry's law atmosphere-air equilibrium is not reached.

3.3.4 Components from Algal Metabolism

Besides the increase in biomass, the algal metabolism consumes and releases components into the growth medium that change its composition and have the ability to change its pH. The components considered here are oxygen and hydroxide ions. For more in-depth details on the reactions, products and reactants of photosynthesis, refer to 3.2.

3.3.4.1 Oxygen

One of the main products of photosynthesis is oxygen which is first dissolved in the medium until its equilibrium concentration (with regard to its current Henry Constant) is reached and then exits the medium into the atmosphere through the means of atmospheric exchange described in the previous section 3.3.2.

In order to calculate the equilibrium concentrations of oxygen, Eq. (3-27) and Eq. (3-28) can be used analogously to carbon dioxide. For oxygen, the Henry's law values of interest are: $H^{ref} = 1.3 * 10^{-5}\, mol/(m^3 * Pa)$ at $T^{ref} = 298.15\, K$ and $-\Delta_{sol}H/R = 1500\, K$ [83], which shows that the molar solubility of oxygen in water is an order of magnitude smaller than that of carbon dioxide.

Since oxygen can be limiting on algal growth at high concentrations in the medium as previously outlined in 3.1.2.5, special care should be given to designing the membrane to be capable of meeting the oxygen transport needs.

3.3.4.2 Hydroxide Ion Production

In the process of algal growth, the nitrate metabolism requires hydrogen ions to turn nitrate into amines, which are found in proteins. These hydrogen ions are taken from breaking up water, in the process of which, hydroxide ions are released into the medium, as outlined in the the discussion of the *Photosynthesis Module* (see 3.2.2.1).

Unlike oxygen, the hydroxide ions are not exchanged with the atmosphere and contribute to the overall acid-base equilibrium in the medium and therefore influence the pH.

3.3.5 Changes of Composition and pH due to acid-base-reactions

The pH of the medium can be a limiting factor on algal growth if it is outside of the tolerable boundaries, as outlined in 3.1.2.2. Therefore, the knowledge of the current medium pH is a vital piece of information when determining the possible algal growth. Many of the components of the Bold's Basal Medium and those added through algal metabolism and atmospheric exchange can alter the medium's pH by contributing or consuming hydrogen ions in equilibrium reactions.

Substances that have the ability to provide a proton (i.e. positively charged hydrogen ion) in an aqueous solution are acids. Those that can accept or receive a hydrogen ion from another substance are called bases [87].

Acid-base reactions in water can be described by the generalized equilibrium reaction as shown in Eq. (3-36)

$$HA + H_2O \overset{K_a}{\Leftrightarrow} B^- + H_3O^+ \qquad \textbf{Eq. (3-36)}$$

In this equation, HA stands for an acid with an attached hydrogen atom, and B^- is the resulting conjugated base that results from the acid, when the hydrogen ion is passed to a water molecule. $\overset{K_a}{\Leftrightarrow}$ indicates that the reaction can go in both directions and the equilibrium is dictated by the equilibrium constant K_a.

The mass action law dictates that the equilibrium concentrations of all involved species follow the equilibrium constant relation as shown in Eq. (3-37). The water concentration is regarded to remain constant throughout the reaction if it is the solvent for the acids and bases involved and is therefore included in the equilibrium constant (see simplifications in 3.3.5.1), which, when talking about acids, is also often known as acidity constant.

$$K_a = \frac{\{B^-\} * \{H^+\}}{\{HA\}} \qquad \textbf{Eq. (3-37)}$$

In the above equation, the curved brackets indicate the unitless molar activities of the respective substances. The molar activity represents an effective concentration which is lower than the actual concentration of a substance in a non-ideal solution and can be obtained by multiplying the concentration with an activity constant [41]. H^+ is the hydrogen ion, which is regarded without the water molecule to which it is attached.

Instead of the K_a value, acids and bases are often characterized by the better readable pK_a value, which is the negative logarithm of a reaction's equilibrium constant as shown in Eq. (3-38).

$$pK_a = -\log_{10}(K_a) \qquad \textbf{Eq. (3-38)}$$

Since the K_a value (and the pK_a as an easier readable version of it) determines how far on the side of the reaction products the equilibrium of a reaction lies, it can be used to characterize the strength of an acid or base. The smaller the pK_a value is, the more likely the acid is to transfer a hydrogen ion into solution and thereby decreasing the pH. A strong acid has a very small pKa and completely deprotonates in water, whereas a weak acid only partially deprotonates [87] (potentially only at high pH).

Some acids are polyprotic (like EDTA salt and potassium phosphate in the Bold's Basal Medium) or polybasic and can provide more than one hydrogen ion each at a different pK_a. The fact that each mole of substance can provide or accept more than one mole of hydrogen ions means they can have a strong impact on medium pH.

Even though bases in an aqueous solution are typically characterized by their pK_b value, which describes their likeliness to accept protons (the smaller, the stronger), they can be characterized by the pK_a value of their conjugate acid (one hydrogen ion more) through the relation shown in Eq. (3-39). A direct result is, that a very weak acid (high pKa) has a very strong conjugate base (low pKb).

$$pK_a + pK_b = 14 \qquad \textbf{Eq. (3-39)}$$

This subchapter outlines the calculation of medium pH depending on the concentrations and equilibrium constants of various components – either added manually or taken up through atmospheric exchange and the algal metabolism. Since the calculation is relatively complicated, some simplifications and assumptions are outlined in 3.3.5.1, the required set of reaction equations is presented in 3.3.5.2 and the pH calculation mechanism is described in 3.3.5.3.

3.3.5.1 Required Simplifications

Bold's Basal Medium consists of 16 different components (including water), of which the acids or bases were identified in order to know which components are relevant for the pH calculation. They are shown in Table 3-7 with their pKa values.

Table 3-7: Basic and acidic components of Bold's Basal Medium

Substance	pKa at 25° C	Acid or Base
Boric Acid	9.324 [88]	weak acid
Disodium EDTA Salt	2.0, 2.4, 6.2, 10.3 [89] First and second protonation of EDTA have 0.26 and 0.96 [90]	Medium strong acid, pure EDTA would be strong acid.
Potassium Hydroxide	23-29 of hydroxide ion [88]	strong base
Dibasic Potassium Phosphate	12.325 of HPO_4 [88]	medium weak base
Monobasic Potassium Phosphate	7.207 of $H2PO_4$[88]	medium weak acid

Since Boric Acid is only a weak acid and its concentration in Bold's Basal Medium is fairly low, it is left out of calculations in the following. Furthermore, the acidity of minerals and ions other than those stated above,

When calculating mass and charge balances, the current concentrations of the regarded substances are required. However, when calculating mass action law equations with equilibrium constants, activities are required [91]. Ions in solution react with each other and show a behavior that suggests a concentration that appears to be lower, than it actually is. In order to account for this behavior, unitless activity constants are introduced that allow for the calculation of an effective concentration. In an ideally dilute solution (concentration tending to zero), the activity constant becomes 1 and the effective concentration matches the actual concentration [41].

The demonstrated calculations in this chapter assume an ideally dilute solution and therefore use concentrations instead of activities in order to calculate chemical equilibria with mass action law equations. Eq. (3-37) can then be rewritten with concentrations (in brackets) instead of activities (in curly brackets) as shown in Eq. (3-40) and since the constant concentration of water is included in the equilibrium constant, K_a by definition becomes the unit $[mol/m^3]$ in order to maintain the equations correct unit.

$$K_a = \frac{[B^-] * [H^+]}{[HA]}$$ **Eq. (3-40)**

Water is considered to remain at a constant concentration throughout all reaction and calculation steps since its concentration is considerably higher compared to the other medium components and therefore hardly varies. At a density of $\rho_{H_2O} = 1000\,kg/m^3$, the concentration of water is $55.56\frac{mol}{m3}$ as can be calculated with Eq. (3-74).

$$c_a(H_2O) = [H_2O] = \frac{\rho_{H_2O}}{M_{H_2O}}$$ **Eq. (3-41)**

In the above equation $c_a(H_2O)$ and $[H_2O]$ are both representations of the concentrations of water in water in $mol/m3$, ρ_{H_2O} ist he density of water in $kg/m3$ and M_{H_2O} the molar mass of water in $\mathrm{kg/mol}$.

The calculated $55.56\,mol/m3$ are more than 40 times higher than the highest concentration of added reacting substance in the medium, which is dihydrogen phosphate (H_2PO_4) at $1.3\,mol/m3$.

3.3.5.2 Acid-Base Reactions in the Medium

In order to calculate the medium pH, the concentrations and acidity constants of all acids and bases involved in the contribution and consumption of hydrogen ions are required.

As a first step, all added salts of the Bold's Basal Medium are assumed to completely split up into their ions in water. When only regarding the acidic or basic components of the Bold's Basal Medium, four substances have to be considered as outlined in 3.3.5.1. Their ionization reactions can be seen in Eq. (3-42) - Eq. (3-45).

$$Na_2EDTA \rightarrow EDTA^{2-} + 2\,Na^+$$ **Eq. (3-42)**

$$KOH \rightarrow K^+ + OH^-$$ **Eq. (3-43)**

$$KH_2PO_4 \rightarrow K^+ + H_2PO_4^-$$ **Eq. (3-44)**

$$K_2HPO_4 \rightarrow 2 * K^+ + HPO_4^{2-}$$ **Eq. (3-45)**

Henceforth, only the acidic or basic ions $EDTA^{2-}$, OH^-,$H_2PO_4^-$ and HPO_4^{2-} are regarded for the calculations and the metal ions regarded as inactive but still dissolved in the medium.

In the medium, the added salts further speciate and can form different states depending on the pH of the medium. Even states with more hydrogen atoms than those, that were initially added can be reached depending on the overall pH of the medium and therefore must also be regarded as possible reactions in the medium. These reactions are shown in Eq. (3-46) - Eq. (3-52). For simplification the weakly acidic fifth and sixth deprotonation of EDTA are not regarded.

$$EDTA \overset{K_{a_{EDTA}}}{\Longleftrightarrow} EDTA^- + H^+$$ **Eq. (3-46)**

$$EDTA^{-} \overset{K_{a_{EDTA^{-}}}}{\Longleftrightarrow} EDTA^{2-} + H^{+} \qquad \textbf{Eq. (3-47)}$$

$$EDTA^{2-} \overset{K_{a_{EDTA^{2-}}}}{\Longleftrightarrow} EDTA^{3-} + H^{+} \qquad \textbf{Eq. (3-48)}$$

$$EDTA^{3-} \overset{K_{a_{EDTA^{3-}}}}{\Longleftrightarrow} EDTA^{4-} + H^{+} \qquad \textbf{Eq. (3-49)}$$

$$H_3PO_4 \overset{K_{a_{H_3PO_4}}}{\Longleftrightarrow} H_2PO_4^{-} + H^{+} \qquad \textbf{Eq. (3-50)}$$

$$H_2PO_4^{-} \overset{K_{a_{HPO_4^{-}}}}{\Longleftrightarrow} HPO_4^{2-} + H^{+} \qquad \textbf{Eq. (3-51)}$$

$$HPO_4^{2-} \overset{K_{a_{HPO_4^{2-}}}}{\Longleftrightarrow} PO_4^{3-} + H^{+} \qquad \textbf{Eq. (3-52)}$$

The hydroxide ions that were provided by potassium hydroxide are respected in Eq. (3-53), which shows the autoprotolysis of water and is an important aspect of any acid-base-reactions in an aqueous solution.

$$H_2O \overset{K_W}{\Longleftrightarrow} H^{+} + OH^{-} \qquad \textbf{Eq. (3-53)}$$

Furthermore, the previously discussed carbon dioxide speciation to bicarbonate and carbonate can provide hydrogen ions which contribute to the decrease in pH as shown in Eq. (3-54) and Eq. (3-55).

$$CO_2 + H_2O \overset{K_{a_{CO_2^{*}}}}{\Longleftrightarrow} HCO_3^{-} + H^{+} \qquad \textbf{Eq. (3-54)}$$

$$HCO_3^{-} \overset{K_{a_{HCO3^{-}}}}{\Longleftrightarrow} CO_3^{2-} + H^{+} \qquad \textbf{Eq. (3-55)}$$

3.3.5.3 Determination of Medium pH

Since the hydrogen ion H^{+} is a part of all equations in Eq. (3-42) - Eq. (3-74), and the concentrations of some substances are present in more than one equation (those of polyprotic acids) the reactions cannot be solved individually with their respective equilibrium constants. A set of linear equations, that links all the equations together, must be derived and solved for the concentration of the hydrogen ion in order to obtain the pH. When the concentration of the hydrogen is known, it can be used to solve the set of linear equations for the concentration of each substance involved.

Overall, the reaction equations Eq. (3-42) - Eq. (3-74) yield the following unknown concentrations:

$$[H^{+}], [OH^{-}], [K^{+}], [Na^{+}], [EDTA], [EDTA^{-}], [EDTA^{2-}], [EDTA^{3-}], [EDTA^{4-}], [CO_2], [HCO_3^{-}], [CO_3^{2-}], [H_3PO_4], [H_2PO_4^{-}], [HPO_4^{2-}], [PO_4^{3-}]$$

Since there are 16 unknown concentrations of involved substances, 16 equations are required to solve the system for the hydrogen ion concentration $[H^{+}]$.

Following the algorithm presented in [92] and adapting it to a larger system, formulating a charge balance is the first step to solving the system and acts as the first required equation. Every unknown concentration listed above goes into the equation once. If the ion has a positive charge it goes on the left of the equation, concentrations of

negatively charged ions are placed on the right. If the ion has more than one negative or positive charge, that goes as a factor in front of the component.

$$[H^+] + [K^+] + [Na^+] = [EDTA^-] + 2 * [EDTA^{2-}] + 3 * [EDTA^{3-}] + 4 * [EDTA^{4-}] + [HCO_3^-] + 2 * [CO_3^{2-}] + [H_2PO_4^-] + 2 * [HPO_4^{2-}] + 3 * [PO_4^{3-}] + [OH^-] \quad \textbf{Eq. (3-56)}$$

The aim is to find an expression for each concentration in the charge balance, which is solely dependent on known values (such as initially added concentrations of a certain substance or the acidity constant) and the hydrogen ion concentration, for which the charge balance should be solved in the end.

Further equations are provided through the mass action laws of all involved substances as shown in Eq. (3-57) - Eq. (3-66).

$$K_{a_{EDTA}} = \frac{[EDTA^-] * [H^+]}{[EDTA]} \quad \textbf{Eq. (3-57)}$$

$$K_{a_{EDTA^-}} = \frac{[EDTA^{2-}] * [H^+]}{[EDTA^-]} \quad \textbf{Eq. (3-58)}$$

$$K_{a_{EDTA^{2-}}} = \frac{[EDTA^{3-}] * [H^+]}{[EDTA^{2-}]} \quad \textbf{Eq. (3-59)}$$

$$K_{a_{EDTA^{3-}}} = \frac{[EDTA^{4-}] * [H^+]}{[EDTA^{3-}]} \quad \textbf{Eq. (3-60)}$$

$$K_{a_{H_3PO_4}} = \frac{[H_2PO_4^-] * [H^+]}{[H_3PO_4]} \quad \textbf{Eq. (3-61)}$$

$$K_{a_{HPO_4^-}} = \frac{[HPO_4^{2-}] * [H^+]}{[H_2PO_4^-]} \quad \textbf{Eq. (3-62)}$$

$$K_{a_{HPO_4^{2-}}} = \frac{[PO_4^{3-}] * [H^+]}{[HPO_4^{2-}]} \quad \textbf{Eq. (3-63)}$$

$$K_{a_{CO_2^*}} = \frac{[HCO_3^-] * [H^+]}{[CO_2]} \quad \textbf{Eq. (3-64)}$$

$$K_{a_{HCO3^-}} = \frac{[CO_3^{2-}] * [H^+]}{[HCO_3^-]} \quad \textbf{Eq. (3-65)}$$

$$K_w = [OH^-] * [H^+] = 10^{-14} \quad \textbf{Eq. (3-66)}$$

Further equations can be obtained by formulating mass balance equations. The concentration of all species of a certain substance in the medium have to come from what was initially added of that substance as shown in Eq. (3-67) - Eq. (3-70). In an open system, the carbon dioxide concentration is a function of its partial gas pressure above the medium and can therefore be easily calculated with the Henry constant in Eq. (3-71).

$$[EDTA] + [EDTA^{-}] + [EDTA^{2-}] + [EDTA^{3-}] + [EDTA^{4-}] = C_{Na_2EDTA_{initial}}$$ **Eq. (3-67)**

$$[Na^{+}] = 2 * C_{Na_2EDTA_{initial}}$$ **Eq. (3-68)**

$$[K^{+}] = C_{KOH_{initial}} + C_{KH_2PO_{4_{initial}}} + 2 * C_{K_2HPO_{4_{initial}}}$$ **Eq. (3-69)**

$$[H_3PO_4] + [H_2PO_4^{-}] + [HPO_4^{2-}] + [PO_4^{3-}] = C_{K_2HPO_{4_{initial}}} + C_{KH_2PO_{4_{initial}}} = C_{phosphate_{total}}$$ **Eq. (3-70)**

$$[CO_2] = H_{CO_2} * p_g(CO_2) = C_{CO_{2_{initial}}}$$ **Eq. (3-71)**

The 16 equations Eq. (3-56) - Eq. (3-71) are sufficient to solve the system for the 16 unknown equations and ultimately calculate the concentration of hydrogen ions and pH. The equations have to be rearranged to only be dependent on known values such as initial concentrations or acidity constants and the hydrogen ion concentration. These expressions can be found in Appendix B.1.

The rearranged expressions can then be integrated into the charge balance Eq. (3-56), terms with equal exponent can be collected and the equation can then be numerically solved for the hydrogen ion concentration. In this case, the final equation is a polynomial of 10th order of the shape shown in Eq. (3-73). Since the actual equation is rather extensive it can be found in the Appendix B.1.

$$a * [H^{+}]^{10} + b * [H^{+}]^{9} + c * [H^{+}]^{8} + d * [H^{+}]^{7} + e * [H^{+}]^{6} + f * [H^{+}]^{5} + g * [H^{+}]^{4} + h * [H^{+}]^{3} + i * [H^{+}]^{2} + j * [H^{+}]^{1} + k = 0$$ **Eq. (3-72)**

Once the hydrogen ion concentration is known through numerical solving, the previously arranged terms representing the species concentrations (which are only dependent on known values and the now known hydrogen ion concentration) can be used to calculate the concentration of each species in the system.

3.4 Photosynthetically Active Radiation Module

Photosynthetically active radiation provides the required energy for the endothermic reactions of the photosynthetic carbon metabolism [38]. Since the transformation of carbon dioxide to biomass is the main purpose of photosynthesis, photosynthetically active radiation – together with carbon dioxide – can be regarded as the backbone of photosynthesis and therefore algal growth.

The photosynthetically active radiation, which plants can use as energy source for photosynthesis, lies within the same wave spectrum of 400-700 nm as the radiation that the human eye can sense as light [7]. However, the term “light” or more precisely “visible light” is defined as the radiation between 400 and 700 nm wavelength, which the human eye can detect [6] and since plants do not receive energy or information through eyes, the term light should not be used when referring to plant research [7]. Despite the fact that the source of photosynthetically active radiation for algal photosynthesis can be seen by the human eye as light, this part of the simulation is not called *Light Module* but *Photosynthetically Active Radiation Module*.

3.4.1 Photosynthetically Active Radiation as Energy Source

The energy an electromagnetic wave carries is a function of its wavelength or frequency. If the electromagnetic waves lie within the boundaries of photosynthetically active radiation, their radiant energy can be absorbed by photosynthetically active organisms where it is transformed to chemical energy stored in biomass-molecules along with heat losses.

3.4.1.1 Radiometric Characterization of Radiation

Since growth is the increase of biomass over time, a defining factor for biomass growth is how much energy in the photosynthetically active radiation band can be provided to a photosynthetically active organism within a time interval to enable growth. The measurement of electromagnetic radiation properties such as energy in Joules and Power in Watts is called radiometry [93].

The rate of energy a radiation source emits per time unit is called radiant flux and is measured in Watts in SI-units. With increasing distance to the source, the radiant flux is spread over an increasingly large area where the incoming radiation per area can be measured as irradiance in Watts per square meter in SI-units. It should be noted that in radiometry and photometry *intensity* actually refers to a property of the radiation source and should not be used for describing the *irradiance* on a receiving surface [7].

3.4.1.2 Quantum Characterization of Radiation

The quantum mechanical concept of particle-wave duality allows to describe electromagnetic radiation either in form of continuous waves or as discrete quanta, which are called photons in this case. In terms of photosynthetically active radiation the description of radiation phenomena with photons is favorable over treating the radiation as a wave [7] and will be used hereafter.

Each photon travels at the speed of light and has an energy that is a function of its wavelength which can be calculated with Eq. (3-73).

$$E_{ph} = \frac{h * c_{light}}{\lambda} \qquad \textbf{Eq. (3-73)}$$

E_{ph} is the photon's energy in J, $h = 6.63 * 10^{-34}\, J * s$ is the Planck's Constant, $c_{light} = 3 * 10^{8}\, m/s$ the speed of light and λ refers to the photon's wavelength in meters.

Similar to the radiometric concept of radiant flux, a radiation source can be regarded as emitting a certain number of photons per time unit, which is called photon flux and measured in photons per second. With increasing distance from the source, this photon flux spreads out over an increasing area where it can be measured as photon flux density, which is equivalent to the radiometric irradiance. Photosynthetic photon flux density is measured as photons per second per square meters. If only the photons from the photosynthetically active radiation band are considered, the photon flux density is called photosynthetic photon flux density and the number of photons is commonly counted in micro moles [94].

3.4.1.3 Conversion of Units

For a mechanistic approach towards biological growth, a photon-based description of photosynthetically active radiation is favorable. However, when considering energy absorption and heat losses, radiometric units are advantageous and the need for conversion between the two arises.

A monochromatic radiation source only emits photons of a single wavelength, which makes the conversion between photon and radiometric units a trivial task as seen in Eq. (3-74).

$$I = \frac{P_m * 10^{-6} * N_A * h * c_{light}}{\lambda} \qquad \textbf{Eq. (3-74)}$$

I is the radiometric irradiance in $[W/m^2]$, P_m the monochromatic photon flux density in $[\mu mol/(m^2 * s)]$, $N_A = 6.022 * 10^{23}$ is the Avogadro Constant, $h = 6.63 * 10^{-34}\, J * s$ is the Planck's Constant, $c_{light} = 3 * 10^8\, m/s$ the speed of light and λ the photon's wavelength in meters.

A polychromatic radiation source emits photons of different wavelengths at the same time. Most sources used to provide photosynthetically active radiation, artificial light sources and daylight are polychromatic as shown in Figure 3-21. A monochromatic radiation source would only be a vertical line at a certain wavelength in this graph.

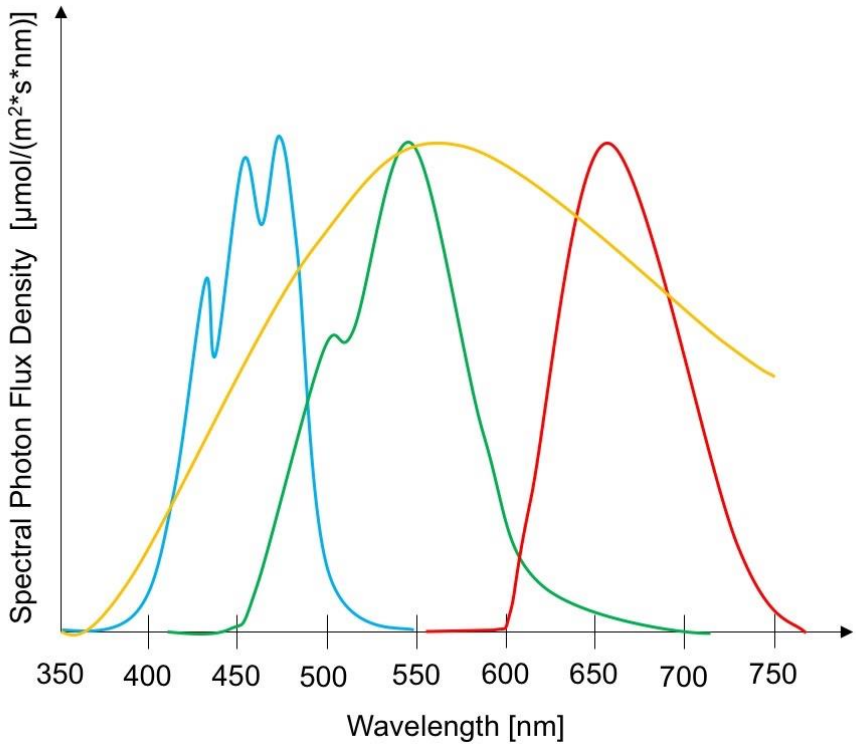

Figure 3-21: Qualitative graph of spectral photon flux density profiles of different polychromatic radiation (in this case light). Blue, green and red lines stand for lights of the respective color (adapted from [95]), the yellow line represents daylight (adapted from [96]).

For a polychromatic radiation source, the transformation of units is more difficult and requires detailed knowledge of the spectral photon flux density profile $P_{T_p}(\lambda)$ and

integration over the photosynthetically active radiation band of 400 to 700 nm as seen in Eq. (3-75). (This is to determine what is relevant to photosynthetic organisms, parts of the profile could lie outside the waveband and would thereby be disregarded.)

$$I = \int_{400*10^{-9}}^{700*10^{-9}} \frac{P_p(\lambda) \ * 10^{-6} * N_A * h * c}{\lambda} \, d\lambda \qquad \textbf{Eq. (3-75)}$$

I is the radiometric irradiance in $[W/m^2]$ and $P_p(\lambda)$ the spectral photon flux density profile in $[\mu mol/(m^2 * s * m)]$.

Since the spectral photon flux profile (which results in a spectral photon flux density profile when measured at a distance of the source) is a unique feature of every radiation source and difficult to measure, the determination of the irradiance of a polychromatic light source is challenging. Further details, conversion formulas and algorithms can be found in [7], [94] and [95].

3.4.2 Photosynthetically Active Radiation Growth Domains

The energy provided through photosynthetically active radiation enables photosynthetically active organisms to metabolize carbon dioxide to biomass and releases oxygen from water.

From a mechanistic standpoint, for each oxygen molecule (O_2) released in the process of photosynthesis, 8 photons are required but realistically a number between 9 and 10 photons is required per oxygen molecule due to inefficiencies. This fact holds true for most photosynthetic organisms from microalgae to vascular plants [2], [42].

When the evolution of oxygen molecules is used as an indicator for photosynthetic activity and photosynthetic biomass growth in general, a relationship between photon availability and growth can be formulated. This relationship is plotted qualitatively in Figure 3-22.

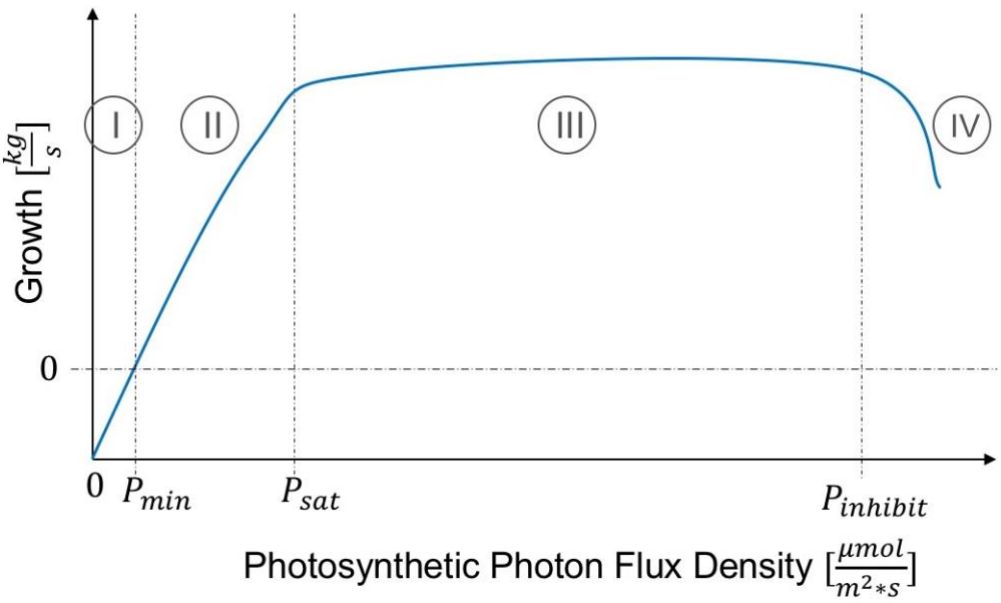

Figure 3-22: Radiation saturation curve of photosynthesis with growth domains. I: respiration, II: linear growth, III: photo-saturated growth and IV: photo-inhibited growth. Adapted from [42].

3.4.2.1 Domain I: Respiration

At a photon flux below the required minimum P_{min}, the available energy is not sufficient to enable photosynthetic growth. The microalgae cultures only respire. In this process, enzymes enable biomass to be oxidized and carbon dioxide to be released from the biomass instead of fixed. This leads to a destruction of biomass or, in other words, negative growth [97].

In fact, this process can be assumed to be independent of the photon flux [47] and therefore continuously occurs while a photosynthetic organism is growing. In high oxygen concentration media [7] and the longer an algal culture is exposed to conditions where not enough energy is provided (e.g. dark conditions), this effect can become more significant when looking at overall growth [98].

3.4.2.2 Domain II: Linear Growth

When more than the minimum photon flux P_{min} is provided, growth rises linearly with the provided photosynthetically active radiation power. This domain is hence called the linear growth domain.

In the linear growth domain, radiation energy absorption and radiation energy related photosynthetic reactions are the limiting factor on photosynthetic growth and the growth is therefore light-limited [42]. This behavior can be pictured as a number of cells in a two-dimensional microalgae culture that all require a certain number of photons to fix a carbon dioxide molecule. Until every algal cell is provided with enough photons to perform photosynthesis, the growth potential of the entire culture is not fully exploited.

3.4.2.3 Domain III: Saturation

The linear behavior of photosynthetic growth is limited to a certain range of photon flux values and stops at the saturation photon flux P_{sat}. From this point onward, the growth does not increase any further with increasing photon flux and is therefore called the saturated growth domain.

While absorption and transformation of photosynthetically active radiation power are the limiting factors in the linear growth domain, this is not the case here since enough energy per time unit is now available to allow all cells in the culture to grow. However, the (endothermic) chemical reactions that are enabled by the absorbed energy require a certain time to complete and therefore limit the growth in the saturated growth domain. Most prominently, the carbon reactions (slow enzyme catalysis) and electron transfer are limiting the growth [42].

Consequently, a two-dimensional microalgae culture with a photon flux density higher than saturation penetrating its surface could be regarded as energy-inefficient since the additional photons only generate heat and do not contribute to photosynthetic growth. However, when regarding the culture as a three-dimensional volume, a surface irradiated above saturation can have a positive effect on the overall growth of the culture volume. Photons become absorbed and scattered by the layers of algal cells close to the surface and shadow the lower lying cells. If more photons than required for the top-most layer are available, they can penetrate deeper into the volume and enable growth in deeper lying cells despite absorption and scattering [42]. This behavior becomes increasingly important in dense algal cultures and is discussed in more detail in 3.4.4.

3.4.2.4 Domain IV: Photoinhibition

Increasing the photon flux well above P_{sat} will cause a rapid drop in growth and eventually fatal damage to the algal culture. The point at which these effects start is called inhibition point $P_{inhibition}$ and this domain of algal growth is therefore called photoinhibited domain.

When exposed to photon flux beyond $P_{inhibition}$, the photosynthetic activity is photoinhibited which results in a rapid decrease in growth. Some parts of the photosynthetic apparatus (e.g. the photosystem II) are sensitive to strong irrandiances and therefore the weak part of photosynthesis with regard to high photon flux [43]. Photoinhibition is a protective measure of the photosynthetic organism to prevent photosynthesis happening at a rate that would trigger a damagingly high electron transfer [2].

When all growth is inhibited, and the photon flux is further increased, photooxidation (also called pigment bleaching) occurs, which results in irreversible cell damage and death. Irradiance levels beyond the inhibition point should therefore be avoided, especially for extended periods of time [99].

3.4.3 Optimum Wavelength within the Photosynthetically Active Radiation Band for Chlorella Vulgaris cultivation

Photons of the photosynthetically active radiation waveband can be absorbed by Chlorella vulgaris' radiation receptors carotenoids and chlorophyll a and b. Carotenoids can absorb photons of the whole photosynthetically active radiation spectrum and are passed on as energy to chlorophyll a and b in the photosystem II and I, where they are transformed to chemical energy in the process of photosynthesis [79]. However, since chlorophyll a and b can absorb radiation energy and directly transform it to chemical energy, the blue and red wavelengths, which can be directly absorbed by these pigments, are more efficient for microalgal growth [79].

In the case of Chlorella vulgaris, radiation of 680 nm is most suitable to achieve high biomass concentrations with the least electrical energy usage [55]. Radiation in this waveband is perceived as the color red by the human eye. It should be noted that different radiation wavelengths can yield a different macromolecular composition (proteins, carbohydrates) of Chlorella vulgaris cells [79].

For energy-efficient growth of a culture with a high biomass concentration, providing radiation only in the most growth-efficient wavelength is necessary. Due to their narrow bandwidth, with close to monochromatic behavior, low energy consumption compared to other sources, high reliability and longer life-span, light emitting diodes are the most suitable radiation sources [100].

3.4.4 Energy Attenuation in Microalgae Cultures

At high biomass concentrations, cells further away from the irradiated surfaces receive less light due to photon absorption from higher lying cells and scattering of photons. The combined effects of absorption (uptake of photons into matter), refraction and scattering are called attenuation, which describes the gradual loss of photon flux density while photons are passing through a medium [101].

3.4.4.1 Photon Absorption and Non-Photochemical Quenching

The cells in top layers absorb more photons than they can use for photosynthesis or can even be photoinhibited. They release the excess energy through a process called non-photochemical quenching. This energy, which dissipates into the medium as heat, cannot be used for photosynthesis by other cells and is the most important reason for reduced efficiency and algal culture productivity [42].

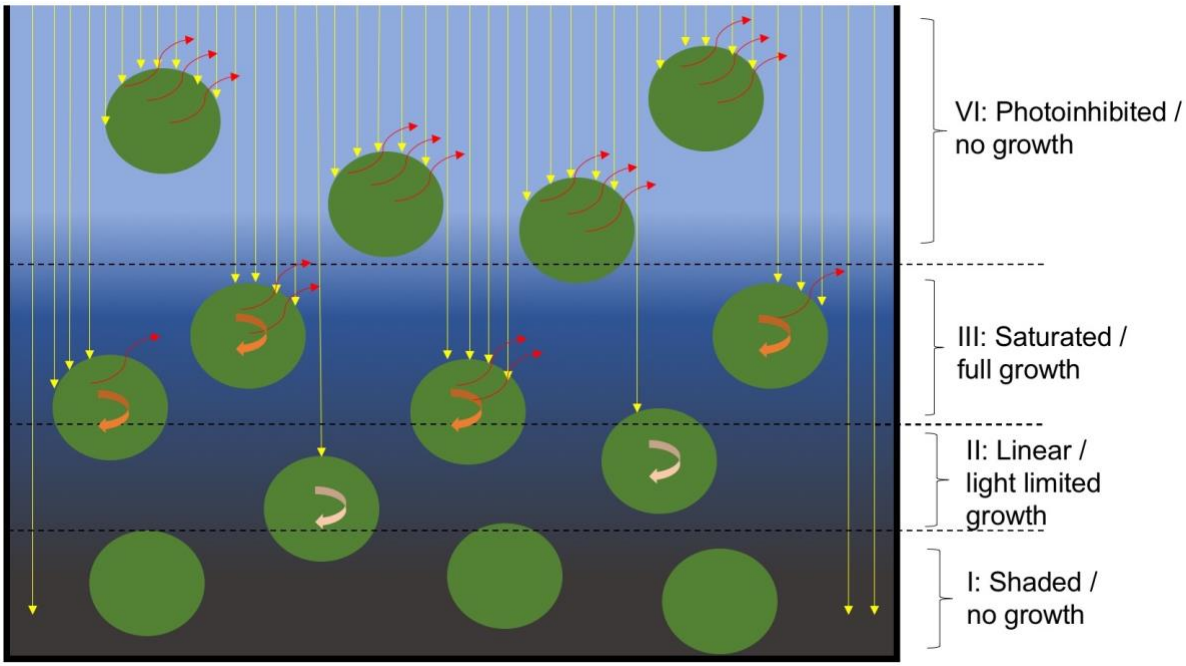

Figure 3-23: Over-absorption of photosynthetically active radiation (yellow arrows) by microalgae (green circles) and heat-loss due to non-photochemical quenching (red arrows) lead to spatially separated growth domains in the culture volume. Orange arrows in the cells indicate full growth, light colored arrows indicate limited growth. Inspired by [42].

3.4.4.2 Radiation Attenuation in Microalgae Cultures

When considering absorption of photons not as a chemical cellular property but as an optical property of a medium, the concept of radiation attenuation becomes of importance. Attenuation describes the loss of photon flux through a medium due to absorption and scattering [102] as a function of the medium's optical density properties, the radiation's pathway through the medium and radiation wavelength [95].

Knowing the photon flux at the irradiated surface of the culture medium P_0 and assuming no surface reflection, the photon flux P at any point L below the surface of the medium can be calculated with Eq. (3-76) [95].

$$P = P_0 * e^{-L*A(\lambda,\rho_b)} \qquad \textbf{Eq. (3-76)}$$

P is the photon flux in $[\mu mol/(m^2 * s)]$ at any point L below the surface, P_0 is photon flux at the surface of the culture medium in $[\mu mol/(m^2 * s)]$, L is any point inside the culture medium below the irradiated surface in $[m]$ and $A(\lambda, \rho_b)$ is the wavelength/radiation source and biomass concentration dependent attenuation coefficient in $[1/m]$.

The attenuation coefficient characterizes the mediums absorption and scattering properties with regard to the traversing radiation. For an algal culture medium, it is primarily dependent on the wavelength (monochromatic) or radiation source (polychromatic) and biomass concentration and therefore has to be recalculated each time one of these parameters change. However, different models can be used to determine the attenuation coefficient as a function of biomass concentration [95]. Three models, along with experimental data points are shown in Figure 3-24.

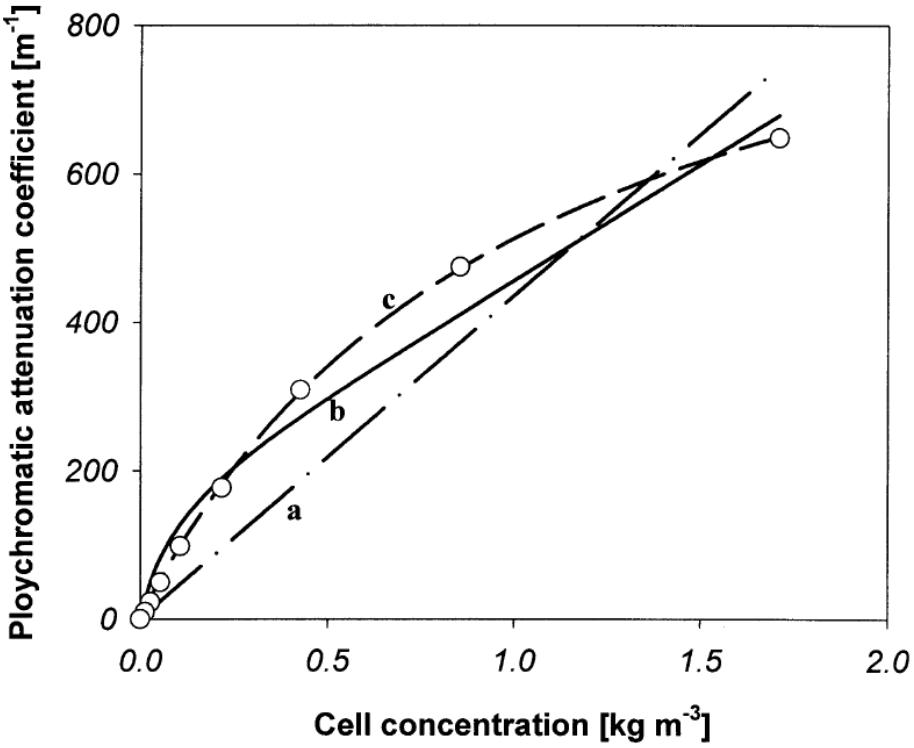

Figure 3-24: Different models to characterize the attenuation coefficient $A(\lambda, \rho_b)$ as a function of biomass concentration (called cell concentration in the graph) for daylight. The linear Beer-Lambert model is line a, the Cornet-model is line b and the empirical hyperbolic model is line c. Experimental data points are included as circles. Graph copied from [95].

The linear Beer Lambert model is the simplest one and rises linearly with cell density. However, this model is not applicable to heterogenous solutions such as an algal solution. A better fit to the actual behavior is the mechanistic Cornet model. It considers absorption and scattering but also cannot predict the behavior of the experimental data perfectly. The best fit can be achieved through a hyperbolic model which is derived from the experimental data. The drawback of an empirical approach is the lack of mechanistic representation of the physical effects that cause the light attenuation [95].

The hyperbolic model allows to calculate the attenuation coefficient with Eq. (3-77) [95]:

$$A(\lambda, \rho_b) = \frac{A_{max}(\lambda) * \rho_b}{b(\lambda) + \rho_b} \qquad \textbf{Eq. (3-77)}$$

$A_{max}(\lambda)$ is a radiation source dependent empirical maximum attenuation coefficient in $[1/m]$ and $b(\lambda)$ is a radiation source dependent empirical constant. Values for the

parameters of the hyperbolic model for different radiation / light sources are given in Table 3-8.

Table 3-8: Empirical Parameters for different radiation sources. Data and Table copied from [95].

Parameter	Red	Yellow	Green	Blue	Daylight
$\boldsymbol{A_{max}(\lambda)}$	1283	1025	945.6	1719	1041
$\boldsymbol{b(\lambda)}$	1.36	1.04	0.92	1.79	1.03

When the hyperbolic model is used to calculate the attenuation coefficient of daylight, which penetrates the surface of the earth at around $P_0 = 2000\ \mu mol/(m^2 * s)$, it would reach to a depth of around $L = 1\ cm$ in a pond with an algal culture of $\rho_b = 1\ kg/m^3$. A graph of the light attenuation can be seen in Figure 3-25.

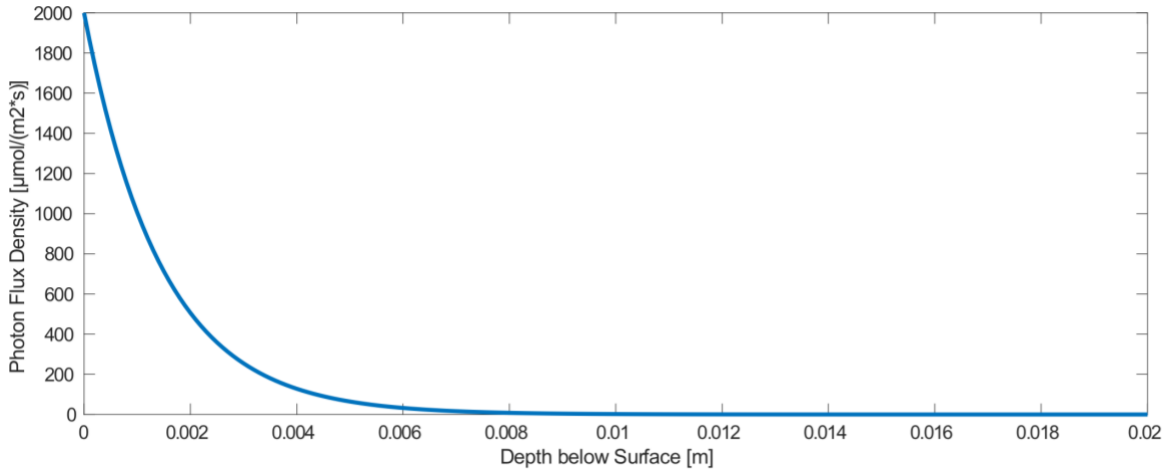

Figure 3-25: Light attenuation below the surface of an algal pond irradiated by sunlight. Points that mark the boundaries of the growth domains (generic values) are indicated as dashed lines.

3.4.5 Spatial Separation of Growth Domains in Photobioreactors

Due to radiation attenuation, the growth regimes described in 3.4.2 are not just a function of different surface irradiances but can also exist in a spatial dimension perpendicularly inward from the surface of a photobioreactor. While top layers of the medium can receive too much radiation and are therefore inhibited from growing, lower layers can show saturated and linear growth. Even further away from the surface, there might be too little radiation power to support growth at all. For example, a medium with a culture depth of 10 mm could be photoinhibited until a depth of 2 mm, saturated until a depth of 5 mm, show linear radiation-growth behavior between 5 mm and 8 mm and be below the minimum photon flux density between 8 mm and 10 mm.

Not all of the four growth domains have to exist in a culture volume at all times. The inhibited growth area can only exist, if the algae's inhibition point lies below the surface photon flux and the saturated zone only if it is above the algae's saturation point. In early phases of culture growth, the biomass concentration is low and most radiation can pass through, which leads to all of the culture being similarly irradiated, possibly inhibited if the surface irradiance is too high. At higher cell densities all four growth zones can exist in the medium at the same time but are spatially separated. A visual

comparison of a low, medium and high biomass concentration medium is shown in Figure 3-26.

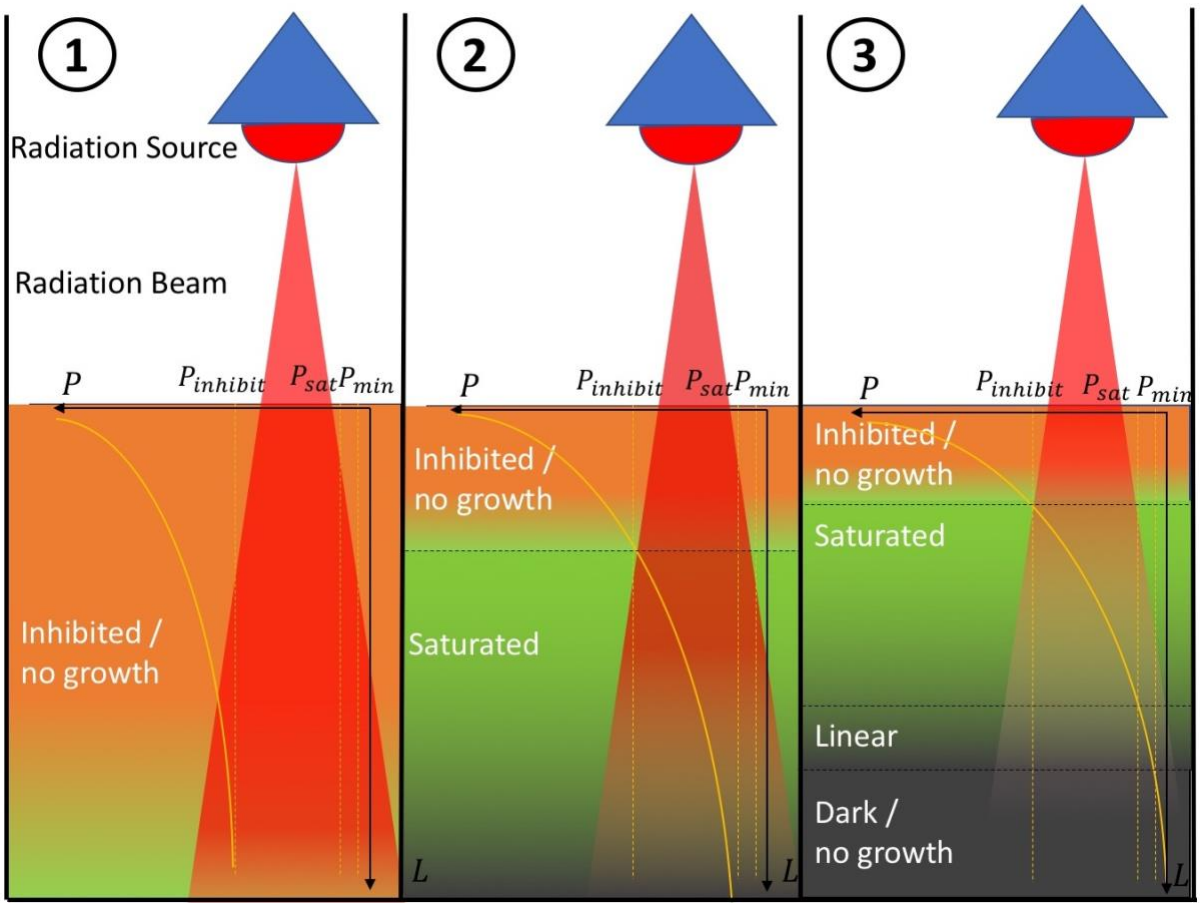

Figure 3-26: Comparison of light attenuation and resulting spatially separated growth zones in a photobioreactor for 1: low biomass concentration, 2: medium biomass concentration, 3: high biomass concentration. Photon flux at the surface is assumed to be higher than the algal specie's inhibition photon flux. Photon flux as a function of depth is shown in the overlaid graph.

For all three configurations shown in Figure 3-26, the radiation source irradiates the surface with the same photon flux, which lies above the algae's inhibition photon flux $P_{inhibit}$. At low biomass concentrations (1), only a small fraction of the surface radiation is attenuated as it is transmitted through the medium and the entire reactor is irradiated above $P_{inhibit}$. At higher biomass concentrations (2), enough light is attenuated in layers close to the surface, so a saturated growth domain can exist in the reactor volume. At very high concentrations (3), all the surface photon flux is attenuated in the reactor's volume as it is transmitted and all four growth domain exist.

The radiation profile in the saturated growth volume is not of much interest, since the growth rate is not dependent on the availability of radiation in this domain. However, it is important in the linear growth domain, since the growth rate of the algae rises linearly with the availability of photon flux density in this domain (see 3.4.2.2). The average availability of photon flux density in the linear growth domain is therefore calculated by integrating the attenuation function over the boundary positions of the linear growth domain and dividing it by its thickness as shown in Eq. (3-78).

$$P_{avg_{lin}} = \frac{1}{L_{min}-L_{sat}} * \int_{L_{sat}}^{L_{min}} P_0 * e^{-L*A}\, dL \qquad \textbf{Eq. (3-78)}$$

In the above equation $P_{avg_{lin}}$ in $[\mu mol/(m^2 * s)]$ is the average photon flux density in the linear growth domain, L_{min} in $[m]$ the position of the lower end of the linear growth domain, L_{sat} in $[m]$ the position of the upper end of the growth domain and P_0 in $[\mu mol/(m^2 * s)]$ the surface photon flux density.

Attenuation is not linear but exponential with depth. As a consequence, a very thin linear growth domain (photon flux density does not reach the minimum photon flux density before exiting the photobioreactor at the bottom), has a higher average photon flux density than a thick one (extending all the way to the minimum photon flux density) and can therefore grow at a higher rate. A thick linear growth volume is therefore disproportionately more disadvantageous than a small one, since the growth rate does not decrease linearly but exponentially with the growth domain's thickness/depth.

In order to achieve highest algal productivity and energy efficiency, the photobioreactor's entire volume should be growing in the saturated growth domain with its base being irradiated at the saturated growth domain's lower boundary P_{sat} (whole volume in saturated radiation growth domain but not wasting energy).

In order to adapt to an increasing biomass concentration, a variable irradiance is advantageous for energy efficiency. When the photobioreactor's base starts to be shaded due to attenuation, the photon flux density at the surface has to be increased in order for the photobioreactor to remain in the saturated growth zone. A limit is reached, when the surface is irradiated with $P_{inhibit}$. Any further increase will lead to an increasingly large inhibition domain at the top or, with a constant surface photon flux, to decreasing saturation and linear domains.

3.4.6 Efficiency of Photosynthetic Energy Conversion and Heat Generation

Considering the effects of non-photochemical quenching, refraction and scattering, the question arises, what fraction of the penetrating number of photons is actually utilized for photosynthesis and what fraction is transformed to heat energy.

The best conversion efficiency of solar energy to biomass η_{solar} is achieved in the linear growth domain [42]. Despite the high energy conversion efficiency of growing algae in the linear domain, operation of a photobioreactor in the linear domain is not feasible since it would not be volume and mass efficient.

Literature values and observations on the overall conversion efficiency vary but are in the same order of magnitude. Sources state conversion efficiencies as low as 3-5% [46] or 3-10% [103] for Chlorella vulgaris, others list 6% [104] and 8-10% [42] and another source states that microalgal cultivation can achieve an overall conversion efficiency of 10% [44]. These values indicate that only 3-10% of the attenuated photons are used for photosynthesis and the rest is transformed to heat energy.

The flux of attenuated photons P_{att} in $[\mu mol/(m^2 * s)]$ can be calculated with Eq. (3-79) by comparing the surface irradiance P_o in $[\mu mol/(m^2 * s)]$ with the photon flux density P_{exit} in $[\mu mol/(m^2 * s)]$ leaving the culture volume on the opposite side of a photobioreactor's irradiated surface. This can either be done by measuring the exit photon flux density or by calculations with Eq. (3-76) where the length L is set to be the entire depth below the photobioreactor's surface. In dense cultures, likely no

photons leave the volume and therefore the entire photon flux at the surface is attenuated and either used for photosynthesis or transformed to heat.

$$P_{att} = P_o - P_{exit} \qquad \textbf{Eq. (3-79)}$$

Of the attenuated photon flux density, depending on the solar conversion efficiency η_{solar} only 3-10% are used for photosynthesis and the other 97-90% are transformed to a heat photon flux density P_{heat} in $[\mu mol/(m^2 * s)]$.

$$P_{heat} = P_{att} * (1 - \eta_{solar}) \qquad \textbf{Eq. (3-80)}$$

The generated heating power $\dot{Q}_{PAR}$in $[W]$ entering the culture medium depends on the energy of the penetrating photons and therefore their wavelength or frequency as shown in Eq. (3-73). The heating power $\dot{Q}_{PAR}$in $[W]$ of the absorbed photon power can then be calculated with Eq. (3-81) by multiplying the absorbed photon flux power with the surface area A_o in $[m^2]$ of the irradiated surface.

$$\dot{Q}_{PAR} = P_{heat} * \frac{h * c}{\lambda} * A_o \qquad \textbf{Eq. (3-81)}$$

Depending on the heat capacity c_p in $[J/K]$ and mass m in $[kg]$ of the medium, the heating power $\dot{Q}_{PAR}$ in $[W]$ leads to a temperature increase ΔT in $[K]$ over time Δt in $[s]$ that can be calculated with Eq. (3-82).

$$\Delta T = \frac{\dot{Q}_{PAR} * \Delta t}{m * c_p} \qquad \textbf{Eq. (3-82)}$$

Since algae react sensitively to high temperatures, high density cultures, in which a lot of the penetrating light is attenuated and transformed to heat, must be cooled in order to keep the culture alive.

4 Implementation of Chlorella Vulgaris Model in V-HAB

The scientific relations and mechanisms of the dynamic algae model, as previously described in chapter 3, are implemented in the virtual habitat simulation tool V-HAB. This spacecraft life support system simulation tool allows further integration of the dynamic algae model into a higher-level cabin environment, which is presented in chapter 6.

This chapter introduces the used simulation tool V-HAB in 4.1, presents the general functionality and architecture of the dynamic algae model in 4.2 and then describes the various calculation modules of the dynamic algae model in the following sub-chapters 4.3 - 4.6.

The four sub-chapters about the calculation modules 4.3 - 4.6. introduce no new effects but should be regarded as an extensive guide to future users of the algae model. For readers not concerned with the specific V-HAB implementation, only reading chapters 4.1 and 4.2 will provide sufficient information about the model.

4.1 The V-HAB Life Support System Simulation Tool

The Virtual Habitat (V-HAB) is a dynamic life support system simulation tool that has been under development at the Institute of Astronautics at the Technical University of Munich since 2006. In a collaborative effort of PhD, Master and Bachelor students, the MATLAB based simulation system has been continuously expanded and now allows detailed simulations of individual life support system technology components to large systems like the International Space Station [4].

V-HAB was specifically designed to eliminate average-based estimations of a life support system (e.g. the Equivalent System Mass methodology) and rather model them from a mechanistic background, detailing the actual behavior. Following this bottom-up design philosophy, the simulations are based on the flow and property changes of matter represented by a stoichiometric composition [4].

The simulated matter can be stored in and moved between different phases and stores by physics-based solvers, which are available at different levels of detail for simulation time concerns. Furthermore, matter processors are available to change the phase (e.g. evaporation) or even the composition of mass from one matter to another (e.g. chemical reactions). Individually definable and automatically adaptable time-steps for all involved components allow fast simulation of (near) steady-state behavior and high resolution depiction of transient processes [4]. This fact makes V-HAB well suited for large system simulations, which are based on high-detail individual processes, such as the detailed algae model, which is based on stoichiometric chemical reactions and is integrated into a large context of a simulated spacecraft cabin.

Various components of different areas of life support system technologies (carbon dioxide removal, oxygen production, water processing) are available and can be combined to an overall system. Furthermore, a human model is available that can be integrated in the system for human-in-the-loop simulations, as is done in this thesis. Further information on the used human model is given in 6.2.2.2.

4.2 Dynamic Algae Model Implementation Overview

The model can be viewed and described from two perspectives. One perspective can describe the succession of calculation steps within a time step, another perspective can look at the overall architecture from the matter-based V-HAB framework. This subchapter therefore initially describes what the model does by explaining the calculation mechanism and then shows how it does that in the V-HAB framework.

4.2.1 Calculation Mechanism

Since the algal growth, as a consumer of carbon dioxide and oxygen as its photosynthetic product, is what determines the reactor's quality as a life support system the calculation mechanism is explained here with special focus on the growth rate calculation. A schematic overview is shown in Figure 4-1.

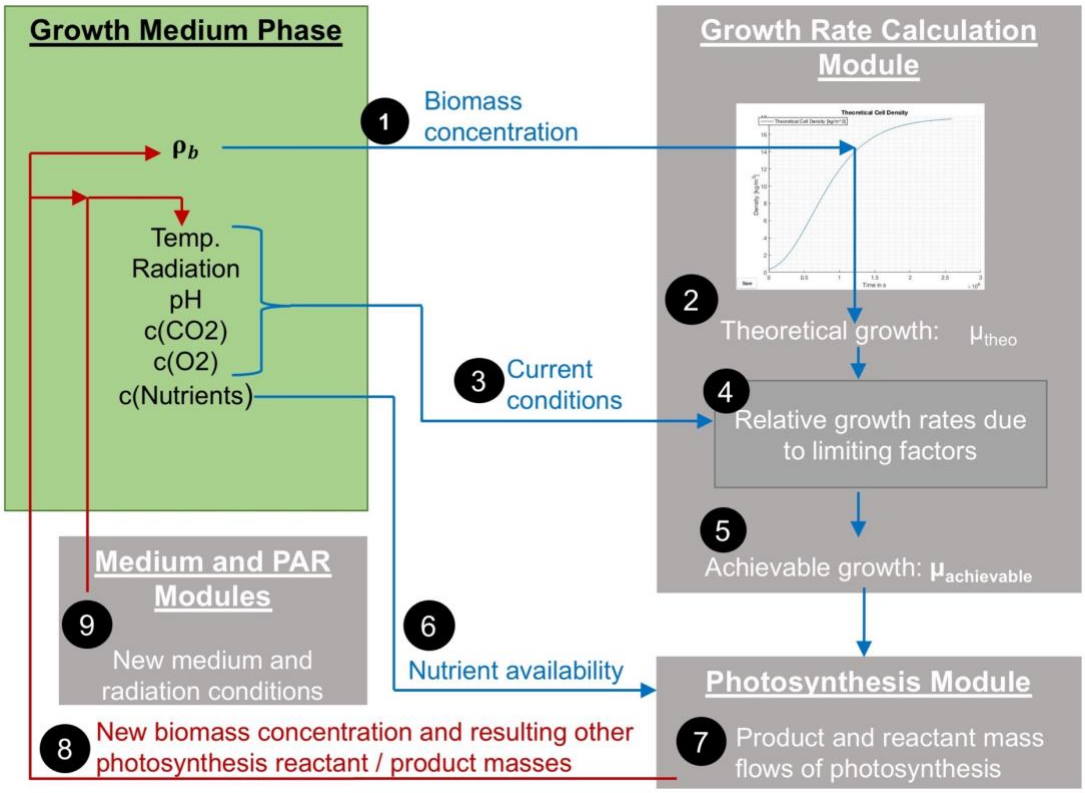

Figure 4-1: Calculation mechanism of changes in the dynamic algae model. Numbers in black circles show the succession of calculation steps. Blue arrows indicate the passing of an information to a next calculation step, red arrows indicate passing of information that directly influences the growth medium and algal culture.

The current biomass concentration in the growth medium phase (1) serves as baseline to determine the current optimum growth rate (2). The growth calculation module then gathers the current condition in the medium of those factors that could limit the growth (3), which are used in the next steps to calculate the relative growth rates for the limiting factors (4). By multiplying the relative growth rates, which represent how close the growth rate can be to the optimum when influenced by limiting factors, the achievable growth rate is calculated (5).

From the growth rate calculation module, the achievable growth rate, which is the optimum growth rate decreased through the influence of growth limiting factors, is passed to the photosynthesis module. The photosynthesis module determines the availability of all reactants for the photosynthetic growth, also referred to as nutrients (6). Based on the achievable growth rate and availability of nutrients, the actual growth rate is determined and then used in the stoichiometric reaction equations (nutrient and Chlorella stoichiometry dependent) to calculate the masses of all photosynthesis reactants and products (7). These masses are then passed back to the growth medium phase, where the masses are changed accordingly (8).

In the meantime, the growth medium module calculates changes that happen in the growth medium, such as gas exchange with the atmosphere or the speciation of substances due to a changed pH (9). Furthermore, the photosynthetically active radiation module recalculates the positions of the growth domains based on the increased biomass concentration (9).

4.2.2 V-HAB Model Architecture

From a V-HAB perspective, the model is implemented in the Chlorella in Media system, which holds a matter store with two phases, matter processors for phase and matter changes and calls calculation classes, the so-called modules, where the behavior of all the algal growth and medium related processes is determined. A sketch of the system, the V-HAB modelling classes (stores, phases, matter processors and flows), calculation modules and selected information flows is shown in Figure 4-2.

The Chlorella in Media system comprises one Growth Chamber store with the Air flow phase and the Medium mixture phase. A manipulator is integrated in the medium phase and is responsible for the matter changes due to photosynthesis and chemical reactions. Two phase to phase processors – one for oxygen and one for carbon dioxide – simulate the membrane transport according to Henry's law. Furthermore, matter branches interface with the photobioreactor parent system, once the model is integrated into it (see chapter 6).

Calculation modules (as outlined in the previous chapter 3) are the actual backbone of the simulation of algal growth and all related medium changes and matter transports. In these modules the physical, chemical and biological mechanisms defining and affecting algal growth are implemented.

The four calculation modules interface with each other and the matter processors in order to enable the simulation of a dynamic behavior. While all of the modules use information (mainly matter properties such as temperature or composition) from one or both of the two phases in the growth chamber store, they are also linked among each other.

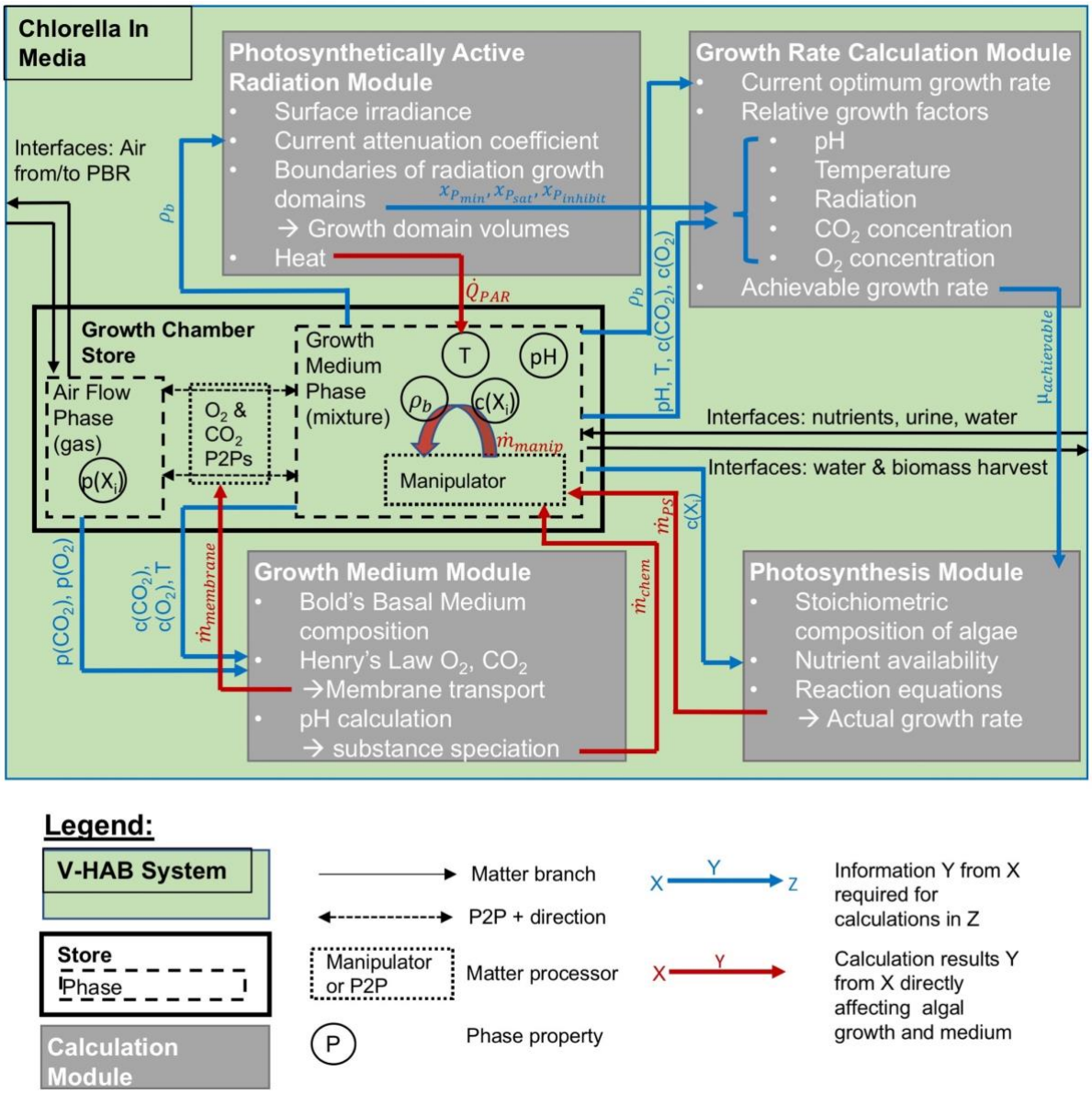

Figure 4-2: System sketch of the dynamic algae model with the V-HAB modelling classes (stores, phases matter flows and processors), calculation modules, and selected information flows.

4.3 Growth Rate Calculation Module Implementation

The growth rate calculation module determines the optimum biomass concentration increase rate depending on the current biomass concentration in the medium and calculates relative growth rates for potentially limiting factors (temperature, pH, availability of photosynthetically active radiation, concentrations of oxygen and carbon dioxide). When the potentially limiting relative growth rates are multiplied with the optimum biomass concentration increase rate the achievable growth rate is calculated (after the biomass concentration increase rate was multiplied with the culture volume to yield a mass growth rate).

The module is implemented as a V-HAB base child class and initially called and stored as an object in the Chlorella in Media system. It comprises the biomass concentration increase rate calculation based on the Gompertz growth model parameters, calls

further classes and instantiates objects responsible for the relative growth rates of the limiting factors, and determines the achievable mass growth rate.

The growth model parameters can be entered in the growth rate calculation module's class constructor to enable the simulation of different growth behaviors. The class constructor also calculates the initial Chlorella biomass based on the growth parameters and current culture volume. Furthermore, the biomass concentration increase rate is derived to find the biomass concentration where it has its maximum. This maximum growth biomass concentration is passed back to the photobioreactor parent system to establish the set point for the harvester. Additionally, the calculation mechanism for the achievable mass growth rate can be defined to be based on a multiplicative or minimum threshold model here.

The update function of the growth module class calls three separate functions in the same class that update the theoretical optimum growth rate (see 4.3.1), call the update functions in the stored objects calculating the relative growth rates of the limiting factors (see 4.3.2) and finally the function to calculate the achievable mass growth rate (see 4.3.3).

4.3.1 Theoretical Optimum Growth

The Gompertz Model, as introduced in 3.1.1 is used to calculate the theoretical optimum biomass concentration increase rate.

During the lag time, the time dependent form is used as introduced in 3.1.1.1, since this is a time-dependent behavior. After the lag time, the biomass concentration increase rate is not time dependent anymore and is calculated with its biomass concentration dependent form as introduced in 3.1.1.2.

Since this calculation yields a biomass concentration increase rate, it is multiplied with the culture volume to yield a mass growth rate.

4.3.2 Limiting Factors

The theoretical optimum growth rate is multiplied with relative growth rate factors [μ/μ_{opt}] which represent the deviation the achievable growth rate has from its optimum. These factors are calculated in separate classes' update functions, which are called and instantiated as objects stored in the growth rate calculation module. The behavioral mechanisms of these growth limiting factors can be changed in the individual classes without having to change anything else in the model. The only thing that has to remain consistent with the current implementation is the output of a relative growth factor between 0 and 1.

All of the relative growth rates range between 0, which represents a total inhibition of growth to 1, which means that the growth is not limited by this factor.

4.3.2.1 Temperature

The temperature influence class's class constructor allows the definition of the upper and lower extreme boundaries beyond which no growth is possible, and of the temperature influence curve. In two separate vectors, temperature data points can be entered with corresponding relative growth rates, which should be 0 at the extreme lower and upper boundary and 1 around the optimum growth rate. The data is then

automatically approximated with the MATLAB curve fitting tool to create a 4th order polynomial curve, which represents the growth rate with varying medium temperature. The currently implemented behavior follows that introduced in 3.1.2.1 shown in Figure 3-6.

The update function of the temperature influence class calculates the current relative growth rate as a function of medium temperature. The relative growth rate is set to 0, if the medium temperature is below the lower or above the upper extreme temperature limit and follows the behavior defined in the class constructor. If the upper extreme temperature boundary is exceeded, a Boolean parameter is set to true, which indicates that the culture is dead. This parameter is passed back to the growth calculation module along with the relative growth rate and prevents any further growth from happening.

4.3.2.2 pH

The boundaries of the pH relative growth depend on the growth medium temperature, as presented in 3.1.2.2. The pH influence class constructor allows the vectoral definition of the temperature dependent behavior of the pH boundaries. The data is automatically approximated with the MATLAB curve fitting tool to create four 3rd order polynomial curves, which represents the upper and lower boundaries beyond which no growth can occur and the upper and lower boundaries between which the optimum growth can occur. The currently implemented behavior follows that introduced in 3.1.2.2.

The update function of the pH influence class initially calculates the current 4 boundary points of the pH growth curve, based on the 4 polynomials created in the class constructor. Since these curves are only valid between the upper and lower extreme boundaries, the relative growth is automatically set to zero when the current growth medium pH is outside of these boundaries. Otherwise as a function of the current growth medium pH, the relative growth rate rises linearly from 0 to 1 between the extreme lower and lower boundary of optimum growth, remains at 1 between the lower and upper boundary of optimum growth and falls linearly to 0 between the upper boundary of optimum growth and the upper extreme boundary.

4.3.2.3 Photosynthetically Active Radiation Limitation

The photosynthetically active radiation limitation class is closely linked to the photosynthetically active radiation module, from which it retrieves calculation results.

The update function initially calls the photosynthetically active radiation module to calculate the positions below the reactor surface, where the boundary points of the radiation saturation curve are reached. These positions are calculated depending on the current biomass dependent attenuation coefficient (e.g. culture depth of 10 mm: inhibited until 2 mm, saturated until 5 mm, linear until 8 mm dark beyond 8 mm). These positions are then used to calculate the volumes of the sub-minimum, linear, saturated and inhibited growth domains, which have to add up to the total culture volume. These volumes are passed back to the photosynthetically active radiation limitation object.

For each of these four volumes, the relative growth rate is calculated. For the no-growth volume (irradiated below minimum photon flux density and above inhibition photon flux density), the relative growth rate is 0. For the saturated growth domain volume, the

relative growth rate is 1. In the linear growth domain, the relative growth rate is determined by relating the current average photon flux in this zone, which is obtained from the photosynthetically active radiation module, to the saturation photon flux density, as defined in the photosynthetically active radiation module.

The overall relative growth rates due to photosynthetically active radiation limitation is comprised of the three relative growth rates from the growth domains (no, linear and saturated growth). Each of the volume's growth factors is weighted with the relation of how much the respective growth domain volume takes up of the total culture volume as presented in 3.1.2.3.

The overall relative growth factor due to photosynthetically active radiation limitation is then passed back to the growth calculation module.

4.3.2.4 Oxygen

The oxygen concentration influence class constructor allows the vectoral definition of the maximum equivalent partial pressure of oxygen (more information on equivalent partial pressures of substances in a liquid, see 3.3.2.2) at which the optimum growth can occur (i.e. below which growth is not limited) and to what level the relative growth rate falls at 100 kPa partial pressure.

The update function calculates the current equivalent partial pressure of oxygen in the medium by using information from the Henry's law oxygen phase to phase processor, which is part of the growth medium module. It then calculates the relative growth rate depending on the behavior entered in the class constructor. Mathematically, the relative growth rate could fall to below zero when it is high above the maximum partial pressure due to its linearly decreasing behavior. For this reason, a check is implemented, which allows 0 as the lowest relative growth rate. Currently the second behavior outlined in 3.1.2.5 is implemented.

4.3.2.5 Carbon Dioxide

The carbon dioxide influence class constructor allows the vectoral definition of the maximum equivalent partial pressure of carbon dioxide (more information on equivalent partial pressures of substances in a liquid, see 3.3.2.2) at which the optimum growth can occur (i.e. below which growth is not limited) and to what level the relative growth rate falls at 100 kPa partial pressure. It is important to note, that this limitation is not due to the absence of carbon dioxide as a nutrient for photosynthesis, but due to high concentrations, which can also limit algal growth, see 3.1.2.6.

The update function calculates the current equivalent partial pressure of carbon dioxide in the medium by using information from the Henry's law carbon dioxide phase to phase processor, which is part of the growth medium module. It then calculates the relative growth rate depending on the behavior entered in the class constructor. Mathematically, the relative growth rate could fall to below zero when it is high above the maximum partial pressure due to its linearly decreasing behavior. For this reason, a check is implemented, which allows 0 as the lowest relative growth rate. Currently the behavior outlined in 3.1.2.6 is implemented.

4.3.3 Achievable Growth

Depending on the specification in the class constructor, the achievable growth rate is calculated by multiplying all of the relative growth rates with the optimum growth rate (multiplicative), or only with the most limiting one (minimum threshold model). The achievable growth rate is a mass growth rate [kg/s], which is called by the photosynthesis module. Both models are available to select from, the multiplicative model is used for simulations in this thesis, since small deviations are expected and these should all be respected.

4.4 Photosynthesis Module Implementation

The photosynthesis module calculates the changes due to the algal growth rate as determined by the growth calculation modules. The mass flows are calculated based on the stoichiometric growth equations for different sources of nitrogen.

The module is implemented as a V-HAB base child class and initially called and stored as an object in the Chlorella in Media system. It comprises an update function that governs the stoichiometric growth reactions and separate functions to simulate the growth on nitrate and urine. The update function is called by the growth medium changes substance manipulator in the growth medium phase.

The class constructor allows to change the stoichiometric relations of the growth equations. However, these reactions only change, if the algal composition changes, and therefore the matter table also has to be updated for a new molar mass if other algal compositions and resulting reactions should be used. The V-HAB human model does not contain any urea in its urine, but rather *urine solids*, which represent an average composition of the solid matter diluted in urine. The urine solids are similar to the composition of urea but have an additional COH_2 group attached. Currently, urine solids are treated to be metabolized like urea and the COH_2 group is left behind in the medium. This has to be respected in the stoichiometric reactions. Currently, the uptake of phosphorus is not modelled in the equations, since the V-HAB human model does not contain phosphorus in its urine.

As a first calculation step of this module, the mass growth rate from the growth rate module is translated to a molar growth rate based on the relative molar mass of Chlorella vulgaris cells in the V-HAB matter table. This is required since stoichiometric reactions are based on molar relations and all calculations in this module are based on these reaction equations.

The availability of nitrogen sources in the media is checked thereafter. When both nitrate and ammonium/ammonia are available in the growth medium, algal cells seem to prefer the uptake of ammonium since it requires less energy [71]. Therefore, if urine is available, its use is given precedent over the consumption of nitrate in this model. This check simply determines if urine is available and does not guarantee that sufficient nitrogen-nutrient is available, since that depends on the stoichiometric equations, which are treated in separate functions.

Based on whether urine or nitrate shall be consumed, the respective functions are called with the input of how many moles of Chlorella shall be produced. The function then initially determines the required molar changes for all involved substances as a first step. Since the availability of all required nutrients is mandatory for the full growth to happen in the current timestep, their availability is checked in the functions. If only a

fraction of what is required is available, the algal cells only grow until this limited nutrient is depleted to avoid negative masses. If one of the reactants is completely unavailable, no growth can happen and all mass flows from this function are set to 0.

The stoichiometric growth functions for nitrate and urea calculate all changes in molar terms and only in the last step convert them to mass flow rates with the molar masses of the respective substances. A negative prefix indicates that a substance is being consumed and a positive one that it is being created.

These mass flows, along with availability factors of the required reactants carbon dioxide and the nitrogen nutrient, are then passed back to the governing update function. Depending on the nitrogen source, the current assimilation coefficient is calculated and stored, which can be used later as a means of improving the nutritional mix for the algae, when trying to match the respiration and assimilation coefficients of human and algae.

The mass flows for all involved substances are then passed back to the substance manipulator, which also considers the flow rates of medium changes due to acid/base reactions calculated by the growth medium module, which is discussed in the next sub-chapter 4.5. The substance manipulator in the growth medium phase considers the flow rates from both these modules and conducts the actual matter changes in the phase.

4.5 Growth Medium Module

In the growth medium module those parts of the dynamic algae model are integrated that are responsible for substances entering and exiting the medium (e.g. added growth medium components or atmospheric exchange) and for the medium changes as a result of acid/base reactions.

The growth medium module is not comprised of one single class but by a class to calculate the initial concentrations of Bold's Basal Medium, presented in 4.5.1, two phase to phase processors for the oxygen and carbon dioxide atmospheric exchange, presented in 4.5.2 and a class for the acid base calculations of all involved components, presented in 4.5.3.

4.5.1 Bold's Basal Medium Composition

Bold's Basal Medium is used as algal growth medium in the simulations of this thesis. As for a real photobioreactor, the growth medium components have to be added in the correct amount (depending on the simulated water volume) in the beginning of each simulation run.

The Bold's Basal Medium Composition class is implemented as a V-HAB base child class and initially called and stored as an object in the Chlorella in Media system. It is comprised only of the class constructor since this class is only required to calculate the composition once. Despite being only called once, it was still decided to store this part of the module as an object and not implement it as a function in order to be able to store the information about the initial masses and concentrations of the added substances for later reference (e.g. the pH calculation and nitrate resupply rely on this information being available).

The class constructor uses the targeted culture volume (defined in the photobioreactor system, see 6.2.1) and the target concentrations as defined by the recipe (more information, see 3.3.1) to calculate the masses required to reach those concentrations.

Although all the recipe concentrations are stored, only those substances are actually instantiated that either serve as a modeled nutrient to the algal culture (in this case sodium nitrate) or are acidic or basic (list, see 3.3.5.1). Additionally, water is used to make up for the remaining mass

Once the masses are determined, that are needed to reach the desired concentrations in the growth medium volume, they are combined in a struct with their respective masses. In this struct they are defined to be split into their ions, which would happen in water anyway (however, V-HAB currently has no mechanism for this) and is needed for later calculations for the algal photosynthetic metabolism and pH calculations.

The struct with the Bold's Basal Medium components and masses is combined with the initial algal biomass concentration (as defined by the growth calculation module) in the calling Chlorella in Media system and then used in the instantiation of the growth medium phase. Currently, the Disodium-EDTA salt is implemented to be added at 1.16 times of its recipe mass. This 16 % increase in mass is required to bring the simulated pH in line with the measured one of Bold's Basal Medium.

4.5.2 Atmospheric Exchange Phase to Phase Processors

The atmospheric exchange phase to phase processors are the interface between the air flow phase and the growth medium mixture phase. In these phase to phase processors, the solubility of the respective substance in the growth medium is determined based on Henry's law (more information, see 3.3.2.1) and a transport through a membrane is simulated (more information, see 3.3.2.2).

The atmospheric exchange is implemented as a stationary V-HAB phase to phase processor and set between extract-merge processors of the growth medium and air phase in the growth chamber store. By entering a substance property as an input, it is defined which substance – oxygen or carbon dioxide – the instance of this processor is responsible for.

The class constructor sets the Henry's law properties according to the substance and the membrane material, which is set in the photobioreactor definition (see 6.2.1). Different commercially available membranes, or no membrane at all can be selected.

When the update function is called, it calculates the current Henry's constant based on the growth medium temperature. Using the partial pressure of the respective substance (oxygen or carbon dioxide) in the air phase, it calculates what concentration of this substance should be in the medium in equilibrium with the atmosphere. If no membrane is used, the flow rate from the air phase to the growth medium phase through the phase to phase processor is set by comparing the current concentration and what the concentration should be in equilibrium. This model assumes that the water surface itself does not limit the transport itself, which is not true in reality. However, the assumption is based on the idea that for a photobioreactor a membrane will be used in most cases, especially in a zero-g environment, and that the used membrane will pose a much stronger resistance to matter transport than the water surface, which can therefore be neglected.

When a membrane is used, the transport can be limited through this membrane. Since the concentration in the growth medium changes by mass from the air phase being transported through a membrane into the growth medium phase, the membrane transport capability is calculated in the next step. As outlined in 3.3.2.2, the membrane transport is driven by a pressure gradient and therefore the current concentration in the medium is transformed to an equivalent partial pressure. This equivalent partial pressure is based on Henry's law and would be equal to the air phase partial pressure if the concentration were at equilibrium with the partial pressure in the air phase. The flow rate can then be calculated in the next step by factoring in the membrane properties.

Besides the membrane properties, a flow factor is recorded which compares the current membrane transport to what is being consumed (carbon dioxide) or produced (oxygen) by the photosynthetic processes. When assuming that there should be a steady state between photosynthetic flow rate and membrane flow rate, this factor can give an indication whether the membrane is sufficiently sized. However, this should be viewed as an indication and not a definitive measure, since the growth medium poses as a buffer that has the capability to store oxygen and carbon dioxide, which can equalize short term differences in these flows. One example would be that the membrane flow is too low to support the oxygen flow from photosynthesis, the flow factor drops below 1. The concentration in the water rises and thereby also raises the equivalent partial pressure, which increases the driving force and thereby the membrane transport. As long as the driving force is strong enough before the effect of oxygen becomes limiting on algal growth, the membrane transport does not limit growth and this factor should therefore be viewed only as an indication.

4.5.3 pH Calculation

Another major part of the growth medium module is the pH calculation and the speciation of substances due to the change in pH. For example, this determines the short-term availability of carbon dioxide in the growth medium, as outlined in 3.3.3.

The calculation is implemented as a V-HAB base child class and initially called by the Chlorella in Media system. It comprises an update function that governs the chemical acid base reactions with all the involved substances. The update function is called by the growth medium changes substance manipulator in the growth medium phase.

The class constructor instantiates the initial masses of the substances added through the Bolds Basal Medium Composition and the equilibrium constants for all involved acid base reactions.

The update function, which is called by the growth medium changes substance manipulator, initially gathers the current molar concentrations of all acid/base active substances in the medium (currently 14). Based on the current molar concentrations of all involved substances and the initial molar concentrations of the added acid/base-active ions, an 11th order polynomial is solved to determine the hydrogen ion concentration. The polynomial is solved with the MATLAB roots function, which yields a vector with a number of polynomial roots equivalent to one more than the polynomial's order. Since the roots represent the target hydrogen ion molar concentration, only one of these roots can be the correct solution. Therefore, all negative and imaginary roots are eliminated. This leaves one real and positive solution,

which represents the molar concentration of the hydrogen ions in the medium given the current molar concentration of substances in the medium.

With the target molar concentration of hydrogen ions, the resulting equilibrium molar concentrations for all involved substances can be calculated in the next step. When comparing the current and the target molar concentrations, the difference between them defines what currently is in the medium and what should be. This molar difference can then be multiplied with the molar mass to yield a mass difference, which is divided by the current time step to yield a mass flow rate. The mass flow rate is then passed to the calling substance manipulator. There it is combined with flow rates from the photosynthesis module to change the matter in the growth medium phase.

The polynomial that is used to determine the hydrogen ion concentration cannot be created by hand calculations due the large number of involved equilibrium equations and its resulting size. Therefore, a separate function is provided that uses the MATLAB Symbolic Toolbox to determine the polynomial. This function, which takes the involved chemical equilibrium equations and other constraints of the linear equation system (information, see 3.3.5) as input can be used to determine a new polynomial, if different substances should be used.

4.6 Photosynthetically Active Radiation Module Implementation

The photosynthetically active radiation module determines the availability of radiation power for photosynthesis in the medium and calculates the heat transfer into the medium due to absorbed, but unused energy.

The module is implemented as a V-HAB base child class and is initially called and stored as an object in the *Chlorella in Media* system. It comprises a class constructor specifying the radiation growth curve and attenuation relevant parameters, an update function that calculates the defining positions of the radiation-growth curve based on the current attenuation coefficient and a function that calculates the heat transfer into the medium.

The class constructor allows the definition of the photon flux densities that define the radiation growth curve's shape. They are the minimum, saturation and inhibition photon flux density (more information, see 3.1.2.3 and 3.4), which are defined by the algal species used. Currently the experimentally determined ones (more information, see 5.3). Furthermore, the class constructor takes a radiation source as an input and instantiates the attenuation parameters accordingly. Radiation sources available come from literature sources (more information, see 3.4.4.2) and experiments conducted within the scope of this thesis (more information, see 5.4). The radiation source can be specified in the Photobioreactor system and is called by the class constructor.

4.6.1 Calculation of Growth Domain Volumes

The update function of this module is called by the class calculating the relative growth due to photosynthetically active radiation limitation. Its purpose is to determine the positions below the irradiated surface where the photon flux density values are reached that define the boundaries of the radiation saturation curve (e.g. culture depth of 10 mm: inhibited until 2 mm, saturated until 5 mm, linear until 8 mm dark beyond 8 mm). From these positions, growth volumes can be calculated that determine what

part of the photobioreactor is in what radiation growth domain (inhibited, saturated, linear, shaded off).

The first step of the update function is to calculate the current attenuation coefficient based on the biomass concentration in the medium and the specified radiation source. This attenuation coefficient can then be used as specified in 3.4.4.2 to calculate the positions of the radiation growth curve's boundary photon flux densities. These positions can lie outside of the actual culture volume due to the nature of the equations, which simply calculate a position away from the irradiated surface (positive or negative), where the respective photon flux density is reached with a constant attenuation coefficient. To correct this, the positions have to be set to lie on the surface if they lie above it or set to lie on the bottom of the reactor if they lie below it. For example, the position, where saturation starts is calculated to lie at -3 mm (i.e. 3 mm above the surface). When multiplied with a surface area, this would yield a volume, which extends to 3 mm above the photobioreactor (which does not make any sense since the reactor only reaches to its surface defined at 0 mm). When the saturation position is set to 0 mm (on the reactor surface), only that volume is counted to be in the saturated growth domain, which is between the reactor surface and the beginning of the linear growth domain.

Once the positions are established, the corresponding growth domain volumes can be calculated by multiplying the depth of each growth domain with the surface area of the photobioreactor. In this step the photoinhibited volume and sub-minimum photon flux density volume are combined to form one no-growth volume, since no growth is possible in both of them. Currently, only the calculation for a flat panel photobioreactor is implemented.

The radiation profile in the saturated growth volume is not of much interest, since the growth rate is not dependent on the availability of radiation in this domain. However, it is important in the linear growth domain, since the growth rate of the algae rises linearly with the availability of photon flux density in this domain. The average availability of photon flux density in the linear growth domain is therefore calculated by integrating the attenuation function over the boundary positions of the linear growth domain as explained in more detail in 3.4.5.

The growth domain volumes and the average photon flux in the linear growth domain are passed to the object calculating the relative growth rate due to photosynthetically active radiation limitation.

4.6.2 Heat Transfer into the Medium

The heat transfer calculation function determines the absorption in the different radiation growth domains by assuming that all attenuated radiation is absorbed (no scattering and refraction) and subtracting the radiation energy used for photosynthesis.

The first calculation steps determine the photon flux density attenuated in each of the growth domains. This is done by subtracting the exiting and incoming photon flux densities of the respective growth domains and assuming that all the photon flux attenuated in-between is absorbed.

Thereafter the amount of energy turned to heat and used for photosynthesis is determined. In the photoinhibited domain, all absorbed energy is assumed to be transformed to heat, since no photosynthesis is happening there. In the saturated and

linear growth domains the photosynthetic efficiency determines how much is used for photosynthesis and the rest of the absorbed energy is assumed to be transformed to heat.

The heat flux of the absorbed photon flux is calculated as outlined in 3.4.6 with the assumption that the light is monochromatic to avoid having to integrate over an unknown spectral curve. The representative wavelength used for this assumption is stored in the object's properties and set in the class constructor along with the attenuation parameters of the selected radiation source.

In a last step the heat flux is multiplied with the irradiated surface of the photobioreactor to yield a heating power. This heating power is used by the *Chlorella in Media* system thermal structure to set the thermal power of a heat source in the growth medium.

Currently a simple cooler (heat source with negative heating power) is also implemented there to take away all the entering power and therefore keep the temperature constant. This can be exchanged for a more sophisticated cooling system at a later point in time.

5 Experiments

The reported values on certain aspects of algal growth have high variance or are scarcely available. Among those with high variance are the growth rate and maximum achievable biomass concentration presented in 3.1.1 and the lighting growth parameters, presented in 3.1.2.3. Very scarce data is available on the attenuation of light in an algal culture, especially Chlorella vulgaris, with varying biomass concentration as described in 3.4.4. In fact, only one source [95] was found regarding this subject.

This chapter presents experiments that were performed in order to generate data in fields where a large variance of reported data exists, or data is scarcely available.

Initially, this chapter introduces the experimental procedure of determining cell concentration and translating that to a biomass concentration in 5.1. The documentation of the performed experiments is separated with regard to three different areas: the determination of the growth model parameters is presented in 5.2, the determination of the boundaries of the photosynthetically active radiation growth domains is presented in 5.3 and the energy attenuation with regard to the current biomass concentration is presented in 5.4.

Each of the sub-chapters documenting the experiments initially present the aims of the experiments in this area, then describe the hardware setup and procedure and finally present the results of the performed experiments.

5.1 Measuring Biomass Concentration

The tracking of biomass concentration ρ_b in $[\frac{kg}{m^3}]$ is of paramount importance for all the experiments conducted within the scope of this thesis. For the growth and radiation growth curve domain experiments, the evolution of biomass concentration must be measured and documented over time and for the energy attenuation experiments the biomass concentration is required to determine a biomass concentration dependent attenuation coefficient.

Most conveniently, the biomass is determined by measuring the dimensionless optical density through a defined culture depth, correlating the optical density to a cell concentration (typically stated in $[cells/ml]$) through an experimentally determined lookup table, and then multiplying the cell concentration with an averaged cell mass in order to obtain the biomass concentration (in this thesis treated as $[kg/m^3]$).

The steps of this process are outlined in this sub chapter, which is further divided into a description of obtaining the cell concentration from the optical density in 5.1.1 and a subsequent description of using an average cell mass to calculate the biomass concentration in 5.1.2.

5.1.1 Optical Density to Cell Concentration

As light passes through the algal culture, some of its energy is lost due to absorption and scattering. In the case of an algal culture, the radiation is mostly scattered rather than absorbed and therefore leads to the reduced irradiance when it exits the culture [105]. The optical density is a measurement for how much of the radiation energy is lost as it passes through the culture. Mathematically speaking, the optical density is

the negative decadic logarithm of the relation between the exiting and entering a medium as shown in Eq. (5-1) [106](error in source, missing minus).

$$OD = -\log_{10}(\frac{P}{P_0}) \qquad \textbf{Eq. (5-1)}$$

In the above equation, OD refers to the unitless optical density. Other units of irradiance (e.g. $[\frac{W}{m^2}]$) can also be used instead of photon flux density, as long as the same units are used for P and P_0.

The optical density can be measured with a device such as the Thermo Scientific Multiskan FC, which was used for the experiments within the scope of this thesis. A picture of the device is shown in Figure 5-1.

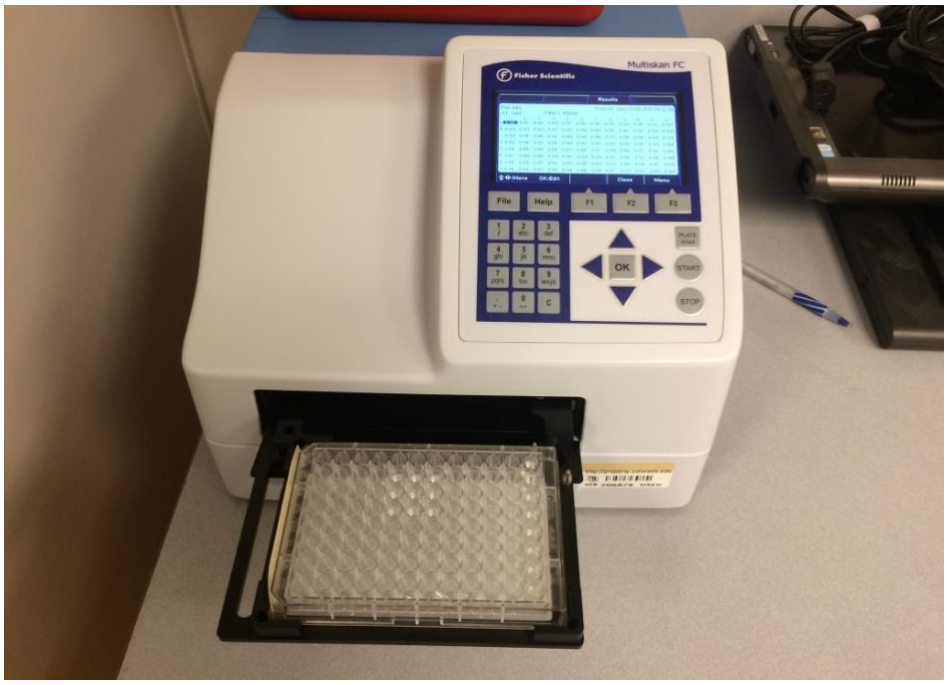

Figure 5-1: Thermo Scientific Multiskan FC at laboratories of Bioserve Space Technologies. Device used to measure the optical density of probes in 200 µl wells of cell culture plates, which are placed on a retractable tray (shown in the extended position with an inserted well plate, is drawn in for measurements).

The measured optical density can then be correlated to a cell concentration in $[cells/ml]$. The correlation between optical density and cell concentration was determined in previous cell count experiments and documented in unpublished findings from T. Niederwieser. The correlation, along with two trend lines shown in Figure 5-2.

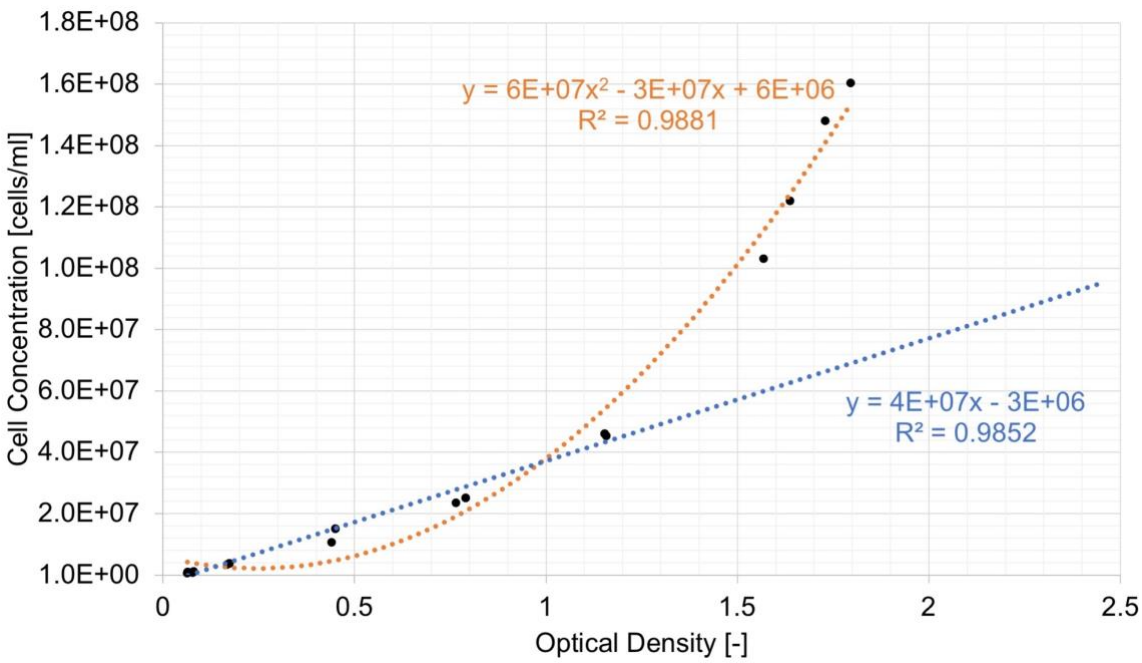

Figure 5-2: Experimentally determined correlation between cell concentration and measured optical density. Black dots are measured data points, orange line is a quadratic trendline encompassing all data points, blue line is a linear trend line, of optical density values between 0 and 1.15 for calculations with a corrected optical density. Both stated with the relating equation. Measurements and correlation obtained from unpublished documentations from T. Niederwieser.

By using the chart and equations in Figure 5-2, the current cell concentration can be determined based on the measured optical density.

However, at optical densities larger than a critical optical density, the correlation becomes unreliable. The probe has to be diluted to obtain a measurement below the critical density and then multiplied with the dilution factor to generate a corrected optical density OD_{corr} [105]. The critical optical density is reported as $OD_{crit} = 0.4$ by one source [105] while another source uses $OD_{crit} = 1$ for experiments [100]

For the purpose of this thesis, the dilution factor is defined as the ratio of solution to solute as shown in Eq. (5-2) and is used in the calculation of the corrected optical density as shown in Eq. (5-3).

$$f_{dil} = \frac{V_{solution}}{V_{solute}} \qquad \textbf{Eq. (5-2)}$$

$$OD_{corr} = OD_{dil} * f_{dil} \qquad \textbf{Eq. (5-3)}$$

The dilution factor f_{dil} is unitles, $V_{solution}$ is the total volume of the solution in $[m^3]$, which is the sum of the solvent (here: water) and solute (here: high concentration algal culture). V_{solute} is the volume of solute in $[m^3]$, which is the high concentration algal culture in this case. OD_{dil} is the unitless optical density of the diluted solution and the calculated OD_{corr} the unitless corrected optical density.

For example, one part of the initial algal culture and 9 parts water yield a dilution factor of 10, the measured optical density of the diluted solution, must be multiplied with 10 in order to obtain the corrected optical density.

This optical density can then be used with the linear trend line, which is shown in Figure 5-2, and formulated in Eq. (5-4), to calculate the current cell concentration:

$$C_{cells} = 4 * 10^7 * OD_{corr} - 3 * 10^6 \qquad \textbf{Eq. (5-4)}$$

The cell concentration is C_{cells} and measured in $[cells/ml]$, and OD_{corr} is the corrected optical density.

For the experiments performed within the scope of this thesis, the dilution was done for optical densities larger than $OD_{crit} = 1$. The rationale is that the experimentally determined linear relation between cell concentration and optical density holds true until around $OD = 1.15$ as shown in Figure 5-2.

5.1.2 Cell Concentration to Biomass Concentration

Since the simulation model operates on the absolute biomass concentration in $[kg/m^3]$, the cell concentration $[cells/ml]$ has to be multiplied with an averaged cell mass $[kg/cell]$ to obtain the biomass concentration. A compilation of literature values for the averaged cell mass is shown in Table 5-1.

Table 5-1: Compilation of literature values for the averaged mass of a Chlorella vulgaris cell.

Source	Cell Mass $\left[\frac{kg}{cell}\right]$	Comment
[74]	6.2×10^{-14}	For Chlorella in general, not vulgaris. Calculated from stated cell- and biomass concentration.
[107]	$(2.24\pm0.16)\times10^{-14}$	
[48]	1×10^{-14}, 1.5×10^{-14}, $1.7\ 1\times10^{-14}$	Depending on growth media used, but Bold's Basal Medium not analyzed. Graphically extracted.

In general, very few sources are available that state the mass of an individual cell or even state a biomass concentration along with a cell concentration, which would allow the calculation of an averaged cell mass. Although all the stated values in Table 5-1 seem extremely small, the largest value is still 6 times larger than the smallest. This variance becomes critical, when the cell concentration is used to calculate the biomass concentration, which can then also have a difference of the factor 6.

Since an experimental determination of cell mass was not possible within the scope of this thesis, an assumption has to be made. The average of the stated values stated in the three different sources is formed, while the three values stated in [48] are treated as one averaged value to not give this source more weight than the others. The average is then $m_{cell} = 3.34 * 10^{-14}\ kg$ and shall be used henceforth.

The biomass concentration can be calculated from the optical density by combining the previously stated equation for cell concentration and the information on the average cell mass with Eq. (5-5).

$$\rho_b = (4 * 10^{13} * OD_{corr} - 3 * 10^{12}) * m_{cell} \qquad \textbf{Eq. (5-5)}$$

OD_{corr} is the unitless corrected optical density, and m_{cell} the averaged cell mass of a Chlorella vulgaris cell in $[kg/cell]$.

5.2 Growth Model Parameter Experiments

The main set of experiments is performed to determine the parameters of the Gompertz growth model, which is presented in 3.1.1. In the simulation, the growth model is used to determine the optimum growth. Hence, the parameters of the growth model must be determined under optimum conditions in order to represent the optimum growth.

The obtained parameters can then be entered in the simulation model in order to generate a realistic growth behavior during the simulation.

5.2.1 Aim of Experiments

The main goal of the growth model parameter experiments is the determination of the parameters of the Gompertz growth model in three different scenarios:

- Still algal culture under a membrane
- Stirred algal culture under a membrane
- Algal culture with air bubbling

For each of these scenarios the growth parameters shall be determined. The three growth model parameters, as outlined in 3.1.1, are:

- the lag time t_{lag} $[s]$
- the maximum growth rate μ_{max} $[kg/m^3 * s]$
- the asymptote of the maximum biomass concentration $\rho_{b_{max}}$ $[kg/m^3]$

A requirement for obtaining the best possible growth model parameters is to provide and maintain optimum growth conditions while these experiments are being performed. Therefore, the determination of conditions that deviate from the optimum conditions and identification of operational constraints during experiments and the operation of a photobioreactor, is also an aim of the growth model parameter experiments.

5.2.2 Experimental Setup

The Chlorella vulgaris cells were taken from the stock culture kept at the laboratories of Bioserve Space Technologies at the University of Colorado, Boulder The stock culture sample was diluted to $1*10^6$ cells/ml and prepared with Bold's Basal Medium by mixing a 50x concentrate [80] and deionized water.

The algal cells were initially cultured in 96 well cell culture plates under a Sigma Aldrich "Breathe Easy" membrane. The rationale of choosing a very small cell culture volume (200 µL per well) was to provide sufficient radiation energy throughout the culture. Furthermore, the well plates offer the capability of providing experiment replicates with very similar conditions (e.g. surface irradiance, temperature) due to their small spatial separation.

After evaporation problems that were determined during the first set of experiments, algae were later cultured in 20 ml tissue flasks. Both, a tissue flask and well plate are shown in Figure 5-3.

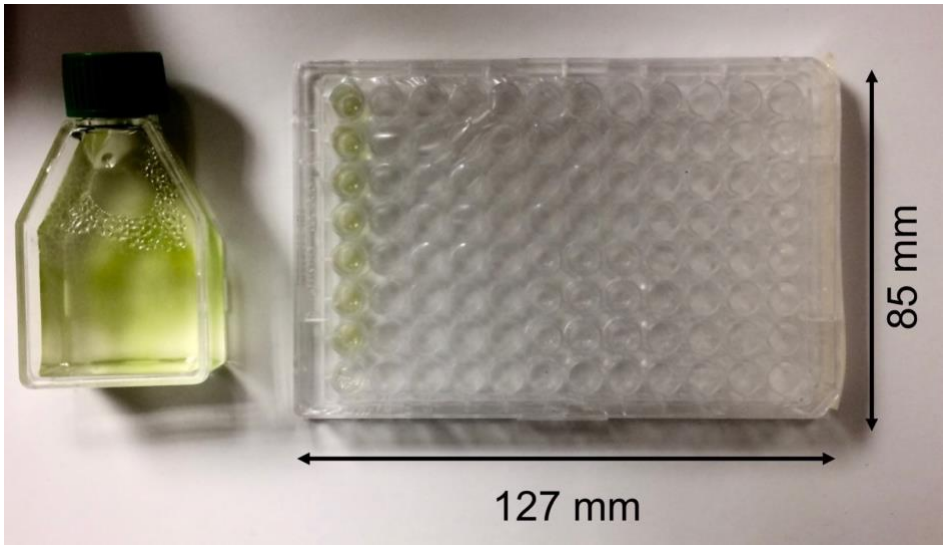

Figure 5-3: Top view of tissue flask (left) and 96 well cell culture plate (right) with dimensions. Ripples visible on the well plate are from the attached membrane and the green tint in the flask and some of the wells stems from the Chlorella vulgaris culture.

In order to maintain optimum growth conditions, Chlorella vulgaris cells were cultured in a Percival Scientific incubator. This incubator is capable of controlling temperature, relative humidity and carbon dioxide content in the internal atmosphere. A picture of the used incubator is shown in Figure 5-4

Figure 5-4: Percival Scientific incubator with description of components and control equipment.

The temperature was maintained through an integrated heater and cooler and set to 28.5 °C in accordance with the optimum temperature range previously shown in Table

3-1. Furthermore, fans were used in direct proximity of the algal culture and LED in order to achieve an even heat distribution.

The carbon dioxide content was controlled through controller / sensor combination and a solenoid valve which were attached to a > 99 % carbon dioxide high pressure gas bottle, which acted as carbon dioxide supply. The carbon dioxide content in the incubator was set to 6 %, which equates to a partial pressure of around 5 kPa, when the altitude of Boulder, CO is taken into account, where the absolute atmospheric pressure is roughly 20 % less than at sea level (1624 m above mean sea level, $p_{abs_{Boulder}} \approx 84\ kPa$ at $T = 298\ K$ [108]). The controller was calibrated by filling a flexible volume from a 5 % (w/w) carbon dioxide high pressure supply, reading and then adjusted for the decreased absolute atmospheric pressure in Boulder, CO by adding 20 % (5 % * 1.2 = 6 %) of the control value in order to represent the sea level partial pressure equivalent to 5 % (i.e. 5 kPa). The high carbon dioxide content was chosen to always provide sufficient carbon dioxide to the culture and to have a strong partial pressure gradient across the membrane.

The relative humidity was set to be controlled at 100 % in order to keep evaporation from the culture medium at a minimum. Due condensation of humidity on a cooling plate, the relative humidity usually was not able to rise above 90-95 %.

Inside the incubator, a HE Photo Red LED from CREE at 1.1 A and 2.85 V provided radiation energy to the growing algal culture. This specific LED was chosen since it has a narrow radiation bandwidth around 660 nm [109], which is in the band where Chlorella vulgaris cells absorb radiation energy at high efficiency as outlined in 3.4.3. The power for the LED was provided by a laboratory power supply, which was placed inside the incubator. The LED was attached to a frame that allowed height adjustments in order to control the surface photon flux density and allowed accurate positioning of the well plate.

5.2.2.1 Unstirred Algal Culture Under a Membrane

Initial experiments determined the growth rate of an unstirred algal culture in 96 well cell culture plates. The well plates were separated from the surrounding environment by a semi-permeable Sigma Aldrich Breathe Easy membrane. The setup is shown in in Figure 5-5.

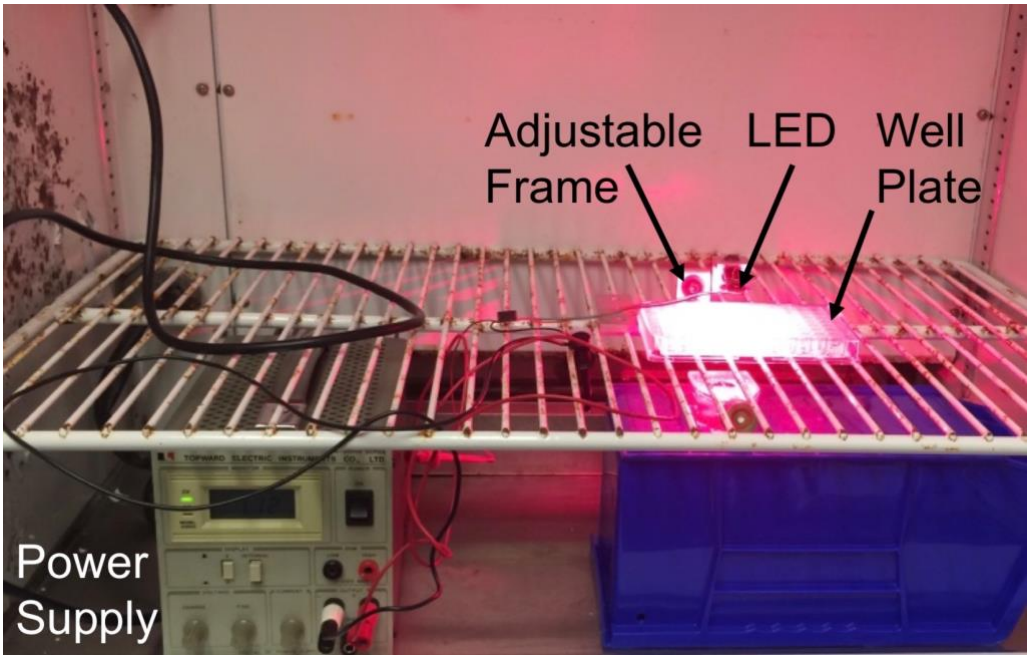

Figure 5-5: Setup inside the incubator with power supply, adjustable frame with an attached LED and a well plate. Not shown are two small fans that were placed on either side of the well plates to carry away heat produced by the LED.

This experiment's setup was later changed to be done with tissue flasks, since strong evaporation was observed through the membrane on the cell culture plate, as outlined in 5.2.4.1. The tissue flasks have an integrated membrane in the lid and were also not stirred during growth. It was placed so that the medium surface was 62 mm below the LED.

5.2.2.2 Stirred Algal Culture Under Membrane

In a different setup the growth rate of a stirred algal culture was determined. Since the volume in the well plates is too small to include a magnetic stirrer, and evaporation was a problem (determined in preceding experiments), these experiments were performed in a tissue flask with a magnetic stirrer. It was placed so that the medium surface was 62 mm below the LED.

This setup was chosen to determine the different growth rates between a sole membrane transport and bubbling, because bubbling air through a reactor is impossible in a zero-g environment but is often used in terrestrial applications. In this setup, the sole means of carbon dioxide supply and oxygen removal is the transport through the membrane in the lid of the culture flask.

The setup used a magnetic stirrer inside a tissue flask, which was placed on a magnetic stirring table under the previously described LED.

5.2.2.3 Algal Culture with Air Bubbling

At a later point, the setup was extended to include a pump and hose connection to the algal culture to determine the effects of air bubbling on algal growth. Although air bubbling is not possible in space, many previous experiments and terrestrial applications employ this method and therefore the results allow a comparison with

other experiments. A tissue flask was used since the wells of a cell culture plate have too small a volume for an operational implementation of air bubbling without significant evaporation loss. It was placed so that the medium surface was 64 mm below the LED.

The pump provided a steady stream of air through the culture medium, which provided carbon dioxide, carried away oxygen and also stirred the medium to counter sedimentation of algal cells. In order to keep evaporation of the medium at bay, the air was enriched with water by bubbling it through a water bottle before directing it to the flask containing the algal culture. The air then left the flask through a vent hole at the top. This setup is shown in Figure 5-6.

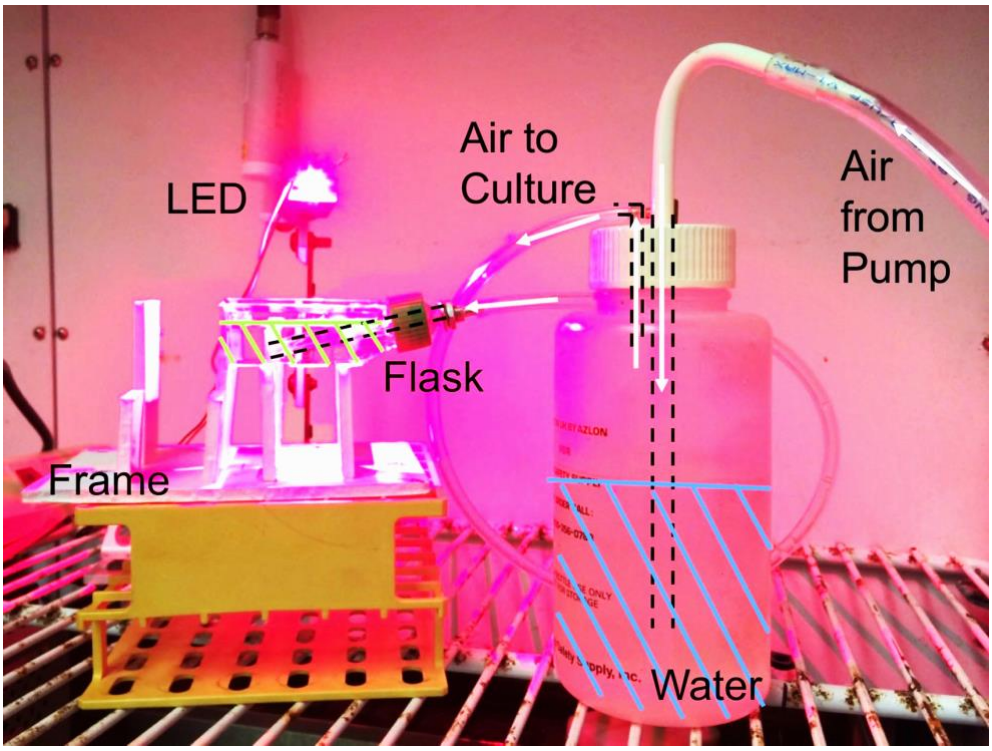

Figure 5-6: Experiment configuration with air supply into medium. Augmented with visual guides for better visibility. The air is pumped from the incubator's internal atmosphere, directed through a water bottle in order to enrich it with water vapor and prevent evaporation as it passes through the culture medium, where it provides the culture with carbon dioxide, removes oxygen and induces a constant movement to prevent algal sedimentation. The air leaves the culture flask through a vent hole in the top.

5.2.3 Experimental Procedure

The cell culture was initially prepared at a cell concentration of $1*10^6$ cells/mL with Bolds Basal Medium. Multiple wells of the cell culture plates were filled in close proximity to create replicates. When tissue flasks were used, only one was filled. Due to their size, uniform lighting properties could not be guaranteed with the use of one LED (only one was available), which would have made replicates useless.

During the growth period, the optical density was usually measured and documented twice daily, on some days only once, but not less. The optical density was then used to calculate the current biomass concentration as outlined in 5.1. Experiments in cell culture plates were measured directly (and the optical density of the membrane subtracted), and for experiments performed in tissue flasks, 200 µl of the culture were placed in a well of a cell culture plate for measurement and then replaced into the flask.

Each measurement was done with at least one duplicate to average over and hence mitigate measurement errors. Along with each documentation of biomass concentration, the current temperature, humidity and atmospheric carbon dioxide content were documented.

The experiments were stopped, when no noticeable growth could be observed anymore and an asymptotic behavior of the biomass concentration over time could be observed.

The biomass concentration over time was plotted after all the data was gathered and the growth rate determined by calculating the differential between the current measurement and the next one, mathematically speaking a forward differential. This approach leads to the growth rate curve being slightly shifted to the left, since the growth rate that would be observed between two data points is attributed to the first of the two data points. The absolute values, which are of concern for the growth model, are still correct. Furthermore, the growth rate at the last documented time is not representable, since no forward value is available for calculation. Using a central difference, which produces less error, would sacrifice the growth rate at the first and last data point and was therefore also not chosen due to the rather low number of measurements (usually 10-15).

At the end of each experiment run, limiting factors on the growth (e.g. temperature, surface irradiance, nutrient resupply, evaporation, membrane transport) were identified and changes implemented for the next one.

5.2.4 Results

Initially, some results on the operation of growth experiments, membrane transport and medium maintenance are presented that came up during the growth experiments. Thereafter results of the growth experiments themselves are presented grouped with regard to the previously introduced three different scenarios: still/stirred with membrane and air bubbling.

5.2.4.1 Experiment Operation, Membrane Transport and Medium Maintenance

The growth parameter experiments were initially planned to be done in cell culture plates with Sigma Aldrich Breathe Easy membranes, which allow the exchange of carbon dioxide and oxygen with the atmosphere. The rationale behind this setup was to choose a small volume that is always sufficiently lit.

However, despite the high relative humidity in the incubator, these membranes also allowed a high degree of medium evaporation, most likely water, from the wells of the cell culture plates, which made the determination of algal growth almost impossible. In order to compensate the evaporation loss, the mass was tracked, and the wells refilled according to the lost mass, as shown in Figure 5-7.

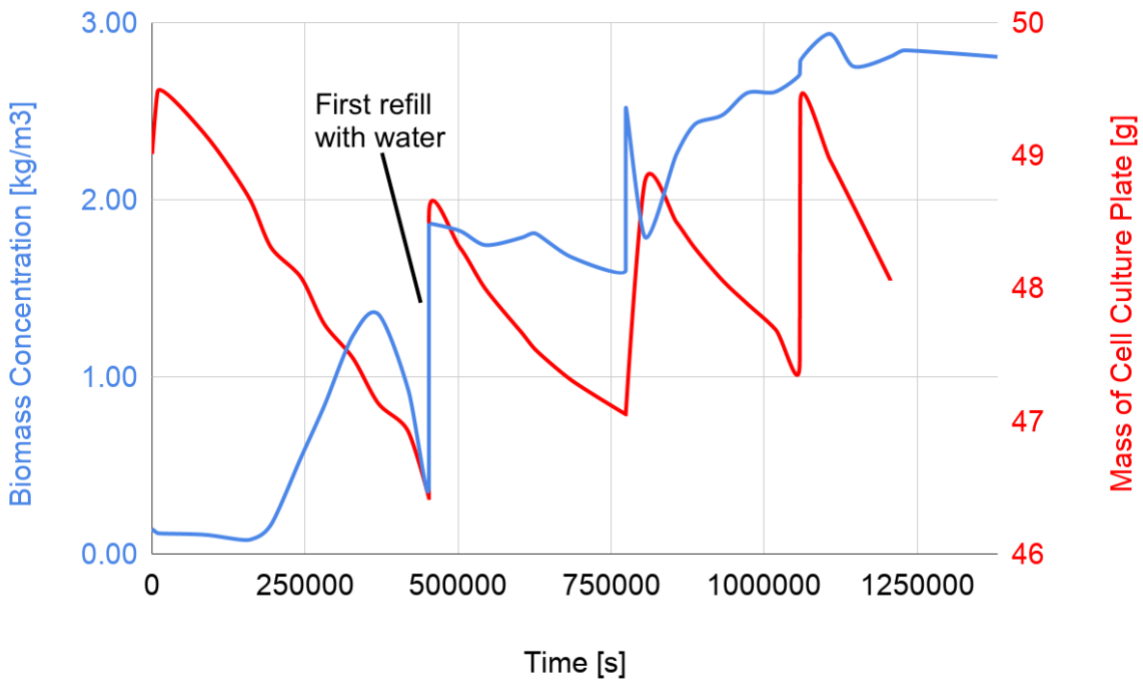

Figure 5-7: Cell culture plate experiment showing strong fluctuations in biomass concentration due to evaporation mass loss. The blue line represents the evolution of biomass over time, the red line the varying mass of the cell culture plate and its volume due to evaporation. Vertical red lines represent times where the wells were refilled.

The overall growth behavior trend, which was previously described in 3.1.1, can be seen to contain an initial lag phase, then a growth phase, and an eventual stationary phase. However, the biomass concentration evolution in Figure 5-7 shows very strongly fluctuating values due to the fluctuations in medium mass as a result of evaporation. The strongest mass loss of 3 g total, before the first refill, equates to 37.5 % of the 8.2 g total mass of the 41 filled wells in this experiment. It should be noted, that 5 wells were used for pH testing, and therefore the first refill does not reestablish the initial mass, since these 5 plates were not refilled.

What can be clearly seen is that a decreased culture volume due to evaporation, yields lower measurements (or even decreasing, when the culture should actually be grown.), than would be expected. This is clearly seen before the first refill. The wells therefore have to be refilled, in this case with water. This is a challenge in itself, since not all wells showed a uniform evaporation loss and therefore could not be refilled with the lost mass evenly divided over all the used wells.

After the first refill the cell concentration was measured in the expected range, however, the next measurements showed almost no increase in cell concentration, which leads to the assumption, that the culture has to adapt to the refill with a new lag time, as clearly seen after the first refill, when the biomass concentration almost does not change over time.

In order to mitigate this lag time after refilling, another experiment was performed, where one half of the wells were refilled with water, and the other with Bolds Basal Medium, and the biomass concentrations of these two groups tracked separately. The results are graphically shown in Figure 5-8.

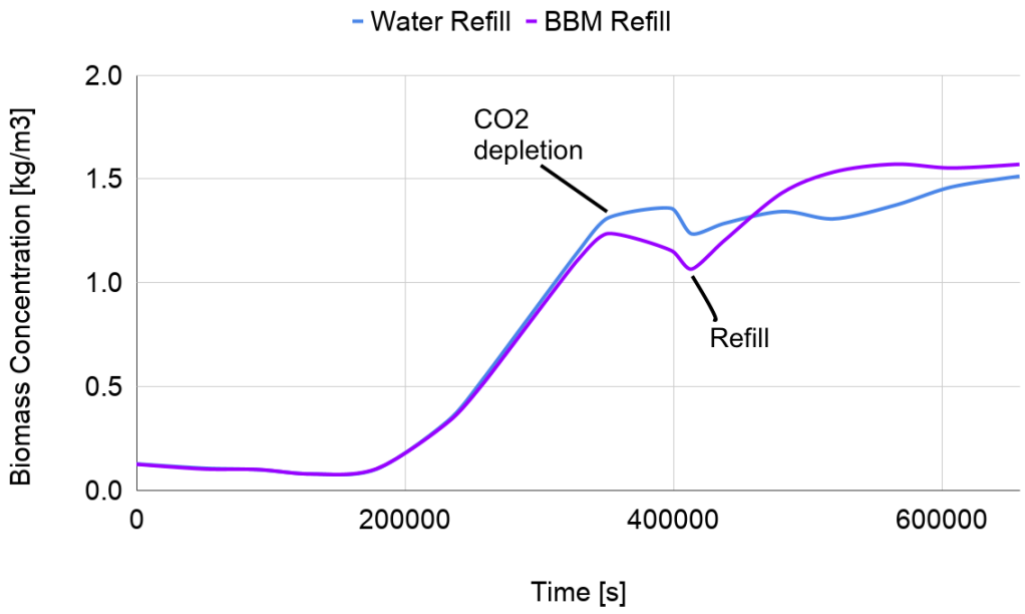

Figure 5-8: Evolution of biomass concentration over time for comparison of refilling evaporation loss with water and Bold's Basal Medium. The blue line represents the growth in the wells refilled with water, the purple line the growth in the wells that were refilled with Bold's Basal Medium.

Figure 5-8 shows that although the refill with Bold's Basal Medium is slightly better than the refill with water, both do not see a significant improvement of growth after the procedure. In fact, as was seen in the other experiments, the biomass concentration can rise to more than double of what is seen in this graph. What is also seen in this graph is that the culture adapted to a depletion of the carbon dioxide supply, which was reestablished as the culture was refilled with water and Bolds Basal Medium.

A further concern of the use of membranes for atmospheric exchange on cell culture plates is that some of the experiments showed limited gas transport capability across the membrane. This was observed through air bubbles (of unknown composition) forming underneath the membrane as shown in Figure 5-9. This leads to the conclusion, that despite the small volume of algal culture in the cell culture plates, the membrane transport capability is limited.

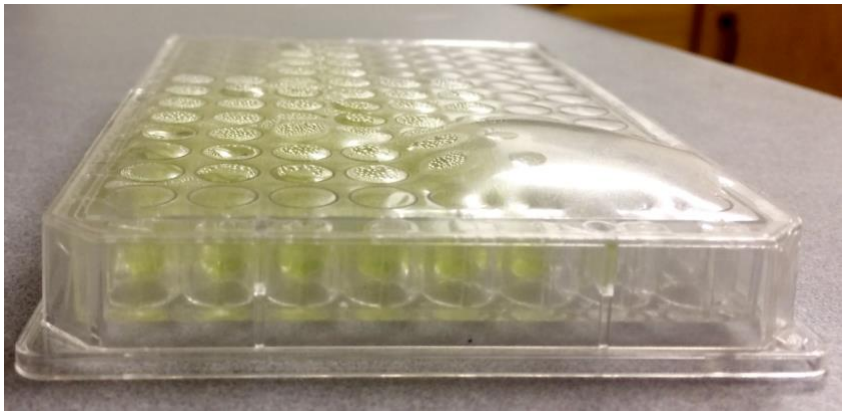

Figure 5-9: Formation of an air bubble between the cell culture plate and Sigma Aldrich Breathe Easy membrane. Indicating a limited transfer capability of the membrane.

The experiments using cell culture plates showed that they pose a challenge to algal growth experiments. The extremely small volume of the wells reacts very sensitively to evaporation. In general, refilling evaporated medium with water or medium solution seems to create a lag time, which is unfavorable. However, in order to compensate evaporation loss of the wells of cell culture plates, they have to be refilled and are therefore not suited for long term algae experiments.

Tissue flasks with an integrated membrane were eventually chosen for the growth parameter experiments due to their larger volume, after cell culture plates were deemed not useful.

5.2.4.2 Growth Parameters of Unstirred Algal Culture Under a Membrane

Initially, the growth experiments using a membrane, were designed to be done with cell culture plates under a Sigma Aldrich Breathe Easy membrane. However evaporation from the extremely low volume of only 200 µl per well through the membrane, made these experiments impossible to produce accurate results. Efforts of compensating the evaporation loss with water or bolds basal medium were unsuccessful as previously outlined in 5.2.4.1.

After restarting well plate with membrane experiments 6 times and trying to overcome membrane- and small-volume-related challenges, a tissue flask with an integrated membrane was chosen for these experiments. The rationale was that the 100 times larger volume of the tissue flask (20 ml) compared to wells of a cell culture plate (200 µl) would not be as sensitive to evaporation.

Despite showing some fluctuations the data shows the trends previously described for the mathematical Gompertz growth model. The data of the best experiment integration using an unstirred algal culture in a tissue flask is shown in Figure 5-10.

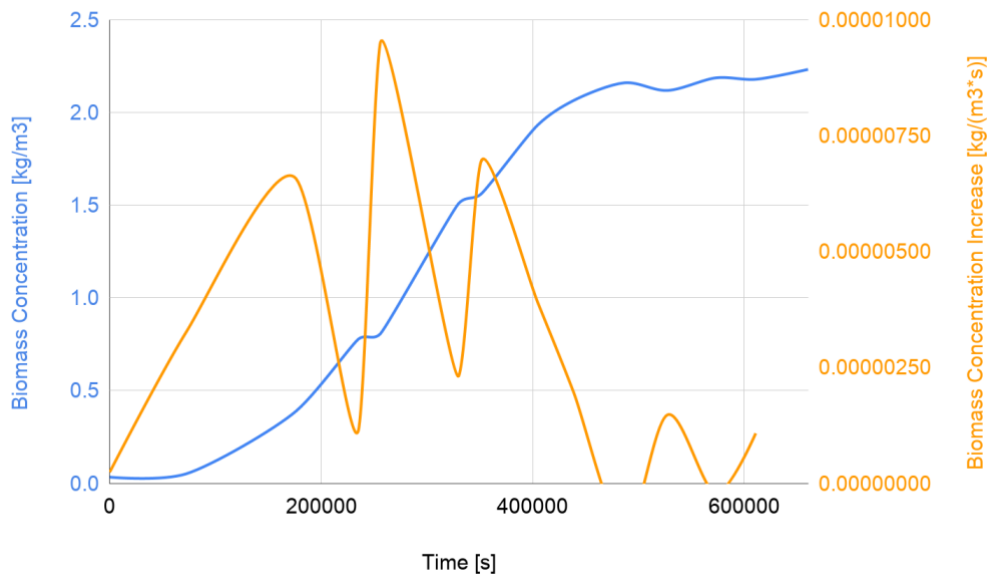

Figure 5-10: Experimental results of Chlorella vulgaris growth in a controlled environment. This experiment used a tissue flask with a membrane to grow the algal culture in. The culture was only stirred on a shaker, twice daily before measurements. The blue line represents the evolution of biomass concentration over time and the orange line represents the biomass concentration increase (i.e. growth rate) over time.

From the behavior of biomass concentration and growth rate over time, the parameters of the Gompertz model can be gathered. For the unstirred culture under a membrane, they are:

- the lag time $t_{lag} = 109230\ s$
- the maximum growth rate $\mu_{max} = 9 * 10^{-6} \frac{kg}{m^3 * s}$
- the asymptote of the maximum biomass concentration $\rho_{b_{max}} = 2.2 \frac{kg}{m^3}$

The strong fluctuations in the growth rate are due to short measurement intervals that did not show major increases in biomass concentration, as shown by the plateaus in the blue line representing the biomass concentration. An interesting conclusion can be drawn from this circumstance. It seems like the culture has to adapt even to small changes, such as a few seconds of shaking before a measurement. This process is necessary to mix the sedimented algae into the growth medium and allow a correct measurement of an evenly dispersed cell culture. However, after the measurement, when the flask is placed back in the incubator, the growth seems to be inhibited for some time due to this disturbance, which leads to a similar biomass concentration at the next measurement. An algal culture, that is constantly stirred, but also shaken before the measurement, does not show this behavior as shown in the following sub-chapter 5.2.2.2.

5.2.4.3 Growth Parameters of stirred Algal Culture Under a Membrane

In the previously described experiments with an unstirred algal culture, in both cell culture plates and tissue flasks, strong sedimentation of algal cells was visible. A tissue flask was therefore equipped with a magnetic stirrer and placed on a stirring table in order to counteract sedimentation. The growth behavior of this experiment is shown in Figure 5-11.

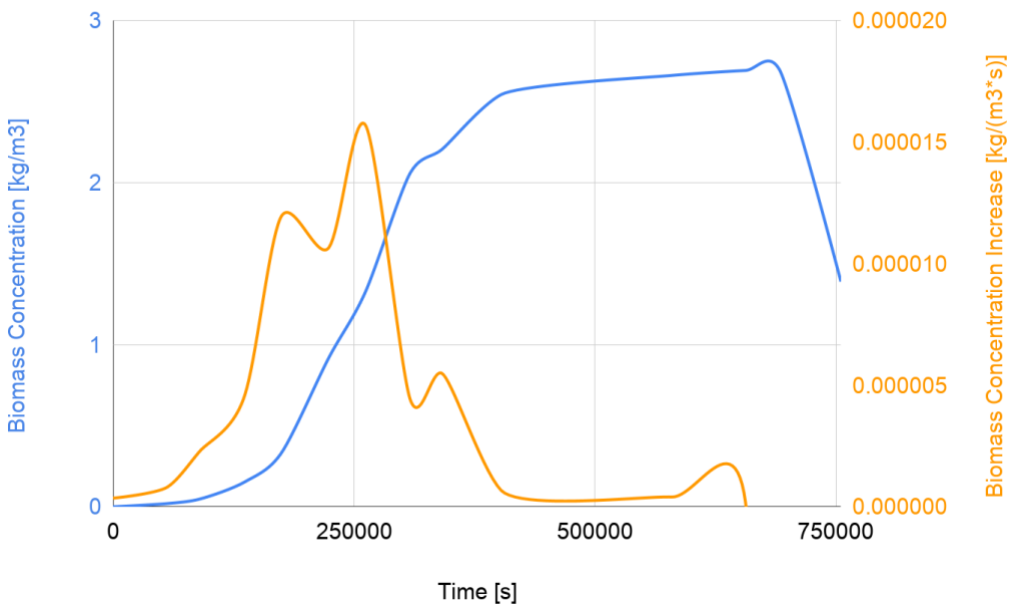

Figure 5-11: Experimental results of Chlorella vulgaris growth in a controlled environment. This experiment used a tissue flask with a membrane to grow the algal culture in. The culture was stirred with a magnetic stirrer The blue line represents the evolution of biomass concentration over time and the orange line represents the biomass concentration increase (i.e. growth rate) over time.

From the behavior of biomass concentration and growth rate over time, the parameters of the Gompertz model can be gathered. For the unstirred culture under a membrane, they are:

- the lag time $t_{lag} = 142080\ s$
- the maximum growth rate $\mu_{max} = 1.6 * 10^{-5} \frac{kg}{m^3 * s}$
- the asymptote of the maximum biomass concentration $\rho_{b_{max}} = 2.65 \frac{kg}{m^3}$

The lag time is larger than for the unstirred culture. However, since the lag time of the Gompertz model is defined by the time, when the algal culture has 6.6 % of its maximum biomass concentration [32], and not an absolute biomass concentration, the comparison is not easily possible. When the time is compared, where the algal culture reaches a certain absolute concentration, the stirred culture reaches it faster, which is also a result of the higher growth rate the stirred culture can reach (almost double that of the unstirred culture).

In this experiment, another interesting observation could be made. After the stationary phase at the maximum biomass concentration was reached, the culture crashed on the 8th day after the experiment was started. The crash caused a rapid decrease in biomass concentration, visible color loss from dark green to brown, and white residue forming on top of the culture medium as shown in Figure 5-12. The reason for the crash unknown, since no further examination of the medium was done, but could result from contamination.

Figure 5-12: Culture after crash at the end of stirred algal culture under membrane experiment. Results were white substance on medium and strong color loss.

5.2.4.4 Growth Parameters of Algal Culture With Air Bubbling

The experiment that employed a pump to bubble air through the culture showed the smoothest results with regard to biomass concentration and growth rate evolution over time as shown in Figure 5-13.

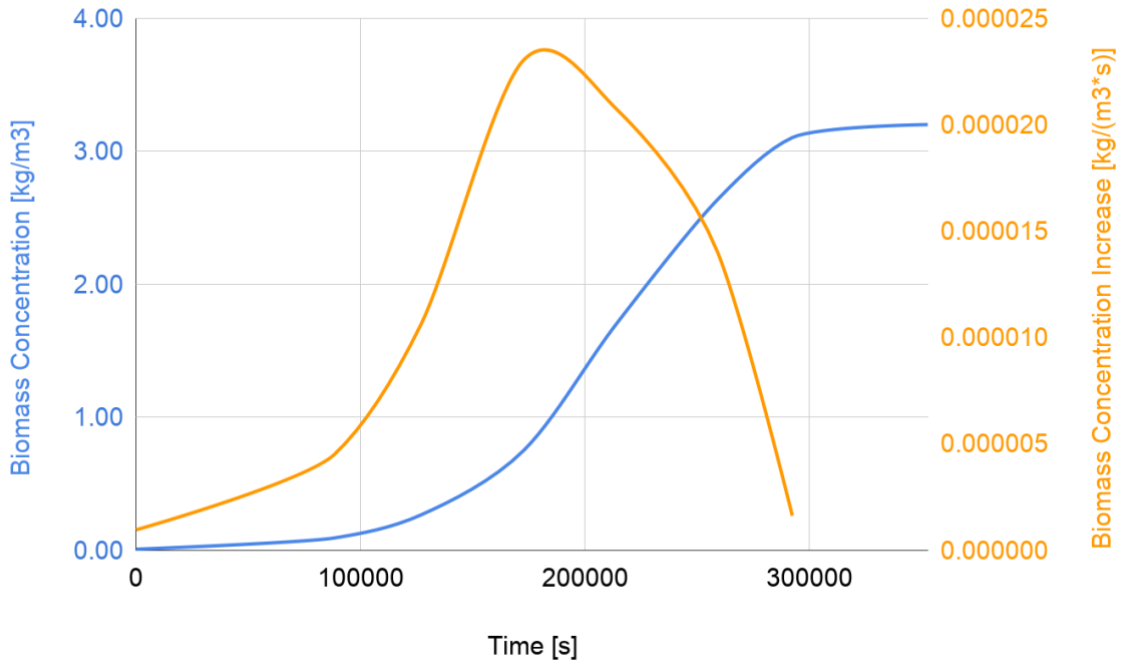

Figure 5-13: Experimental results of Chlorella vulgaris growth in a controlled environment using air bubbling through the growing culture. The blue line represents the evolution of biomass concentration over time and the orange line represents the biomass concentration increase (i.e. growth rate) over time.

With the maximum growth rate recorded at a biomass concentration of $\rho_b = 1.02\, kg/m^3$, which is 33 % of the maximum, this behavior matches the mathematical Gompertz growth model best, which sees the maximum growth rate at 36.8 % of the final biomass concentration. The parameters for the Gompertz model, which can be obtained from the experimental data are:

- the lag time $t_{lag} = 117547\ s$
- the maximum growth rate $\mu_{max} = 2.4 * 10^{-5} \frac{kg}{m^3 * s}$
- the asymptote of the maximum biomass concentration $\rho_{b_{max}} = 3.2 \frac{kg}{m^3}$

The lag time of this experiment was the shortest, the maximum growth rate the highest and the reached maximum biomass concentration was also the highest. Therefore the conclusion can be drawn, that air bubbling is the most efficient way to grow Chlorella vulgaris.

It should be noted though, that air bubbling, as was done in this experiment, is not possible in a zero-g environment, since bubbles cannot rise upward and leave the reactor in a controlled manner, as they do when under the influence of gravity. Nevertheless, this experiment can act as a baseline with regard to what algal growth is possible.

5.3 Radiation Growth Curve Parameter Experiments

Four growth domains exist, when growth is regarded as a function of the available radiation energy, as outlined in 3.4.2. The relative growth rate follows a distinct radiation growth curve, when plotted over the photon flux density. At low irradiances, growth is inhibited due to the lack of sufficient radiation power for photosynthetic growth. When the minimum required photon flux density is reached, the relative growth rate rises linearly with increasing photon flux density until a saturation point is reached. Above that the relative growth rate does not further increase with rising photon flux density, until the inhibition photon flux is reached. Above the inhibition photon flux, the growth decreases rapidly and algal cells eventually take lethal damage.

There is large variance on the reported photon flux density values, that mark the boundaries of the growth domains and therefore determine the shape of the radiation growth curve, as outlined in 3.1.2.3.

5.3.1 Aim of Experiments

The aim of the radiation growth curve parameter experiments is to determine the photon flux density values that mark the boundaries of the radiation growth curve domains. They are:

- Minimum Photon Flux Density P_{min}
- Saturation Photon Flux Density P_{sat}
- Inhibition Photon Flux Density $P_{inhibition}$

5.3.2 Hardware Setup

The algal culture was prepared in the same way as for the growth model parameter experiments (see 5.2.2) and filled into multiple tissue flasks. The culture was grown in 20 ml tissue flasks in the previously described incubator. The temperature was controlled at 28.5 °C, the humidity was around 90 % throughout the experiment and the carbon dioxide partial pressure around 5 kPa.

The tissue flasks were placed at different distances from the LED (50/62/74/86 mm), which were in a range previously identified as being the range, where the sought-after values would most likely be reached.

The previously described HE Photo Red LED from CREE was used as radiation source, while running at 2.85 V and 1.1 A. In order to determine the profile of the photosynthetic photon flux density as a function of distance away from the LED, measurements were made. The Photosynthetic photon flux densities were measured with a LI-COR LI-190R Quantum sensor. This sensor had not been calibrated for 22 years when it was used, but was the only available sensor capable of reliably measuring in the used LED's waveband of around 660 nm. It was therefore cross calibrated with newer sensors and different light sources. It showed a deviation of only 0.85 % below the measurement of a new sensor, when the sunlight at noon was measured (old Li-COR LI-190R: 2007 µmol/m^{2}s, new Apogee MQ200 1990 µmol/m^{2}s) and 5.6 % above the newer sensor measurement of a white LED. The sensor was therefore deemed sufficiently capable of measuring the 660 nm LED.

5.3.3 Experimental Procedure

The cell culture was initially prepared at a cell concentration of $1*10^6$ cells/mL with Bolds Basal Medium. The culture and medium were then filled into four 20 ml tissue flask, which have a membrane in the lid that allows the exchange of oxygen and carbon dioxide. The content of the flasks was not stirred.

During the growth period, the optical density was usually measured and documented twice daily, on some days only once, but not less. The optical density was then used to calculate the current biomass concentration as outlined in 5.1. Each measurement was done with at least one duplicate to average over and hence mitigate measurement errors.

Along with each documentation of biomass concentration and pH, the current temperature, humidity and atmospheric carbon dioxide content were documented.

The experiment was stopped, when no noticeable growth could be observed anymore and an asymptotic behavior of the biomass concentration over time could be observed.

After the growth period, the radiation values at the respective positions of the flasks and further points (larger / smaller distances than the flasks) were measured in order to relate the achieved culture growth to the lighting conditions and eventually determine the boundaries of the radiation growth curve domains.

5.3.4 Results

After initial growth experiments, which placed the algae between 17 mm and 30 mm away from the LED, showed no growth at all, the distance was increased gradually to determine where algae would grow.

At a distance of 40 mm away from the LED, growth was observed despite slow, indicating that growth was photoinhibited, but not to a degree where growth is impossible. In other words, around 40 mm away from the LED, the photon flux is decreased to a level, where it reaches the upper boundary of the saturated growth domain. Moving the probe further away will expose it to photon flux densities that lie within the saturated growth zone.

This sub-chapter presents the measured photon flux density over distance profile, results of growth experiments at different distances from the radiation source and draws a conclusion on the parameters of the radiation growth curve.

5.3.4.1 Photosynthetic Photon Flux Density Profile

The photosynthetic photon flux density profile with increasing distance from the used LED was measured as described in 5.3.2. Since the LED reacts to the power it is being fed, it is important to note, that the LED was powered with 2.65 V and 1.1 A during the growth experiments and the measurements. The profile is shown in Figure 5-14.

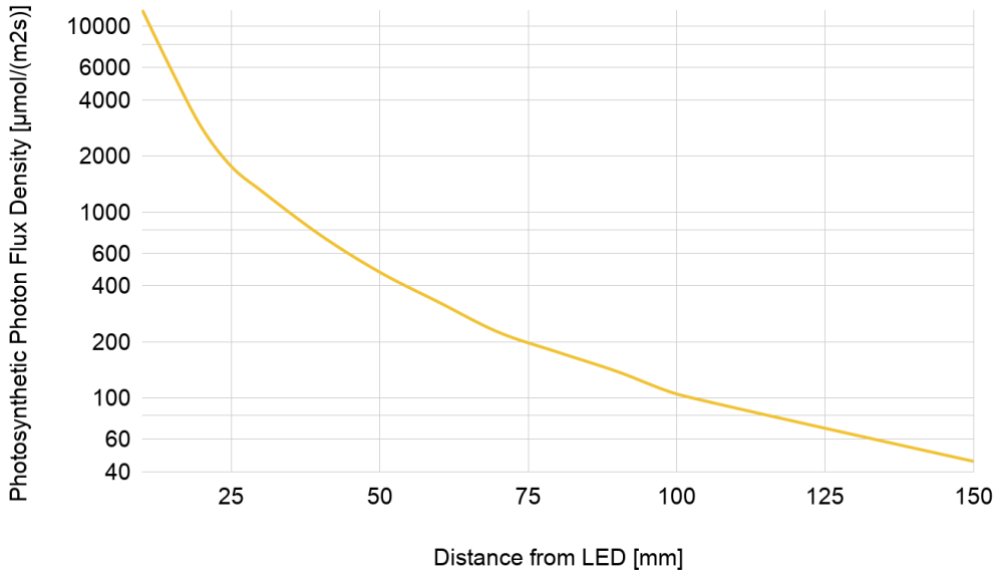

Figure 5-14: Profile of photosynthetic photon flux density with increasing distance from the CREE HE Photo Red LED powered with 2.65 V and 1.1 A. Logarithmic scale on vertical axis to cover wide band width of measurements.

As seen in Figure 5-14, the band width of measured photosynthetic photon flux densities is rather large and decreases exponentially with increasing distance from the LED. While the measurements at very small distances seem extremely high, they lie in the photoinhibited zone anyway, so an accurate measurement is not as important, as of the values from 40 mm onwards, where the algal cultures started growing.

5.3.4.2 Boundaries of the Radiation Curve Growth Domains

Operating the radiation profile of a photobioreactor close to the upper boundary of the saturated growth zone is advantageous. This has the effect that the radiation can penetrate as deep as possible into the medium without inhibiting growth in the upper layers. It was therefore especially of importance to find this upper boundary of the saturated growth domain.

Four tissue flasks were placed in the incubator at the same time at different distances of the LED. The evolution of biomass concentration of all four of them is shown in Figure 5-15.

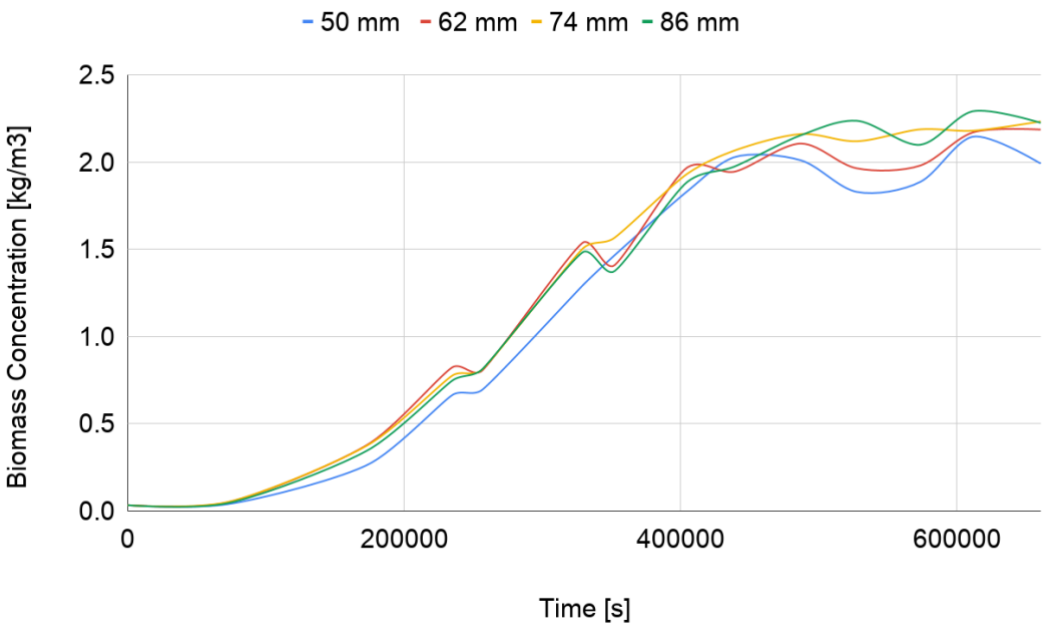

Figure 5-15: Evolution of biomass concentration of four flasks placed at 50 mm, 62 mm, 74 mm and 86 mm distance from the LED in order to determine the upper boundary of the saturated growth zone.

As seen in Figure 5-15, the biomass concentration of the three flasks at 62 mm,74 mm and 86 mm rises almost simultaneously, while the growth in the flask placed at 50 mm away from the LED is slightly slower. The conclusion can be drawn, that the photoinhibited growth zone starts at a photosynthetic photon flux density measured between 50 mm and 62 mm away from the LED.

Although the achieved growth in the flask at 50 mm away from the LED is only slightly lower than in the other three, the difference in color is a visual indicator for different growth conditions, as can be seen in Figure 5-16.

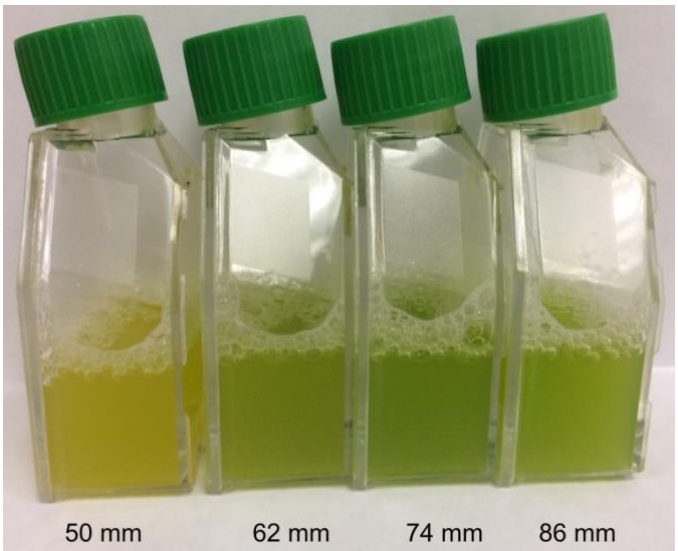

Figure 5-16: Four tissue flasks with algal culture grown in different photosynthetic photon flux densities (achieved by different distances from the LED, as indicated in the picture). Visible difference in color of the closest flask.

When all conducted experiments and their achieved growth is overlaid with the previously introduced radiation-distance-profile, the boundaries can be determined. The graph is shown in Figure 5-17.

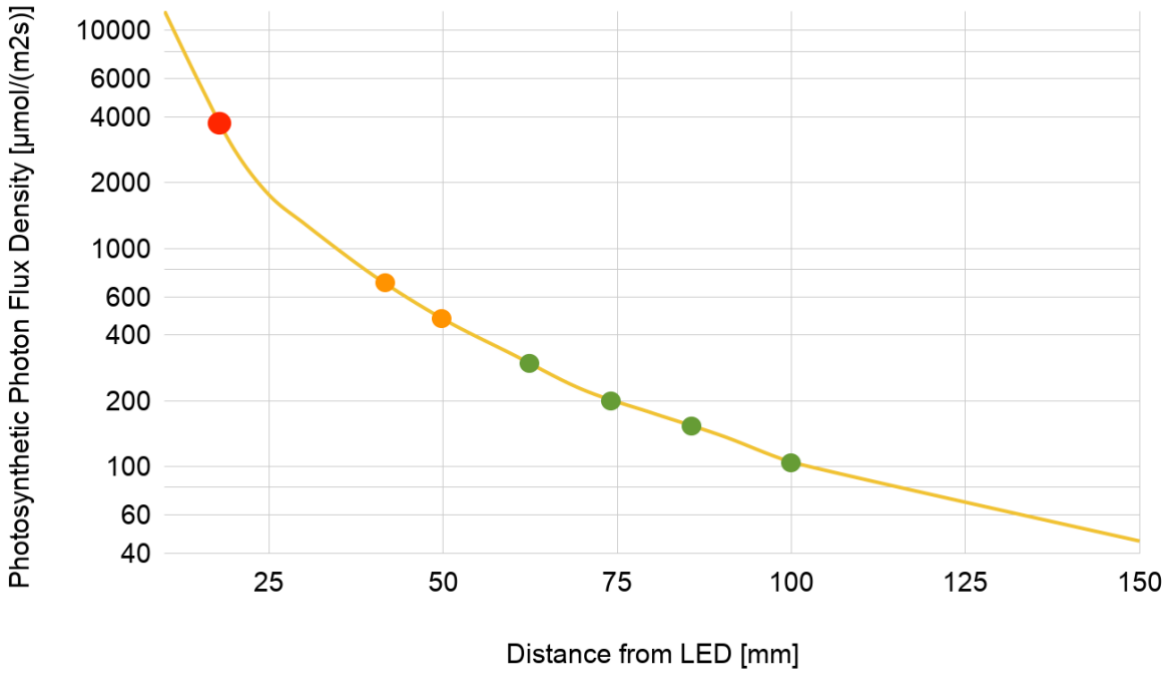

Figure 5-17: Radiation profile of used LED overlaid with experiments conducted at different distances and their achieved maximum biomass concentration as color coded dots. Red represents no growth, orange represents some, but limited, growth, and green represents full growth.

Since the model treats photoinhibition with immediately setting the growth rate to zero, the distances where some growth was observed (indicated as orange dots), can be assumed to yield no growth in the model. Analyzing Figure 5-17 allows to determine the upper boundary of the saturated growth domain of the radiation growth curve. The inhibition photon flux density $P_{inhibition}$ lies somewhere close to 50 mm as can be concluded from the data presentend in Figure 5-15, where the flask placed at 50 mm ($P = 474\ \mu mol/(m^2 * s)$) shows a slightly lower growth rate than the one placed at 62 mm ($P = 320\ \mu mol/(m^2 * s)$). A conservative approximation, by using the middle between the two values, $P_{inhibition} = 400\ \mu mol/(m^2 * s)$ will be used henceforth as the experimentally determined inhibition photon flux density.

Although the minimum and saturation photosynthetic photon flux density could not be determined in the performed experiments, they can be estimated.

For the photon flux density that marks the end of the linear growth domain and start of the saturated growth domain, no data could be experimentally determined. What can be concluded is, that it lies below $P = 100\ \mu mol/(m^2 * s)$, as can be seen in the data presented in Figure 5-17. As a conservative estimate, $P_{sat} = 100\ \mu mol/(m^2 * s)$ will therefore be assumed henceforth.

The minimum photon flux density, below which no growth occurs at all, was not observed experimentally and will be used as stated in literature $P_{min} = 10\ \mu mol/(m^2 * s)$ [46].

5.4 Energy Attenuation Experiments

The attenuation of radiation energy as it passes through the algal culture seems to be a field that is not well documented. Only one literature source was found that documents a varying attenuation coefficient as function of the biomass concentration.

However, this knowledge is vital from an operational view point for the optimization of radiation profiles (e.g. always provide sufficient photon flux but never too much to save power on electricity on cooling). Furthermore, it is of high importance for the simulation in order to calculate the volumes of the different growth domains as described in 3.4.5.

In order to generate some additional data to the one source that was found, a set of experiments were performed with regard to the energy attenuation with varying algal biomass concentration in a culture medium.

5.4.1 Aim of Experiments

The aim of the energy attenuation experiments is the determination of the attenuation coefficient $A(\lambda, \rho_b)$ as a function of biomass concentration and wavelength. Furthermore, the generated data should be able to fit the hyperbolic model, which was outlined in 3.4.4.2 and the parameters $A_{max}(\lambda)$ and $b(\lambda)$ determined.

Since radiation that is visible to the human eye as the red colored light is most efficient for energy conversion by algal cells (see 3.4.3), and the experiments performed within the scope of this thesis were also done with a red LED (narrow waveband around 660 nm of CREE HE Photo Red), the focus of these experiments lies on the determination of the attenuation of radiation in this waveband.

5.4.2 Experimental Setup

This set of experiments did not require to grow algae. Different stages of biomass concentration were generated by diluting the high-biomass-concentration stock culture and performing measurements.

The stock solution with a high optical density (measured at 450 nm) was diluted with deionized water to a multitude of different dilution factors and placed in wells of cell culture plates as shown in Figure 5-18.

Figure 5-18: Initial state of differently diluted algal cultures in wells of cell culture plates. From the top left downward each row has 20 µl more water and 20 µl less algal culture. The range is from 200 µl algal cells / 0 µl water in the top left to 20 µl algae /180 µl water on the lower of the two probes on the right.

The cell and biomass concentration in the wells was measured as outlined in 5.1. The attenuation of red light was measured with the same Thermo Scientific Multiskan FC that is used for the determination of cell concentration, but with a different filter for red light (670 nm).

5.4.3 Experimental Procedure

The stock solution with a high optical density (measured at 450 nm) was diluted with deionized water to a multitude of different dilution factors and placed in wells of cell culture plates as shown in Figure 5-18. The dilution factor ranged from 1 (no water) to 10 (20 µl stock culture and 180 µl water). Each level of dilution was measured with one duplicate to average over and hence mitigate measurement errors.

The wells were then measured at 450 nm to generate data on the current cell concentration. This data was used to calculate the biomass concentration as outlined in 5.1. In order to generate data on the attenuation of red light at 690 nm with varying biomass concentration, the optical density of each well was also measured with red light and documented.

These optical density measurements with red light at 690 nm are eventually used to determine the attenuation coefficient, which can be calculated with Eq. (5-6).

$$A = \frac{-\ln(10^{-OD})}{L} \qquad \textbf{Eq. (5-6)}$$

Since the lowest dilution factor of 10 still yielded a higher cell concentration than the lowest concentration used in the previous growth and pH experiments, further experiments were performed to generate data over a large area of biomass concentration. After the initial set of 10 dilution factors, the content of the wells was

further diluted in 50 % steps, the biomass concentration documented, the optical density of the current red light measured and the process repeated until the cell concentration was as low as $1*10^6$ cells per ml. The well plate with further diluted algal culture is shown in Figure 5-19.

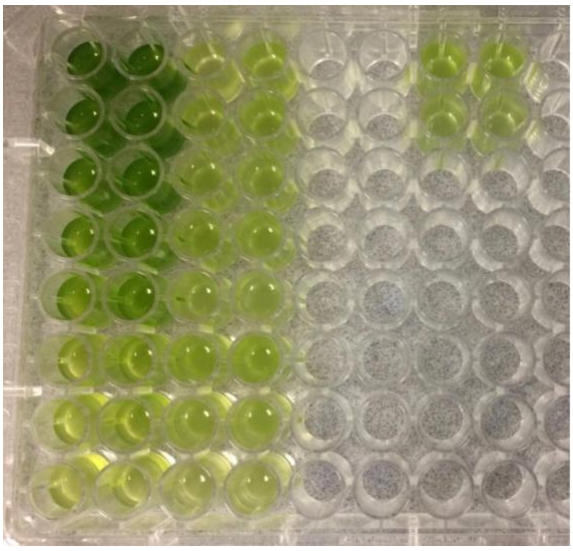

Figure 5-19: Well plate with algal culture at further levels of dilution than initially measured after the highest dilution level still had a cell concentration higher than the lowest level used in other experiments. Each level with one duplicate. Further levels of dilution, which were mixed after the picture was taken, were also measured to generate data over a wide range of cell concentrations.

5.4.4 Results

The aim of this set of experiments was to generate data on the biomass concentration dependent attenuation coefficient of red light (as it is used in these experiments). The measured data points, along with a polynomial trend line, are plotted in Figure 5-20.

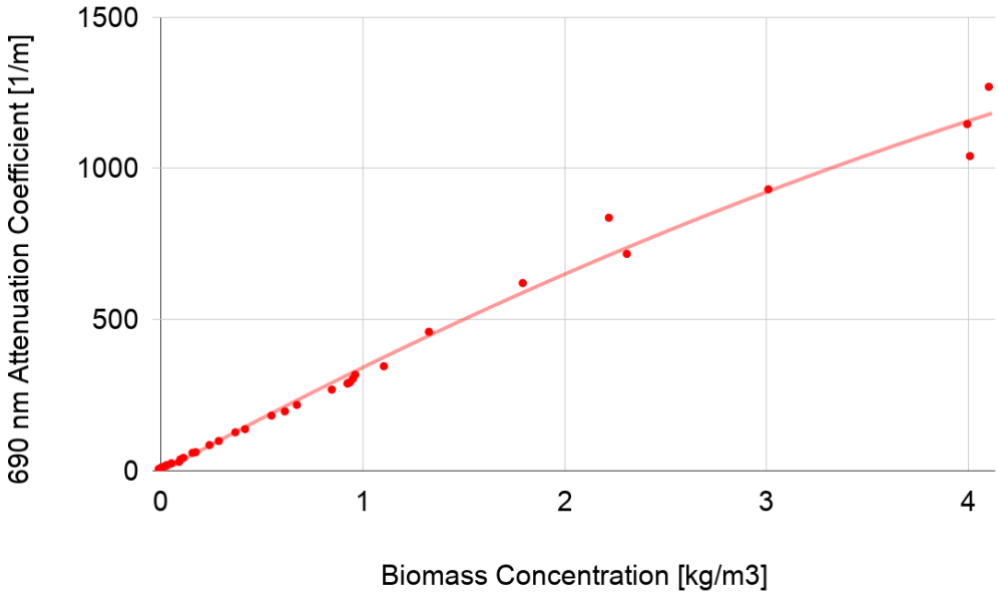

Figure 5-20: Attenuation coefficient of red light depending on biomass concentration. Dots are measured data points, line is 2nd order polynomial trend line.

The measured results show attenuation coefficients that are on the same order of magnitude, but slightly smaller than those reported by another source [95]. While the source states an attenuation coefficient of $A = 600\,1/m$ at $\rho_b = 1.5\,kg/m^3$, the experimentally measured data shows the attenuation coefficient to be $A = 500\,1/m$, which is 20 % more. The experimentally determined values therefore allow a deeper algal culture under otherwise same lighting conditions, since less light is attenuated as it passes through the media, than was previously assumed from the data stated in the obtained literature source [95].

Furthermore, the experimentally generated data covers a wider range of biomass concentration (0 - 4 kg/m^3) than the data stated in the source (0 - 1.5 kg/m^3) [95].

The trend line generated from the data points is a second order polynomial and is given in Eq. (5-7).

$$A = -18.325 * \rho_b^2 + 363.24 * \rho_b - 3.1281 \qquad \textbf{Eq. (5-7)}$$

When fitted to the hyperbolic form used in [95], which was previously introduced in 3.4.4.2, the two required parameters can be defined as $A_{max} = 3619$ and $b = 8.379$.

6 Simulation of an Algal Life Support System

The developed dynamic algae model is used to simulate a biological life support system in a spacecraft that is based on algae. More specifically, the algal photobioreactor is sized to be able to perform air revitalization for one crew member and furthermore, process urine to produce potable water and produce biomass that can be harvested and supplemented to the astronaut's diet.

The V-HAB simulation system is used to integrate a photobioreactor into a spacecraft cabin in which an astronaut is simulated by the V-HAB human model. Besides the human model and the photobioreactor, the spacecraft cabin contains a common cabin air assembly which keeps the humidity and temperature in the cabin constant. Furthermore, food, water, urine and feces storages are modeled in the cabin, of which some interface with the photobioreactor.

The photobioreactor design and integration architecture is based on a proposal by Tobias Niederwieser from the University of Colorado, Boulder, which was presented at the 69th International Astronautical Congress [5]. One of the overall aims of this thesis is to verify the functionality of this design and identify areas for future optimization.

This chapter introduces the simulation environment of the photobioreactor in a spacecraft cabin with an astronaut in the loop. Initially, the design of the proposed photobioreactor design and integration architecture by Niederwieser is introduced in 6.1, followed by a description of the programmatic integration into the V-HAB simulation environment and the used V-HAB systems in 6.2. Finally, three simulation scenarios are presented in 6.3.

6.1 Niederwieser Photobioreactor Design

The aim of the proposed photobioreactor design is to provide one astronaut with sufficient steady state air revitalization capability, while also producing potable water from urine and producing food supplement by harvesting biomass. It was sized in a first order feasibility analysis by using optimistic values gathered from previous research. The design was presented at the 69th International Astronautical Congress in Bremen, Germany in 2018 [5].

The proposed design captures 1.04 kg of carbon dioxide and produces 0.816 kg of oxygen per day (see Table 6-1), which is sufficient for one astronaut. Furthermore, urine is processed, nutrients supplied and water and biomass harvested [5].

Table 6-1: Mass Balance of proposed photobioreactor [5]. Prefixes changed from source to reflect photobioreactor point of view, not cabin (+ is into reactor, - is out).

Substance	Productivity [kg/d]
Oxygen	- 0.816
Carbon Dioxide	+ 1.040
Biomass	- 0.255
Nutrients	+ 0.11
Pre-Processed Water	- 1.589
Urine	+ 1.6

In order to maintain breathable air for one astronaut, 15 liters of culture volume are required, which are housed in a photobioreactor of 0.407 m^3 total volume. The whole system has a mass of 127 kg and requires 3992 watts of power, which is mainly attributed to the LEDs. These parameters make the system lighter and smaller, but more power consuming, than the current International Space Station systems it could replace (oxygen generation assembly and urine processing assembly) [5].

At the core of the design by Niederwieser is a flat panel photobioreactor that consists of a stack of panels. They are each made up of a flow channel at the core, through which the algal culture flows. They are enclosed by transparent air exchange membranes, over which the air flows on the outside to supply carbon dioxide to and carry oxygen away from the algae. The outermost layer of each panel is made up of a fiber optics panel on either side, which transmit photosynthetically active radiation from an LED panel on the outside of the reactor through the air gap and membrane to the growing algal culture [5]. A sketch is shown in Figure 6-1.

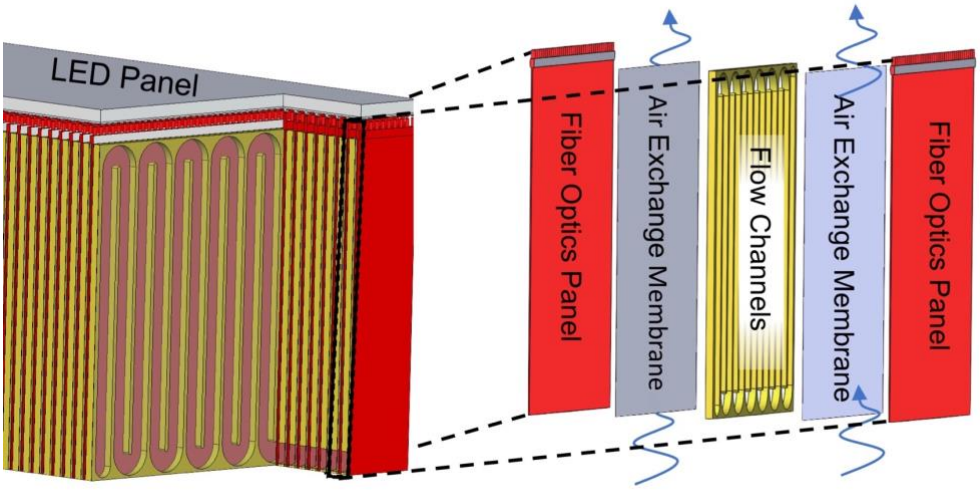

Figure 6-1: Flat panel photobioreactor design by T. Niederwieser. On the left the stack of panels is shown that makes up the photobioreactor. On the right is an exploded view that shows the composition of an individual panel. Compiled from two images in [5] and augmented with visual guides and descriptions.

Each of the flow channel sheets has dimensions of 20 x 20 x 0.5 cm, with 0.127 mm thick air exchange membranes on either side. One sheet can hold a volume of 163 ml, which requires a total of 92 sheets to contain the 15 liters of required culture volume. The 0.8 mm thick fiber optics panels are used instead of directly mounting LEDs on either side in order to achieve a denser packaging and implement a less complex cooling system that carries away the heat from the LEDs [5].

One significant feature of the proposed architecture is the air supply for the photobioreactor. The air supply does not directly interface with the cabin, since it is designed to use a higher carbon dioxide and lower oxygen partial pressure in order to create favorable conditions for the membrane transport of carbon dioxide into and oxygen out of the algal culture. The air passing over the membranes has a carbon dioxide partial pressure of 95 kPa and the oxygen partial pressure is regulated at 5 kPa. This is realized by selectively removing carbon dioxide from the cabin through a removal system and enriching the air that is circulated through the photobioreactor.

The achieved pressure gradients make a membrane area of 4.9 m^2 sufficient to fulfill the gas exchange needs of the photobioreactor without limiting algal growth [5].

Furthermore, the design incorporates an ultrasonic harvester (currently at low technology readiness level), which separates the algae from the medium surrounding it. This enables the harvesting of 70 % of the algal biomass passing through the harvester at 25 mL/min [110]. The harvested biomass can then be collected, dried and supplemented to the astronauts' daily diet. Furthermore water is harvested, which has to be fed to a processor to produce potable water [5].

A schematic overview of the integrated architecture is shown in Figure 6-2.

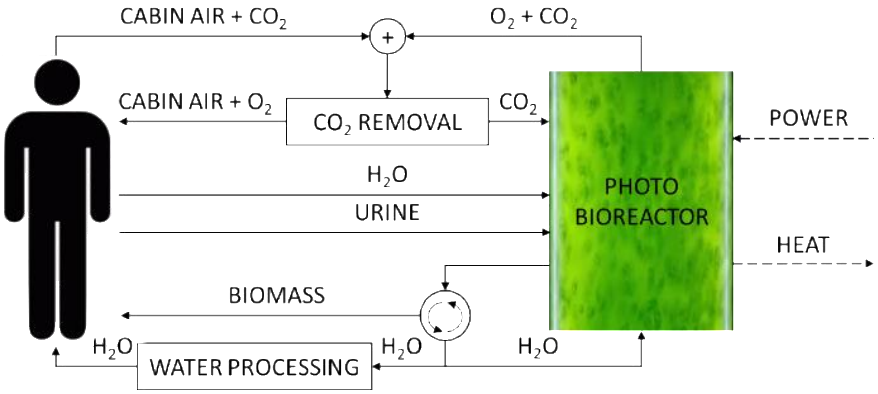

Figure 6-2: Proposed architecture for integration of photobioreactor into cabin environment. Copied from [5].

6.2 V-HAB Integration

This sub-chapter describes the implementation of the previously presented photobioreactor and integration architecture into the V-HAB simulation environment. From the perspective of this thesis, there are two parts that have to be connected in the simulation. The photobioreactor with the dynamic algae model which is described in 6.2.1, and the rest of the V-HAB cabin environment, including further subsystems, described in 6.2.2.

The dynamic algae model is integrated in a photobioreactor based on the operational principle of that proposed by Tobias Niederwieser [5]. The photobioreactor sets boundary conditions for the algae model, provides the required supply of nutrients and lighting and has an integrated harvester that harvests algal biomass and water.

The photobioreactor is integrated into a spacecraft cabin that also houses an astronaut, which is represented through the V-HAB human model. A common cabin air assembly is also integrated into the cabin to regulate humidity and temperature of the spacecraft cabin air. The human model, the common cabin air assembly and the photobioreactor are child systems of the spacecraft cabin system. The photobioreactor is connected to the air, water, food and urine stores of the spacecraft cabin to create a dynamic interaction between the photobioreactor and the human, which is also connected to these stores. A full system overview is provided in Figure 6-3.

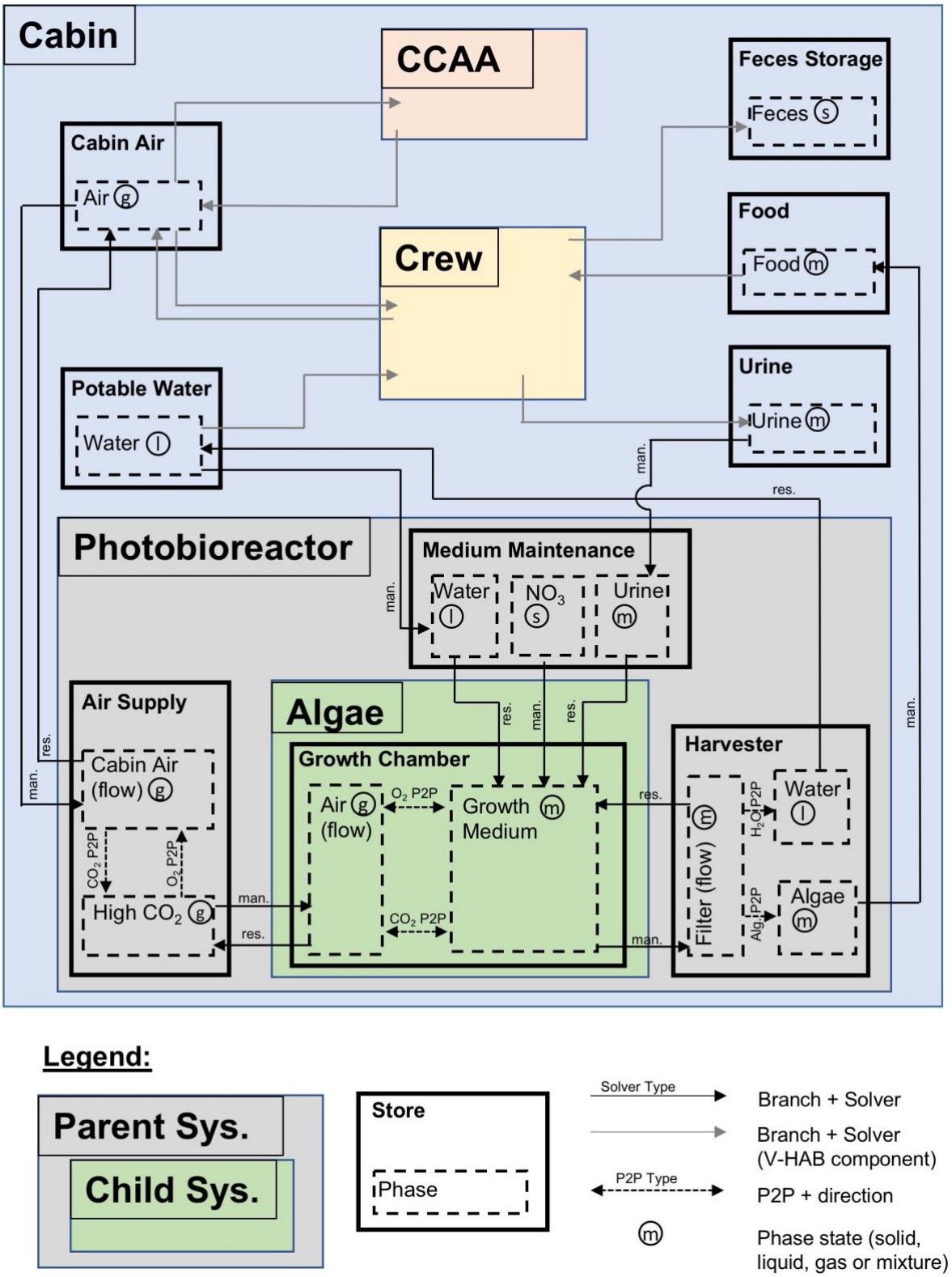

Figure 6-3: Schematic overview of the developed dynamic Chlorella vulgaris model in the photobioreactor and integration into the cabin environment. Colored boxes represent V-HAB systems, solid black boxes stores of the system they share the same color with and dashed boxes are phases in the stores. The state of the phase is given in a black circle. Black arrows represent branches directly connected to the photobioreactor or algae model, grey lines represent branches of the V-HAB components used but not developed for this simulation. Dashed arrows are V-HAB phase to phase processors.

6.2.1 Photobioreactor Integration

They dynamic algae model, which was described in chapters 3 and 4, is integrated in a photobioreactor that follows the design and architecture proposed by Tobias Niederwieser [5].

The definition of the photobioreactor system allows to set design and operation parameters. The reactor size is defined by setting the growth volume and depth below surface (important parameter for the photosynthetically active radiation module) for the algal culture. The membrane surface and thickness, as well as the membrane type (different commercially available membranes available to select from) are defined. The radiation conditions are set by defining the photosynthetic photon flux density on the reactor surface and the light color. Furthermore, the use of urine to supply nutrients can be activated.

Besides housing the algal culture in a child system and providing important design parameters, the photobioreactor system incorporates three modules, that interact with the dynamic Chlorella vulgaris model.

6.2.1.1 Air Supply Module

The air supply module provides high carbon content and low oxygen content air to the algal photobioreactor to ensure a sufficient pressure gradient over the membrane interfacing with the growth medium.

The cabin air is circulated through a buffer flow phase in the photobioreactor subsystem. Through phase to phase processors for carbon dioxide and oxygen, this flow phase interfaces with a high carbon dioxide content phase. From this high carbon dioxide content phase, the air is circulated through the air flow phase in the growth chamber, which is part of the previously described dynamic algae model. This air flow phase is the interface to the growth medium.

Since the algal growth becomes limited at high carbon dioxide concentrations (see 3.1.2.5), the proposed constant high carbon dioxide partial pressure of 95 kPa from Niederwieser cannot be implemented. This value was therefore set to 60 kPa equivalent partial pressure, since growth is not limited then. If membrane transport becomes a critical issue due to the reduced partial pressure, a dynamically increasing partial pressure could be implemented, which matches the membrane transport rate to the photosynthetic uptake but ensures that the concentration in the medium does not reach critical levels.

As the algal culture consumes carbon dioxide and produces oxygen, the partial pressures of these two substances in the high carbon dioxide content phase change. In order to keep the partial pressures at their desired values, phase to phase processors transfer oxygen out to the cabin air flow phase (i.e. increasing the cabin air oxygen content) and resupply carbon dioxide from the cabin air flow phase (i.e. lowering the cabin air carbon dioxide content). The previously mentioned dynamically calculated pressure set point is used as the middle of a hysteresis controller for the phase to phase transfer rate between the cabin air flow and the high carbon dioxide content phase, while oxygen is regulated statically at 5 kPa with a hysteresis controller.

6.2.1.2 Harvesting Module

The harvesting module is responsible for harvesting algal biomass and water from the photobioreactor.

The algal biomass is circulated through the harvesting filter, which is represented through a flow phase and based on the ultrasonic harvester [110] used in the Niederwieser design [5]. It shows a 70 % filtration efficiency at a circulation flow rate of 25 ml/min [110]. From the filter flow phase, phase to phase processors can selectively harvest algae (at 70 % filtration efficiency) and water and transfer them to algae and water phases in the harvesting store. These substance phases in the harvester store then interface with the food store and potable water storage, to where the algae and water are transferred respectively and can be consumed by the V-HAB human model.

Harvesting biomass is not only vital for the production of edible biomass, but also for maintaining growth in the photobioreactor at the highest possible rate. The growth rate peaks at a certain biomass concentration, which lies at 38.7 % of the maximum biomass concentration in the Gompertz model. In order to ensure the maximum possible consumption of carbon dioxide and production of oxygen, the photobioreactor should always be operated at a biomass concentration, where the growth rate peaks.

The control logic in the harvesting module determines this optimum biomass concentration automatically based on the current settings of the growth module. This is done by deriving the growth rate equation, which is based on the Gompertz equation as presented in 3.1.1.2, to obtain the biomass concentration where the growth has its maximum value. The biomass concentration, at which the highest growth rate occurs is then used as control point for the harvester. The harvester is implemented as a hysteresis controller and starts to harvest biomass when the biomass concentration is 5 % above the control point and stops, when it has fallen to below 5 % of the control point.

The water harvester is implemented to respond to the input of urine. The amount of water in the urine supplied to the medium (the amount of urine is determined by the nutrient demand) translates to the amount of water harvested by the water harvester phase to phase processor in the harvester module. Harvested water is directly transferred to the potable water store in the cabin system without further processing. This procedure is not in accordance with the Niederwieser design, which uses a water processing assembly to clear contaminants [5]. In the implemented simulation environment, the contaminants are left behind in the growth medium since the phase to phase processor only withdraws pure water from the filter flow.

6.2.1.3 Medium Maintenance Module

The medium maintenance module of the photobioreactor is responsible for supplying water to the photobioreactor and maintaining the growth medium in an optimum condition with regard to nutrient supply.

The medium maintenance store has three phases, one buffer phase for water, one storage phase for nitrate and one buffer phase for urine. The urine and water buffer phases are connected to their respective counterparts in the cabin system.

When urine or water is supplied to the medium, their buffer phases in the photobioreactor are kept at a constant mass, while the cabin stores are gradually emptied.

When the urine supply is activated in the photobioreactor system (defined through Boolean urine use parameter in class constructor), urine can be used to supply nutrients to the growing algal culture. The supply is implemented as a hysteresis controller and starts, when the nitrogen equivalent is at or lower than 10 % of the initial nitrate concentration in Bold's Basal Medium and ends when the amount of nitrogen supplied through the urine is equivalent to the initial nitrate concentration in Bold's Basal Medium. Since urea (and the urine solids in the V-HAB matter table) contains 2 nitrogen atoms per molecule and nitrate only one, the nitrogen equivalent is reached after only half the molecules of urine solids or urea, than would be required with nitrate. An amount equivalent to the amount of water in the supplied urine is harvested at the same time by the harvesting module of the photobioreactor system.

Since urine is not necessarily always available or should not be used for other reasons, nitrate can also be used to supply nitrogen to the algal culture. It is stored in abundance in the nitrate phase of the photobioreactor's medium maintenance store.

The processes of photosynthesis and nutrient metabolism consume water, which has to be refilled from time to time, especially when urine is not being used. The water phase in the medium maintenance store can provide this water. A control logic automatically activates the water supply from this phase, when the water mass in the growth medium falls below 95 % of the initial value and stops the process of refilling, as soon as the initial level is reached.

6.2.2 V-HAB Cabin Environment

The photobioreactor is integrated in a spacecraft cabin to simulate its use as a life support system. The V-HAB human model is used to simulate the reciprocal influences between photobioreactor performance and crew activities. Furthermore, a model of the International Space Station's common cabin air assembly is used in the spacecraft cabin to keep the temperature and humidity within tolerable bounds for the astronauts.

The human model, its integration into a spacecraft cabin (along with the instantiation of supply and waste stores and phases) and the common cabin air assembly were not developed within the scope of this thesis. However, they were used to create a realistic image of a spacecraft environment that is influenced by crew activities and the developed photobioreactor. They are therefore not documented in detail here, but only described at a level that is sufficient to understand their purpose in the simulation environment and in- and outputs.

6.2.2.1 V-HAB Spacecraft Cabin

The V-HAB spacecraft cabin (in this case, based on the human model tutorial) acts as a parent system to the common cabin air assembly, the human model and the photobioreactor and has the ability to connect these child systems.

In the case of this simulation environment, the cabin system contains five stores that are designed for the human to interact with:

- The cabin air, which holds the cabin air phase with a varying composition depending on the crew activities and photobioreactor performance.
- The food store, which contains different types of stored foods
- The potable water store, which holds potable water for the crew to drink from and, in this case, to resupply water to the photobioreactor

- The urine store, which holds urine that is produced by the human and can be transferred to the photobioreactor from there if desired
- The feces store, which holds the feces produced by the human.

The most connected of these stores is the cabin air store with its gaseous cabin air phase. The volume of this store and phase defines what is commonly understood as the spacecraft cabin volume, since it defines what volume the pressurized part of the spacecraft has in which the astronauts live. The cabin air phase interfaces with the crew through respiration and heat transfer, with the common cabin air assembly where it is cooled and dried and with the photobioreactor, to which it supplies carbon dioxide and from which it is supplied with oxygen.

6.2.2.2 V-HAB Human Model

The V-HAB human model creates in- and outputs of the substances it consumes and produces while it performs a set of daily activities governed by a schedule.

A schedule for each crew member can be implemented with various daily activities of different levels of intensity. The metabolic and respiratory system of the model react to these different levels of intensity and demand a related amount of oxygen, water and food. An amount of carbon dioxide relative to the consumed oxygen and current respiratory coefficient is exhaled along with respiratory water. The respiratory coefficient, which relates the produced carbon dioxide to consumed oxygen, reacts to different food sources. Urine and feces are produced in relation to the consumed water and food. A heat flux equivalent to an activity's intensity level leaves the simulated human and enters the cabin air phase.

The processes relevant to the interaction of the human with a photobioreactor as life support system are graphically presented in Figure 6-4.

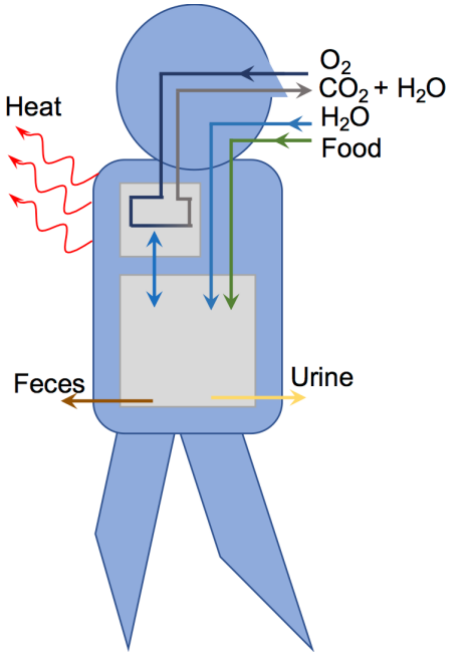

Figure 6-4: Overview of in-, outputs and internal processes of the V-HAB human model relevant to this thesis.

6.2.2.3 V-HAB Common Cabin Air Assembly

A model of the common cabin air assembly, which is used on the International Space Station, is included in the simulation environment to control humidity and temperature of the cabin air phase.

The astronaut exhales water and releases a heat flux to the cabin atmosphere. Both at a level depending on the intensity level of the performed activity level. Without regulation and disregarding any other means of heat transport (e.g. radiation to space), the cabin would heat up and become extremely humid. In order to keep the temperature and humidity at tolerable values, the common cabin air assembly regulates these two parameters.

Since the common cabin air assembly does not directly interface with the photobioreactor, no detailed knowledge of this subsystem's functionality, beyond what was previously explained, is required within the scope of this thesis.

6.3 Simulation Cases

The simulation architecture presented in the previous article is used to simulate the behavior of a photobioreactor as a biological life support system. This sub-chapter describes the different cases that are simulated. While the boundary conditions are the same, the differences between the simulated cases are the use of a growth model that is more optimistic than the growth model that is used otherwise and the volume of the simulated photobioreactors.

The boundary conditions are the same for all simulated cases by simulating one human with the same schedule in all three cases. The cabin air volume is set to 65 m^3, which equates to roughly one sixth of the habitable volume of the International Space Station [111]. The rationale for choosing the habitable volume over the (larger) total

pressurized volume is to reduce effects of the buffering capability of a large air mass since the simulation only covers seven days.

The aim of all cases is to demonstrate that a photobioreactor can sufficiently produce oxygen for one crew member over the course of one week. Since the lag time before growth even starts is around 1.5 days, it is set to zero or the purpose of these simulations. This choice allows to reach a steady state of carbon dioxide consumption and oxygen evolution faster.

6.3.1 Niederwieser Photobioreactor with Optimistic Growth Model

The first set of simulations is connected to the originally proposed design of the Niederwieser photobioreactor. The main difference of the Niederwieser design and the algae model of this thesis is the attained growth rate and maximum biomass concentration.

Since this design was done in a first order feasibility analysis with averaged values, a dynamic evaluation of the design is yet to be done. The first simulation case therefore accepts the optimistic growth model and uses it for the simulation model.

The optimistic growth model, is based on an assumed oxygen evolution of $\mu_{O_2} = 53.1\,\mathrm{g/L{*}d} = 6.146 * 10^{-4}\,\mathrm{kg/(m^3{*}s)}$ [5]. When the photosynthesis equation for urine consumption (no phosphorus) is used, each algal molecule produced yields 1.115 molecules of oxygen. This relation leads to a biomass growth rate of $\mu_{max} = 3.89{*}10^{-4}\,\mathrm{kg/m^3{*}s} = 33.6\,\mathrm{g/L{*}d}$, which is 24 times higher than the experimentally determined maximum growth rate of $\mu_{max} = 1.6 * 10^{-5}\,\mathrm{kg/(m^3{*}s)}$ for a stirred algal culture under a membrane (see 5.2.2.2).

Furthermore, a cell concentration of $\rho_{cells} = 2 * 10^8\,cells/ml = 2 * 10^{15}\,\mathrm{cells/m^3}$ is assumed in the paper [5]. By using an average cell mass of $m_{cell} = 3.34 + 10^{-14}\,kg/cell$ the biomass concentration can be calculated as $\rho_{b_{opt}} = 6.68\,\mathrm{kg}/m3$. It is insinuated that the reactor is continuously operated at this biomass concentration. It will be therefore treated as the biomass concentration of optimum growth for this simulation case. The mathematical relations of the Gompertz growth model yield the maximum biomass concentration to be $\rho_{b_{max}} = 18.15\,\mathrm{kg}/m3$. This value is high, but higher ones have been reported [100].

On a side note, there seems to be a misconception about the relation between high biomass concentration and efficiency of a photobioreactor. The source states that $\rho_{cells} = 2 * 10^8\,cells/ml$ is a good compromise between high cell concentration and radiation penetration depth [5], which can be interpreted to suggest that a high cell concentration is of advantage. It is the growth rate that determines the biomass productivity, carbon dioxide consumption and oxygen evolution and not a high biomass concentration. Even if cell cultures that reach a higher cell concentration could possibly also have a higher growth rate, the cell concentration is not the determining factor for the quality of an efficient photobioreactor, the maximum growth rate is. In a batch culture, the high biomass concentration has the advantage of enabling a longer growth period and therefore more overall biomass yield and oxygen production. Since the growth rate peaks at a certain biomass concentration $\rho_{b_{opt}}$, and a continuously growing culture should be kept at this optimum, a higher than optimum growth rate has no advantage in a continuously growing culture.

In brief: the aim of this simulation case is to verify the functionality of the proposed design including the optimistic growth rate and compare the initially presented results of inputs and outputs to those of the dynamic simulation.

The used parameters for the photobioreactor design for this simulation case are summarized in Table 6-2.

Table 6-2: Photobioreactor and growth calculation inputs to the simulation for the simulation case using an optimistic growth rate.

Parameter	Value	Unit
Light Color	Red Experimental	-
Surface Photon Flux Density	400	$\frac{\mu mol}{m^2 s}$
Growth Volume	0.015	m^3
Depth Below Surface	0.0025	m
Membrane Material	SSP-M823 Silicone	-
Membrane Surface	5	m^2
Membrane Thickness	0.0001	m
Lag Time	0	s
Max. Growth Rate	$3.89*10^{-4}$	$\frac{kg}{m^3*s}$
Max. Biomass Conc.	18.15	$\frac{kg}{m3}$

6.3.2 Niederwieser Photobioreactor with Experimental Growth Model

Since the first simulation case is done with an optimistic growth rate, this simulation case uses the previously introduced experimentally determined growth rate with an otherwise same design. Most importantly, the culture volume is left at 15 liters as proposed

The aim of this simulation case is to verify the functionality of the proposed design without the optimistic growth rate and compare the initially presented results of inputs and outputs from [5] to those of the dynamic simulation with the experimentally determined growth rate.

The used parameters for the photobioreactor design for this simulation case are summarized in Table 6-3.

Table 6-3: Photobioreactor and growth calculation inputs to the simulation for the simulation case using the experimentally determined growth rate.

Parameter	Value	Unit
Light Color	Red Experimental	-
Surface Photon Flux Density	400	$\frac{\mu mol}{m^2 s}$
Growth Volume	0.015	m^3
Depth Below Surface	0.0025	m
Membrane Material	SSP-M823 Silicone	-
Membrane Surface	5	m^2
Membrane Thickness	0.0001	m
Lag Time	0	s
Max. Growth Rate	$1.6*10^{-5}$	$\frac{kg}{m^3*s}$
Max. Biomass Conc.	2.65	$\frac{kg}{m3}$

6.3.3 Sufficiently sized Niederwieser Photobioreactor with Experimental Growth Model

While the first two cases verify a design, this case determines a design. This simulation case is aimed at finding the volume of a sufficiently sized photobioreactor capable of providing oxygen to a human over the course of 7 days.

Since the first simulation case is done with an optimistic growth rate and the second one with a much lower experimentally determined one but still uses the rather small growth volume of just 15 liters, this simulation case uses the previously introduced experimentally determined growth rate but a scaled-up volume, that is actually capable of providing sufficient oxygen to a human over the course of one week.

The aim of this simulation case is to find a reactor design that matches the inputs and outputs and present the deviations in design from [5] that are necessary to attain the presented inputs and outputs.

The used parameters for the photobioreactor design for this simulation case are summarized in Table 6-4.

Table 6-4: Photobioreactor and growth calculation inputs to the simulation for the simulation case to determine design parameters.

Parameter	Value	Unit
Light Color	Red Experimental	-
Surface Photon Flux Density	400	$\frac{\mu mol}{m^2 s}$
Growth Volume	tbd → result	m^3
Depth Below Surface	tbd → result	m
Membrane Material	SSP-M823 Silicone	-
Membrane Surface	tbd → result	m^2
Membrane Thickness	0.0001	m
Lag Time	0	s
Max. Growth Rate	$1.6*10^{-5}$	$\frac{kg}{m^3*s}$
Max. Biomass Conc.	2.65	$\frac{kg}{m3}$

7 Simulation Results

This chapter presents the simulation results of different photobioreactor configurations as core of a biological life support system with a human in the loop.

All simulations are run with the design of the Niederwieser photobioreactor (see 6.1) in the previously introduced spacecraft cabin integration architecture (see 6.2.2). The cases differ by the attained algal biomass growth rate and the photobioreactor size as outlined in 6.3.

The results are grouped in the same categories as the previous description of the simulation cases. For comparison, baseline values without a simulated photobioreactor are given in 7.1. In 7.2 the simulation results of the published Niederwieser photobioreactor design with an optimistic growth model are presented and some means of optimization and their results presented in the sub-chapters, which also demonstrates the optimization capabilities the developed model provides. 7.3. presents the results of the next simulation, which uses the experimentally determined growth rate from 5.2.4.3 instead of the published optimistic one case. The simulation results of a scaled-up Niederwieser design that uses the experimentally determined growth rate is presented in 7.4.

While the main focus of result presentation lies on the ability of the photobioreactor to provide sufficient carbon dioxide assimilation and oxygen production capability, other results are also shown. These additional results are related to urine processing, food production and other interesting findings.

7.1 Comparison Baseline without Photobioreactor

The results presented in this sub-chapter represent a comparison baseline that was created without an active photobioreactor in the loop (achieved by turning of the photobioreactor's radiation energy source). Therefore, air is not revitalized, the urine not processed and no algal food supplement created. This baseline allows to assess the quality of a photobioreactor's performance, by comparing the baseline values with the simulated results, when an active photobioreactor is in the loop.

As shown in Figure 7-1, the oxygen partial pressure declines to around 11 kPa partial pressure, which is low but still survivable, since it equates to an altitude on Earth of about 5000 m above sea level. Following the almost linear downward trend of oxygen evolution, the oxygen partial pressure will further drop to a level not survivable for humans after a few ore simulation days. The carbon dioxide partial pressure rises to a level above 8 kPa over the course of 7 days. Even for just one hour of exposure, the maximum allowable carbon dioxide content is only 2 kPa for a spacecraft cabin [112].

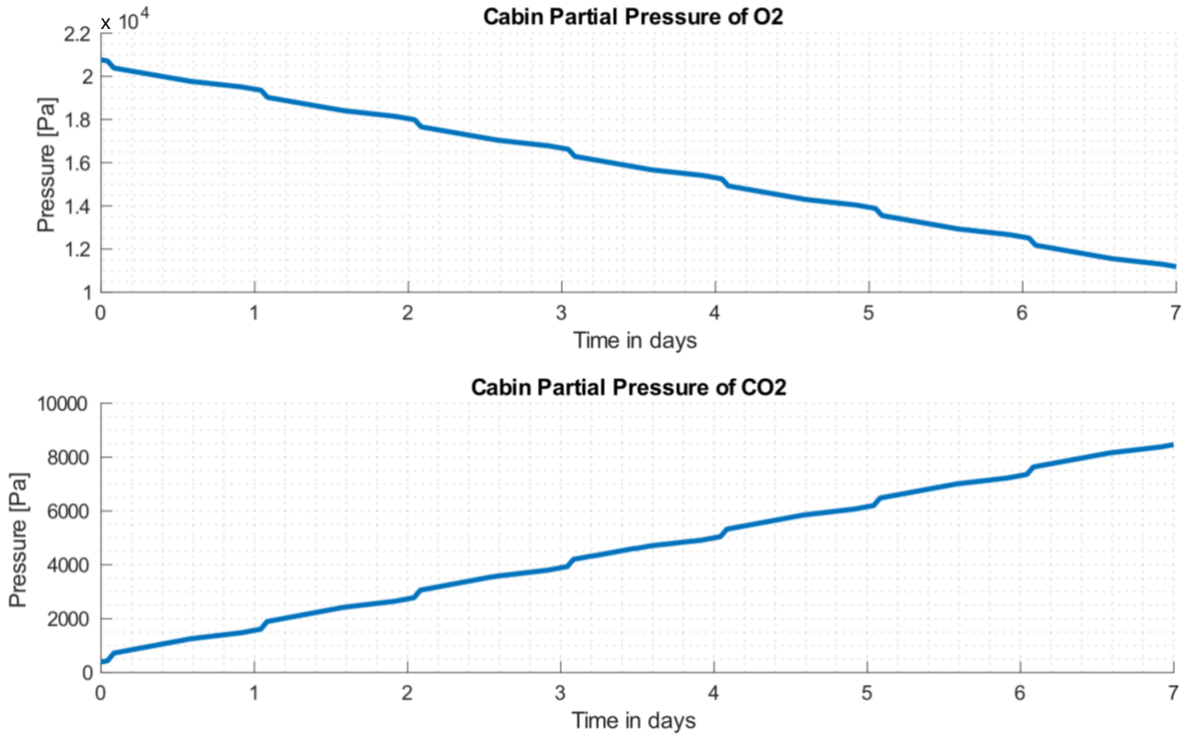

Figure 7-1: Baseline of oxygen (top) and carbon dioxide (bottom) partial pressure evolution over the course of 7 days in a spacecraft cabin with a human but without any means of air revitalization.

The steps in the oxygen and carbon dioxide partial pressure occur, when the human is exercising. During this short time period the intensity level is strongly increased, to which the human model responds by requiring more oxygen (step downward in graph) and producing more carbon dioxide (step upward in graph) than normal. Not pictured here are the visible increase in humidity (due to increased respiration and connected exhaling of water) and the increased temperature (heat transfer from human) of the cabin atmosphere.

An assumption made for the simulation is that potable water can be directly harvested from the photobioreactor, in the proposed Niederwieser design a water processing assembly would be required [5]. Without a photobioreactor in the loop, which has the potential to turn urine into potable water, the potable water store is reduced by 22.74 kg over the course of seven days (see Figure 7-3), and the urine store filled with 17.75 kg (see Figure 7-2). The mass difference between the two arises through the production of respiratory water which is captured by the common cabin air assembly, where it is stored and not further processed in this simulation. The food store is depleted by 14.52 kg over the course of the seven simulated days (see Figure 7-4).

The stepped shape of the displayed graphs is not a sign of low data resolution but due to the fact that the water and food are not ingested continuously but in lumps during meal and drink times and urine only excreted during bathroom breaks.

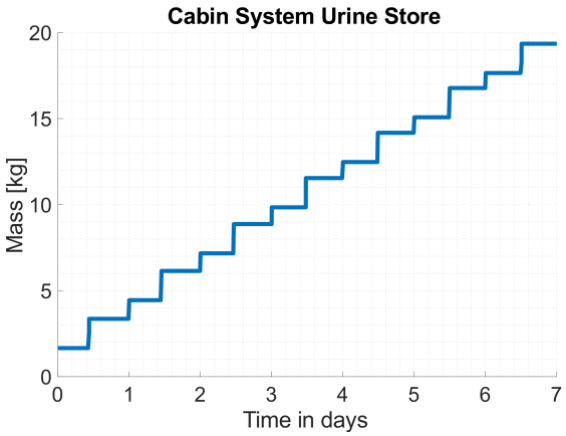

Figure 7-2: Baseline for evolution of urine store mass

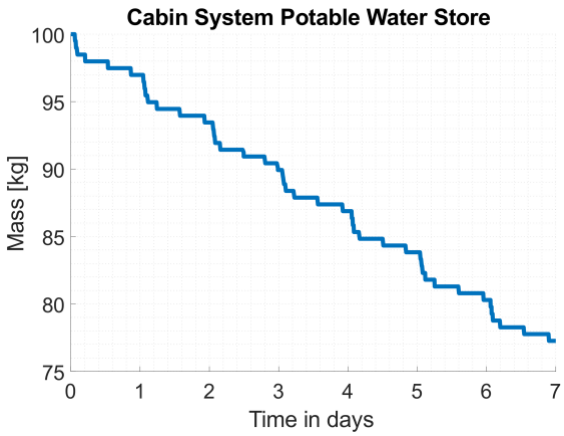

Figure 7-3: Baseline for evolution of potable water store mass

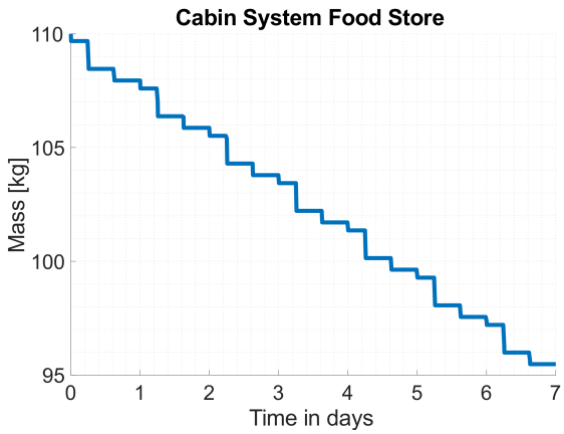

Figure 7-4: Baseline for evolution of food store mass

7.2 Niederwieser Photobioreactor with Optimistic Growth Model

The photobioreactor with the optimistic growth model provides some, yet insufficient, air revitalization capability, when compared to the baseline without a photobioreactor.

The evolution of oxygen and carbon dioxide partial pressures in the cabin air is given in Figure 7-5. Over the course of seven days, the oxygen partial pressure falls to around 15 kPa, which is unproblematic since it is roughly the same oxygen partial pressure as in Boulder, CO. However, the carbon dioxide partial pressure is definitely problematic, since it rises to a partial pressure of above 5 kPa during this time period. That is well beyond, the upper threshold for what humans are allowed to be exposed to as defined by the National Aeronautics and Space Administration's Human Integration Design Handbook [112].

Overall the air revitalization capability of this configuration is insufficient since the oxygen partial pressure follows a downward trend that will eventually reach critical levels and the carbon dioxide concentration already reaches a dangerously high partial pressure at the end of day 2, where even the threshold for short term exposure of 2 kPa [112] is passed.

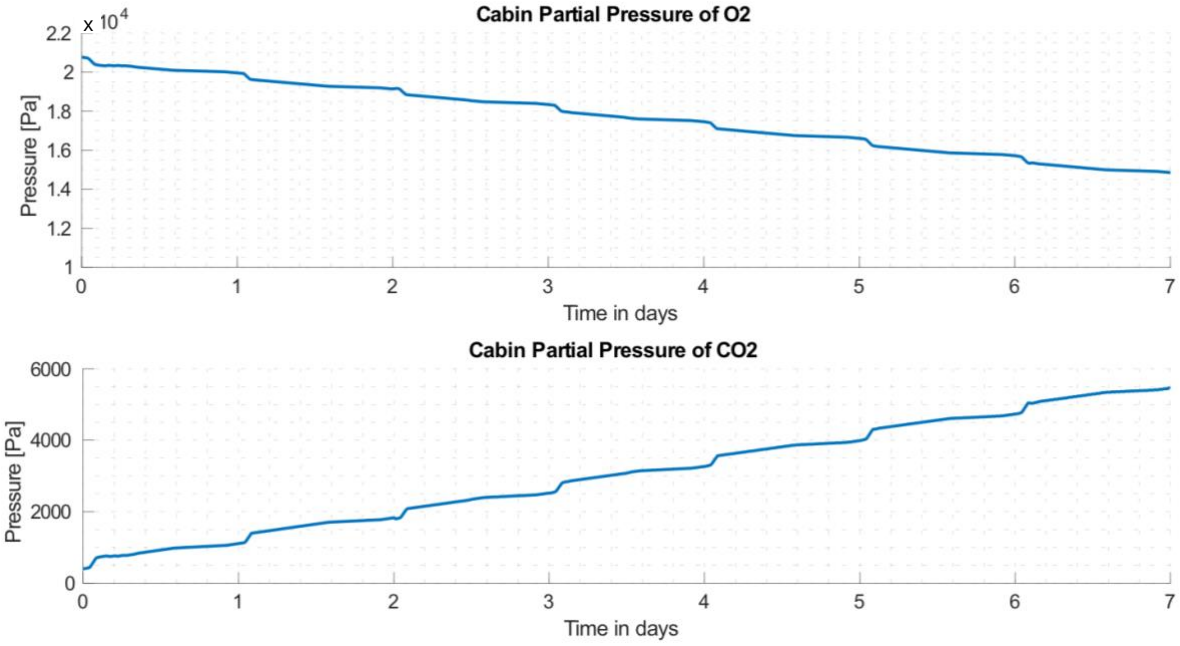

Figure 7-5: Evolution of oxygen (top) and carbon dioxide (bottom) partial pressures in the cabin air with Niederwieser photobioreactor and optimistic growth model.

The urine processing and water generation capability of the configuration reduces the net generated (and stored) urine mass from 17.75 kg (as shown in the comparison baseline values) to 0.852 kg as seen in Figure 7-6 (the store is initially filled with 1.6 kg of urine). This represents a urine recovery capability of 95 %. Instead of 22.74 kg depleted potable water in the comparison baseline, the potable water store is only depleted by 6.14 kg when the photobioreactor is continuously feeding processed urine into it, as shown in Figure 7-7. This scenario can therefore reduce the traditional urine processing system capability by 95 % and the required potable water storage by 73 %. Additionally, 2.075 kg of algal biomass are harvested and could be added as food supplement. If added in total, this food supplement could reduce the stored food mass by 14 %.

Since the urine store is never fully depleted, urine is always available as nitrogen source for the algal culture and therefore no further nutrients have to be added, which is in contrast to the initially proposed design by Niederwieser [5]. The photobioreactor's overall mass balance of matter in- and outflows is given in Table 7-1 as daily averages over the course of seven days.

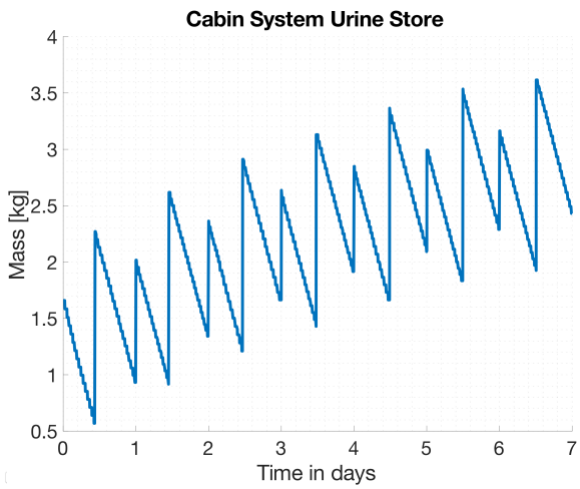

Figure 7-6: Evolution of urine store mass with optimistic growth rate

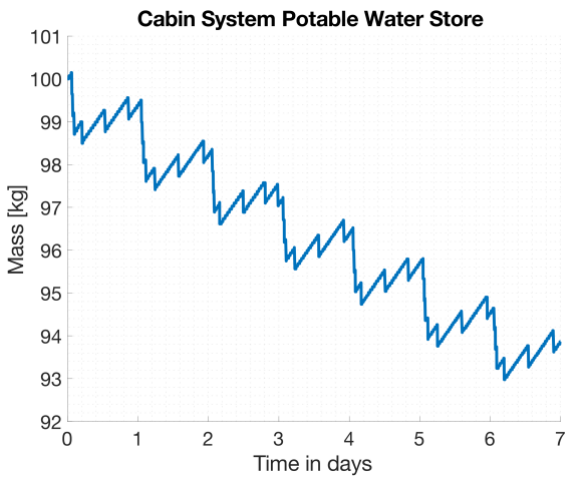

Figure 7-7: Evolution of potable water store mass with optimistic growth rate

Table 7-1: Overall mass balance of matter in- and outflows. Left column shows the values originally proposed by Niederwieser [5] and the right column the averaged values of the simulated results (+ is into reactor, - is out).

Substance	Niederwieser Proposal [kg/d]	Simulation case averages [kg/d]
Oxygen	- 0.816	- 0.463
Carbon Dioxide	+ 1.040	+ 0.527
Biomass	- 0.255	- 0.296
Nutrients	+ 0.11	0
Pre-Processed Water	- 1.589	- 2.33
Urine	+ 1.6	+ 2.417

Since this design was calculated to be capable of providing sufficient oxygen production and carbon dioxide removal capability with the optimistic growth rate, the question arises, why the simulation shows that it is not. As seen in Figure 7-8, the achievable growth rate is only at around 60 % of its theoretical maximum while the biomass concentration is regulated successfully at the concentration where maximum growth should actually be occurring, in this case $\rho_{b_{opt}} = 6.68\,\mathrm{kg}/m3$.

On a side note: the theoretical biomass growth rate (absolute value $[\mathrm{kg}/s]$, not biomass concentration increase $[\mathrm{kg}/m^3 * s]$) is slightly decreasing over time due to water being used for photosynthesis, thus increasing the biomass concentration. The harvester reacts by harvesting more algal cells until the biomass concentration set point is reached again, which reduces the overall culture size and therefore less algal culture is available to perform photosynthesis.

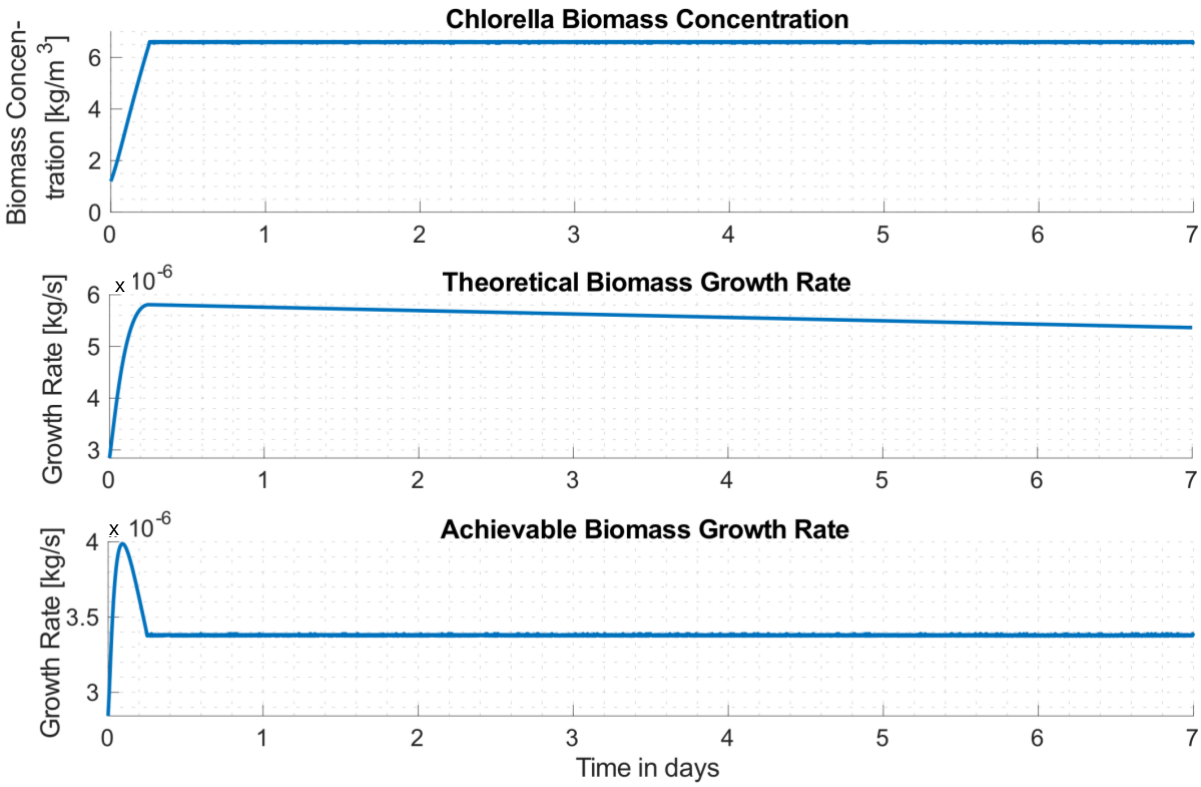

Figure 7-8: Evolution of biomass concentration (top) regulated to remain at the cultures highest growth rate, the biomass concentration-dependent theoretical biomass growth rate (middle) and the possible growth rate (bottom) over the course of seven simulated days.

The answer to the question about the reduced growth rate can be found in the photosynthetically active radiation available to the growing algal culture. In fact, the reason for the limited growth is due to two thirds of the algal culture being in the linear, “light limited”, and not saturated growth domain as seen in Figure 7-9.

As the biomass concentration increases (see Figure 7-8), the attenuation coefficient rises. The more radiation is attenuated as it passes from the photobioreactor’s surface through the algal culture, the less radiation reaches the lower lying layers of the algal culture. As seen in the graph in the middle of Figure 7-9, only about 0.85 mm below the surface is irradiated in the saturated growth domain, where full growth can occur. Between 0.85 mm and 2.5 mm below the irradiated surface, the algae are light limited and can only grow at a less than optimum growth rate. The larger the linear growth zone becomes, the less photon flux density is available inside of it on average. Almost 10 liters of the culture volume, two thirds of the entire reactor, are growing at only about 30 % (calculated by simulation, data not shown here) of the theoretical optimum. Consequentially, the resulting overall growth factor representing the effect of photosynthetically active radiation is 0.6 (see Figure 7-9 bottom graph) and decreases the theoretically possible growth by 40 %.

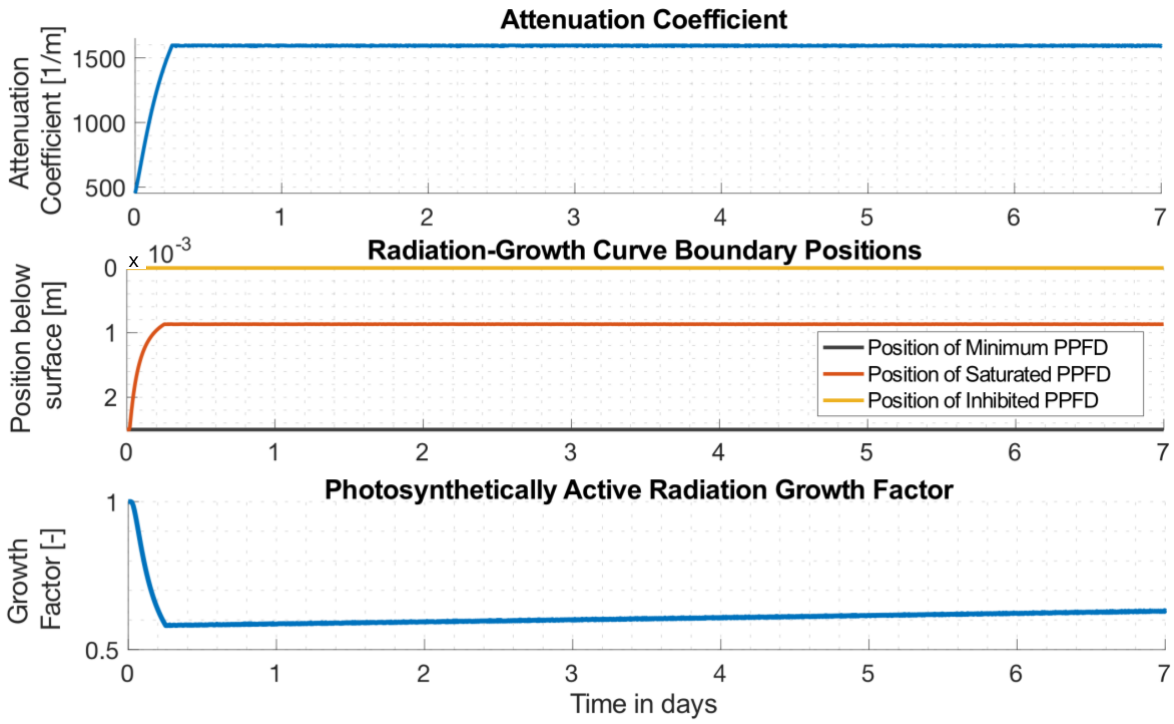

Figure 7-9: Evolution of attenuation coefficient (top), the radiation-growth curve's boundary positions (middle) and the resulting photosynthetically active radiation growth factor (bottom).

7.2.1 Photobioreactor Performance Increase Optimization

The information in Figure 7-8 and Figure 7-9 can be used in a next step to optimize the design toward an increased growth rate in two different ways.

One option is related to changing the set point of the biomass harvest controller to a lower biomass concentration, which is outlined in 7.2.2.

Another option is connected to decreasing the plate thickness (also called culture depth) of the photobioreactor to eliminate the linear growth zone altogether. This means of optimization is outlined in 7.2.3.

7.2.2 Optimization with Harvest Controller Set Point Variation

In this case, one has to accept that some of the photobioreactor's volume will be in the linear growth zone, but it should be kept as small as possible.

The graph at the bottom of Figure 7-8 shows, that initially the achievable growth rate increases but then starts to fall again after a peak at $\mu_{achievable_{opt}} = 3.987 * 10^{-6}\, kg/s$ due to the increasingly strong effect of attenuation. Although it is not the absolute optimum growth, which is $\mu_{achievable} = 5.835 * 10^{-6}\, kg/s$, it is better than the $\mu_{achievable} = 3.379 * 10^{-6}\, kg/s$ that is reached in the steady state.

The biomass harvest controller is set for the biomass concentration at which the theoretical optimum growth rate occurs. However, this theoretical growth rate is not reachable in this case because the simulation shows that it is decreased due to the strong attenuation of photosynthetically active radiation. If the harvest controller is set to the biomass concentration, at which the achievable optimum growth occurs, the

growth rate will remain at that point constantly. In this case, the achievable optimum growth rate $\mu_{achievable_{opt}} = 3.987 * 10^{-6}\, kg/s$ occurs at $\rho_b = 3.149\, \mathrm{kg}/m3$, which shall be treated as new harvester set point for this optimization analysis. All other parameters, especially the membrane surface of 5 square meters and the culture volume of 15 liters are left the same.

The simulation results show, that the volume of the photobioreactor in the saturated growth domain has increased from 5 L to 6.5 L and furthermore, the average photon flux density in the linear growth volume (9 L) has increased from 30 to 60 µmol/m^{2}s. As a result, the growth limitation due to the attenuation of photosynthetically active radiation decreases from 40 % to 15 %. This leads to an improved effect on the cabin atmosphere, as seen in Figure 7-10.

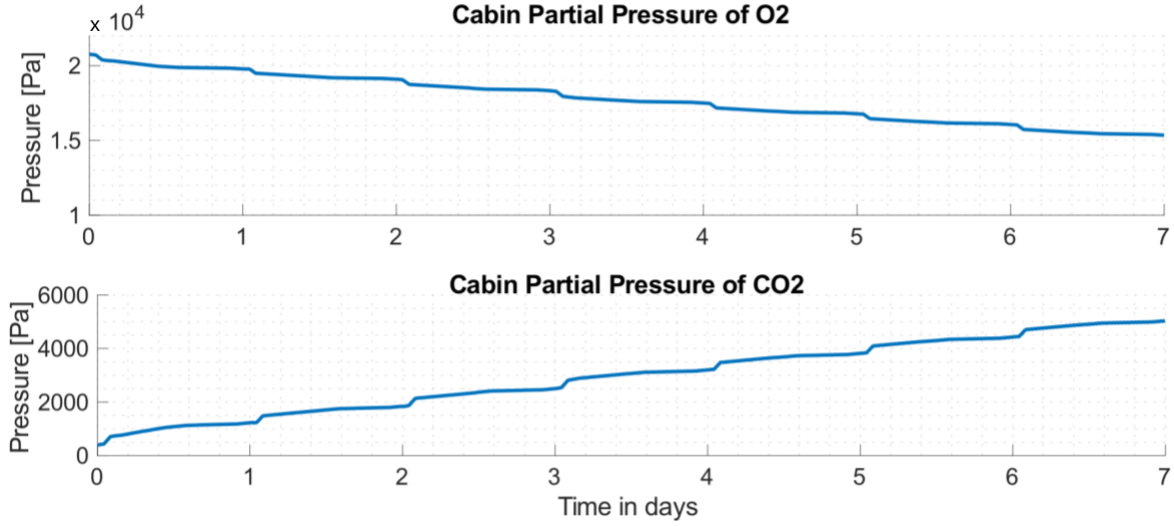

Figure 7-10: Evolution of oxygen (top) and carbon dioxide (bottom) partial pressures in the cabin atmosphere with a decreased harvest controller set point.

While the effect of this optimization is not very strong, some differences can be observed. The oxygen partial pressure only decreases to 15.4 kPa and the carbon dioxide partial pressure increases to 5 kPa.

This case reaches a 100 % urine regeneration capability, as seen in Figure 7-11 and supplies 18.6 kg of potable water to the potable water store as seen in Figure 7-12. The net water usage over the course of seven days is at 18 % (a large part of this is attributed to the respiration water captured by the common cabin air assembly, which is currently not used any further) During the course of 7 days, 2.5 kg of dry Chlorella biomass is generated as seen in Figure 7-14. Since the urine is slightly insufficient in this case to provide all the nitrogen to the algal culture, some additional nitrate is supplied as shown in Figure 7-13.

An overall balance of masses that enter and leave the photobioreactor as daily averages over the course of seven days is shown in Table 7-2.

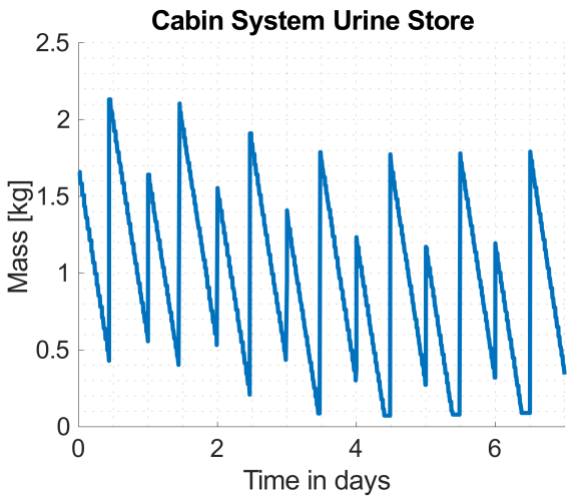

Figure 7-11: Evolution of urine store mass with optimistic growth rate and harvest controller set point optimized.

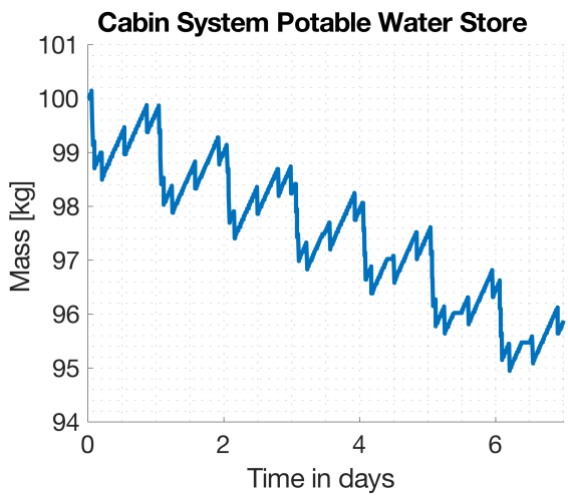

Figure 7-12: Evolution of potable water store mass with optimistic growth rate and harvest controller set point optimized.

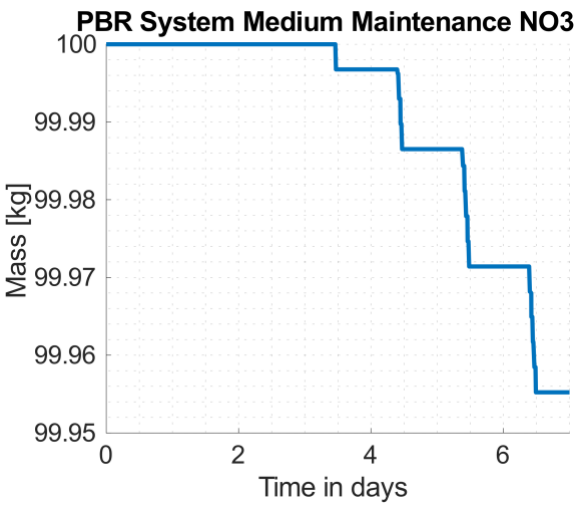

Figure 7-13: Evolution of nitrate supply mass with optimistic growth rate and harvest controller set point optimized

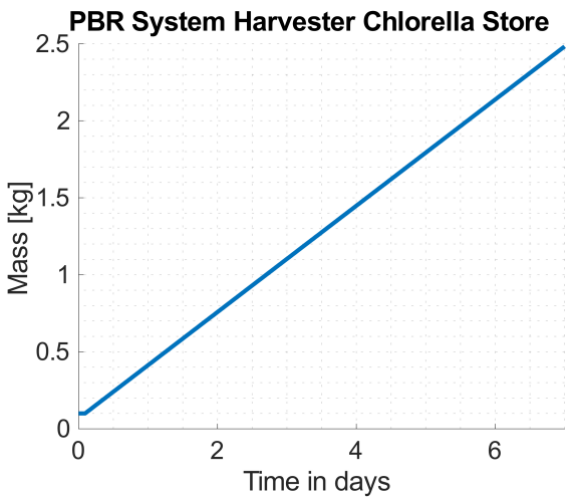

Figure 7-14: Evolution of the harvested Chlorella mass with optimistic growth rate and harvest controller set point optimized.

Table 7-2: Overall mass balance of matter in- and outflows. Left column shows the values originally proposed by Niederwieser [5], the middle column the averaged values of the simulated results of the proposed design and the right column the averaged results of the optimized design with a changed harvest controller set point (+ is into reactor, - is out).

Substance	Niederwieser Proposal [kg/d]	Simulation case averages [kg/d]	Optimized Averages [kg/d]
Oxygen	- 0.816	- 0.463	- 0.550
Carbon Dioxide	+ 1.040	+ 0.527	+ 0.619
Biomass	- 0.255	- 0.296	- 0.355
Nutrients	+ 0.11	0	+ 0.006
Pre-Processed Water	- 1.589	- 2.33	- 2.62
Urine	+ 1.6	+ 2.417	+ 2.714

Since the optimization did not lead to a large improvement in oxygen and carbon dioxide cabin atmosphere partial pressures, the reactor's volume is scaled up to a size, where – with the optimistic growth model and a culture depth of 2.5 mm, optimized with a varied harvest controller set point – it can support one human over the course of one week in terms of air revitalization.

7.2.2.1 Optimization with Harvest Controller Set Point Variation and Increased Volume

The previously described photobioreactor using a decreased harvest controller set point is scaled up to a volume of 32 L and the is then capable of providing sufficient air revitalization, as seen in Figure 7-15. The membrane surface area is left at 5 m^2.

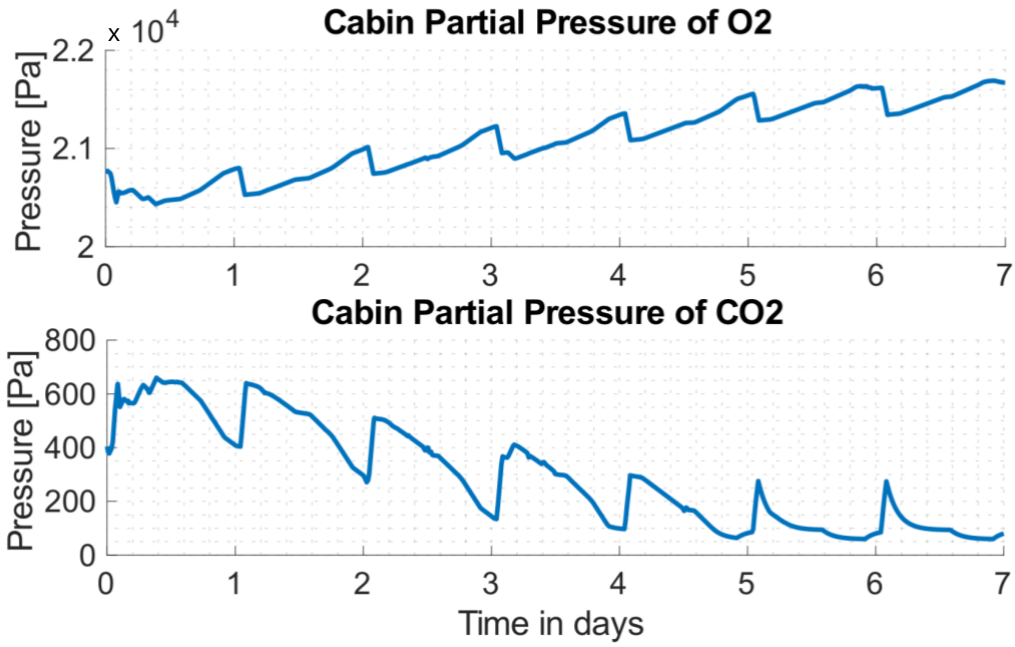

Figure 7-15: Evolution of oxygen (top) and carbon dioxide (bottom) partial pressures in the cabin atmosphere with a decreased harvest controller set point and scaled up volume to 32 L.

The oxygen partial pressure fluctuates with about 300 Pa throughout the course of the day, but shows an overall upward trend after a slight initial drop and does not fall below its starting value after day 2. The carbon dioxide partial pressure fluctuates with about 300 Pa throughout the course of the day and shows an overall downward trend. The carbon dioxide partial pressure does not climb above 680 Pa, which is the 180 day long term exposure limit defined by the National Aeronautics and Space Administration's Human Integration Design Handbook [112]. The lag time is not simulated in this case to achieve a steady behavior faster. However, the time it takes for the biomass concentration to reach the point where the algal culture is growing in its optimum takes about three hours (in this case not the absolute optimum, since the reactor design was optimized for a given plate thickness). In these three hours, less than the exhaled carbon dioxide is consumed by the algae leading to an increase in carbon dioxide partial pressure which has an effect over the next 2 days. This fact shows that even a short downtime on the scale of hours has a noticeable adverse effect on the cabin atmosphere, which can be noticed over the scale of days, since the photobioreactor is sized to be as small as possible and has no extra capacity. A larger photobioreactor could compensate this more easily but would be limited in growth by the lack of carbon dioxide at least some of the time and therefore not operating in its optimum.

This simulation case also provides urine processing and food production capability. Since the algae are now growing at a higher growth rate than previously, the urine provided by one human is insufficient and nitrate must be added additionally. The mass evolution of the stored urine is shown in Figure 7-16, where the times of urine depletion (regulated to always leave 0.1 kg of mass in the store) can be seen as horizontal lines and nitrate is supplied during these times, as seen in Figure 7-18. This scenario shows a 100 % urine processing capability and about 1 kg of nitrate are used additionally over the course of seven days, while producing a total 4.8 kg of algal biomass (see Figure 7-19). With a net water usage of only 3.94 kg over this time period, the algal photobioreactor shows the potential to reduce water usage by 83 %. Since all the urine is processed, the 17 % of water "lost", can be attributed to the stored feces, to be consumed by the biomass in the process of photosynthesis and most importantly, captured by the common cabin air assembly from respiratory water.

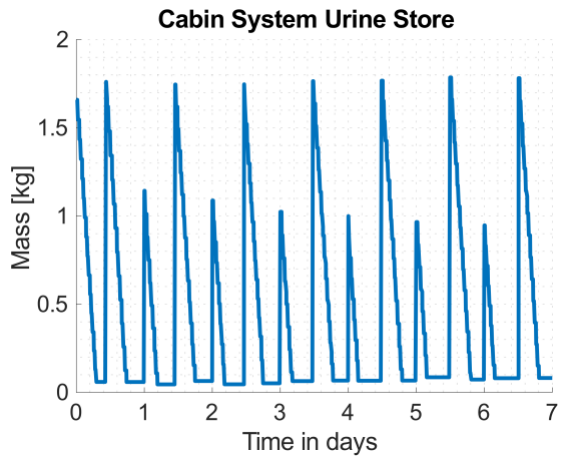

Figure 7-16: Evolution of urine store mass with optimistic growth rate, harvest controller set point optimized and scaled up.

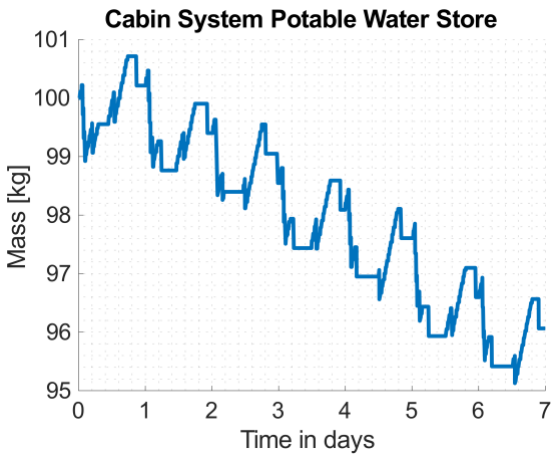

Figure 7-17: Evolution of potable water store mass with optimistic growth rate, harvest controller set point optimized and scaled up.

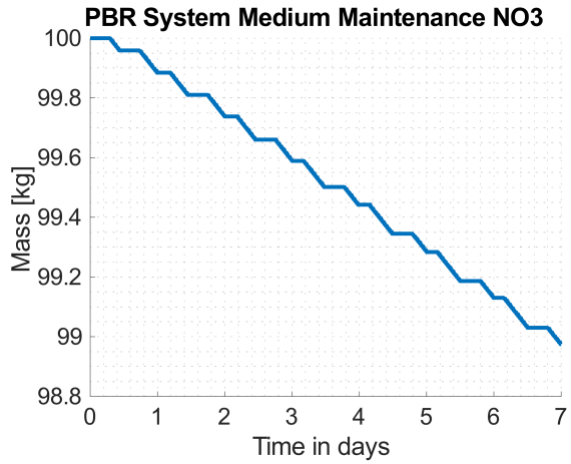

Figure 7-18: Evolution of nitrate supply mass with optimistic growth rate, harvest controller set point optimized and scaled up

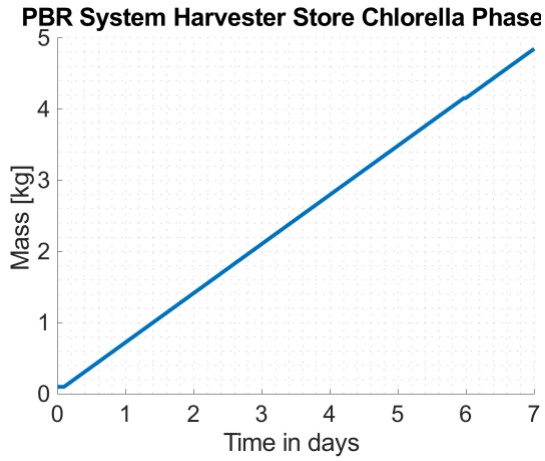

Figure 7-19: Evolution of the harvested Chlorella mass with optimistic growth rate, harvest controller set point optimized and scaled up.

A consequence of the use of nitrate is the release of hydroxide ions into the medium as outlined in 3.2.2.1, which increases the pH of the medium. The evolution of the medium pH is shown in Figure 7-20. At first glance it seems to be of low resolution due to the visible steps, especially during day 1 and 2. However, the steps are a result of discontinuous nitrate supply. Due to the nitrate metabolism, the pH increases during the times, when nitrate is supplemented. If urine is available, its supply has precedent over nitrate, which can be seen in the horizontal parts of the pH evolution graph, since the urine metabolism in algae has no impact on the pH. Another observation that can be made from the graph in Figure 7-20 is the strong impact the phosphate and bicarbonate buffers have on the medium pH evolution. While nitrate is supplied at rather continuous intervals (see Figure 7-18), the pH does not increase significantly over the first five days once it reaches a value of around seven.

A further interesting observation can be made with regards to the medium pH being affected by carbon dioxide. As shown in Figure 7-20, it increases rather smootly until day 5 and then shows strong fluctuations. The effect for this can be found in the low carbon dioxide partial pressure in the cabin from day 5 onward (see Figure 7-15), which translates to a decreased partial pressure of carbon dioxide in the photobioreactor air supply. The membrane transport can not be kept sufficiently high and the concentration of carbon dioxide in the medium drops. Besides not being available for photosynthesis, which is also shown through the CO_2 availability factor in Figure 7-20, the lack of carbon dioxide leads to a decrease of total inorganic carbon and a hydrogen ion consuming shift to the left in the total inorganic carbon balance (see 3.3.3), which means that less hydrogen ions are in the medium and thus the pH rises.

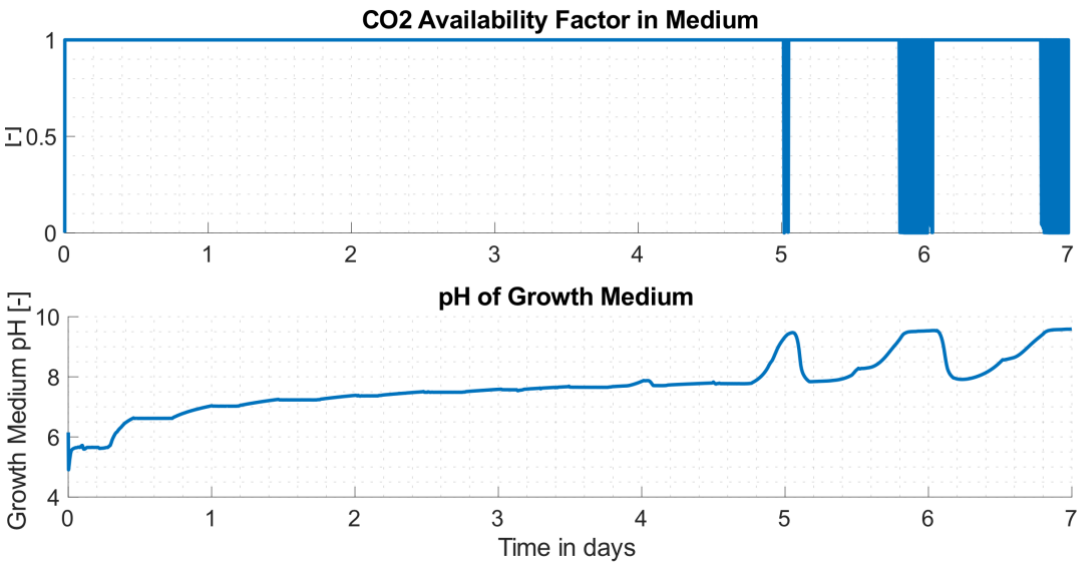

Figure 7-20: Growth Medium pH increase as a result of carbon dioxide deprivation.

An overall mass balance of the simulation case and this optimization is given in Table 7-3.

Table 7-3: Overall mass balance of matter in- and outflows. Left column shows the values originally proposed by Niederwieser [5], the middle column the averaged values of the simulated results of the proposed design and the right column the averaged results of the optimized design with a changed harvest controller set point (+ is into reactor, - is out).

Substance	Niederwieser Proposal [kg/d]	Simulation case averages [kg/d]	Optimized Averages [kg/d]
Oxygen	- 0.816	- 0.463	- 1.286
Carbon Dioxide	+ 1.040	+ 0.527	+ 1.338
Biomass	- 0.255	- 0.296	- 0.6925
Nutrients	+ 0.11	0	+ 0.146
Pre-Processed Water	- 1.589	- 2.33	- 2.66
Urine	+ 1.6	+ 2.417	+ 2.75

7.2.3 Optimization with Decreased Culture Depth

Since the position below the surface, where the linear growth domain begins is known, and it is desirable to keep the entire photobioreactor in the saturated growth domain, this information can be used as a means of optimization.

The new depth below surface of the photobioreactor is decreased to the thickness, that the previous simulation showed to be in the saturated growth domain. In this case the depth below the surface, where the saturated growth domain ends and the linear growth domain starts, is at just 0.85 mm below the surface. When irradiated from two sides, like proposed by Niederwieser, then the culture depth of 0.85 mm would result in a 1.9 mm plate thickness.

All other parameters, especially the membrane surface of 5 square meters and the culture volume of 15 liters are left the same. Furthermore, the harvester biomass concentration set point is set to $\rho_{b_{opt}} = 6.68\,\mathrm{kg}/m3$, which is where the absolute optimum growth rate of this growth model occurs (as opposed to the previous sub-chapter, where it was reduced).

The simulation results show, that all the algal cells are now in the saturated growth for the entire duration of seven days. Another proof for this is that the photosynthetic photon flux density exiting the photobioreactor is above the saturation photon flux density of $P_{sat} = 100\,\mu mol/(m^2 * s)$. The growth is now no longer limited as seen in Figure 7-21.

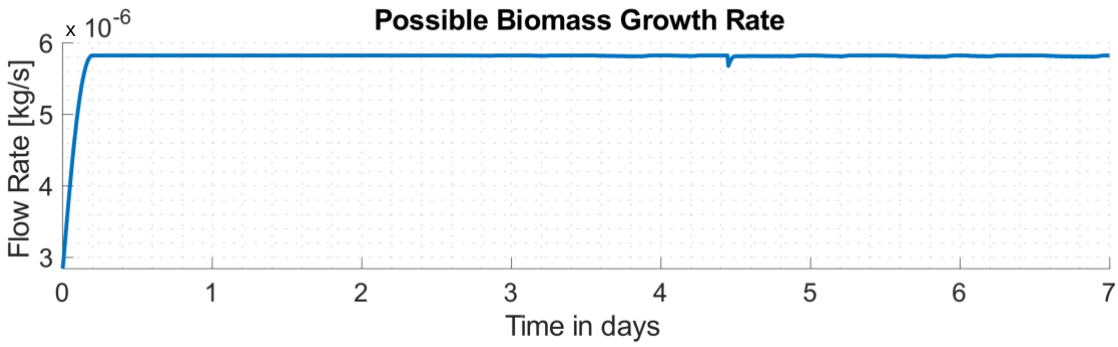

Figure 7-21: Possible biomass growth rate with optimistic growth rate in its optimum with a culture depth below surface of 0.85 mm.

The evolution of oxygen and carbon dioxide partial pressures is shown in Figure 7-22. While the oxygen partial pressure now only falls by 3 kPa to 18 kPa, the carbon dioxide pressure still rises to levels way above acceptable limits.

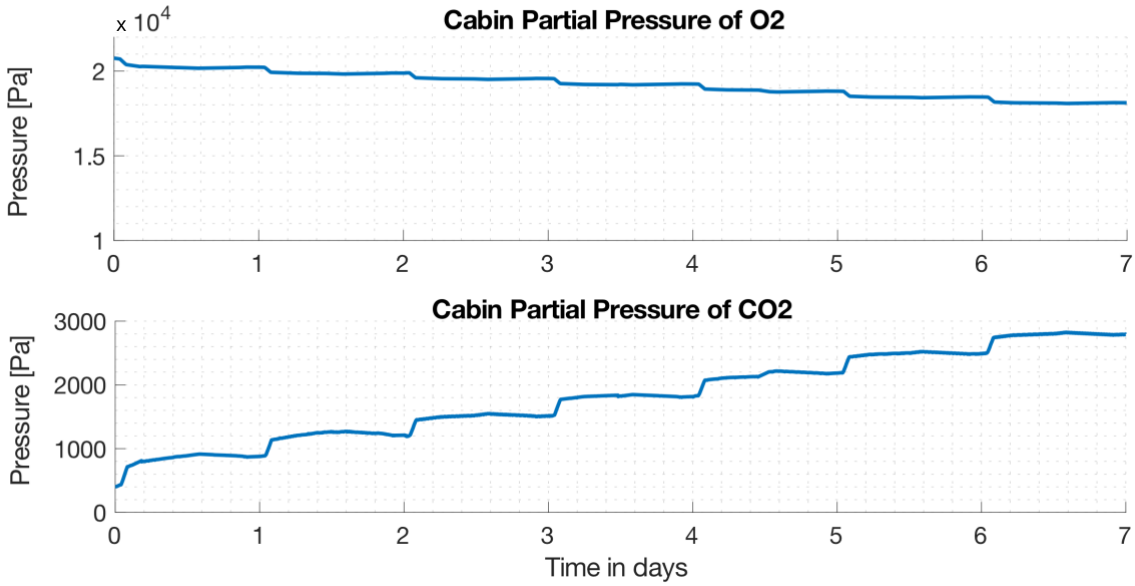

Figure 7-22: Evolution of oxygen (top) and carbon dioxide (bottom) partial pressures with optimistic growth rate and optimized by decreased culture depth of 0.85 mm.

This simulation case also provides urine processing and food production capability. Since the algae are now growing at a higher growth rate than previously, the urine provided by one human is insufficient (Figure 7-23) and nitrate must be added additionally. A direct consequence of a 100 % urine recovery is a 83% water savings capability as previously described in 7.2.2.1 Figure 7-25 shows that a total of 0.5 kg nitrate are used additionally over the course of seven days. Figure 7-26 shows that this scenario produces 3.5 kg of dry algal biomass over the course of seven days.

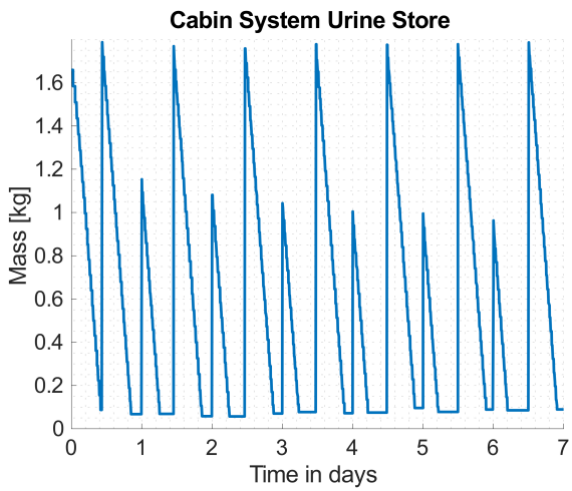

Figure 7-23: Evolution of urine store mass with optimistic growth rate and depth optimized.

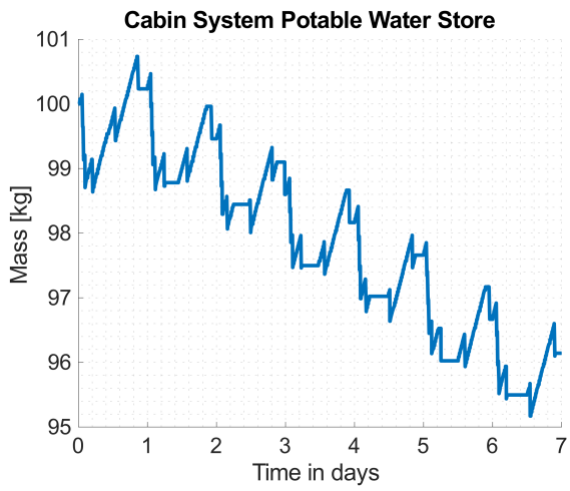

Figure 7-24: Evolution of potable water store mass with optimistic growth rate and depth optimized.

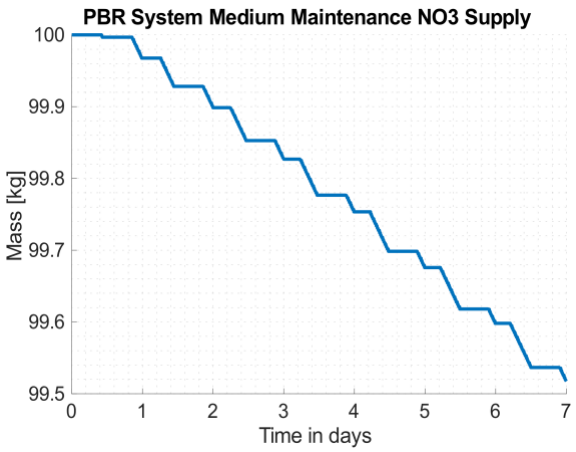

Figure 7-25: Evolution of nitrate supply mass with optimistic growth rate and depth optimized.

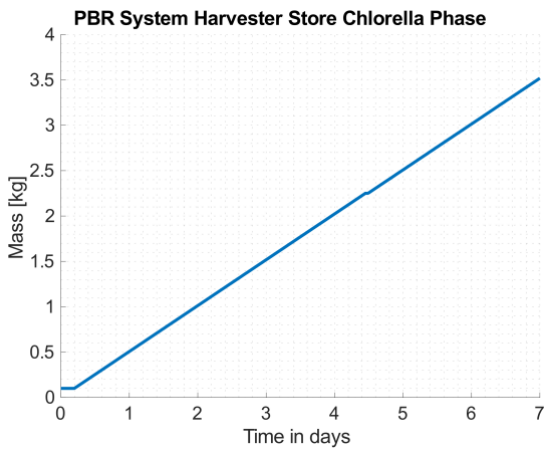

Figure 7-26: Evolution of the harvested Chlorella mass with optimistic growth rate and depth optimized.

The reactor is still not capable to sustain a breathable cabin atmosphere for a human in the long run, since oxygen is decreasing over time and carbon dioxide increasing (albeit at a slower rate than before). This can also be attributed to the fact, that the assumptions for the human oxygen consumption and carbon dioxide production in the Niederwieser proposal deviate from those simulated by the V-HAB human model (e.g. 1.37 kg/d CO_2 and 1.15 kg/d O_2 on day 1). The values presented in Table 7-4, show that the optimized reactor (culture volume 15 liters, depth 0.85 mm) reactor would already be able to support the Niederwieser assumption for human oxygen consumption, but not yet fully clear all the carbon dioxide. This is due to the fact that the algal assimilation coefficient does not perfectly match the human respiration coefficient – a challenge which is also discussed in the next sub-chapter 7.2.3.1.

Table 7-4: Overall mass balance of matter in- and outflows. Left column shows the values originally proposed by Niederwieser [5], the middle column the averaged values of the simulated results of the proposed design and the right column the averaged results of the optimized design with reduced depth (+ is into reactor, - is out).

Substance	Niederwieser Proposal [kg/d]	Simulation case averages [kg/d]	Optimized Averages [kg/d]
Oxygen	- 0.816	- 0.463	- 0.86
Carbon Dioxide	+ 1.040	+ 0.527	+ 0.925
Biomass	- 0.255	- 0.296	- 0.5
Nutrients	+ 0.11	0	+ 0.068
Pre-Processed Water	- 1.589	- 2.33	- 2.65
Urine	+ 1.6	+ 2.417	+ 2.75

Since the growth is now occurring at the optimum of what the algal culture can achieve, the only further means of optimization and reaching sufficient air revitalization capability is to scale the reactor up.

7.2.3.1 Optimization with Decreased Culture Depth and Increased Volume

Even with a decreased culture depth to just 0.85 mm below the irradiated surface and the optimistic growth rate proposed by Niederwieser, the photobioreactor with 15 liters of culture volume is still not capable of supporting a human over the course of one week. The only further improvement that can be made in this case is to scale up the reactor. For this optimization case it is increased by 43 % to a volume of 21.5 liters, the membrane was kept at 5 m^2.

The evolution of the cabin atmosphere oxygen and carbon dioxide partial pressures is shown in Figure 7-27. The oxygen partial pressure fluctuates over the course of each day but never falls below less than 300 Pa of the starting value of 20.8 kPa. In fact, there is an upward trend of oxygen partial pressure over the course of the seven simulated days, ending at 21 kPa partial pressure. The carbon dioxide partial pressure also fluctuates throughout the course of the day with a steep increase during times when the human exercises and a decrease during daily activities and sleep. The carbon dioxide partial pressure remains below 680 Pa for most of the day, which is the 180 day long term exposure limit defined by the National Aeronautics and Space Administration's Human Integration Design Handbook [112]. It climbs slightly above that for around 7 hours after the exercise with a peak at 720 Pa, which is still below the 24 hour exposure limit of 1.3 kPa. Slightly increasing the reactor volume would push these peaks to below 680 Pa if required.

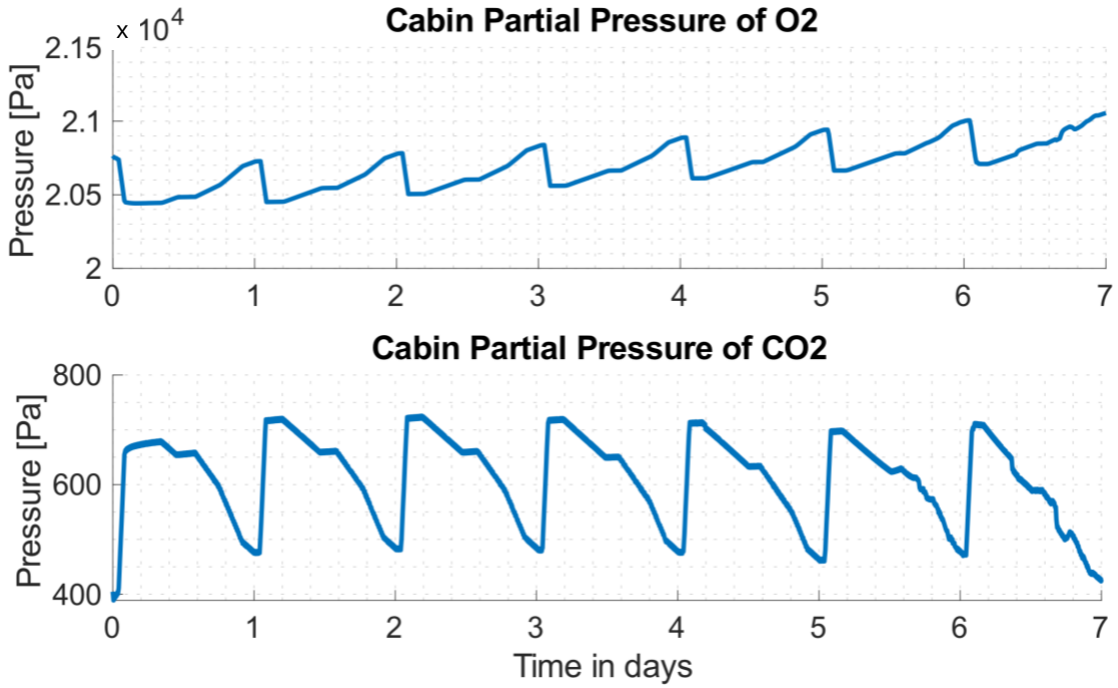

Figure 7-27: Evolution of oxygen (top) and carbon dioxide (bottom) partial pressures with optimistic growth rate, decreased culture depth of 0.85 mm and scaled-up volume of 20 liters.

An interesting observation that can be made when looking at the results from this simulation case is the deviation of carbon dioxide and oxygen partial pressure trends: the carbon dioxide partial pressure remains rather constant, while the oxygen partial pressure increases in the long run. The reason is that the human respiration coefficient (mol CO2 exhaled per mol O2 consumed) and algal assimilation coefficient do not match each other perfectly. While the human respiration coefficient varies depending

on the consumed food, the algal respiration coefficient varies due to what nitrogen nutrient is used. Overall the algal assimilation coefficient is lower than the human respiration coefficient as shown in Figure 7-28. This means that for a given amount of carbon dioxide exhaled by the human and consumed by the algal culture, the algae produce more oxygen than is taken up by the human to produce that amount of carbon dioxide.

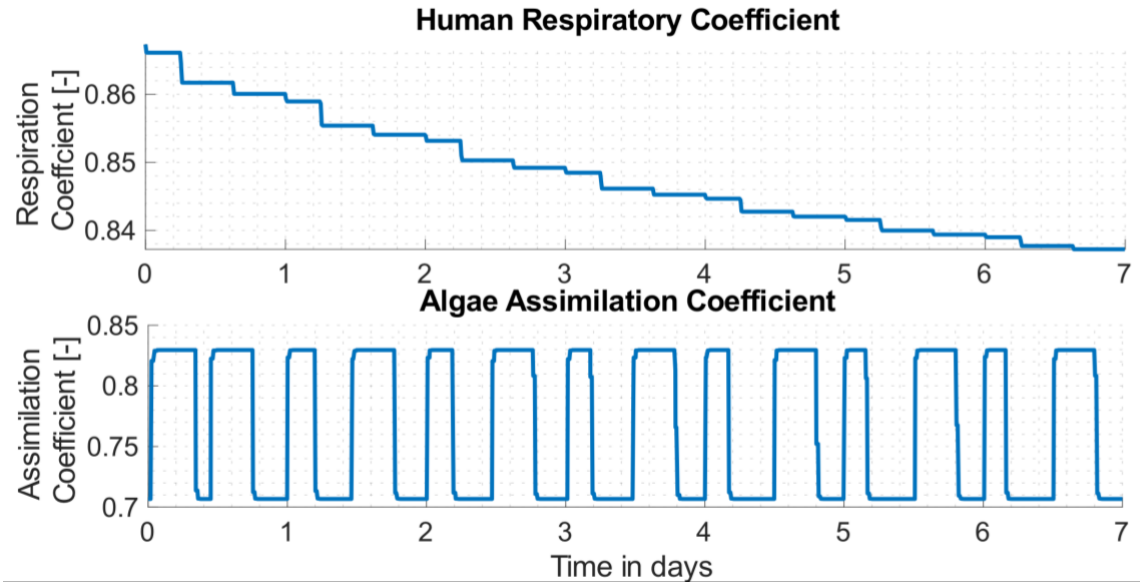

Figure 7-28: Comparison between human respiration coefficient and algae assimilation coefficient (mol CO2 consumed per mol O2 produced). Respiration coefficient is decreasing due to diet and algae assimilation coefficient fluctuating due to nitrogen nutrient variation (urine vs nitrate).

This simulation case provides urine processing and food production capability. Since all available urine is used (Figure 7-29), the reactor provides a 100 % urine processing and 83 % water savings (see Figure 7-30), capability, as in previous cases. A total 1 kg nitrate is supplied during times of urine depletion, as seen in Figure 7-31. Figure 7-32 shows that this scenario produces 4.5 kg of dry algal biomass over the course of seven days.

The summary with the overall mass balance of this optimization is provided in Table 7-5. From where a further result of this simulation case and the following optimization can be obtained: the Niederwieser model assumes too low rates of oxygen consumption and carbon dioxide production, when compared to the V-HAB human model, since 20 % more carbon dioxide removal capability are required than initially assumed.

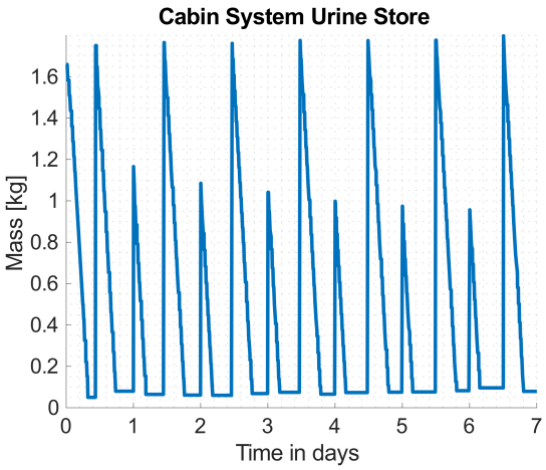

Figure 7-29: Evolution of urine store mass with optimistic growth rate, depth optimized and scaled up.

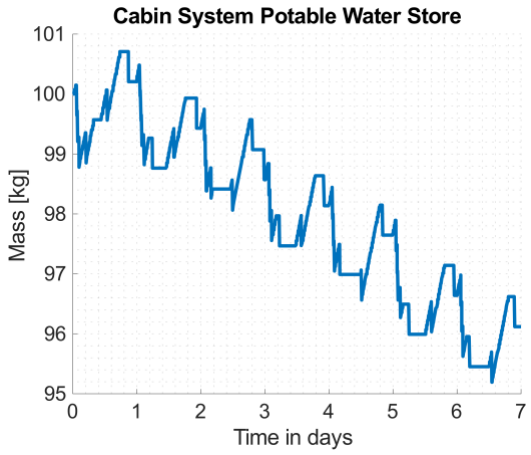

Figure 7-30: Evolution of potable water store mass with optimistic growth rate, depth optimized and scaled up

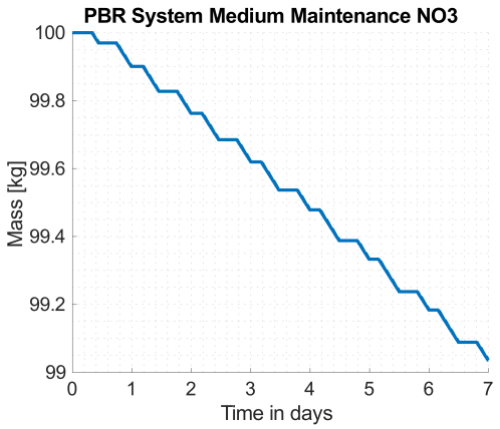

Figure 7-31: Evolution of nitrate supply mass with optimistic growth rate, depth optimized and scaled up.

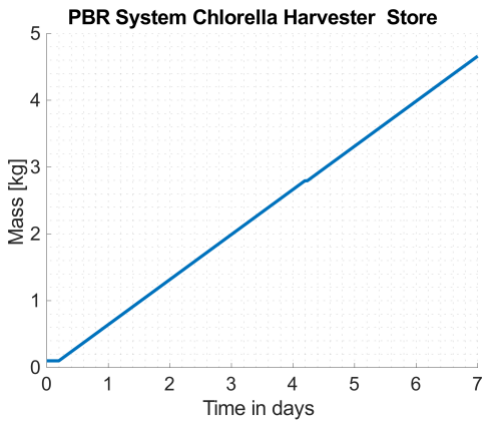

Figure 7-32: Evolution of the harvested Chlorella mass with optimistic growth rate, depth optimized and scaled up.

Table 7-5: Overall mass balance of matter in- and outflows. Left column shows the values originally proposed by Niederwieser [5], the middle column the averaged values of the simulated results of the proposed design and the right column the averaged results of the optimized design with reduced depth and increased volume (+ is into reactor, - is out).

Substance	Niederwieser Proposal [kg/d]	Simulation case averages [kg/d]	Optimized Averages [kg/d]
Oxygen	- 0.816	- 0.463	- 1.194
Carbon Dioxide	+ 1.040	+ 0.527	+ 1.251
Biomass	- 0.255	- 0.296	- 0.666
Nutrients	+ 0.11	0	+ 0.137
Pre-Processed Water	- 1.589	- 2.33	- 2.66
Urine	+ 1.6	+ 2.417	+ 2.75

7.3 Niederwieser Photobioreactor With Experimental Growth Model

When the small volume of 15 liters of the Niederwieser photobioreactor design is combined with the experimentally determined growth rate, it is not capable to sufficiently turn carbon dioxide into oxygen.

The evolution of carbon dioxide and oxygen partial pressures over the course is shown in Figure 7-33. The oxygen partial pressure drops to levels as low as 11.44 kPa, just 200 Pa above the comparison baseline, where no photobioreactor was used. The carbon dioxide level increases to 8.2 kPa, which is 20 times the level of its initial concentration and well above any tolerable limits for humans defined by the National Aeronautics and Space Administration's Human Integration Design Handbook [112].

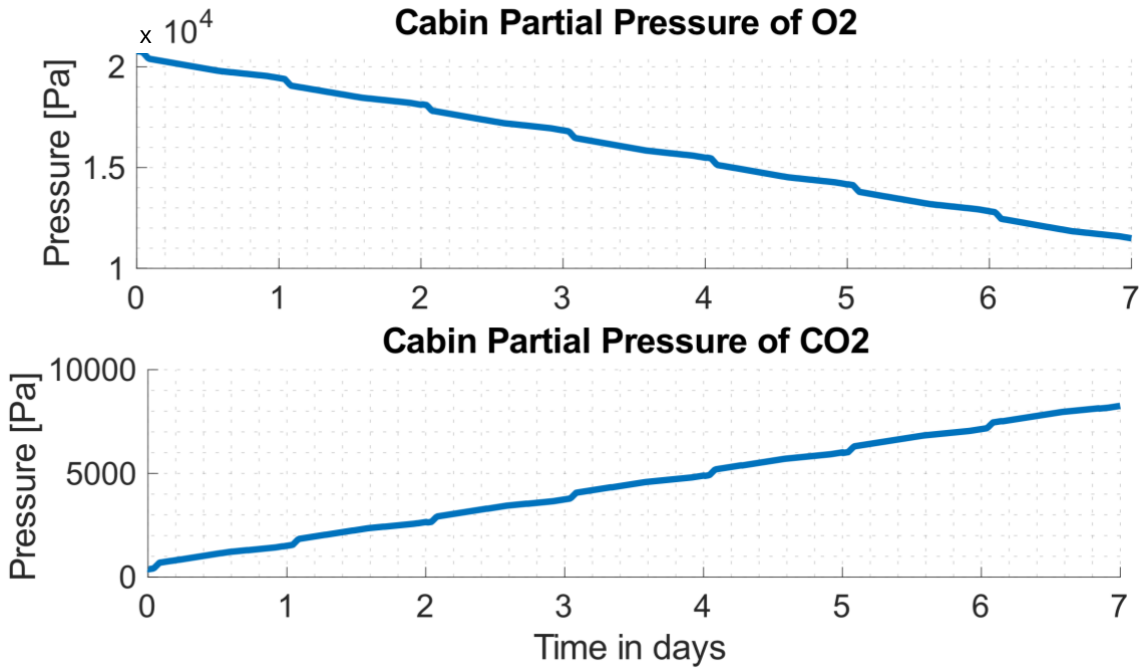

Figure 7-33: Evolution of oxygen (top) and carbon dioxide (bottom) partial pressures with Niederwieser design (15 L volume and 2.5 mm culture depth) with experimentally determined growth rate.

This simulation case provides almost no urine processing and food production capability. The mass evolution of the stored urine mass is shown in Figure 7-34, which climbs to only 1 kg below the baseline, where no photobioreactor is used. This scenario therefore shows a 5.6 % urine processing capability. Consequentially the net water usage is only 1 kg below the comparison baseline as seen in Figure 7-35. Since the urine is never depleted, no nitrate must be added and the store remains at its initial value of 100 kg as seen in Figure 7-36. As a result of harvesting to maintain the optimum growth rate, Figure 7-37 shows that this scenario only produces 0.23 kg of dry algal biomass over the course of seven days.

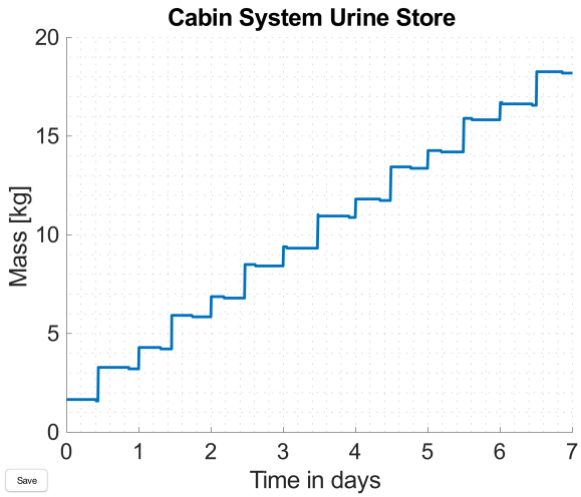

Figure 7-34: Evolution of urine store mass in Niederwieser design (15 L) with experimental growth rate.

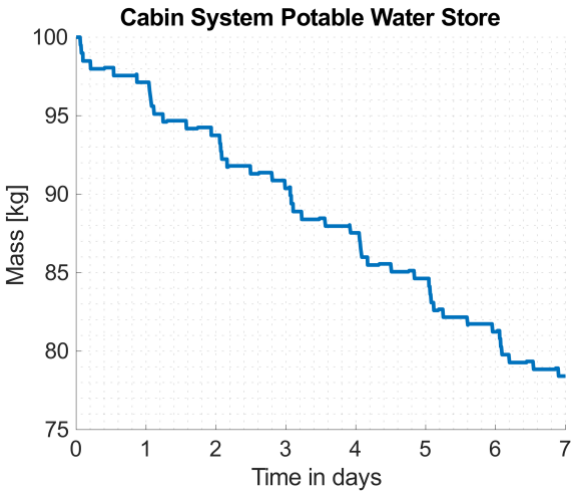

Figure 7-35: Evolution of potable water store mass in Niederwieser design (15 L) with experimental growth rate.

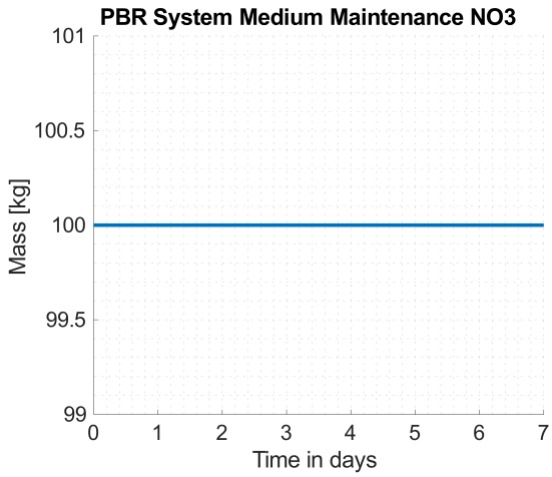

Figure 7-36: Evolution of nitrate supply mass in Niederwieser design (15 L) with experimental growth rate.

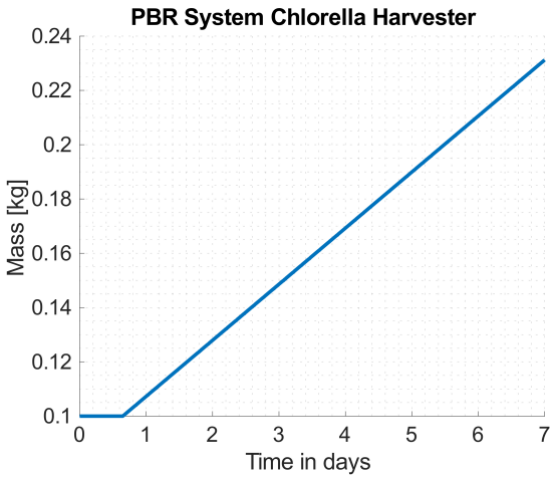

Figure 7-37: Evolution of the harvested Chlorella mass in Niederwieser design (15 L) with experimental growth rate.

The Niederwieser photobioreactor combined with the experimentally determined growth rate is too small to support a human in terms of air revitalization and also only provides insignificant amounts of urine processing and food production as shown in Table 7-6.

The simulation results show, that no factor is limiting the algal growth but the low growth rate itself. The experimental growth rate, combined with the very small volume of just 15 L is insufficient to support a human. When the experimentally determined growth rate is used, the photobioreactor has to be scaled up significantly to provide sufficient air revitalization. This is done in the next sub-chapter 7.4.

Table 7-6: Overall mass balance of matter in- and outflows. Left column shows the values originally proposed by Niederwieser [5] and the right column the averaged values of the simulated results with the experimentally determined growth rate (+ is into reactor, - is out).

Substance	Niederwieser Proposal [kg/d]	Simulation case averages [kg/d]
Oxygen	- 0.816	- 0.032
Carbon Dioxide	+ 1.040	+ 0.037
Biomass	- 0.255	- 0.033
Nutrients	+ 0.11	0
Pre-Processed Water	- 1.589	- 0.141
Urine	+ 1.6	+ 0.146

7.4 Sufficiently sized Niederwieser Photobioreactor with experimental Growth Model

Using the experimentally determined growth rate, the originally proposed design by Niederwieser must be scaled up significantly in order to be able to support a human in terms of air revitalization. The scaling is done through iterations, where too large designs are characterized by being able to provide sufficient air revitalization but being growth limited through a lack of carbon dioxide at times. Too small designs are shown to have increasing carbon dioxide and decreasing oxygen partial pressures as shown in some of the previous simulation cases.

A size that works sufficiently has a culture volume of 500 L and is therefore 33 times larger than the originally proposed design by Niederwieser. This is on the order of magnitude of a 24 times higher growth rate and accounting for the fact that the originally proposed Niederwieser design is not sufficiently able to support the simulated oxygen consumption and carbon dioxide production of the V-HAB human model (even when its plate thickness is reduced to not be limited by the available photosynthetically active radiation). The evolution of oxygen and carbon dioxide partial pressure in the cabin atmosphere are shown in Figure 7-38.

The trend of oxygen partial pressure is slightly increasing and carbon dioxide slightly decreasing, while both are showing fluctuations between 200 and 300 Pa throughout the day. This behavior is already described in detail for other results in the previous sections of this chapter.

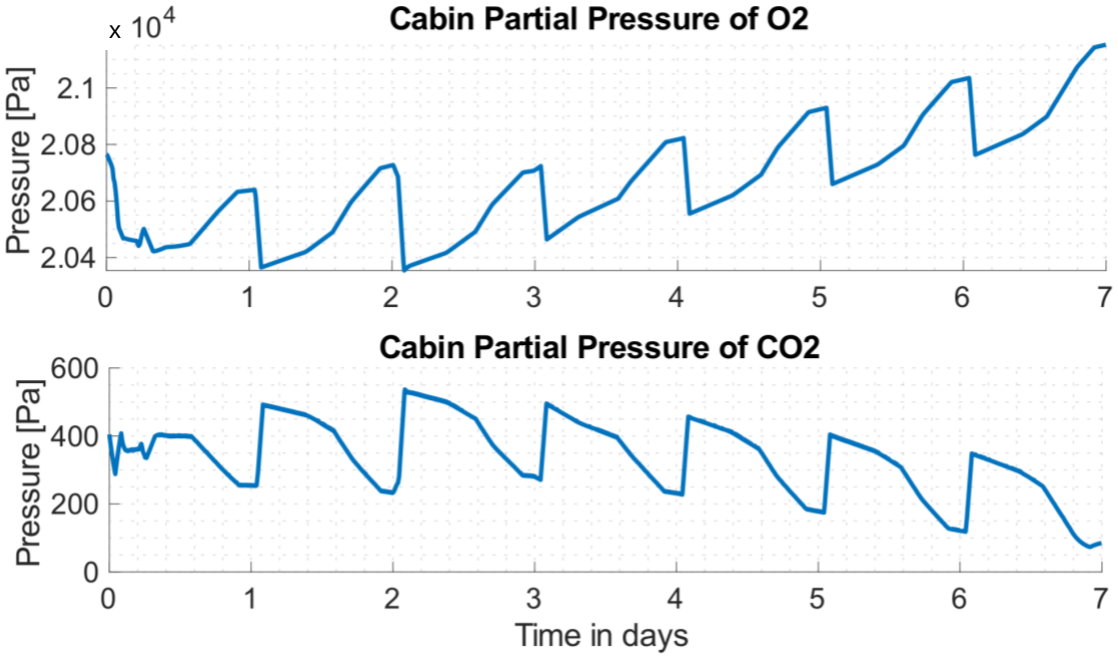

Figure 7-38: Evolution of oxygen (top) and carbon dioxide (bottom) partial pressures with scaled up Niederwieser design (500 L volume, 5 m^2 membrane and 2.5 mm culture depth) with experimentally determined growth rate.

One interesting observation can be made here, since the initial phase of carbon dioxide evolution differs from previous results. Previous results show a stark increase in carbon dioxide partial pressure, which builds up until the reactor is producing oxygen at the maximum growth rate and then takes 3-5 days for the photobioreactor to catch up with. Here the trend is different, the carbon dioxide partial pressure sees an initial drop in the beginning of the simulation, and only peaks on day 2. This is despite the fact that the maximum growth rate is not reached until 17 hours into the simulation, compared to only 3-4 hours with the optimistic growth rate. The decrease is due to the reactor's large volume, which can dissolve about 0.36 kg of carbon dioxide with a carbon dioxide partial pressure above the membrane of 60 kPa. This amount equates to around 30 % of what the V-HAB human model produces in an entire day. For oxygen this is not the case, since it is les soluble in water and the growth chamber partial pressure is only at 5 kPa, which results in only 0.006 kg being dissolved in the growth chamber in steady state.

Interestingly, the simulation results show that a membrane surface of 5 m2 is still sufficient even at a 33 fold increased volume. The reason can be found in the mechanism of the membrane transport, which is driven by a pressure gradient. The larger volume of the reactor leads to a larger buffering capacity until concentrations become critical or the driving force strong enough. Once a steady state between membrane transport and photosynthesis is reached, the pressure difference is the same as with the smaller volume and the membrane transport through a 5 m^2 membrane sufficient.

A further observation, presented in Figure 7-39, is that this culture volume has less of an increase in pH than the results of previous simulations with smaller reactors, which are also able to support a human over the course of seven days.

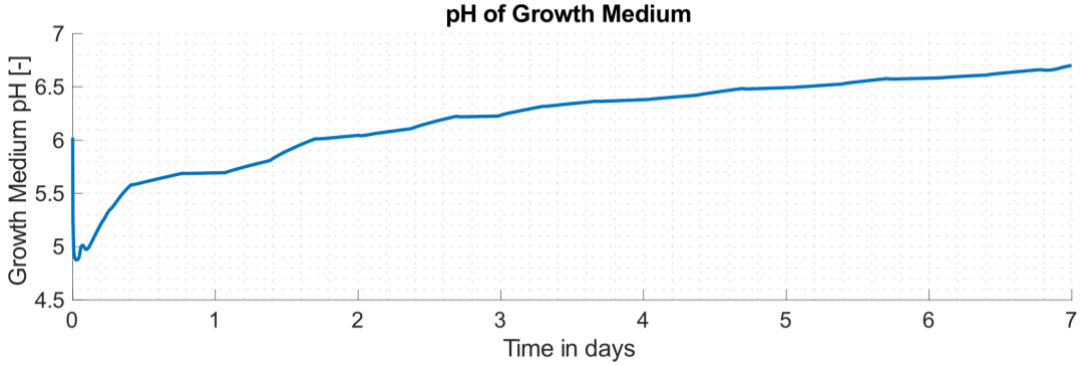

Figure 7-39: Evolution of growth medium pH over time in the scaled up Niederwieser reactor (500 L) with the experimental growth rate.

The pH only rises to 6.7 in this simulation case, while it rises to 7.8 (when carbon dioxide is sufficiently available) in the harvester set point optimized and scaled up simulation case (see 7.2.2.1). The reason for this differing behavior can be found in the Bold's Basal Medium components, which are added in the beginning of the simulation to match the recipe concentrations. Since the growth medium volume of this simulation case is so much larger, a higher total mass than in a smaller volume is required to reach the required concentrations. Nevertheless, the amount of released hydroxide ions is still the same in both cases, since the amount of added nitrate is also the same. However, in the larger volume the hydroxide ions have less impact, since the absolute number of hydrogen ions, which have to be equalized by hydroxide ions to increase the pH, is so much larger.

This simulation case provides similar urine processing and water savings capability as the previous cases that were able to support a human in terms of air revitalization. The reactor provides a 100 % urine processing (see Figure 7-40) and 83 % water savings (see Figure 7-41) capability, as in previous cases. A total 1 kg nitrate is supplied during times of urine depletion, as seen in Figure 7-42. Furthermore, Figure 7-43 shows that this scenario produces 4.45 kg of dry algal biomass over the course of seven days.

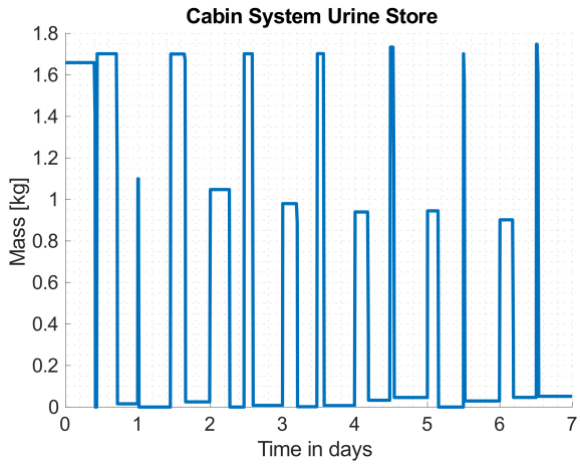

Figure 7-40: Evolution of urine store mass in Niederwieser design (15 L) with experimental growth rate.

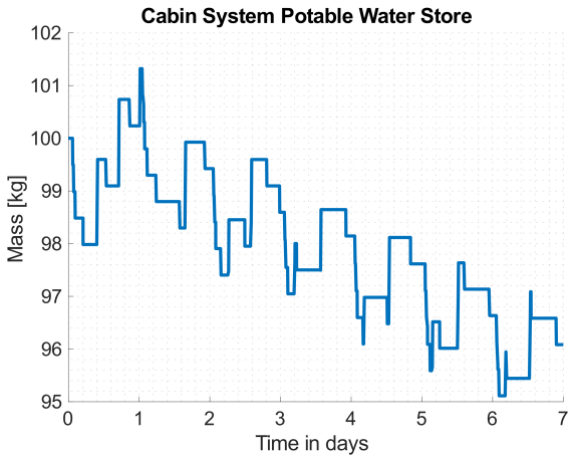

Figure 7-41: Evolution of potable water store mass in Niederwieser design (15 L) with experimental growth rate.

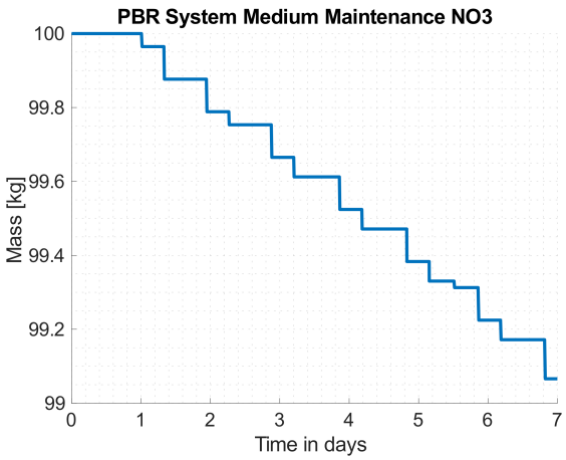

Figure 7-42: Evolution of nitrate supply mass in Niederwieser design (15 L) with experimental growth rate.

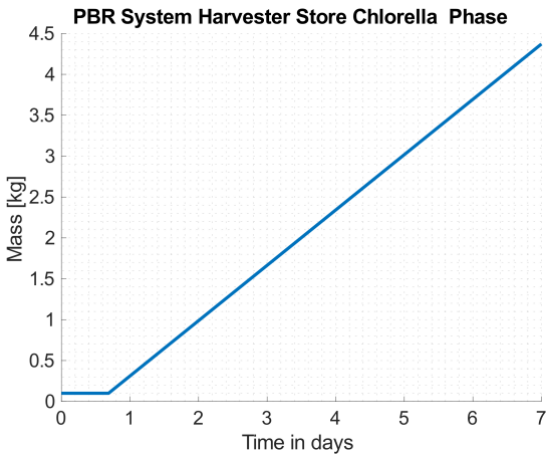

Figure 7-43: Evolution of the harvested Chlorella mass in Niederwieser design (15 L) with experimental growth rate.

When comparing the urine and water tank mass evolution over time in Figure 7-40 and Figure 7-41 to those of previous results where the reactor is able to maintain a breathable cabin atmosphere, the graphs presented here look more step than spike shaped. This behavior can be traced back to the supply logic of nitrate, which is refilled to its initial concentration in Bolds Basal Medium. Since the volume of the reactor is so much larger than that of previous results, the concentration can only be reached with a higher absolute mass. This can also be seen in the evolution of the nitrate mass tank in Figure 7-42, which has less but larger steps. Since the algal culture is still consuming it at a comparable rate to previous results, once the nitrate is added it lasts longer. Therefore, the urine can remain in the tank longer until the nitrate is used up, the urine is supplied and water harvested.

An overall mass balance of averaged in and outflows of the reactor in this simulation case is given in Table 7-7.

Table 7-7: Overall mass balance of matter in- and outflows. Left column shows the values originally proposed by Niederwieser [5] and the right column the averaged values of the simulated results with the scaled up reactor and experimentally determined growth rate (+ is into reactor, - is out).

Substance	Niederwieser Proposal [kg/d]	Simulation case averages [kg/d]
Oxygen	- 0.816	- 1.22
Carbon Dioxide	+ 1.040	+ 1.273
Biomass	- 0.255	- 0.624
Nutrients	+ 0.11	0.133
Pre-Processed Water	- 1.589	- 2.66
Urine	+ 1.6	+ 2.71

8 Conclusion

This chapter wraps up the conducted work by critically discussing the work and results of this thesis in 8.1, provides a summary of the model and the obtained experimental and simulation results in 8.2, draws conclusions in 8.3 and outlines some steps for future work to further improve and build upon the presented model in 8.4.

8.1 Discussion

This subchapter highlights and discusses some assumptions and architectural decisions that are made for the model and critically discusses the results of the experiments and simulations.

8.1.1 Model

A model is an abstraction of reality, which requires assumptions to be made. Especially with regard to simulating biological phenomena, such as algal growth, assumptions and generalizations are key to being able to formulate relations and mechanisms in a mathematical manner.

8.1.1.1 Growth Rate Calculation Module

One important aspect of this model is that it reacts to multiple environmental influences happening at the same time, no model could be found in literature that takes into account as many varying influences as this one does. Most other existing models only simulate, for example, growth as a function of the available nutrients or as a function of the available photosynthetically active radiation or maybe a combination of two influence factors - this model factors them in all at once. While this is definitely one of the strong suits of this model, this also leaves a lot of room for discussion.

Especially with regard to the modeled relative growth rates, the architectural decisions can be challenged. The achievable growth rate is calculated by factoring in multiple relative growth rates from various influence factors. The minimum threshold model only picks the worst relative growth rate to be factored in and at the same time disregards other non-ideal factors. It therefore possibly calculates a best case when multiple factors are deviating from optimum. The multiplicative model leads to a worsening achievable growth rate with the number of non-ideal conditions factored in.

For example, when 5 factors affecting the algal growth are factored in and all currently have a relative growth rate of 0.9, the minimum threshold model will only multiply one of them with the optimum growth rate, while the multiplicative model will multiply it with 0.9^5=0.59. If the number of factors is increased to 10, again all at 0.9, the minimum threshold model will still only use the worst of them – 0.9 – and the multiplicative model will now determine the overall relative growth factor to be 0.9^{10}=0.35, which is a lot less than the 0.9 of each of the individual factors.

A similar effect happens for a small number of factors, when they are strongly deviating. Where the actual relative growth rate lies is difficult to determine, since it would require to model the cross-influence between the factors affecting the growth, which in turn requires experiments on the cross-influence of all these factors. This is usually done for 2 factors, for example temperature and radiation [39], but not for more.

The model is therefore not ideal to represent strong deviations from optimum in multiple factors at the same time, since their cross influence is unknown and.

However, it works well for deviations by one factor at a time or small deviations of multiple ones. And since the model is intended to simulate a photobioreactor in a spacecraft, which commonly is a well-controlled environment, one can expect possibly one component to fail (e.g. radiation source, cooling or the harvester), but not all of them at once, since broken parts will be exchanged quickly.

The relative growth rates were taken from many different sources, which is why for many of the implementation choices in the model, a table is provided in this thesis that gives an overview over the range of reported values. Since so many different sources were used, one has to accept that not all the experiments were conducted under the same conditions. Nevertheless they are treated as “ideal” in this thesis, which is another assumption one has to accept, when using data from multiple different sources. Furthermore, not all values could be obtained for Chlorella vulgaris exclusively, since they sometimes were only available for the Chlorella species or “microalgae” in general.

8.1.1.2 Photosynthesis Module

As already addressed in the description of the photosynthesis module, abstractions have to be made with regard to the stoichiometric composition and especially the growth reactions. This thesis regards the cell as a black box, since the modelling of cell internal processes is a highly complex subject, which should be left to biologists. However, for example the assimilation of nitrate is defined by cell internal processes, which have to be represented to at least some extent, since an important part of the nitrate metabolism is not just the incorporation of the ion into the cell but a preceding metabolism. This releases hydroxide into the medium and therefore has the potential to change the composition of the medium by altering its pH. However, the amount of hydroxide ions released into the medium is reported differently, as outlined in 3.2.2.1, and the final assumption of this model to use one hydroxide ion per nitrate ion consumed, can and should be challenged in future works.

Furthermore, the consumption of phosphorus by the algae was excluded since the V-HAB human model does not excrete any phosphorus in its urine. Nevertheless, phosphorus is often regarded as the fifth important element in the algal composition (besides C, H, O, N) and theoretically could be taken from the phosphate in Bold’s Basal Medium. This was excluded from the simulation for reasons of simplifications although it would have an effect on the medium pH by removing ions from the phosphate buffer.

8.1.1.3 Medium Module

The growth medium is based on Bold’s Basal Medium, of which only the higher concentrated and acid/base relevant components are modelled. It is questionable though, if this should be exchanged for water, since it does not provide any nutrients to the algal culture modeled in this simulation (e.g. trace models) besides nitrate, which can be exchanged for urine (if available) and has to be refilled rather quickly when the algae grow.

Theoretically one could argue that there is no necessity to model the medium. Nevertheless, there are some benefits. Due to the initially low pH of around 4.5, the culture can grow for longer without supplying any substance to decrease the pH before reaching growth limiting levels. Furthermore, the buffering effect of the phosphate buffer is advantageous for the same reason.

The EDTA mass concentration in the simulation had to be increased by 16 %, when compared to the recipe concentrations to match measured pH values of Bold's Basal Medium. While this is only one component and concentrations of Bold's Basal Medium overall are rather low, the question arises why this was necessary. Possibly it is due to the fact that not all of the medium's components were modelled (e.g. boric acd was left out, since it only has a low concentration), or the obtained values for the acidity constants are slightly incorrect. This could be the case, since the acidity constant values for disodium-EDTA could only difficultly be obtained and were only available from one source. They can be changed in the model if desired.

8.1.1.4 Photosynthetically Active Radiation Module

The photosynthetically active radiation module involves geometric calculations, which are rather simple for a cuboid shape but become more complex for cylinders. Despite the fact that cylinders are a commonly used shape for photobioreactors, the model currently does not offer the opportunity to model the radiation propagation through a cylindrical photobioreactor.

Since this model was specifically designed with the goal to simulate the flat panel photobioreactor by Niederwieser the possibility to include a cylindrical shape was never implemented. Especially with regard to how thin the culture depths have to be for a high (volume) efficient growth, it could be interesting to have different options to choose from with regard to geometry.

8.1.2 Experiment Results

Although they were not the main focus of this thesis, some experiments were also conducted to gather data in areas, where the reports were varying or only scarcely available.

The largest uncertainty with regards to the experiments is the conversion between cell concentration, which is used for measurements, and biomass concentration, which is used in the model (e.g. for stoichiometric relations and radiation attenuation). The conversion is done with an average cell mass. Not only is there scarce reporting on the average cell mass, the reported values also differ from the lowest to the largest by a factor of 6. When looking at the absolute number in the order of 10^{-14} kg/cell, this might not seem much, however one has to consider, that this propagates to the biomass concentration. For example, this could either be 2 kg/m^3 or 12 kg/m^3 for the same cell concentration, which is a major difference in absolute values. Even more important for this model is that the growth rate, and therefore carbon dioxide fixation and oxygen production can also differ by a factor of 6 due to this uncertainty. The used average is in the middle of the reported values but can definitely be challenged since it's variance probably has one of the largest effects on the overall performance of a simulated photobioreactor's performance.

Furthermore, the procedural requirement of having to use a corrected optical density, when above a critical optical density was not known during the first experiments and therefore only the actual optical density measured. This led to the loss of some data from previous experiments, which could not be repeated due to time constraints. Due to the corrected optical density, the values of measured cell concentration are lower than if they were measured with an uncorrected optical density. When analyzing literature, the question arises, if this requirement is known to all the experimenters reporting values measured by optical density (which is the most common method of measurement).

The growth rate curves do not show very smooth behavior but generally follow the profile known from literature sources. In relative terms the results are as expected, the absolute values however are questionable by the previously discussed cell mass assumptions. Furthermore, the determined growth rates are among the lower ones reported, which begs the question, if the growth rates designed to be an optimum-baseline can actually be used as such. They are used nevertheless but should be regarded as a more conservative estimate, when evaluating the performance they show in a photobioreactor.

8.1.3 Simulation Results

Interestingly, a V-HAB simulation has an opposing design philosophy from the evaluated paper by Niederwieser. While V-HAB uses a bottom up approach, which models molecular-level mechanisms and sees how they perform on a larger scale, the paper by Niederwieser uses a top-level approach that does not take these mechanisms into account and uses averages to represent them.

As characterized in the title of the simulation case using the very optimistic growth rate suggested by Niederwieser, and clearly described in the simulation case description, the growth rate used for this model is considerably higher than the experimentally determined one. It should therefore be regarded as a very-best-case scenario. Some assumptions had to be made since it is based on an oxygen evolution rate and was transformed to an absolute biomass concentration growth rate with the modeled stoichiometric equations, which could yield potential sources of error.

When accepting the optimistic growth rate, the design still cannot provide sufficient air revitalization for a human over the course of seven days for two reasons.

Firstly, the V-HAB human model produces more carbon dioxide and consumes more oxygen than the baseline assumed in the Niederwieser design proposal. Since the human model is simply used for the simulations and is not developed or even changed in this simulation, these values are simply accepted.

Secondly, the design is strongly limited in growth due to the attenuation of photosynthetically active radiation. Instead of a proposed culture depth of 2.5 mm below an irradiated surface (5 mm flow channel thickness), only 0.85 mm would be required to eliminate this limitation. Even when this is combined in a plate with 1.7 mm thickness, which is irradiated from two sides, it is questionable if this could be successfully implemented from a mechanical standpoint. This would also increase the overall volume of the reactor, since more radiation panels per culture volume would be required. Another aspect to consider would be the high sensitivity in the extremely thin plates to heat flux fluctuations, to which it would quickly respond with temperature

changes. A more realistic approach would be to run the photobioreactor at a lower biomass concentration (and therefore growth rate) and double the culture volume to account for the efficiency decrease.

Combining the experimentally determined growth rate with the reactors yields a significantly lower – almost non-existent – performance due to the 24-fold lower growth rate. Only when scaled up to 500 m culture volume, the design is sufficiently large to support one human in terms of air revitalization.

The claim in Niederwieser's proposal [5] that more urine is required than can be provided by one human, is confirmed by the simulation results, where nitrate is supplied additionally. Interestingly, the assumption for urine produced by one human in the Niederwieser proposal are 35 % lower than the urine mass produced by the V-HAB human model. As a consequence of urine consumption by the algal culture, potable water is produced in the simulation, which is transferred to the potable water tank in the cabin. The modeled process is very simplistic, since it only removes an equivalent amount of water to what water was added in the supplied urine. In reality will probably require additional water processing devices as proposed by Niederwieser [5].

Overall, one shortcoming of the developed model and the generated simulation results is that the model was never put to a test itself. The individual mechanisms are based mainly on reviewed journal articles and some conference papers and are therefore trusted to represent the individual mechanisms (e.g. temperature response) correctly. However, they were never validated with test results in combination. No flat panel photobioreactor with membrane air exchange hardware was available for testing, which means that the simulation results could not be verified as a whole. This is a general challenge that arises when something is modeled that has not been built yet and should be usually validated with comparable test data to minimize the error. As the experiments in this thesis show, the behavior of a culture with induced bubbles strongly differs from that of a culture under a membrane, even when it is stirred. This means that the available bubble column reactor hardware could also not be used for model verifications, since the model was developed for a flat panel reactor with membrane air exchange (the reason being that bubble column reactors cannot work in weightlessness).

Noteworthy results of the simulation case are not just the calculated oxygen and carbon dioxide evolutions and resulting required reactor volumes, but the potential to use data generated by the simulation to improve the design iteratively. This is an important feature of the model, since many control values are created during the simulation, which allow to monitor what is currently limiting algal growth in the reactor. This can be an important feature for evaluating different designs in the future.

8.2 Summary

This thesis was done in collaboration between Institute of Astronautics at the Technical University of Munich and the Bioastronautics Department at the University of Colorado Boulder, where most of the work was done. It documents the development of a dynamic algae growth model for the life support system simulation tool V-HAB and its integration in the larger context of a simulated spacecraft cabin with a human in the loop.

The aim was to assess the dynamic behavior of a newly proposed photobioreactor design as a biological life support system component and use the developed model in the V-HAB environment as a basis to demonstrate means of design and operational optimization.

The starting point of this thesis was the goal of using an algae model for the dynamic design verification of an algal photobioreactor proposed by Tobias Niederwieser [5] from the University of Colorado Boulder. After reviewing existing V-HAB implementations of algae models, of which two were too simplistic and inflexible and the other aimed at producing hydrogen instead of oxygen, the decision was made that these could not be used and a new one had to be developed.

The first step of the model development was the identification of factors affecting the growth of microalgae, which was mainly done by reviewing published literature. Personal discussions, with advisors from both involved university departments, about what factors would be interesting to model, further contributed to what bases the model should cover.

Mainly, journal articles were used to quantify and mathematically describe the mechanisms and effects of algal growth. In fields, where no journal articles were available, conference papers, university course materials and technical product sheets were used. In many areas, assumptions and simplifications had to be made, which are clearly outlined throughout this thesis.

The eventually developed algae growth model is implemented in a V-HAB system environment and comprises four calculation modules of different areas. The main functionality of the developed model is that an optimum growth rate is dynamically determined, and external influences can decrease this growth rate when they deviate from their ideal value.

Some experiments were executed in order to generate data for the model in areas where literature data showed a large variance or was only scarcely available. However, some uncertainty with regard to the results exists since a transformation between cell concentration and biomass concentration had to be made via an average cell mass, on which only scarce and varying information is available.

The algae model was integrated in a photobioreactor system, which allows the definition of inputs on geometry, boundary conditions, used materials and the source of photosynthetically active radiation. This photobioreactor system with clearly defined interfaces will be available to future V-HAB users and does not require the deep understanding of the internal mechanisms. The photobioreactor system was then integrated in a cabin environment with a human in the loop to verify the viability of a photobioreactor as a biological spacecraft life support system.

The simulation of the proposed photobioreactor design and integration architecture by Niederwieser [5] showed that it has to be scaled up to a larger growth volume since it is limited due to the attenuation of photosynthetically active radiation and furthermore was designed for oxygen and carbon dioxide flows lower than those produced by the V-HAB human model. Nevertheless, the capability of the model to simulate algal growth and provide means of optimization were demonstrated with the simulation cases and allowed to generate values for a sufficiently sized Niederwieser reactor.

8.3 Conclusions

This thesis demonstrates the successful development of an algal growth simulation model implemented in the V-HAB simulation tool. The model can dynamically react to varying environmental influences and provides the most reliable results, when deviations are small or only one factor is deviating at a time. It records the degree at which influencing factors are limiting the growth for subsequent design and architectural improvements.

The model shows high modularity and is designed so it can be changed in the future, as more information about certain mechanisms is implemented or more growth influencing factors added.

While individual mechanisms are based on credible sources and some experiments, the overall model is not validated with test data of a flat panel photobioreactor with membrane air exchange, since such hardware was unavailable for testing.

The implementation in a V-HAB cabin environment with a simulated human model was successful and uses the photobioreactor design and integration architecture by Niederwieser [5]. The simulation results show that the design uses an extremely optimistic growth model and even then, is still too small to support the human model with sufficient air revitalization. Nevertheless, the developed simulation model can be used to sufficiently size a photobioreactor capable of providing air revitalization for one human and additionally producing potable water and food supplement.

Besides the implementation in this specific cabin and air supply architecture, the modeled PBR works as a standalone system in the V-HAB environment with clearly defined interfaces. A tutorial file is provided with the programing work of this thesis that enables future users to implement an algal photobioreactor without going into the scientific and technical details of algal growth.

The model is well suited for the design verification of photobioreactor life support systems as demonstrated by this thesis. Furthermore, or even more importantly, it can be used in the optimization process of reactor designs by showing limiting factors of the growth in the reactor. Potential optimizations that can be done with the model are the following ones:

- Culture growth volume by monitoring the evolution of cabin atmosphere partial pressures.
- The required plate thickness at a defined biomass concentration design point by using the positions of radiation growth domains.
- The membrane size by comparing what can be transported through the membrane and what is required by the algal culture.
- The optimum growth rate and resulting biomass harvester set point, when accepting growth limiting conditions
- Energy usage by only running lights at a limit necessary to support algal growth at the current biomass concentration. This can also save cooling power.
- Energy usage by only running the carbon dioxide supply system at a pressure necessary to maintain sufficient membrane transport for the current algal carbon dioxide consumption.
- The pH of the growth medium can be optimized or maintained by using different nutritional profiles. Urine for neutral behavior, nitrate to increase pH, ammonium salts to decrease pH.

- The algal assimilation coefficient by supplying different nutrients.

8.3.1 Fulfillment of Requirements

Top-level requirements were defined in the beginning of this thesis, which were derived from a mission statement and main goals that were communicated with the advisors from both departments in Munich and Boulder. They acted as a basis during the work on this thesis and their fulfillment shall be reflected here.

1. A Chlorella vulgaris growth model shall be created capable of dynamically reacting to varying influences of
   1.1. atmospheric pressure
   1.2. carbon dioxide concentration
   1.3. oxygen concentration
   1.4. nitrogen concentration
   1.5. light intensity
   1.6. temperature

While requirements 1.2 – 1.6, which concern the modeling of different environmental influences were fulfilled, one influence not modeled was the atmospheric pressure on the algae itself (requirement 1.1). This was omitted when it became clear that the expected atmospheric pressures in a spacecraft (70 kPa proposed Exploration Atmosphere to about 100 kPa on International Space Station) had no significant effect on algal growth [79]. Additionally to those requirements above, the influence of pH on algal growth was added along with a complex model to calculate the current growth medium pH. This was done since it was identified to have an effect on growth and various mechanisms in the growth medium can alter the pH.

2. The use of urine as a nutrient should be investigated and implemented

The integration of urine processing capability was upgraded from a nice-to-have to a must have requirement during the development process, since this is a vital part of a biological life support system.

3. The algal growth model shall be implemented in V-HAB
4. The algal growth model shall be incorporated in a photobioreactor design in order to simulate
   4.1. carbon dioxide consumption
   4.2. oxygen generation
   4.3. biomass production

The requirements 3 and 4 were fulfilled.

5. Two gas transfer technologies between the photobioreactor and the atmosphere shall be implemented
   5.1. sparging
   5.2. hollow fiber membranes

Both of the requirements 5.1 and 5.2 were not implemented. Sparging is nonsensical for an orbital spacecraft since it relies on gravity and hollow fiber membranes are a very specific implementation of a membrane. A more general membrane transport membrane was implemented, which could be adapted to hollow fiber membranes if their surface area and permeability is known.

6. Areas where biological and hardware tests are sensible shall be identified.

These areas were identified to be the determination of the optimum growth rate, the defining photon flux densities of the radiation growth domains and the biomass concentration dependent radiation attenuation in the Chlorella vulgaris culture.

7. Simulations shall be run that to size a photobioreactor capable of providing sufficient air revitalization capability to a human in a day/night cycle with special consideration of the
   7.1. interplay between assimilation coefficient (algae) and respiration coefficient (human)
   7.2. predicting the waste water input (urine as nutrition) and purified water output
   7.3. predicting the produced biomass

The requirements 7.1-7.3 were fulfilled.

8. The newly proposed photobioreactor design and integration architecture shall be simulated
   8.1. With values exactly as proposed in the paper
   8.2. With the values as implemented in the model (found in other literature sources)

Both requirements 8.1 and 8.2 were fulfilled.

9. Means of optimization shall be identified through the simulation results

Requirement 9 was fulfilled.

While the overall goal of the thesis – the development of an algal growth model and its integration in a V-HAB simulation – was clear from the beginning and did not change, details were updated, old requirements neglected, and new ones added. The involvement of two different universities, thousands of kilometers apart from each other, demanded somewhat of an agile approach to changing aims of the thesis. These changing aims could also be viewed as an upgrade of aims since most of them came about when discussing the topic further and finding newer or better ideas of aspects that would be interesting to implement.

Overall, the conclusion can be drawn that for both of the involved departments – in Boulder and Munich – some useful outcome was created in this thesis, which will be usable for future projects. The model was successfully developed and is available to future V-HAB users and the newly developed photobioreactor was simulated and optimization pathways presented.

8.4 Future Work

During the model development, implementation and simulation, new ideas arise constantly that could enhance the model. However, not all of these can be implemented due to time constrains. Nevertheless, these ideas are gathered here and provide an outlook on how to further improve the model in the future or how it could be put to use. Furthermore, an overview of planned publications in relation to this thesis is given.

8.4.1 Model Updates

The model was purposefully designed so it could be modified and extended.

The most important piece of future work is to gather some overall model validation data with some tests on a flat panel photobioreactor with membrane air exchange. This

could not be done in this thesis due to the unavailability of a flat panel photobioreactor and the lack of time to build one. Nevertheless, it is strongly suggested to design tests and build hardware in order to gain higher confidence in the model as a whole and its generated predictions. Another first step in this direction would be the implementation of a cylindrical geometry and bubble column air exchange in order to be able to use the existing photobioreactor at the Bioserve Space Technologies laboratories for model validation.

Some sources suggest a varying macromolecular composition of algal cells with different lighting and medium conditions. This could be implemented in the model by implementing a variable Chlorella composition with one model for ammonia uptake and one for nitrate uptake as outlined in [61]. This would allow the calculation of an overall current composition, which could be changing over time depending on how much of either reactant is used. From a V-HAB perspective, this would require the specification of more than one Chlorella vulgaris cell composition in the matter table.

Although it did not show to be critical over the course of the simulated seven days, the pH showed an upward trend, mainly attributed to the metabolism of nitrate, which has to be supplied additionally to urine. Therefore, maintaining an uncritical pH for long term algal growth is imperative. This could be implemented by automatically supplying nitrate and ammonia as nitrogen, due to their ability to increase (nitrate) or decrease (ammonia) pH [69]. A challenge to consider is that algae prefer the uptake of ammonia over the metabolism of nitrate, which means that they cannot be supplied by a mix but have to be supplied after the other is used up.

The photosynthetically active radiation module currently is only suited to calculate the radiation propagation through flat panel photobioreactors (cuboid shape). These calculations could be updated to include a cylindrical shape to make the simulation results comparable to a wider range of experiments described in literature. Furthermore, a day night cycle or “flashing-light” influence could be implemented, which is currently not the case, but is reported have a positive effect on algal growth [46].

8.4.2 Further Experiments

A flat panel photobioreactor, or at least a subsection of the proposed Niederwieser design, should be built and tests designed to validate the model developed within the scope of this thesis.

A previously mentioned, the cross influence of various limiting parameters is unknown and therefore the validity of simulated results is unclear, when more than one factor is deviating from its optimum. Experiments to determine the reciprocal influence between multiple parameters are probably complex but would be of great value.

Since the assumed average cell mass has such a large influence on the growth rate and radiation attenuation (which in term influences the plate thickness), it would be ideal to either find/create reliable data for the average cell mass or, even better, find a way of determining biomass concentration in a fast way right away during experiments.

8.4.3 Simulation Cases

The conference paper that presents the Niederwieser design [5], also compares the design to currently used systems on the International Space Station by using a top-level approach with averages. It would be interesting to use V-HAB with its International Space Station life support library components to make a dynamic comparative analysis of the reactor to the physico-chemical systems currently used.

One of the great advantages of a simulation tool is that control mechanisms can be implemented for almost every parameter in the simulation environment, even if this is not or only difficultly possible in real life. This gives a system designer the freedom to test the performance of different control logics and establish if this control mechanism is wort researching more in order to implement it in hardware at a later point in time.

Some of these control mechanisms that could be tested in future simulations are harvesting at varying biomass concentrations set different growth rates according to what is currently needed. This could also be done by implementing a controller that switches the LED panels providing the photosynthetically active radiation on or off. This could be further extended to only switching off part of the reactor in order to achieve different levels of oxygen production, while having some reserve for when more performance is required.

A further control and architectural design considerations that is worth investigating is related to the air supply. It would be interesting to investigate two different architectures and compare their masses and performance. One architecture lets the photobioreactor draw the carbon dioxide it can process from the cabin directly and (if no strong fluctuations should be allowed) accepts that the reactor will be lacking carbon dioxide supply at times of low carbon dioxide production in the cabin and is therefore oversized. An alternative architecture uses a buffer pump and tank that maintain a constant carbon dioxide partial pressure in the cabin (at the cost of higher periphery mass), which will result in a smaller reactor volume and mass while it can always operate in its optimum working point.

8.4.4 Publications

The previously mentioned architectural considerations about implementing a carbon dioxide buffer tank or choosing a larger reactor volume will be evaluated in more detail with the model from this thesis in a paper that will be presented at the International Conference on Environmental Systems in July 2019 in Boston, MA, USA.

Furthermore, a journal article is planned to be written on the simulated design of the Niederwieser reactor and design optimizations that are possible with the simulation model. The article will be handed in for the Acta Astronautical Journal sometime in early 2019.

A References

[1] D. S. Bendall, C. J. Howe, E. G. Nisbet, and R. E. R. Nisbet, “Introduction. Photosynthetic and atmospheric evolution,” *Philos. Trans. R. Soc. B Biol. Sci.*, vol. 363, no. 1504, pp. 2625–2628, Aug. 2008.

[2] J. M. Fernandez Sevilla and D. Lopez Alonso, “Microalgal Biotechnology,” presented at the University of Almeria, University of Almeria, 2014.

[3] M. Li, D. Hu, H. Liu, E. Hu, B. Xie, and L. Tong, “Chlorella vulgaris culture as a regulator of CO2 in a bioregenerative life support system,” *Adv. Space Res.*, vol. 52, no. 4, pp. 773–779, Aug. 2013.

[4] C. Olthoff, D. Pütz, and J. Schnaitmann, “Dynamic Life Support System Simulations with V-HAB,” presented at the Deutscher Luft und Raumfahrtkongress 2015, 2015.

[5] T. Niederwieser and D. Klaus, “Feasibility Study of an Algal-Based Life Support System,” presented at the 69th International Astronautical Congress (IAC), Bremen, Germany, 2018, p. 10.

[6] G. K. Pal, Pal, and G.K, *Textbook of Practical Physiology*. Orient Blackswan, 2001.

[7] O. L. Lange, P. S. Nobel, C. B. Osmond, and H. Ziegler, *Physiological Plant Ecology I*. Springer-Verlag Berlin-Heidelberg, 1981.

[8] R. A. Andersen and R. A. Lewin, “Algae,” *Britannica Academic*. Encyclopaedia Britannica Inc., Dec-2016.

[9] V. Bhola, R. Desikan, S. K. Santosh, K. Subburamu, E. Sanniyasi, and F. Bux, “Effects of parameters affecting biomass yield and thermal behaviour of Chlorella vulgaris,” *J. Biosci. Bioeng.*, vol. 111, no. 3, pp. 377–382, Mar. 2011.

[10] P. Eckart, *Spaceflight life support and biospherics*. Dordrecht; London: Springer, 1996.

[11] “Blue Green Algae,” *Britannica Academic*. Encyclopaedia Britannica Inc., 2007.

[12] R. Hine and E. A. Martin, *A dictionary of biology*. Oxford: Oxford University Press, 2008.

[13] M. W. Beyerinck, “Culturversuche mit Zoochlorellen, Lichenengonidien und anderen niederen Algen,” *Bot. Ztg.*, vol. 45, p. 726, Nov. 1890.

[14] C. Safi, B. Zebib, O. Merah, P.-Y. Pontalier, and C. Vaca-Garcia, “Morphology, composition, production, processing and applications of Chlorella vulgaris: A review,” *Renew. Sustain. Energy Rev.*, vol. 35, pp. 265–278, Jul. 2014.

[15] L. Blinová, A. Bartošová, and K. Gerulová, “Cultivation Of Microalgae (Chlorella vulgaris) For Biodiesel Production,” *Res. Pap. Fac. Mater. Sci. Technol. Slovak Univ. Technol.*, vol. 23, no. 36, pp. 87–95, Jun. 2015.

[16] E. W. Becker, “Micro-algae as a source of protein,” *Biotechnol. Adv.*, vol. 25, no. 2, pp. 207–210, Mar. 2007.

[17] K. Tuantet, M. Janssen, H. Temmink, G. Zeeman, R. H. Wijffels, and C. J. N. Buisman, “Microalgae growth on concentrated human urine,” *J. Appl. Phycol.*, vol. 26, no. 1, pp. 287–297, Feb. 2014.

[18] J. B. K. Park, R. J. Craggs, and A. N. Shilton, “Wastewater treatment high rate algal ponds for biofuel production,” *Bioresour. Technol.*, vol. 102, no. 1, pp. 35–42, Jan. 2011.

[19] S. Chinnasamy, B. Ramakrishnan, A. Bhatnagar, and K. Das, “Biomass Production Potential of a Wastewater Alga Chlorella vulgaris ARC 1 under Elevated Levels of CO2 and Temperature,” *Int. J. Mol. Sci.*, vol. 10, no. 2, pp. 518–532, Feb. 2009.

[20] L. E. González, R. O. Cañizares, and S. Baena, “Efficiency of ammonia and phosphorus removal from a colombian agroindustrial wastewater by the microalgae Chlorella vulgaris and Scenedesmus dimorphus,” *Bioresour. Technol.*, vol. 60, no. 3, pp. 259–262, Jun. 1997.

[21] J. Keppler *et al.*, “The final configuration of the algae-based ISS experiment PBR@LSR,” presented at the 48th International Conference On Environmental Systems, Albuquerque NM, 2018, p. 12.

[22] T. Niederwieser, P. Kociolek, and D. Klaus, “A review of algal research in space,” *Acta Astronaut.*, vol. 146, pp. 359–367, May 2018.

[23] Texas A&M AgriLife, *AgriLife-Algae-FacilityCrane, CC BY-NC-ND 2.0*. 2010.

[24] IGV Biotech, *Photobioreactor CC BY-SA 3.0*. .

[25] M. Beck, “Development of a Dynamic Algae Photobioractor Model for the V-HAB LSS Simulation,” Term Paper (Semesterarbeit), Technical University of Munich, Munich, Germany, 2010.

[26] E. Decker, *moss bioreactor CC BY-SA 1.0*. 2008.

[27] J. Steigenberger, “Dynamic Modeling and Simulation of a Microalgae Photobioreactor,” Bachelor’s Thesis, Technical University of Munich, Munich, Germany, 2014.

[28] D. Schneider, “Development of a dynamic algae model as an element of a Life Support System,” Term Paper (Semesterarbeit), Technical University of Munich, Munich, Germany, 2010.

[29] E. Lee, M. Jalalizadeh, and Q. Zhang, “Growth kinetic models for microalgae cultivation: A review,” *Algal Res.*, vol. 12, pp. 497–512, Nov. 2015.

[30] G. Detrell, S. Belz, J. Bretschneider, A.-I. K. Jost, and Ø. M. Jakobsen, “Design of a test platform for algae cultivation research at different gravitation levels,” presented at the 48th International Conference on Environmental Systems, Albuquerque NM, 2018, p. 13.

[31] M. I. . Halmi, M. S. Shukor, W. L. . Johari, and M. Y. Shukor, “Modeling the Growth Kinetics of Chlorella vulgaris Cultivated in Microfluidic Devices,” *Asian J. Plant Biol.*, vol. 2, pp. 7–10, 2014.

[32] K. M. C. Tjørve and E. Tjørve, “The use of Gompertz models in growth analyses, and new Gompertz-model approach: An addition to the Unified-Richards family,” *PLOS ONE*, vol. 12, no. 6, p. e0178691, Jun. 2017.

[33] M. Stemkovski, R. Baraldi, K. Flores, and H. T. Banks, “Validation of a Mathematical Model for Green Algae (Raphidocelis Subcapitata) Growth and

Implications for a Coupled Dynamical System with Daphnia Magna," *Appl. Sci.*, vol. 6, no. 5, p. 155, May 2016.

[34] M. H. Zwietering, I. Jongenburger, and F. M. Rombouts, "Modeling of the Bacterial Growth Curve," *APPL Env. MICROBIOL*, vol. 56, p. 7, 1990.

[35] A. W. Mayo, "Effects of Temperature and pH on the Kinetic Growth of Unialga Chlorella vulgaris Cultures Containing Bacteria," *Water Environ. Res.*, vol. 69, no. 1, pp. 64–72, 1997.

[36] J. Keppler *et al.*, "From breadboard to protoflight model – the ongoing development of the algae-based ISS experiment PBR@LSR," presented at the 47th International Conference on Environmental Systems, Charleston, South Carolina, 2017, p. 11.

[37] M. Javanmardian and B. O. Palsson, "High-density photoautotrophic algal cultures: Design, construction, and operation of a novel photobioreactor system," *Biotechnol. Bioeng.*, vol. 38, no. 10, pp. 1182–1189, Dec. 1991.

[38] S. Daliry, A. Hallajsani, J. M. Roshandeh, H. Nouri, and A. Golzary, "Investigation of optimal condition for Chlorella vulgaris microalgae growth," *Glob. J. Environ. Sci. Manag.*, no. 2, Apr. 2017.

[39] Y. Bartosh and C. J. Banks, "Algal growth response and survival in a range of light and temperature conditions: implications for non-steady-state conditions in waste stabilisation ponds," *Water Sci. Technol.*, vol. 55, no. 11, pp. 211–218, Jun. 2007.

[40] *Compendium of Chemical Terminology - Gold Book*, vol. 2.3.3. International Union of Pure and Applied Chemistry, 2014.

[41] H. Kalka, *Short Lecture 2017: Acid-Base Systems & pH Buffers.* 2017.

[42] A. Melis, "Solar energy conversion efficiencies in photosynthesis: Minimizing the chlorophyll antennae to maximize efficiency," *Plant Sci.*, vol. 177, no. 4, pp. 272–280, Oct. 2009.

[43] P. Leukart and K. Lüning, "Minimum spectral light requirements and maximum light levels for long-term germling growth of several red algae from different water depths and a green alga," *Eur. J. Phycol.*, vol. 29, no. 2, pp. 103–112, May 1994.

[44] J. Kim, J.-Y. Lee, and T. Lu, "A model for autotrophic growth of Chlorella vulgaris under photolimitation and photoinhibition in cylindrical photobioreactor," *Biochem. Eng. J.*, vol. 99, pp. 55–60, Jul. 2015.

[45] C. Yan, Y. Zhao, Z. Zheng, and X. Luo, "Effects of various LED light wavelengths and light intensity supply strategies on synthetic high-strength wastewater purification by Chlorella vulgaris," *Biodegradation*, vol. 24, no. 5, pp. 721–732, Sep. 2013.

[46] J. Degen, A. Uebele, A. Retze, U. Schmid-Staiger, and W. Trösch, "A novel airlift photobioreactor with baffles for improved light utilization through the flashing light effect," *J. Biotechnol.*, vol. 92, no. 2, pp. 89–94, Dec. 2001.

[47] Y.-S. Yun and J. M. Park, "Kinetic modeling of the light-dependent photosynthetic activity of the green microalgaChlorella vulgaris," *Biotechnol. Bioeng.*, vol. 83, no. 3, pp. 303–311, Aug. 2003.

[48] M. A. Chia, A. T. Lombardi, and M. D. G. G. Melao, “Growth and biochemical composition of Chlorella vulgaris in different growth media,” *An. Acad. Bras. Ciênc.*, vol. 85, no. 4, pp. 1427–1438, Oct. 2013.

[49] R. Filali, S. Tebbani, D. Dumur, A. Isambert, D. Pareau, and F. Lopes, “Growth modeling of the green microalga Chlorella vulgaris in an air-lift photobioreactor,” *IFAC Proc. Vol.*, vol. 44, no. 1, pp. 10603–10608, Jan. 2011.

[50] T. Niederwieser, R. Wall, J. Nabity, and D. Klaus, “Development of a testbed for flow-through measurements of algal metabolism under altered pressure for bioregenerative life support applications,” presented at the 47th International Conference on Environmental Systems, Charleston, South Carolina, 2017, p. 9.

[51] C.-H. Hsieh and W.-T. Wu, “Cultivation of microalgae for oil production with a cultivation strategy of urea limitation,” *Bioresour. Technol.*, vol. 100, no. 17, pp. 3921–3926, Sep. 2009.

[52] M. Baba and Y. Shiraiw, “High-CO2 Response Mechanisms in Microalgae,” in *Advances in Photosynthesis - Fundamental Aspects*, M. Najafpour, Ed. InTech, 2012.

[53] R. C. Hodson and J. F. Thompson, “Metabolism of Urea by Chlorella vulgaris,” *PLANT Physiol.*, vol. 44, no. 5, pp. 691–696, May 1969.

[54] T. Ogawa, T. Fujii, and S. Aiba, “Effect of oxygen on the growth (yield) of Chlorella vulgaris,” *Arch. Microbiol.*, vol. 127, no. 1, pp. 25–31, Aug. 1980.

[55] C.-G. Lee and B. ⧫. Palsson, “High-density algal photobioreactors using light-emitting diodes,” *Biotechnol. Bioeng.*, vol. 44, no. 10, pp. 1161–1167, Nov. 1994.

[56] S. Raso, B. van Genugten, M. Vermuë, and R. H. Wijffels, “Effect of oxygen concentration on the growth of Nannochloropsis sp. at low light intensity,” *J. Appl. Phycol.*, vol. 24, no. 4, pp. 863–871, Aug. 2012.

[57] M. Watts Pirt and S. J. Pirt, “The Influence of Carbon Dioxide and Oxygen Partial Pressures on Chlorella Growth in Photosynthetic Steady-state Cultures,” *Microbiology*, vol. 119, no. 2, pp. 321–326, Aug. 1980.

[58] S. J. Pirt, Y.-K. Lee, A. Richmond, and M. W. Pirt, “The photosynthetic efficiency of Chlorella biomass growth with reference to solar energy utilisation,” *J. Chem. Technol. Biotechnol.*, vol. 30, no. 1, pp. 25–34, 1980.

[59] H. A. Spoehr and H. W. Milner, “The Chemical Composition of Chlorella Effect Of Environmental Conditions,” *PLANT Physiol.*, vol. 24, no. 1, pp. 120–149, 1948.

[60] T. Oh Hama and S. Miyachi, “Chlorella,” in *Microalgal Biotechnology*, M. A. Borowitzka and L. J. Borowitzka, Eds. Cambridge: Cambridge University Press, 1988, pp. 3–26.

[61] R. K. Mandalam and B. Palsson, “Elemental balancing of biomass and medium composition enhances growth capacity in high-densityChlorella vulgaris cultures,” *Biotechnol. Bioeng.*, vol. 59, no. 5, pp. 605–611, Sep. 1998.

[62] M. T. Myint, A. Ghassemi, and N. Nirmalakhandan, “A generic stoichiometric equation for microalgae–microorganism nexus by using clarified domestic wastewater as growth medium,” *Desalination Water Treat.*, vol. 51, no. 34–36, pp. 6632–6640, Oct. 2013.

[63] W. J. Oswald, “Microalgae and Wastewater Treatment,” in *Microalgal Biotechnology*, M. A. Borowitzka and L. J. Borowitzka, Eds. Cambridge: Cambridge University Press, 1988, pp. 357–394.

[64] R. Muñoz and B. Guieysse, “Algal–bacterial processes for the treatment of hazardous contaminants: A review,” *Water Res.*, vol. 40, no. 15, pp. 2799–2815, Aug. 2006.

[65] S. John Pirt, “The Thermodynamic Efficiency (Quantum Demand) and Dynmics of Photosynthetic Growth,” *New Phytol.*, vol. 102, no. 1, pp. 3–37, Jan. 1986.

[66] K. Tuantet, H. Temmink, G. Zeeman, M. Janssen, R. H. Wijffels, and C. J. N. Buisman, “Nutrient removal and microalgal biomass production on urine in a short light-path photobioreactor,” *Water Res.*, vol. 55, pp. 162–174, May 2014.

[67] A. Fuggi, V. Di Martino Rigano, V. Vona, and C. Rigano, “Nitrate and ammonium assimilation in algal cell-suspensions and related pH variations in the external medium, monitored by electrodes,” *Plant Sci. Lett.*, vol. 23, no. 2, pp. 129–138, Nov. 1981.

[68] M. Taziki, H. Ahmadzadeh, M. A. Murry, and S. R. Lyon, “Nitrate and Nitrite Removal from Wastewater using Algae,” *Curr. Biotechnol.*, vol. 4, no. 4, pp. 426–440, Jan. 2016.

[69] M. L. Scherholz and W. R. Curtis, “Achieving pH control in microalgal cultures through fed-batch addition of stoichiometrically-balanced growth media,” *BMC Biotechnol.*, vol. 13, no. 1, p. 39, 2013.

[70] J. Jeanfils, M.-F. Canisius, and N. Burlion, “Effect of high nitrate concentrations on growth and nitrate uptake by free-living and immobilizedChlorella vulgaris cells,” *J. Appl. Phycol.*, vol. 5, no. 3, pp. 369–374, Jun. 1993.

[71] P. M. Glibert *et al.*, “Pluses and minuses of ammonium and nitrate uptake and assimilation by phytoplankton and implications for productivity and community composition, with emphasis on nitrogen-enriched conditions: Pluses and minuses of NH4+ *and* NO3−,” *Limnol. Oceanogr.*, vol. 61, no. 1, pp. 165–197, Jan. 2016.

[72] J. C. Goldman and P. G. Brewer, “Effect of nitrogen source and growth rate on phytoplankton-mediated changes in alkalinity1,” *Limnol. Oceanogr.*, vol. 25, no. 2, pp. 352–357, Mar. 1980.

[73] S. Schubert and F. Yan, “Nitrate and ammonium nutrition of plants: Effects on acid/base balance and adaptation of root cell plasmalemma H+ ATPase,” *Z. Für Pflanzenernähr. Bodenkd.*, vol. 160, no. 2, pp. 275–281, 1997.

[74] W. Choochote, K. Paiboonsin, S. Ruangpan, and A. Pharuang, “Effects of Urea and Light Intensity on the Growth of Chlorella sp.,” p. 8.

[75] T. Berman, “Algal growth on organic compounds as nitrogen sources,” *J. Plankton Res.*, vol. 21, no. 8, pp. 1423–1437, Aug. 1999.

[76] F. P. Healey, “Ammonium and urea uptake by some freshwater algae,” *Can. J. Bot.*, vol. 55, no. 1, pp. 61–69, Jan. 1977.

[77] E. Eustance, R. D. Gardner, K. M. Moll, J. Menicucci, R. Gerlach, and B. M. Peyton, “Growth, nitrogen utilization and biodiesel potential for two chlorophytes

grown on ammonium, nitrate or urea," *J. Appl. Phycol.*, vol. 25, no. 6, pp. 1663–1677, Dec. 2013.

[78] H. Belcher and E. Swale, *Culturing algae: a guide for schools and colleges*. Cambridge: Institute of Terrestrial Ecology, 1988.

[79] T. Niederwieser, P. Kociolek, and D. Klaus, "Spacecraft cabin environment effects on the growth and behavior of Chlorella vulgaris for life support applications," *Life Sci. Space Res.*, vol. 16, pp. 8–17, Feb. 2018.

[80] "Product Information Sheet: Bold's Basal Medium, 50x." PhytoTechnology Laboratories, 2014.

[81] "Basal medium," *Biology-Online Dictionary*. .

[82] W. Henry, "Experiments on the Quantity of Gases Absorbed by Water, at Different Temperatures, and under Different Pressures," *Philos. Trans. R. Soc. Lond.*, vol. 93, no. 0, pp. 29–274, Jan. 1803.

[83] R. Sander, "Compilation of Henry's law constants (version 4.0) for water as solvent," *Atmospheric Chem. Phys.*, vol. 15, no. 8, pp. 4399–4981, Apr. 2015.

[84] W. Knoche, "Chemical Reactions of CO2 in Water," in *Biophysics and Physiology of Carbon Dioxide*, C. Bauer, G. Gros, and H. Bartels, Eds. Berlin, Heidelberg: Springer Berlin Heidelberg, 1980, pp. 3–11.

[85] R. G. Burauand and R. J. Zasoki, "SSC 102 - Soil Chemistry, Course Notes Section 5: Chemistry of carbonate systems." University of California Davis, 2002.

[86] H. Kalka, "The Open Carbonate System." [Online]. Available: http://www.aqion.de/site/161. [Accessed: 04-Nov-2018].

[87] *McGraw-Hill dictionary of chemistry*, 2nd ed. New York: McGraw-Hill, 2003.

[88] D. D. Perrin, "Dissociation Constants of Inorganic Acids and Bases in Aqueous Solution." De Gruyter, Australian National University, Canberra, 1965.

[89] "Product Information Sheet: Ethylenediaminetetraacetic acid disodium salt dihydrate." Sigma-Aldrich, Inc.

[90] Deutsche Forschungsgemeinschaft and Commission for the Investigation of Health Hazards of Chemical Compounds in the Work Area, Eds., "Ethylendiamintetraessigsäure (EDTA) und ihre Alkalisalze [MAK Value Documentation in German language, 2009]," in *The MAK-Collection for Occupational Health and Safety*, Weinheim, Germany: Wiley-VCH Verlag GmbH & Co. KGaA, 2012, pp. 1–33.

[91] H. Kalka, "The Closed Carbonate System." [Online]. Available: http://www.aqion.de/site/160. [Accessed: 04-Nov-2018].

[92] K. Ganesh, R. Soumen, Y. Ravichandran, and Janarthanan, "Dynamic approach to predict pH profiles of biologically relevant buffers," *Biochem. Biophys. Rep.*, vol. 9, pp. 121–127, Mar. 2017.

[93] D. Schreuder, Ed., "Radiometry and photometry," in *Outdoor Lighting: Physics, Vision and Perception*, Dordrecht: Springer Netherlands, 2008, pp. 85–108.

[94] W. Biggs, "Principles of Radiation Measurement," LI-COR Company.

[95] Y.-S. Yun and J. . Park, “Attenuation of monochromatic and polychromatic lights in Chlorella vulgaris suspensions,” *Appl. Microbiol. Biotechnol.*, vol. 55, no. 6, pp. 765–770, Jun. 2001.

[96] R. J. Ellingson, “Integrating the Solar Spectrum,” presented at the University of Toledo: PHYS 4400, Principles and Varieties of Solar Energy, 2013.

[97] F. J. Los, “Algal respiration: A literature review,” Jun. 1979.

[98] M. Huesemann *et al.*, “A validated model to predict microalgae growth in outdoor pond cultures subjected to fluctuating light intensities and water temperatures,” *Algal Res.*, vol. 13, pp. 195–206, Jan. 2016.

[99] S. B. Powles, “Photoinhibition of Photosynthesis Induced by Visible Light,” *Annu. Rev. Plant Physiol.*, vol. 35, pp. 15–44, 1984.

[100] W. Fu, O. Gudmundsson, A. M. Feist, G. Herjolfsson, S. Brynjolfsson, and B. Ø. Palsson, “Maximizing biomass productivity and cell density of Chlorella vulgaris by using light-emitting diode-based photobioreactor,” *J. Biotechnol.*, vol. 161, no. 3, pp. 242–249, Oct. 2012.

[101] Kuma, “Difference Between Attenuation and Absorption,” *Pediaa.Com*, 16-Aug-2016. [Online]. Available: http://pediaa.com/difference-between-attenuation-and-absorption/. [Accessed: 12-Oct-2018].

[102] “attenuation,” *The Free Dictionary*. .

[103] J. Kim, J.-Y. Lee, and T. Lu, “Effects of dissolved inorganic carbon and mixing on autotrophic growth of Chlorella vulgaris,” *Biochem. Eng. J.*, vol. 82, pp. 34–40, Jan. 2014.

[104] T. Niederwieser, “First-order sizing analysis for an algal photobioreactor to accomplish spacecraft air revitalization,” presented at the International Conference on Environmental Systems, Albuquerque NM, Jul-2018.

[105] F. Widdel, “Prakctical Course ‘Mikrobiologie’, University of Bremen: Theory and Measurement of Bacterial Growth.” 2010.

[106] “User Manual: Thermo Scientific Multiskan FC.” Thermo Fisher Scientific Inc., 2015.

[107] W. Hu, “Dry Weight and Cell Density of Individual Algal and Cyanobacterial Cells for Algae Research and Development,” Master’s Thesis, University of Missouri-Columbia, Columbia, MO, 2014.

[108] “Air Pressure at Altitude Calculator,” *Mide Technology*. [Online]. Available: https://www.mide.com/pages/air-pressure-at-altitude-calculator. [Accessed: 26-Nov-2018].

[109] “Product Family Data Sheet: Cree XLamp XP-E-LEDs.” CREE, Inc., Durham NC, 2018.

[110] E. H. Gomez, “DEVELOPMENT OF A CONTINUOUS FLOW ULTRASONIC HARVESTING SYSTEM FOR MICROALGAE,” PhD Thesis, Colorado State University, Fort Collins, CO, 2014.

[111] M. Garcia, “International Space Station Facts and Figures,” *NASA*, 28-Apr-2016. [Online]. Available: http://www.nasa.gov/feature/facts-and-figures. [Accessed: 30-Nov-2018].

[112] D. R. Lickowsky and W. W. Seitz, “Human Integration Design Handbook (HIDH).” National Aeronautics and Space Administration, 2014.

B Appendices

B.1 Further pH-Calculation Equations

Equations representing the concentrations of acid/base contributing substances as a function of known values and the hydrogen ion concentration.

$$[EDTA^-] = \frac{C_{Na_2EDTA} * [H^+]^3 * K_{a,EDTA}}{[H^+]^4 + K_{a,EDTA} * [H^+]^3 + K_{a,EDTA} * K_{a,EDTA^-} * [H^+]^2 + K_{a,EDTA} * K_{a,EDTA^-} * K_{a,EDTA^{2-}} * [H^+] + K_{a,EDTA} * K_{a,EDTA^-} * K_{a,EDTA^{2-}} * K_{a,EDTA^{3-}}}$$

$$[EDTA^{2-}] = \frac{C_{Na_2EDTA} * [H^+]^2 * K_{a,EDTA} * K_{a,EDTA^-}}{[H^+]^4 + K_{a,EDTA} * [H^+]^3 + K_{a,EDTA} * K_{a,EDTA^-} * [H^+]^2 + K_{a,EDTA} * K_{a,EDTA^-} * K_{a,EDTA^{2-}} * [H^+] + K_{a,EDTA} * K_{a,EDTA^-} * K_{a,EDTA^{2-}} * K_{a,EDTA^{3-}}}$$

$$[EDTA^{3-}] = \frac{C_{Na_2EDTA} * [H^+] * K_{a,EDTA} * K_{a,EDTA^-} * K_{a,EDTA^{2-}}}{[H^+]^4 + K_{a,EDTA} * [H^+]^3 + K_{a,EDTA} * K_{a,EDTA^-} * [H^+]^2 + K_{a,EDTA} * K_{a,EDTA^-} * K_{a,EDTA^{2-}} * [H^+] + K_{a,EDTA} * K_{a,EDTA^-} * K_{a,EDTA^{2-}} * K_{a,EDTA^{3-}}}$$

$$[EDTA^{4-}] = \frac{C_{Na_2EDTA} * K_{a,EDTA} * K_{a,EDTA^-} * K_{a,EDTA^{2-}} * K_{a,EDTA^{3-}}}{[H^+]^4 + K_{a,EDTA} * [H^+]^3 + K_{a,EDTA} * K_{a,EDTA^-} * [H^+]^2 + K_{a,EDTA} * K_{a,EDTA^-} * K_{a,EDTA^{2-}} * [H^+] + K_{a,EDTA} * K_{a,EDTA^-} * K_{a,EDTA^{2-}} * K_{a,EDTA^{3-}}}$$

$$[HCO_3^-] = \frac{C_{Carb_{tot}} * K_{a_{CO2+H2O}} * [\mathrm{H}^+]}{[\mathrm{H}^+]^2 + K_{a_{CO2+H2O}} * [\mathrm{H}^+] + K_{a_{CO2+H2O}} * K_{a_{HCO3}}}$$

$$[CO_3^{2-}] = \frac{C_{Carb_{tot}} * K_{a_{CO2+H2O}} * K_{a_{HCO3}}}{[\mathrm{H}^+]^2 + K_{a_{CO2+H2O}} * [\mathrm{H}^+] + K_{a_{CO2+H2O}} * K_{a_{HCO3}}}$$

$$[H_2PO_4^-] = \frac{[H^+]^2 * K_{a_{H_3PO_4}} * \left(C_{phosphate_{total}}\right)}{[H^+]^3 + K_{a_{H_3PO_4}} * [H^+]^2 + K_{a_{H_3PO_4}} * K_{a_{HPO_4}} * [H^+] + K_{a_{H_3PO_4}} * K_{a_{HPO_4}} * K_{a_{HPO_4^{2-}}}}$$

$$[HPO_4^{2-}] = (\frac{[H^+] * K_{a_{H_3PO_4}} * K_{a_{HPO_4}} * \left(C_{phosphate_{total}}\right)}{[H^+]^3 + K_{a_{H_3PO_4}} * [H^+]^2 + K_{a_{H_3PO_4}} * K_{a_{HPO_4}} * [H^+] + K_{a_{H_3PO_4}} * K_{a_{HPO_4}} * K_{a_{HPO_4^{2-}}}}$$

$$[PO_4^{3-}] = \frac{K_{a_{H_3PO_4}} * K_{a_{HPO_4}} * K_{a_{HPO_4^{2-}}} * \left(C_{phosphate_{total}}\right)}{[H^+]^3 + K_{a_{H_3PO_4}} * [H^+]^2 + K_{a_{H_3PO_4}} * K_{a_{HPO_4}} * [H^+] + K_{a_{H_3PO_4}} * K_{a_{HPO_4}} * K_{a_{HPO_4^{2-}}}}$$

$$[OH^-] = \frac{K_w}{[H^+]}$$

10th order polynomial to solve the system for the hydrogen ion concentration

$$0 = [H^+]^{10}$$

$$+[H^+]^9 * \left(C_{KH_2PO_{4initial}} + 2 * C_{K_2HPO_{4initial}} + C_{KOH_{initial}} + K_{a_{H_3PO_4}} + K_{a_{EDTA}}\right)$$

$$+[H^+]^8 * \left(C_{K_2HPO_{4initial}} * K_{a_{H_3PO_4}} - C_{CO_{2initial}} * K_{a_{CO2+H2O}} - K_w - C_{NA_2EDTA} * K_{a_{EDTA}} + C_{KH_2PO_{4initial}} * K_{a_{EDTA}} + 2 * C_{K_2HPO_{4initial}} * K_{a_{EDTA}} + C_{KOH_{initial}} * K_{a_{H_3PO_4}} + C_{KOH_{initial}} * K_{a_{EDTA}} + K_{a_{H_3PO_4}} * K_{a_{HPO_4}} + K_{a_{H_3PO_4}} * K_{a_{EDTA}} + K_{a_{EDTA}} * K_{a_{EDTA^-}}\right)$$

$$+[H^+]^7 * \left(C_{K_2HPO_{4initial}} * K_{a_{H_3PO_4}} * K_{a_{EDTA}} - K_{a_{EDTA}} * K_w - 2 * C_{CO_{2initial}} * K_{a_{CO2+H2O}} * K_{a_{HCO3}} - C_{CO_{2initial}} * K_{a_{CO2+H2O}} * K_{a_{H_3PO_4}} - C_{KH_2PO_{4initial}} * K_{a_{H_3PO_4}} * K_{a_{HPO_4}} - C_{NA_2EDTA} * K_{a_{H_3PO_4}} * K_{a_{EDTA}} - C_{CO_{2initial}} * K_{a_{CO2+H2O}} * K_{a_{EDTA}} - K_{a_{H_3PO_4}} * K_w - 2 * C_{NA_2EDTA} * K_{a_{EDTA}} * K_{a_{EDTA^-}} + C_{KH_2PO_{4initial}} * K_{a_{EDTA}} * K_{a_{EDTA^-}} + 2 * C_{K_2HPO_{4initial}} * K_{a_{EDTA}} * K_{a_{EDTA^-}} + C_{KOH_{initial}} * K_{a_{H_3PO_4}} * K_{a_{HPO_4}} + C_{KOH_{initial}} * K_{a_{H_3PO_4}} * K_{a_{EDTA}} + C_{KOH_{initial}} * K_{a_{EDTA}} * K_{a_{EDTA^-}} + K_{a_{H_3PO_4}} * K_{a_{HPO_4}} * K_{a_{HPO_4^{2-}}} + K_{a_{H_3PO_4}} * K_{a_{HPO_4}} * K_{a_{EDTA}} + K_{a_{H_3PO_4}} * K_{a_{EDTA}} * K_{a_{EDTA^-}} + K_{a_{EDTA}} * K_{a_{EDTA^-}} * K_{a_{EDTA^{2-}}}\right)$$

$$+[H^+]^6 * \Big(C_{K_2HPO_4 initial} * K_{a_{H_3PO_4}} * K_{a_{EDTA}} * K_{a_{EDTA^-}} - K_{a_{H_3PO_4}} * K_{a_{EDTA}} * K_w - K_{a_{EDTA}} * K_{a_{EDTA^-}} * K_w - 2 * C_{CO_2 initial} * K_{a_{CO2+H2O}} * K_{a_{HCO3}} * K_{a_{H_3PO_4}} - C_{CO_2 initial} * K_{a_{CO2+H2O}} * K_{a_{H_3PO_4}} * K_{a_{HPO_4}} - 2 * C_{KH_2PO_4 initial} * K_{a_{H_3PO_4}} * K_{a_{HPO_4}} * K_{a_{HPO_4^{2-}}} - C_{K_2HPO_4 initial} * K_{a_{H_3PO_4}} * K_{a_{HPO_4}} * K_{a_{HPO_4^{2-}}} - 2 * C_{CO_2 initial} * K_{a_{CO2+H2O}} * K_{a_{HCO3}} * K_{a_{EDTA}} - C_{CO_2 initial} * K_{a_{CO2+H2O}} * K_{a_{H_3PO_4}} * K_{a_{EDTA}} - C_{NA_2EDTA} * K_{a_{H_3PO_4}} * K_{a_{HPO_4}} * K_{a_{EDTA}} - C_{KH_2PO_4 initial} * K_{a_{H_3PO_4}} * K_{a_{HPO_4}} * K_{a_{EDTA}} - 2 * C_{NA_2EDTA} * K_{a_{H_3PO_4}} * K_{a_{EDTA}} * K_{a_{EDTA^-}} - C_{CO_2 initial} * K_{a_{CO2+H2O}} * K_{a_{EDTA}} * K_{a_{EDTA^-}} - K_{a_{H_3PO_4}} * K_{a_{HPO_4}} * K_w - 3 * C_{NA_2EDTA} * K_{a_{EDTA}} * K_{a_{EDTA^-}} * K_{a_{EDTA^{2-}}} + C_{KH_2PO_4 initial} * K_{a_{EDTA}} * K_{a_{EDTA^-}} * K_{a_{EDTA^{2-}}} + 2 * C_{K_2HPO_4 initial} * K_{a_{EDTA}} * K_{a_{EDTA^-}} * K_{a_{EDTA^{2-}}} + C_{KOH initial} * K_{a_{H_3PO_4}} * K_{a_{HPO_4}} * K_{a_{HPO_4^{2-}}} + C_{KOH initial} * K_{a_{H_3PO_4}} * K_{a_{HPO_4}} * K_{a_{EDTA}} + C_{KOH initial} * K_{a_{H_3PO_4}} * K_{a_{EDTA}} * K_{a_{EDTA^-}} + C_{KOH initial} * K_{a_{EDTA}} * K_{a_{EDTA^-}} * K_{a_{EDTA^{2-}}} + K_{a_{H_3PO_4}} * K_{a_{HPO_4}} * K_{a_{HPO_4^{2-}}} * K_{a_{EDTA}} + K_{a_{H_3PO_4}} * K_{a_{HPO_4}} * K_{a_{EDTA}} * K_{a_{EDTA^-}} + K_{a_{H_3PO_4}} * K_{a_{EDTA}} * K_{a_{EDTA^-}} + K_{a_{EDTA}} * K_{a_{EDTA^-}} * K_{a_{EDTA^{2-}}} * K_{a_{EDTA^{3-}}}\Big)$$

$$+ [H^+]^5 * \Big(C_{K_2HPO_4 initial} * K_{a_{H_3PO_4}} * K_{a_{EDTA}} * K_{a_{EDTA^-}} * K_{a_{EDTA^{2-}}} - K_{a_{H_3PO_4}} * K_{a_{HPO_4}} * K_{a_{EDTA}} * K_w - K_{a_{H_3PO_4}} * K_{a_{EDTA}} * K_{a_{EDTA^-}} * K_w - K_{a_{EDTA}} * K_{a_{EDTA^-}} * K_{a_{EDTA^{2-}}} * K_w - 2 * C_{CO_2 initial} * K_{a_{CO2+H2O}} * K_{a_{HCO3}} * K_{a_{H_3PO_4}} * K_{a_{HPO_4}} - C_{CO_2 initial} * K_{a_{CO2+H2O}} * K_{a_{H_3PO_4}} * K_{a_{HPO_4}} * K_{a_{HPO_4^{2-}}} - 2 * C_{CO_2 initial} * K_{a_{CO2+H2O}} * K_{a_{HCO3}} * K_{a_{H_3PO_4}} * K_{a_{EDTA}} - C_{CO_2 initial} * K_{a_{CO2+H2O}} * K_{a_{H_3PO_4}} * K_{a_{HPO_4}} * K_{a_{EDTA}} - C_{NA_2EDTA} * K_{a_{H_3PO_4}} * K_{a_{HPO_4}} * K_{a_{HPO_4^{2-}}} * K_{a_{EDTA}} - 2 * C_{KH_2PO_4 initial} * K_{a_{H_3PO_4}} * K_{a_{HPO_4}} * K_{a_{HPO_4^{2-}}} * K_{a_{EDTA}} - C_{K_2HPO_4 initial} * K_{a_{H_3PO_4}} * K_{a_{HPO_4}} * K_{a_{HPO_4^{2-}}} * K_{a_{EDTA}} - 2 * C_{CO_2 initial} * K_{a_{CO2+H2O}} * K_{a_{HCO3}} * K_{a_{EDTA}} * K_{a_{EDTA^-}} - C_{CO_2 initial} * K_{a_{CO2+H2O}} * K_{a_{H_3PO_4}} * K_{a_{EDTA}} * K_{a_{EDTA^-}} - 2 * C_{NA_2EDTA} * K_{a_{H_3PO_4}} * K_{a_{HPO_4}} * K_{a_{EDTA}} * K_{a_{EDTA^-}} - C_{KH_2PO_4 initial} * K_{a_{H_3PO_4}} * K_{a_{HPO_4}} * K_{a_{EDTA}} * K_{a_{EDTA^-}} - 3 * C_{NA_2EDTA} * K_{a_{H_3PO_4}} * K_{a_{EDTA}} * K_{a_{EDTA^-}} * K_{a_{EDTA^{2-}}} - C_{CO_2 initial} * K_{a_{CO2+H2O}} * K_{a_{EDTA}} * K_{a_{EDTA^-}} * K_{a_{EDTA^{2-}}} - K_{a_{H_3PO_4}} * K_{a_{HPO_4}} * K_{a_{HPO_4^{2-}}} * K_w - 4 * C_{NA_2EDTA} * K_{a_{EDTA}} * K_{a_{EDTA^-}} * K_{a_{EDTA^{2-}}} * K_{a_{EDTA^{3-}}} + C_{KH_2PO_4 initial} * K_{a_{EDTA}} * K_{a_{EDTA^-}} * K_{a_{EDTA^{2-}}} * K_{a_{EDTA^{3-}}} + 2 * C_{K_2HPO_4 initial} * K_{a_{EDTA}} * K_{a_{EDTA^-}} * K_{a_{EDTA^{2-}}} * K_{a_{EDTA^{3-}}} + C_{KOH initial} * K_{a_{H_3PO_4}} * K_{a_{HPO_4}} * K_{a_{HPO_4^{2-}}} * K_{a_{EDTA}} + C_{KOH initial} * K_{a_{H_3PO_4}} * K_{a_{HPO_4}} * K_{a_{EDTA}} * K_{a_{EDTA^-}} + C_{KOH initial} * K_{a_{H_3PO_4}} * K_{a_{EDTA}} * K_{a_{EDTA^-}} * K_{a_{EDTA^{2-}}} + C_{KOH initial} * K_{a_{EDTA}} * K_{a_{EDTA^-}} * K_{a_{EDTA^{2-}}} * K_{a_{EDTA^{3-}}} + K_{a_{H_3PO_4}} * K_{a_{HPO_4}} * K_{a_{HPO_4^{2-}}} * K_{a_{EDTA}} * K_{a_{EDTA^-}} + K_{a_{H_3PO_4}} * K_{a_{HPO_4}} * K_{a_{EDTA}} * K_{a_{EDTA^-}} * K_{a_{EDTA^{2-}}} + K_{a_{H_3PO_4}} * K_{a_{EDTA}} * K_{a_{EDTA^-}} * K_{a_{EDTA^{2-}}} * K_{a_{EDTA^{3-}}} \Big)$$

$$+[H^+]^4 * \Big(C_{K_2HPO_4 initial} * K_{a_{H_3PO_4}} * K_{a_{EDTA}} * K_{a_{EDTA^-}} * K_{a_{EDTA^{2-}}} * K_{a_{EDTA^{3-}}} - K_{a_{H_3PO_4}} * K_{a_{HPO_4}} * K_{a_{EDTA}} * K_{a_{EDTA^-}} * K_w - K_{a_{H_3PO_4}} * K_{a_{EDTA}} * K_{a_{EDTA^-}} * K_{a_{EDTA^{2-}}} * K_w - K_{a_{EDTA}} * K_{a_{EDTA^-}} * K_{a_{EDTA^{2-}}} * K_{a_{EDTA^{3-}}} * K_w - 2 * C_{CO_2 initial} * K_{a_{CO2+H2O}} * K_{a_{HCO3}} * K_{a_{H_3PO_4}} * K_{a_{HPO_4}} * K_{a_{HPO_4^{2-}}} - 2 * C_{CO_2 initial} * K_{a_{CO2+H2O}} * K_{a_{HCO3}} * K_{a_{H_3PO_4}} * K_{a_{HPO_4}} * K_{a_{EDTA}} - C_{CO_2 initial} * K_{a_{CO2+H2O}} * K_{a_{H_3PO_4}} * K_{a_{HPO_4}} * K_{a_{HPO_4^{2-}}} * K_{a_{EDTA}} - 2 * C_{CO_2 initial} * K_{a_{CO2+H2O}} * K_{a_{HCO3}} * K_{a_{H_3PO_4}} * K_{a_{EDTA}} * K_{a_{EDTA^-}} - C_{CO_2 initial} * K_{a_{CO2+H2O}} * K_{a_{H_3PO_4}} * K_{a_{HPO_4}} * K_{a_{EDTA}} * K_{a_{EDTA^-}} - 2 * C_{NA_2EDTA} * K_{a_{H_3PO_4}} * K_{a_{HPO_4}} * K_{a_{HPO_4^{2-}}} * K_{a_{EDTA}} * K_{a_{EDTA^-}} - 2 * C_{KH_2PO_4 initial} * K_{a_{H_3PO_4}} * K_{a_{HPO_4}} * K_{a_{HPO_4^{2-}}} * K_{a_{EDTA}} * K_{a_{EDTA^-}} - C_{K_2HPO_4 initial} * K_{a_{H_3PO_4}} * K_{a_{HPO_4}} * K_{a_{HPO_4^{2-}}} * K_{a_{EDTA}} * K_{a_{EDTA^-}} - 2 * C_{CO_2 initial} * K_{a_{CO2+H2O}} * K_{a_{HCO3}} * K_{a_{EDTA}} * K_{a_{EDTA^-}} * K_{a_{EDTA^{2-}}} - C_{CO_2 initial} * K_{a_{CO2+H2O}} * K_{a_{H_3PO_4}} * K_{a_{EDTA}} * K_{a_{EDTA^-}} * K_{a_{EDTA^{2-}}} - 3 * C_{NA_2EDTA} * K_{a_{H_3PO_4}} * K_{a_{HPO_4}} * K_{a_{EDTA}} * K_{a_{EDTA^-}} * K_{a_{EDTA^{2-}}} - C_{KH_2PO_4 initial} * K_{a_{H_3PO_4}} * K_{a_{HPO_4}} * K_{a_{EDTA}} * K_{a_{EDTA^-}} * K_{a_{EDTA^{2-}}} - 4 * C_{NA_2EDTA} * K_{a_{H_3PO_4}} * K_{a_{EDTA}} * K_{a_{EDTA^-}} * K_{a_{EDTA^{2-}}} * K_{a_{EDTA^{3-}}} - C_{CO_2 initial} * K_{a_{CO2+H2O}} * K_{a_{EDTA}} * K_{a_{EDTA^-}} * K_{a_{EDTA^{2-}}} * K_{a_{EDTA^{3-}}} -$$

$$K_{a_{H_3PO_4}} * K_{a_{HPO_4}} * K_{a_{HPO_4^{2-}}} * K_{a_{EDTA}} * K_w + C_{KOH_{initial}} * K_{a_{H_3PO_4}} * K_{a_{HPO_4}} * K_{a_{HPO_4^{2-}}} * K_{a_{EDTA}} * K_{a_{EDTA^-}} + C_{KOH_{initial}} * K_{a_{H_3PO_4}} * K_{a_{HPO_4}} * K_{a_{EDTA}} * K_{a_{EDTA^-}} * K_{a_{EDTA^{2-}}} + C_{KOH_{initial}} * K_{a_{H_3PO_4}} * K_{a_{EDTA}} * K_{a_{EDTA^-}} * K_{a_{EDTA^{2-}}} * K_{a_{EDTA^{3-}}} + K_{a_{H_3PO_4}} * K_{a_{HPO_4}} * K_{a_{HPO_4^{2-}}} * K_{a_{EDTA}} * K_{a_{EDTA^-}} * K_{a_{EDTA^{2-}}} + K_{a_{H_3PO_4}} * K_{a_{HPO_4}} * K_{a_{EDTA}} * K_{a_{EDTA^-}} * K_{a_{EDTA^{2-}}} * K_{a_{EDTA^{3-}}}\Big)$$

$$+[H^+]^3 * \Big(C_{KOH_{initial}} * K_{a_{H_3PO_4}} * K_{a_{HPO_4}} * K_{a_{HPO_4^{2-}}} * K_{a_{EDTA}} * K_{a_{EDTA^-}} * K_{a_{EDTA^{2-}}} - K_{a_{H_3PO_4}} * K_{a_{HPO_4}} * K_{a_{EDTA}} * K_{a_{EDTA^-}} * K_{a_{EDTA^{2-}}} * K_w - K_{a_{H_3PO_4}} * K_{a_{EDTA}} * K_{a_{EDTA^-}} * K_{a_{EDTA^{2-}}} * K_{a_{EDTA^{3-}}} * K_w - 2 * C_{CO_{2initial}} * K_{a_{CO2+H2O}} * K_{a_{HCO3}} * K_{a_{H_3PO_4}} * K_{a_{HPO_4}} * K_{a_{HPO_4^{2-}}} * K_{a_{EDTA}} - 2 * C_{CO_{2initial}} * K_{a_{CO2+H2O}} * K_{a_{HCO3}} * K_{a_{H_3PO_4}} * K_{a_{HPO_4}} * K_{a_{EDTA}} * K_{a_{EDTA^-}} - C_{CO_{2initial}} * K_{a_{CO2+H2O}} * K_{a_{H_3PO_4}} * K_{a_{HPO_4}} * K_{a_{HPO_4^{2-}}} * K_{a_{EDTA}} * K_{a_{EDTA^-}} - 2 * C_{CO_{2initial}} * K_{a_{CO2+H2O}} * K_{a_{HCO3}} * K_{a_{H_3PO_4}} * K_{a_{EDTA}} * K_{a_{EDTA^-}} * K_{a_{EDTA^{2-}}} - C_{CO_{2initial}} * K_{a_{CO2+H2O}} * K_{a_{H_3PO_4}} * K_{a_{HPO_4}} * K_{a_{EDTA}} * K_{a_{EDTA^-}} * K_{a_{EDTA^{2-}}} - 3 * C_{NA_2EDTA} * K_{a_{H_3PO_4}} * K_{a_{HPO_4}} * K_{a_{HPO_4^{2-}}} * K_{a_{EDTA}} * K_{a_{EDTA^-}} * K_{a_{EDTA^{2-}}} - 2 * C_{KH_2PO_{4initial}} * K_{a_{H_3PO_4}} * K_{a_{HPO_4}} * K_{a_{HPO_4^{2-}}} * K_{a_{EDTA}} * K_{a_{EDTA^-}} * K_{a_{EDTA^{2-}}} - C_{K_2HPO_{4initial}} * K_{a_{H_3PO_4}} * K_{a_{HPO_4}} * K_{a_{HPO_4^{2-}}} * K_{a_{EDTA}} * K_{a_{EDTA^-}} * K_{a_{EDTA^{2-}}} - 2 * C_{CO_{2initial}} * K_{a_{CO2+H2O}} * K_{a_{HCO3}} * K_{a_{EDTA}} * K_{a_{EDTA^-}} * K_{a_{EDTA^{2-}}} * K_{a_{EDTA^{3-}}} - C_{CO_{2initial}} * K_{a_{CO2+H2O}} * K_{a_{H_3PO_4}} * K_{a_{EDTA}} * K_{a_{EDTA^-}} * K_{a_{EDTA^{2-}}} * K_{a_{EDTA^{3-}}} - 4 * C_{NA_2EDTA} * K_{a_{H_3PO_4}} * K_{a_{HPO_4}} * K_{a_{EDTA}} * K_{a_{EDTA^-}} * K_{a_{EDTA^{2-}}} * K_{a_{EDTA^{3-}}} - C_{KH_2PO_{4initial}} * K_{a_{H_3PO_4}} * K_{a_{HPO_4}} * K_{a_{EDTA}} * K_{a_{EDTA^-}} * K_{a_{EDTA^{2-}}} * K_{a_{EDTA^{3-}}} - K_{a_{H_3PO_4}} * K_{a_{HPO_4}} * K_{a_{HPO_4^{2-}}} * K_{a_{EDTA}} * K_{a_{EDTA^-}} * K_w + C_{KOH_{initial}} * K_{a_{H_3PO_4}} * K_{a_{HPO_4}} * K_{a_{EDTA}} * K_{a_{EDTA^-}} * K_{a_{EDTA^{2-}}} * K_{a_{EDTA^{3-}}} + K_{a_{H_3PO_4}} * K_{a_{HPO_4}} * K_{a_{HPO_4^{2-}}} * K_{a_{EDTA}} * K_{a_{EDTA^-}} * K_{a_{EDTA^{2-}}} * K_{a_{EDTA^{3-}}}\Big)$$

$$+[H^+]^2 * \Big(C_{KOH_{initial}} * K_{a_{H_3PO_4}} * K_{a_{HPO_4}} * K_{a_{HPO_4^{2-}}} * K_{a_{EDTA}} * K_{a_{EDTA^-}} * K_{a_{EDTA^{2-}}} * K_{a_{EDTA^{3-}}} - K_{a_{H_3PO_4}} * K_{a_{HPO_4}} * K_{a_{EDTA}} * K_{a_{EDTA^-}} * K_{a_{EDTA^{2-}}} * K_{a_{EDTA^{3-}}} * K_w - 2 * C_{CO_{2initial}} * K_{a_{CO2+H2O}} * K_{a_{HCO3}} * K_{a_{H_3PO_4}} * K_{a_{HPO_4}} * K_{a_{HPO_4^{2-}}} * K_{a_{EDTA}} * K_{a_{EDTA^-}} - 2 * C_{CO_{2initial}} * K_{a_{CO2+H2O}} * K_{a_{HCO3}} * K_{a_{H_3PO_4}} * K_{a_{HPO_4}} * K_{a_{EDTA}} * K_{a_{EDTA^-}} * K_{a_{EDTA^{2-}}} - C_{CO_{2initial}} * K_{a_{CO2+H2O}} * K_{a_{H_3PO_4}} * K_{a_{HPO_4}} * K_{a_{HPO_4^{2-}}} * K_{a_{EDTA}} * K_{a_{EDTA^-}} * K_{a_{EDTA^{2-}}} - 2 * C_{CO_{2initial}} * K_{a_{CO2+H2O}} * K_{a_{HCO3}} * K_{a_{H_3PO_4}} * K_{a_{EDTA}} * K_{a_{EDTA^-}} * K_{a_{EDTA^{2-}}} * K_{a_{EDTA^{3-}}} - C_{CO_{2initial}} * K_{a_{CO2+H2O}} * K_{a_{H_3PO_4}} * K_{a_{HPO_4}} * K_{a_{EDTA}} * K_{a_{EDTA^-}} * K_{a_{EDTA^{2-}}} * K_{a_{EDTA^{3-}}} - 4 * C_{NA_2EDTA} * K_{a_{H_3PO_4}} * K_{a_{HPO_4}} * K_{a_{HPO_4^{2-}}} * K_{a_{EDTA}} * K_{a_{EDTA^-}} * K_{a_{EDTA^{2-}}} * K_{a_{EDTA^{3-}}} - 2 * C_{KH_2PO_{4initial}} * K_{a_{H_3PO_4}} * K_{a_{HPO_4}} * K_{a_{HPO_4^{2-}}} * K_{a_{EDTA}} * K_{a_{EDTA^-}} * K_{a_{EDTA^{2-}}} * K_{a_{EDTA^{3-}}} -$$

$$C_{K_2HPO_4 initial} * K_{a_{H_3PO_4}} * K_{a_{HPO_4}} * K_{a_{HPO_4^{2-}}} * K_{a_{EDTA}} * K_{a_{EDTA^-}} * K_{a_{EDTA^{2-}}} * K_{a_{EDTA^{3-}}} - K_{a_{H_3PO_4}} * K_{a_{HPO_4}} * K_{a_{HPO_4^{2-}}} * K_{a_{EDTA}} * K_{a_{EDTA^-}} * K_{a_{EDTA^{2-}}} * K_w\Big)$$

$$+ [H^+] * \Big(- K_{a_{H_3PO_4}} * K_{a_{HPO_4}} * K_{a_{HPO_4^{2-}}} * K_{a_{EDTA}} * K_{a_{EDTA^-}} * K_{a_{EDTA^{2-}}} * K_{a_{EDTA^{3-}}} * K_w - 2 * C_{CO_2 initial} * K_{a_{CO2+H2O}} * K_{a_{HCO3}} * K_{a_{H_3PO_4}} * K_{a_{HPO_4}} * K_{a_{HPO_4^{2-}}} * K_{a_{EDTA}} * K_{a_{EDTA^-}} * K_{a_{EDTA^{2-}}} - 2 * C_{CO_2 initial} * K_{a_{CO2+H2O}} * K_{a_{HCO3}} * K_{a_{H_3PO_4}} * K_{a_{HPO_4}} * K_{a_{EDTA}} * K_{a_{EDTA^-}} * K_{a_{EDTA^{2-}}} * K_{a_{EDTA^{3-}}} - C_{CO_2 initial} * K_{a_{CO2+H2O}} * K_{a_{H_3PO_4}} * K_{a_{HPO_4}} * K_{a_{HPO_4^{2-}}} * K_{a_{EDTA}} * K_{a_{EDTA^-}} * K_{a_{EDTA^{2-}}} * K_{a_{EDTA^{3-}}}\Big)$$

$$- 2 * C_{CO_2 initial} * K_{a_{CO2+H2O}} * K_{a_{HCO3}} * K_{a_{H_3PO_4}} * K_{a_{HPO_4}} * K_{a_{HPO_4^{2-}}} * K_{a_{EDTA}} * K_{a_{EDTA^-}} * K_{a_{EDTA^{2-}}} * K_{a_{EDTA^{3-}}}$$